Color-superconductivity from a Dyson-Schwinger perspective

Dem Fachbereich Physik
der Technischen Universität Darmstadt

zur Erlangung des Grades
eines Doktors der Naturwissenschaften
(Dr. rer. nat.)

genehmigte Dissertation von
Dipl.-Phys. Marcel Dominik Johannes Nickel
aus Hanau

Darmstadt 2007
D17

Referent: Prof. Dr. Jochen Wambach
Korreferent: Prof. Dr. Jürgen Berges

Tag der Einreichung: 02.05.2007
Tag der Prüfung: 11.06.2007

Farbsupraleitung aus einer Dyson-Schwinger Perspektive

Zusammenfassung

Farbsupraleitende Phasen der Quantenchromodynamik bei verschwindenden Temperaturen und hohen Dichten werden untersucht. Das zentrale Objekt hierfür ist die Ein-Teilchen-Green-Funktion der Fermionen, der sogenannte Quark-Propagator. Dieser wird mit Hilfe seiner Bewegungsgleichungen, den Dyson-Schwinger Gleichungen, bestimmt. Um letztere handhaben zu können, wird ein für das Vakuum erfolgreich angewandtes Trunkierungsschema zu endlichen Dichten erweitert und schrittweise verbessert. Dabei wird insbesondere sichergestellt, dass analytische Ergebnisse bei asymptotisch hohen Dichten reproduziert werden. Auf diese Weise wird erstmalig ein Zugang bei astrophysikalisch relevanten Dichten verwendet, der sowohl im Vakuum als auch bei asymptotisch hohen Dichten bekannte Ergebnisse wiedergibt.

Im ersten Teil der Arbeit wird der Rahmen der Untersuchung mit Schwerpunkt auf die Erweiterung zu endlichen Dichten dargelegt. Es werden auch physikalische Observablen eingeführt, die durch Kenntnis des Propagators bestimmt werden können.

Im Folgenden wird ein minimales Trunkierungsschema vorgestellt. Um die Komplexität unseres Zugangs im Vergleich zu phänomenologischen Modellen der Quantenchromodynamik aufzuzeigen, wird zunächst die normalleitende Phase diskutiert. Im Anschluss folgt die Untersuchung der farbsupraleitenden Phasen für masselose Quarks. Hierbei kann der Gültigkeitsbereich analytischer Ergebnisse, die im schwach wechselwirkenden Regime bei asymptotisch hohen Dichten bestimmt wurden, durch direkte Gegenüberstellung mit numerischen Resultaten für astrophysikalisch relevante Dichten ausgeschlossen werden. Zusätzlich wird die Rolle der Quarkmassen und von Neutralitätsbedingungen für niedrige Dichten studiert. Im Gegensatz zu phänomenologischen Modellen wird die sogenannte CFL Phase als Grundzustand für alle relevanten Dichten gefunden. Diesem Ergebnis liegt die erstmalige Berücksichtigung einer Modifikation der Wechselwirkung im Medium zugrunde. Da Näherungen in diesem Zugang allein auf Ebene der Dyson-Schwinger Gleichung durchgeführt werden und immer auf eine komplett selbstkonsistente Lösung geachtet wird, werden außerdem neue Erkenntnisse zur CFL Phase gewonnen.

In einem weiteren Abschnitt wird die Anwendbarkeit der Maximum-Entropie-Methode zur Extraktion von Spektralfunktionen aus numerischen Ergebnissen in euklidischer Raumzeit demonstriert. Als Beispiel werden die Spektralfunktionen von Quarks in der normalleitenden und farbsupraleitenden Phase bestimmt. Hierdurch werden die Ergebnisse unseres Zugangs neu beleuchtet. So können das Nicht-Fermi-Flüssigkeitsverhalten der normalleitenden Phase und die endliche Breite der Quasiteilchen in der farbsupraleitenden Phase aufgezeigt werden.

Im abschließenden Kapitel dieser Arbeit werden Erweiterungen unseres Trunkierungsschemas insbesondere durch die Rückreaktion sogenannter Goldstonebosonen ausgearbeitet. Da solche Erweiterungen in unserem Zugang auch noch nicht im Vakuum durchgeführt wurden, werden einleitend Modifikationen des Quark-Propagators im Vakuum bestimmt. Danach wird dieser Zugang auf die CFL Phase für masselose Quarks erweitert und gleichzeitig Eigenschaften der Goldstonebosonen untersucht. Schließlich wird eine selbstkonsistente Trunkierung für die Modifikation der Wechselwirkung erarbeitet, welche zusätzlich den Meißner-Ochsenfeld-Effekt implementiert.

Contents

Chapter 1

Introduction

The laws of nature towards smaller distances are nowadays understood down to scales as small as 10^{-18} m. In this regime their 'effective' description in terms of a quantum field theory is the standard model of particle physics [1, 2, 3, 4]. It consists of two main building blocks: the electro-weak model and quantum chromodynamics (QCD).

The electro-weak model unifies electromagnetism and the weak interaction. Its most striking phenomenon is the Higgs mechanism for the generation of masses and, in its current formulation, it can be treated by a perturbative expansion in its coupling constant on the classical ground state. Consequently, current investigations are on the one hand focusing on the precise determination of the parameters of the electro-weak model, such as neutrino masses and CKM matrix elements. On the other hand, its range of validity is one of the open questions in high energy physics when probing the standard model at even smaller distances. Especially the nature of the scalar Higgs boson, which has not been experimentally discovered yet and the underlying mechanism of spontaneous symmetry breaking.

QCD describes the strong interaction, which is only being experienced and mediated by quarks and gluons. The theory is asymptotically free, meaning that the coupling strength vanishes for asymptotically short distances. Similar to the electro-weak model it can therefore be analyzed perturbatively, *i.e.* in particular systematically, at sufficiently small distances. Asymptotic freedom has been a keystone in establishing QCD by comparison with experiment and its discoverers have been awarded the Nobel price of physics [5, 6]. For distances above 0.1 fm this approach is, however, not applicable and a systematic analytical approach is lacking. Therefore QCD in this strongly coupled regime is interesting in its own right. In particular, the situation conceptually differs from the electro-weak model in the sense that the formulation of the theory is surprisingly plain, while the linkage to observables is highly non-trivial. Hence there are two somewhat opposite objectives for

the investigation of QCD in the vacuum: On the one hand, a direct and precise calculation of measured hadronic observables from the QCD Lagrangian as an additional test for the applicability of the theory in the strongly coupled regime and on the other hand a deeper understanding of underlying QCD phenomena.

The most striking properties whose understanding is still elusive are confinement and dynamical chiral symmetry breaking. Confinement refers to the absence of quarks and gluons in the physical spectrum. Dynamical chiral symmetry breaking also leaves its fingerprints in the bound-state spectrum by giving (most) hadrons finite masses of the order of 1 GeV, irrespective of the quarks' current-masses. Interestingly enough both phenomena seem to be interlinked as will also be discussed below.

The conventional method for first-principle calculations is lattice QCD. It formulates the theory on a discretized and finite space-time volume and numerically performs the path integral which is interpreted statistically [7]. This approach has been successfully applied to investigate ground-state properties, although it is not yet applicable to the full theory for physical values of the parameters. Many other questions can be and have been addressed, as long as there is a suitable indicator in terms of an operator, and the finite volume and the discretization do not pose a limitation.

As those limitations have proven to be crucial, *e.g.* for the confinement of gluons, additional continuum methods are highly desirable. In this thesis our method of choice are Dyson-Schwinger equations (DSEs). Those have successfully been used to study fundamental properties of QCD as well as to determine hadronic observables (for corresponding reviews see *e.g.* refs. [8, 9, 10, 11, 12]). The goal of this thesis is an extension of this approach to the QCD phase diagram, in particular an application to color-superconducting phases. Again, lattice QCD is not applicable within this regime, as the path integral can no longer be interpreted statistically at finite densities.

Exploring the QCD phase diagram is one of the most exciting and demanding fields in strong interaction physics. This is also due to the more complicated experimental situation, because strongly interacting matter under extreme conditions only existed in the early universe, resides in the interior of compact stellar objects or is produced in heavy-ion collisions. Thus, a connection of observations and theory is even more challenging. Nevertheless the exploration constitutes a further direction to gain information about features of QCD.

A schematic QCD phase diagram as it is nowadays conjectured is shown in Fig. 1.1. The thermodynamical variables are quark chemical potential μ_q and temperature T. Already shortly after establishing QCD as the theory of the strong interaction it has already been argued that hadrons, consisting of quarks and gluons, should dissociate at high

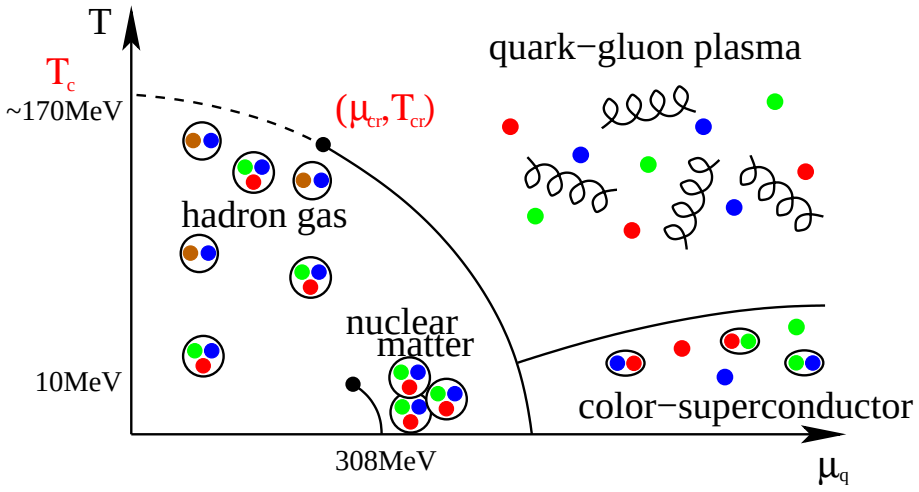

Figure 1.1: A schematic phase diagram of QCD as it is nowadays established. The thermodynamical variables are quark chemical potential μ_q and temperature T.

enough temperatures or densities [13, 14]. In more detail the phase diagram exhibits many interesting regimes, which are however difficult to access experimentally as well as theoretically.

Along the temperature axis lattice QCD calculations are possible to study the chiral and deconfinement phase transition [15]. Many features have attracted attention here in the past years, *e.g.* the precise value of the critical temperature T_c, the nature of the phase transition and the medium properties of the quark-gluon plasma near the phase transition [16, 17, 18, 19]. Experimentally, this regime is and will be in focus of ultra-relativistic heavy-ion experiments performed at CERN (SPS, LHC) and BNL (RHIC). Furthermore, a deeper understanding is of fundamental interest, as for example the chiral and deconfinement phase transition seem to coincide. It is worth noting that such questions have also been addressed by DSE studies for the pure gluonic sector and exhibited non-trivial features [20, 21, 22].

Another interesting regime is the location and vicinity of the chiral critical point and - connected to that - the order of the phase transition. There have been attempts at its determination by lattice QCD calculations which are highly debated [23, 24, 25, 26]. Also ultra-relativistic heavy-ion experiments performed at GSI (FAIR) will challenge this matter.

In this work, however, we will concentrate on the states of quark-matter for (almost) vanishing temperatures and densities beyond hadronic matter. Those are not accessible by lattice QCD calculations and only reside in the interior of compact stars if they are

realized at all. Under these conditions the emergence of color-superconducting phases is expected as the hadrons are dissociated and quarks should form correlated pairs according to Cooper's theorem.

The possible occurrence of different phases in QCD at sufficiently high densities and small temperatures has already been mentioned in 1975 [13] and worked out in [27, 28]. But there was little activity until 1998, when color-superconductivity was rediscovered [29, 30] by revealing the pairing phenomena and therefore also the critical temperatures to be much larger than anticipated. Since then it attracted a lot of interest in recent years (for corresponding reviews see *e.g.* refs. [31, 32, 33, 34, 35, 36, 37]) and numerous scenarios and approaches have been discussed.

Due to asymptotic freedom, color-superconductivity can be systematically studied at asymptotically large densities in a weak coupling expansion [38, 39]. At densities that are relevant for the interior of compact stars one is probing the strongly coupled regime, and such an expansion is lacking. Investigations are usually done within Nambu-Jona–Lasino (NJL)-type models in mean-field approximation. These result are rather sensitive to model parameters [40]. For more reliable statements a non-perturbative approach which is directly based on the QCD degrees of freedom is highly desirable.

This is the aim of this thesis. Starting from a successfully applied truncation scheme of DSEs proposed in the vacuum [41], we find a suitable extension to finite densities so that the commonly applied Hard-Dense-Loop (HDL) approximation at asymptotically high densities is properly recovered. In contrast to NJL-type investigations this also requires the inclusion of a medium modification in the interaction. The approximation is solely done on the level of the DSEs. Hence we also consider the momentum- and energy-dependence of self-energies, which encode non-trivial information about the quasiparticle spectrum, *e.g.* the non-Fermi liquid behavior of the chirally unbroken phase. The latter is especially important for the analysis of superconducting gap functions already in the weakly coupled regime [42].

The thesis is organized as follows:

In chapter 2 we will provide a set-up of DSEs in the vacuum and our framework for the extension to finite densities. All relevant quantities are introduced and some analytic properties are deduced.

In chapter 3 we discuss a minimal truncation scheme that is capable to recover known results in the vacuum as well as at asymptotically large densities and apply it to the strongly coupled regime of color-superconductivity. To illustrate the complexity of our calculations, we present results for the non-Fermi liquid behavior in the unbroken phase. Color-superconductivity in the chiral limit will then serve as an indicator for the applicabil-

ity of analytical results obtained in weak coupling when extrapolating to smaller densities. As the structure of the QCD phase diagram in the color-superconducting regime is strongly dependent on the Fermi surfaces of the pairing quasiparticles, finite strange-quark masses and neutrality conditions are considered in a next step.

The applicability of the Maximum Entropy Method (MEM) [43, 44] to DSE studies performed in Euclidean space is exemplified in chapter 4 and its application will again highlight the complexity of our calculations. The non-trivial features of the quasiparticle spectral functions in the unbroken and color-superconducting phases are presented, and possible applications to Bethe-Salpeter equations (BSEs) are discussed.

Possible extensions of our truncation scheme are elaborated in chapter 5. Focusing on the DSE of the quark propagator (qDSE), we find a trackable truncation scheme which essentially describes a back-reaction of Goldstone bosons on the order parameter in spontaneously broken phases. As this scheme has not yet been applied to the chirally broken phase in the vacuum either, an application to this case serves as an introduction and motivation. In the second part of this chapter, we construct a self-consistent truncation scheme for the medium modification of the effective quark interaction. We find a novel feature in the unbroken phase that might indicate an instability.

The conclusions drawn from our results and possible directions for further investigations are summarized in chapter 6.

Part of this work has already been published: Section 3.2-3.3 of chapter 3 were subject of ref. [45], section 3.4 of ref. [46]. The main part of chapter 4 was elaborated in ref. [47]. Also connected to this thesis is ref. [48].

Chapter 2

Theoretical framework

2.1 Basic aspects of QCD

2.1.1 Generating functional and Lagrangian of QCD

The dynamics of strongly interacting particles, *i.e.* quarks and gluons, is governed by a non-Abelian gauge theory: QCD. Being a quantum field theory, all observables can be deduced from the generating functional of the partition function

$$Z[\chi,\bar{\chi},j] \;=\; \int \mathcal{D}\big[\psi\bar{\psi}A\big]\exp\left(-S_{QCD}\big[\psi,\bar{\psi},A\big]+\int d^4x\left(\bar{\chi}\psi+\bar{\psi}\chi+j^a_\mu A^a_\mu\right)\right), \quad (2.1)$$

where we introduced the classical action $S_{QCD}\big[\psi,\bar{\psi},A\big]$, the quark fields ψ, their conjugates $\bar{\psi}$ and the gluon fields A together with their respective external sources $\bar{\chi}$, χ and j. The quark fields form N_f fundamental representations of $SU(N_c)$ on a Cartesian product of Dirac spinors[1]. The gluons are presented by vector fields taking values in the Lie algebra of $SU(N_c)$ and are therefore locally parameterized by $A_\mu = A^a_\mu T^a$ with an orthogonal basis such that $\mathrm{Tr}_c\left(T^aT^b\right)=\frac{1}{2}\delta_{ab}$ (see Appendix A.2). We assume the path integral, at least after proper renormalization, to be meaningful. Furthermore we already mention that additional constraints on the value of conserved charges can be implemented in the partition function via conjugated Lagrange multipliers.

The (unrenormalized) Lagrangian density $\mathcal{L}_{QCD}\big[\psi,\bar{\psi},A\big]$ of QCD, which determines the classical action $S_{QCD}\big[\psi,\bar{\psi},A\big]=\int d^4x\,\mathcal{L}_{QCD}\big[\psi,\bar{\psi},A\big]$, is constrained by the requirement of renormalizibility, Poincaré invariance, locality, flavor symmetry and gauge symmetry. It locally takes the unique form

$$\mathcal{L}_{QCD}\big[\psi,\bar{\psi},A\big] \;=\; \bar{\psi}\left(-\not{D}+m\right)\psi+\frac{1}{2}\mathrm{Tr}_c\left(F_{\mu\nu}F_{\mu\nu}\right), \quad (2.2)$$

[1]For QCD we have $N_c=3$, but we first consider the more general case of arbitrary N_c.

where we introduced the covariant derivative[2] $D_\mu = \partial_\mu + igA_\mu$ with the (unrenormalized) coupling constant g and the field strength tensor $F_{\mu\nu} = \frac{-i}{g}[D_\mu, D_\nu]$ corresponding to the curvature form. The mass matrix $m = \mathrm{diag}_f(m_u, m_d, \dots)$ implements the current-quark masses in the N_f-dimensional flavor space.

2.1.2 Global symmetries of QCD

Besides being gauge symmetric, the Lagrangian of QCD possesses (approximate) symmetries in flavor space. In the chiral limit it is symmetric under $U_L(N_f) \otimes U_R(N_f)$ acting on the decoupled left-handed $\psi_L = \frac{1-\gamma_5}{2}\psi$ and right-handed $\psi_R = \frac{1+\gamma_5}{2}\psi$ spinors, respectively. With the generators of the $SU(N_f)$ subgroups given by τ^a (see Appendix A.2), a suitable choice of corresponding conserved currents with respect to further explicit, dynamical and anomalous symmetry breaking is given by

$$\begin{aligned} j_\mu &= \bar{\psi}\,\gamma_\mu\,\psi\,, \\ j^5_\mu &= \bar{\psi}\,\gamma_\mu\gamma_5\,\psi\,, \\ j^a_\mu &= \bar{\psi}\,\gamma_\mu\,\frac{\tau^a}{2}\,\psi\,, \\ j^{5,a}_\mu &= \bar{\psi}\,\gamma_\mu\gamma_5\,\frac{\tau^a}{2}\,\psi\,. \end{aligned} \tag{2.3}$$

Including finite masses, these currents obey

$$\begin{aligned} \partial_\mu j_\mu &= 0\,, \\ \partial_\mu j^5_\mu &= 2\,\bar{\psi}\,\gamma_5\,m\,\psi\,, \\ \partial_\mu j^a_\mu &= \bar{\psi}\,\left[\frac{\tau^a}{2}, m\right]\psi\,, \\ \partial_\mu j^{5,a}_\mu &= \bar{\psi}\,\gamma_5\left\{\frac{\tau^a}{2}, m\right\}\psi \end{aligned} \tag{2.4}$$

on a classical level. From this we conclude that only j_μ is conserved for any values of the quark masses. The underlying symmetry is $U(1)_B$ and the corresponding charge is the baryon number. The vector/flavor current j^a_μ connected to the $SU(N_f)_V$ flavor symmetry is explicitly broken by differing quark masses and the axial currents j^5_μ and $j^{5,a}_\mu$ by non-vanishing quark masses. Whereas the vector symmetries in the QCD vacuum, at least for degenerate quark masses, can not be broken dynamically [49], the axial symmetries are. This leads *e.g.* to a non-vanishing chiral condensate and (almost) massless Goldstone

[2]The covariant derivative needs to be considered for different representations of the gauge group or formally speaking in each associated vector bundle.

bosons. On the quantum level j^5_μ becomes non-conserved even in the chiral limit, since the measure of the path integral in Eq.(2.1) is not invariant under the corresponding $U(1)_A$ symmetry leading to an additional source term in Eq.(2.4) [50]. This becomes apparent in the differing masses of the η- and η'-meson.

2.1.3 Gauge fixing

Gauge symmetry implies field configurations (A, ψ) in the same gauge orbit

$$[(A,\psi)] \stackrel{\text{def}}{=} \left\{(UAU^\dagger + UdU^\dagger, U\psi) : U \in \mathbb{R}^4 \times SU(N_c)\right\} \tag{2.5}$$

to have the same classical action. As a result only gauge invariant, *i.e.* observable quantities can be deduced from the generating functional. Since however many theoretical methods, such as perturbation theory and Dyson-Schwinger equations rely on gauge variant correlators, the expression for the path-integral needs to be modified, such that it gives the same results for gauge invariant quantities and non-trivial results for gauge variant quantities.

The key idea is to single out exactly one representative per gauge orbit and absorb the integration along a gauge orbit by rescaling the measure of the path integral. The Faddeev-Popov procedure implements this idea as soon as a functional $F[A]$ is given, such that

$$G\,[A] \stackrel{\text{def}}{=} F\,[A] - \omega \tag{2.6}$$

is vanishing for any given one-form ω exactly once in a given orbit[3]. In linear covariant gauges $F[A] = \partial_\mu A_\mu$ and we get the gauge fixed generating functional

$$\begin{aligned} Z[\chi,\bar\chi,\sigma,\bar\sigma,j] &= \int \mathcal{D}\left[c\bar c\psi\bar\psi A\right] \\ &\quad \exp\left(-\int d^4x\,\mathcal{L}_{QCD,\xi} + \int d^4x\left(\bar\chi\psi + \bar\psi\chi + \bar\sigma c + \bar c\sigma + j^a_\mu A^a_\mu\right)\right), \end{aligned} \tag{2.7}$$

where

$$\mathcal{L}_{QCD,\xi} = \bar\psi\left(-\not{D} + m\right)\psi + \frac{1}{2}\mathrm{Tr}_c\left(F_{\mu\nu}F_{\mu\nu}\right) + \frac{1}{\xi}\mathrm{Tr}_c\left(\partial_\mu A_\mu \partial_\nu A_\nu\right) - i\partial_\mu\bar c D_\mu c\,. \tag{2.8}$$

The Grassmann valued ghost fields c and their conjugated $\bar c$, being in the adjoint representation of $SU(N_c)$, can be viewed as negative degrees of freedom, that cancel the ambiguous

[3] As remarked by Singer [51] this cannot be established by a global cross section, *i.e.* a local functional, for a non-Abelian gauge group, which leads *e.g.* to the problem of Gribov copies [52] in Landau gauge.

and therefore unphysical modes of the gauge freedom and implement the curvature of the gauge orbit. The ghost fields are taken to be real in order to get an hermitian Lagrangian. D_μ is a suitable covariant derivative. The gauge parameter ξ is freely adjustable and we will choose $\xi = 0$ constituting the Landau gauge. This enforces all configurations to fulfill $\partial_\mu A_\mu = 0$.

In the gauge fixed theory, the local symmetry is equivalently imposed by the remaining global symmetry and the BRST symmetry [53, 54]. This leads to a number of advantages when working in this framework. For vacuum studies it allows to formulate criterion and mechanisms to understand confinement and chiral symmetry breaking at least in fixed gauges in terms of originally gauge variant quantities [55, 56, 57]. For medium studies we can distinguish different phases in terms of originally gauge variant order parameters. These are then only meaningful in the gauge fixed theory. Nevertheless this is the only way to circumvent Elitzur's theorem [58], which states that no local gauge symmetry can be broken dynamically.

2.1.4 Renormalization

With the existence of a renormalized BRST algebra being proven [59], the theory given by the Lagrangian in Eq.(2.8) is multiplicative renormalizable. The renormalized Lagrangian is obtained by rescaling the local operators in the unrenormalized Lagrangian

$$\begin{aligned}\mathcal{L}_{QCD,\xi} &= Z_3 \frac{1}{2} A^a_\mu \left(-\partial^2 \delta_{\mu\nu} - \left(\frac{1}{Z_3 \xi} - 1 \right) \partial_\mu \partial_\nu \right) A^a_\nu + \tilde{Z}_3 \, \bar{c}^a \partial^2 c^a + Z_2 \, \bar{\psi} \left(-\not{\partial} + Z_m m \right) \psi \\ &\quad + \tilde{Z}_1 \, g f^{abc} \bar{c}^a \partial_\mu (A^c_\mu c^b) - Z_1 \, g f^{abc} (\partial_\mu A^a_\nu) A^b_\mu A^c_\nu - Z_{1F} \, i g \bar{\psi} \gamma_\mu \frac{\lambda^a}{2} \psi A^a_\mu \\ &\quad + Z_4 \frac{1}{4} g^2 f^{abe} f^{cde} A^a_\mu A^b_\nu A^c_\mu A^d_\nu \,. \end{aligned} \tag{2.9}$$

Focusing on the quark sector of the theory, the quark wave function (Z_2), the fermion mass (Z_m) and the quark-gluon vertex (Z_{1F}) renormalization constants will become of special interest. Note also that Landau gauge is a renormalization fix point, as $\partial_\mu A_\mu = 0$ is not affected by rescalation of the fields. Furthermore $\tilde{Z}_1 = 1$ has been suggested for Landau gauge [60].

As expected from the gauge symmetry of the classical Lagrangian, the (vertex-) renormalization constants of the interaction terms are constraint by gauge symmetry. Slavnov-Taylor identities (STIs) yield [61]

$$Z_1 = Z_g Z_3^{3/2} \,, \qquad \tilde{Z}_1 = Z_g Z_3^{1/2} \tilde{Z}_3 \,, \qquad Z_{1F} = Z_g Z_2 Z_3^{1/2} \,, \qquad Z_4 = Z_g^2 Z_3^2 \,, \tag{2.10}$$

with the coupling renormalization defined by $Z_g g = g_{bare}$.

The renormalization constants in the multiplicative renormalization procedure connect the renormalized expressions $G_i(\nu)$ only depending on a renormalization scale ν to the regularized expressions $G_{i,bare}(\Lambda)$ that depend on an artificially introduced cutoff Λ in the form

$$G_{i,bare}(\Lambda) \;=\; G_i(\nu) Z_i(\nu,\Lambda)\,. \tag{2.11}$$

From this we also conclude $Z(\nu_1,\nu_2)Z(\nu_2,\nu_3) = Z(\nu_1,\nu_3)$ for any ν_1,ν_2.

2.2 Dyson-Schwinger equations in the vacuum

2.2.1 A schematic introduction to DSEs

The hierarchy of Dyson-Schwinger equations for the fields gathered in ϕ is obtained as the set of Taylor coefficients, when expanding the identity

$$\begin{aligned}\left\langle \frac{\delta S}{\delta\phi} - J \right\rangle &\stackrel{\text{def}}{=} -\int \mathcal{D}[\phi]\, \frac{\delta}{\delta\phi} \exp\left(-S + \int d^4x\, J\cdot\phi\right) \\ &= \frac{\delta S}{\delta\phi}\left[\frac{\delta}{\delta J}\right] Z[J] - J Z[J] \\ &= 0 \end{aligned} \tag{2.12}$$

in the external sources J at $J=0$. Obviously this is the quantum analogue of the classical equation of motion $\frac{\delta S}{\delta\phi} = J$. With the n-th Taylor coefficient of $Z[J]$ giving the full n-point function, the latter are then explicitly coupled to higher n-point functions by the interaction terms hidden in $\frac{\delta S}{\delta\phi}$ and implicitly to any higher n-point function. The tower of equations forms a non-perturbative set of self-consistent equations, which are not amenable to a direct solution and which still leaves some indeterminacy [62]. The latter can be fixed by the boundary condition of recovering the free theory for asymptotically small coupling constants and it is possible to apply/recover perturbation theory to get a somewhat systematic solution for the n-point functions.

We will however choose a different strategy, as perturbation theory is not applicable in the strongly coupled regime of QCD and is not suited to explore non-perturbative ground states. Our strategy is to truncate the tower of DSEs and choose the needed higher n-point functions by educated guesses or as input from other investigations.

2.2.2 A truncated set of DSEs for QCD

As an introduction, we will now briefly discuss the structure of the DSEs for the QCD propagators in Landau gauge and how this system of equations can be truncated in order

to become closed. The untruncated set of equations is diagrammatically presented in the upper part of Fig. 2.1. Naturally the coupling to higher n-point functions emerges in form of 1-particle irreducible (1PI) functions (see Appendix C for an exemplary derivation), which will be labeled according to their external fields: c ($\bar{c}$) for (anti-) ghost, q ($\bar{q}$) for (anti-) quark and g for gluon fields. *E.g.* the quark-antiquark-gluon vertex will be labeled $q\bar{q}g$-vertex.

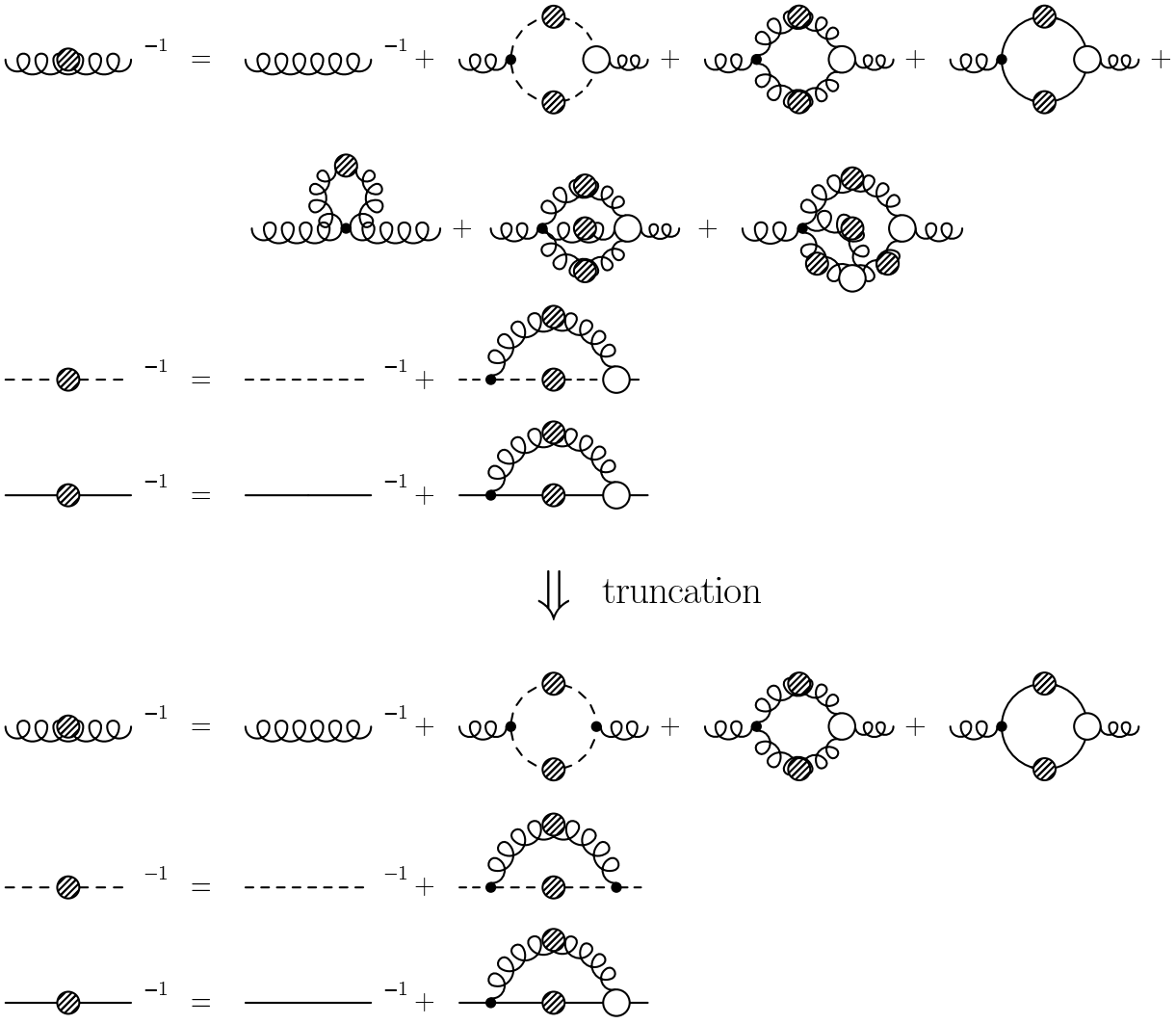

Figure 2.1: The coupled Dyson-Schwinger equations of gluon (curly line), ghost (dashed line) and quark propagator (solid line) in Landau gauge (top) and a suitable truncation (bottom). Shaded circles display connected n-point functions, empty circles 1PI functions. All signs and prefactors have been absorbed in the diagrams.

Considering the Yang-Mills sector, Landau gauge has a number of advantages: It is a renormalization fixed point, which simplifies the renormalization procedure considerably.

Due to this and since it is also covariant, the number of different self-energy contributions to the inverse propagators is comparatively small. Most importantly the $c\bar{c}g$-vertex is finite and is not subject to renormalization [60]. It has furthermore been suggested by Taylor, that it needs to correspond to the bare vertex for small ghost momentum. He therefore conjectured the $c\bar{c}g$-vertex to be only weakly dressed [60]. This has been confirmed by lattice simulations [63] and semi-perturbative DSE investigations [64]. As a consequence the $c\bar{c}g$-vertex can be taken bare in truncated investigations while still maintaining the correct infrared behavior.

Concentrating on the infrared regime first, the DSE for the ghost propagator is then closed on the level of the propagators. Furthermore imposing the Gribov horizon condition [52], which requires the fully dressed ghost propagator - compared to the free propagator - to be strongly enhanced in the infrared, suggests the ghost loop to dominate the gluon self-energy there. This feature allows a systematic study of ghost and gluon propagator in the infrared [65, 66, 67]. As the main result the gluon propagator turns out to be strongly suppressed for small momenta. Using the infrared enhancement of the ghost propagator and the suppression of the gluon propagator, the infrared behavior of all n-point functions in the Yang-Mills theory has been elaborated recently and the neglect of the gluonic contributions to the gluon self-energy in the infrared has been justified *a posteriori* [68]. By a combined analysis of DSEs and renormalization group equations it has in addition been shown that the Gribov horizon condition is required by self-consistency [69].

With respect to the ultraviolet behavior, the 2-loop contributions in the gluon self-energy are sub-leading. Therefore - and for practical reasons - they are neglected in virtually all truncations. The 1-loop gluon diagram is important for a proper ultraviolet behavior and the involved ggg-vertex is chosen to obtain leading order resummed-perturbation theory in the ultraviolet. A suitable choice for the $q\bar{q}g$-vertex is less definite and will be discussed in section 2.2.3.

Summarizing these considerations a reliable, closed and trackable truncation giving the correct infrared and ultraviolet behavior is shown in Fig. 2.1. For the actual solution of this closed set of equations, the gluon propagator $D_{\mu\nu}(p)$, the ghost propagator $D(p)$ and the quark propagator $S(p)$, being all constrained by Poincaré invariance and STIs, are fully parameterized in Landau gauge by

$$\begin{aligned} D_{\mu\nu}(p) &= \frac{Z(p)}{p^2}\left(\delta_{\mu\nu} - \frac{p_\mu p_\nu}{p^2}\right), \\ D(p) &= -\frac{G(p)}{p^2}, \\ S(p) &= \frac{1}{-i\not{p}A(p) + B(p)}, \end{aligned} \tag{2.13}$$

where $Z(p)$, $G(p)$, $A(p)$ and $B(p)$ are referred to as dressing functions and a momentum-subtraction (MOM) scheme is applied[4]. Often the parameterization

$$S(p) \;=\; \frac{Z_f(p)}{-i\not{p} + M(p^2)}\,, \tag{2.14}$$

with the wave function $Z_f(p) = 1/A(p)$ and the quark mass function $M(p) = B(p)/A(p)$ is more appropriate.

Being a continuum approach, DSEs are an interesting complement to first principle lattice calculations. Since they can be solved analytically in the infrared, it is possible to check conditions for confinement criteria as the Kugo-Ojima [70] or Gribov-Zwanziger scenario [56, 57], which are formulated in terms of the dressing functions $G(p)$ and $Z(p)$ for this regime. Furthermore positivity violations of correlators can be studied and in principle the equations can be extended to the complex plane. In the intermediate momentum regime, the approach is uncontrolled, but leads to reasonable agreement with lattice calculations for pure Yang-Mills theory [71, 72], but also for QCD [73, 74].

Apart from the pure Yang-Mills sector, also the confinement of quarks, the spontaneous chiral symmetry breaking and their interrelation are subject of ongoing investigations [75].

2.2.3 The DSE of the quark propagator

Having sketched the status of current investigations for the vacuum propagators in Landau gauge QCD, we will now turn to the DSE of the quark propagator (qDSE) in more detail. This is due to its major role in the forthcoming investigations, to expose the setup of actual calculations, to elucidate our renormalization procedure and to discuss the constraints and ideas for the construction of vertices needed in the calculations.

The renormalized qDSE (see Appendix C for details) in any covariant gauge with appropriate quark wave function renormalization constant Z_2 is then given by

$$S^{-1}(p;\nu) \;=\; Z_2(\nu,\Lambda)S_0^{-1}(p;\Lambda) + Z_2(\nu,\Lambda)\Sigma(p;\Lambda)\,. \tag{2.15}$$

Here

$$S_0^{-1}(p;\Lambda) \;=\; -i\not{p} + m_q(\nu)Z_m(\nu,\Lambda) \tag{2.16}$$

is the inverse bare quark propagator and $\Sigma(p;\Lambda)$ the unrenormalized quark self-energy, which can be parameterized by the vector self-energy $\Sigma_A(p;\Lambda)$ and the scalar self-energy $\Sigma_B(p;\Lambda)$ as

$$\Sigma(p;\Lambda) \;=\; -i\not{p}\Sigma_A(p;\Lambda) + \Sigma_B(p;\Lambda)\,. \tag{2.17}$$

[4]We suppress the dependence on the renormalization scale and refer to section 2.2.3 for a more elaborate discussion.

Furthermore the dependence on the renormalization scale ν and the regularization scale Λ is explicitly pointed out. Multiplicative renormalizibility connects the renormalized propagator $S(p;\nu)$ with the unrenormalized propagator $S(p;\Lambda) = S(p;\nu)Z_2(\nu,\Lambda)$ and automatically ensures the mass function $M(p)$ given in Eq.(2.14) to be independent of the renormalization scale. The self-energy is determined by

$$Z_2(\nu,\Lambda)\Sigma(p;\Lambda) \;=\; Z_{1F}(\nu,\Lambda)g(\nu)^2 \int^{\Lambda}\frac{d^4q}{(2\pi)^4}\,\gamma_\mu\frac{\lambda^a}{2}\,S(q;\nu)\Gamma^b_\nu(q,p;\nu)D^{ab}_{\mu\nu}(k;\nu)\,, \tag{2.18}$$

where we introduced the full $q\bar{q}g$-vertex $\Gamma^b_\nu(q,p;\nu)$ and $k = p-q$. In general it needs to be regularized, as symbolically indicated at the integral. We will adopt the MOM scheme to be consistent with investigations including the Yang-Mills sector [41] and which essentially implies an $O(4)$-regularization with a sharp cutoff Λ. However, as a further advantage of Landau gauge, the integral for the vector self-energy is always finite and for the scalar self-energy at least in the case $m_q = 0$. As a consequence, the regularization procedure will not break chiral Ward-Takahashi identities (see Appendix B.4) for renormalized quantities, although breaking translation symmetry.

The renormalization constants Z_2 and Z_m are determined by requiring

$$S^{-1}(p;\nu)\big|_{p^2=\nu^2} \;=\; -i\not{p} + m_q(\nu)\,. \tag{2.19}$$

From multiplicative renormalizibility we can infer immediately

$$Z_2(\nu_1,\nu_2) \;=\; \frac{1}{A(\nu_1,\nu_2)}\,. \tag{2.20}$$

Since the vector self-energy integral is finite in Landau gauge, the anomalous dimension of Z_2 is vanishing and we have $\lim_{\Lambda\to\infty} Z_2(\nu,\Lambda) = const.$. The behavior of the quark mass function at asymptotically large momenta is known from the operator product expansion [76], which yields

$$M(p) \;\simeq\; -\frac{4\pi\langle\bar{\psi}\psi\rangle_\nu}{3p^2}\frac{\alpha(\nu)^{\gamma_m}}{\alpha(p)^{\gamma_m-1}} + \frac{m_q(\Lambda)}{Z_m(\nu,\Lambda)}\left(\frac{\alpha(p)}{\alpha(\nu)}\right)^{\gamma_m}, \tag{2.21}$$

where the anomalous dimension of the mass function

$$\gamma_m \;=\; \frac{12}{11N_c - 2N_f} \tag{2.22}$$

and the leading order strong running coupling constant

$$\alpha(\nu) \;=\; \frac{\pi\gamma_m}{2\ln\left(\frac{\nu}{\Lambda_{QCD}}\right)} \tag{2.23}$$

have been used. The scale Λ_{QCD} inherits the value of the renormalized coupling at a given scale. The first term on the right-hand side of Eq.(2.21) corresponds to the so-called regular asymptotics, the second term to irregular asymptotics. For non-vanishing unrenormalized quark mass $m_q(\Lambda)$ we therefore find

$$Z_m(\nu_1,\nu_2) \;=\; \left(\frac{\alpha(\nu_2)}{\alpha(\nu_1)}\right)^{\gamma_m} \tag{2.24}$$

for large ν_1, ν_2. In the chiral limit, *i.e.* for $m_q(\Lambda)=0$, a non-vanishing quark mass function spontaneously breaks chiral symmetry and is therefore connected to the order parameter of this symmetry, the chiral condensate $\langle\bar\psi\psi\rangle_\nu := \langle\bar\psi(x)\psi(x)\rangle$. It will be discussed in more detail in section 5.1.2.

The same ultraviolet asymptotics should of course be obtained within the framework of the qDSE as has been clarified by Miransky [77]. This will be a constraint on the construction of the $q\bar qg$-vertex, which is considered the mayor unknown ingredient, as the gluon propagator is sufficiently known and only parameterized by a single function. We require

- multiplicative renormalizibility and therefore a renormalization scale independent mass function $M(p)$,
- the proper anomalous dimension γ_m of the mass function known from resummed-perturbation theory at large momenta.

Considering multiplicative renormalizibility, we have $\tilde Z_1 = 1$ in Landau gauge and therefore

$$\begin{aligned} Z_{1F}(\nu,\Lambda) &= \frac{Z_2(\nu,\Lambda)}{\tilde Z_3(\nu,\Lambda)}\,, \\ 1 &= Z_g(\nu,\Lambda) Z_3(\nu,\Lambda)^{\frac12}\tilde Z_3(\nu,\Lambda)\,. \end{aligned} \tag{2.25}$$

From this we conclude

$$\Sigma(p;\Lambda) \;=\; \frac{\tilde Z_3(\nu,\Lambda)}{Z_2(\nu,\Lambda)}\, g(\Lambda)^2 \int\frac{d^4q}{(2\pi)^4}\,\gamma_\mu\frac{\lambda^a}{2}\,S(q;\Lambda)\Gamma^b_\nu(q,p;\nu)D^{ab}_{\mu\nu}(k;\Lambda)\,, \tag{2.26}$$

leading to

$$\Gamma^a_\mu(q,p;\nu) \;=\; \frac{Z_2(\nu,\Lambda)}{\tilde Z_3(\nu,\Lambda)}\,\Gamma^a_\mu(q,p;\Lambda)\,. \tag{2.27}$$

For the proper anomalous dimension γ_m, the vertex must have the following asymptotic running

$$\frac{1}{Z_2(\nu,\Lambda)\tilde Z_3(\nu,\Lambda)}\frac{g(\nu)^2}{4\pi}\,Z(k;\nu)\,\Gamma^a_\mu(q,q+k;\nu) \;\simeq\; \alpha(k)\,\gamma_\mu\,\frac{\lambda^a}{2}\,. \tag{2.28}$$

The analysis is similar to the one presented in section 2.4.1 for the anomalous dimension of the gap function in a color-superconductor.

We will therefore adopt the approximation[5] used in [41], effectively given by

$$\Gamma^a_\mu(q,p;\nu) \;=\; \frac{\tilde{Z}_3(\nu,\Lambda)}{\alpha_s(\nu)}\,\frac{\alpha_s(k)}{Z(k;\nu)}\,V_\mu(q,p;\nu)\,\frac{\lambda^a}{2}\,, \tag{2.29}$$

with $\alpha_s(\nu) = \frac{g(\nu)^2}{4\pi}$ being the strong running coupling constant defined by the scaling of the $c\bar{c}g$-vertex. The vertex-function $V_\mu(p,q;\nu)$ is taken as an Abelian vertex construction fulfilling the QED Ward-Takahashi identity of the vertex. Putting the pieces together we arrive at

$$Z_2(\nu,\Lambda)\Sigma(p;\Lambda) \;=\; 4\pi Z_2(\nu,\Lambda)\int^\Lambda\!\frac{d^4q}{(2\pi)^4}\,\gamma_\mu\frac{\lambda^a}{2}\,S(q;\nu)V_\nu(q,p;\nu)\frac{\lambda^a}{2}\frac{\alpha_s(k)}{k^2}T_{\mu\nu}(k) \tag{2.30}$$

for the truncated self-energy that is solely determined by the quark propagator and the function $\alpha_s(k)$.

This approximation is motivated by the Slavnov-Taylor identity (STI) of the $q\bar{q}g$-vertex [61]

$$-ig(\nu)G^{-1}(k;\nu)k_\mu\Gamma^a_\mu(q,p;\nu) \;=\; H^a(k,q;\nu)S^{-1}(p;\nu) - S^{-1}(q;\nu)H^a(k,q;\nu)\,, \tag{2.31}$$

where $H^a(k,q)$ is the ghost-gluon scattering kernel $g\left\langle c(x)\bar{c}(z)\psi(y)\bar{\psi}(x)\frac{\lambda^a}{2}\right\rangle$ in momentum space, where the external ghost and quark propagator is amputated. As $H^a(k,q)$ is largely unknown in the strongly coupled regime, with some constraints given in [75, 78], it is assumed to be of the form $H^a(k,q;\nu) \propto f(k)\frac{\lambda^a}{2}$ with a real function $f(k)$ being determined by Eq.(2.29). The upper STI then has a similar form as the WTI in an Abelian theory

$$-ig(\nu)k_\mu\Gamma_\mu(p,q;\nu) \;=\; S^{-1}(p;\nu) - S^{-1}(q;\nu)\,, \tag{2.32}$$

which has been used by Ball and Chiu [79] to constrain/construct transversal parts of the fermion-photon vertex and furthermore by Curtis and Pennington [80], who in addition implemented multiplicative renormalizibility for arbitrary covariant gauges. The construction is generalized to the medium and color-superconducting phases in section 5.3.2.

In the first part of this work, we will however use

$$V_\mu(p,q;\nu) \;=\; \gamma_\mu Z_2(\nu,\Lambda) \tag{2.33}$$

and investigate the sensitivity of our results under the variation of $\alpha_s(k)$. To consider two opposite extremes in the medium, we will use

[5] A class of similar couplings with the correct asymptotic running has been discussed in [41], which give a truncated quark self-energy that depends on the quark propagator and a real function $\alpha_s(k)$ of the gluon momenta only.

- $\alpha_I(k)$ corresponding to the strong running coupling constant determined in the Yang-Mills sector [41], which underestimates chiral symmetry breaking significantly for this approximation;
- $\alpha_{II}(k)$ corresponding to a fit to lattice QCD data for the quark mass function under the assumption of this vertex. We extend the parameterization given in [81] to vary the renormalization point under the constraint of multiplicative renormalizibility.

The parameterization of both couplings is given in Appendix D. Together with the quark mass function in the chiral limit, they are shown in Fig. 2.2 for illustration.

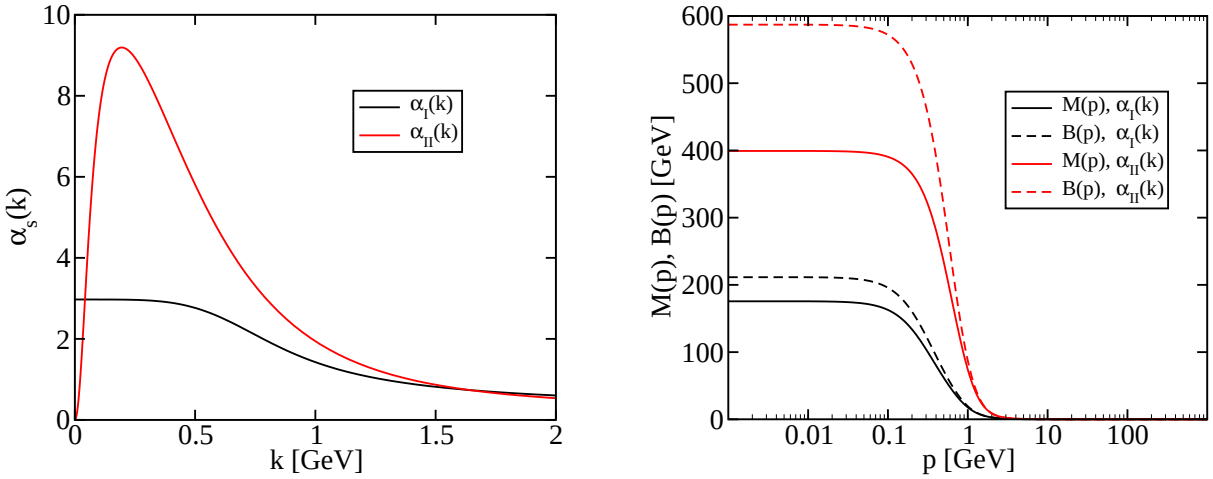

Figure 2.2: Left: Two versions of the strong running coupling used in the numerical solution of the qDSE. The black line represents the coupling $\alpha_I(k^2)$ and the red line $\alpha_{II}(k^2)$. Right: Mass function $M(p)$ (solid) and scalar dressing function $B(p)$ at a renormalization point of $\nu = 2\,\mathrm{GeV}$ (dashed) for the coupling $\alpha_I(k^2)$ (black) and $\alpha_{II}(k^2)$ (red).

We conclude this section with some remark: We have suppressed the flavor dependence of the renormalization constants as the different quarks in the vacuum decouple in our approximation. As the flavor/mass dependence of Z_2 is negligible, we will always use Z_2 obtained in the chiral limit for Eq.(2.33). Secondly we will drop the explicit dependence on the renormalization scale ν and the regularization Λ from now on.

2.3 Dyson-Schwinger equations in the medium

2.3.1 Imaginary time and Nambu-Gor'kov formalism

Having sketched investigations of QCD correlators in the vacuum, we will now turn to thermostatics, which is naturally formulated in imaginary time, that is to say Euclidean space.

In a grand canonical formalism, temperature and non-vanishing charges are introduced in the generating functional by setting

$$S_{QCD}[\psi,\bar{\psi},A] \;=\; \int_0^\beta d\tau \int d^3x \left(\mathcal{L}_{QCD}[\psi,\bar{\psi},A] + \sum_i \mu_i\rho_i\right), \tag{2.34}$$

where $\beta = \frac{1}{T}$ is the inverse temperature, τ is the imaginary time and μ_i the chemical potential that is conjugated to a charge Q_i with density ρ_i. After gauge fixing $\mathcal{L}_{QCD}$ is replaced by $\mathcal{L}_{QCD,\xi}$ from Eq.(2.8). According to the Kugo-Martin-Schwinger relation, quark fields need to obey anti-periodic boundary conditions, whereas gluon and ghost fields periodic boundary conditions. In momentum space, finite temperature is reflected in the Matsubara sum and the boundary condition in the Matsubara frequencies. As we will restrict ourself to the case of vanishing temperatures, the Matsubara sum reduces to the usual energy integration $\frac{1}{\beta}\sum_i \to \int\frac{dq_4}{2\pi}$.

In order to investigate color-superconducting phases and to allow for dynamical symmetry breaking by diquark condensation, the Nambu-Gor'kov [82, 83] formalism is appropriate. Using the charge-conjugation matrix of Dirac spinors, $C = \gamma_2\gamma_4$, we define the $8N_cN_f$-dimensional bispinors Ψ and their conjugate $\bar{\Psi}$ as

$$\Psi = \frac{1}{\sqrt{2}}\begin{pmatrix}\psi\\ \psi_C = C\bar{\psi}^T\end{pmatrix}, \quad \bar{\Psi} = \frac{1}{\sqrt{2}}\left(\bar{\psi}, \bar{\psi}_C = \psi^T C\right). \tag{2.35}$$

With the definition of

$$\mathcal{C} \;=\; \begin{pmatrix}0 & C\\ C & 0\end{pmatrix}, \tag{2.36}$$

they possess the important property

$$\Psi = \mathcal{C}\bar{\Psi}^T, \quad \bar{\Psi} = \Psi^T\mathcal{C}. \tag{2.37}$$

In addition we have

$$\Psi = \begin{pmatrix}\gamma_4 & 0\\ 0 & \gamma_4\end{pmatrix}\bar{\Psi}^\dagger, \quad \bar{\Psi} = \Psi^\dagger\begin{pmatrix}\gamma_4 & 0\\ 0 & \gamma_4\end{pmatrix}. \tag{2.38}$$

As the charge densities corresponding to global symmetries (see Eq.(2.4) for conserved vector currents) can be written as

$$\sum_i \mu_i\rho_i \;=\; \psi^\dagger\mu\psi, \tag{2.39}$$

with a matrix $\mu = \sum_i \mu_i T^i$ and generators T^i, we can express the integrand of the action as

$$\mathcal{L}_{QCD}\big[\psi,\bar{\psi},A\big] + \sum_i \mu_i \rho_i \;=\; \bar{\Psi}\begin{pmatrix} -\not{D} + m + \gamma_4\mu & 0 \\ 0 & -\not{D}_C + m - \gamma_4\mu^T \end{pmatrix}\Psi + \frac{1}{4}F^a_{\mu\nu}F^a_{\mu\nu}\,, \tag{2.40}$$

where $D_{C\mu} = \partial_\mu - igA^T_\mu$ corresponds to the charge-conjugate of the covariant derivative $D_\mu = \partial_\mu + igA_\mu$.

We can also consider the Nambu-Gor'kov spinor Ψ as the underlying degree of freedom, when defining $\tilde{\mathcal{D}}\big[\Psi\bar{\Psi}\big] \stackrel{\text{def}}{=} \mathcal{D}\big[\psi\bar{\psi}\big]$. However in order to avoid a double counting in the path integral, we need to identify Ψ and its conjugate $\mathcal{C}\Psi$ in the measure[6]. Diagrammatic representations are then similar to the ordinary theory, only that closed fermion loops introduce an additional factor of $-\frac{1}{2}$ instead of -1.

2.3.2 qDSE and color neutrality at non-vanishing chemical potential

The qDSE in the Nambu-Gor'kov formalism can be derived as in the vacuum (see Appendix C). It is then given by

$$\mathcal{S}^{-1}(p) \;=\; Z_2\mathcal{S}_0^{-1}(p) + Z_2\Sigma(p), \tag{2.41}$$

where now

$$\mathcal{S}_0^{-1}(p) \;= \begin{pmatrix} -i\vec{p}\cdot\vec{\gamma} - i(p_4 + i\mu + \frac{Z_{1F}}{Z_2}gA_4)\gamma_4 + m & 0 \\ 0 & -i\vec{p}\cdot\vec{\gamma} - i(p_4 - i\mu - \frac{Z_{1F}}{Z_2}gA_4^T)\gamma_4 + m \end{pmatrix} \tag{2.42}$$

is the inverse bare quark propagator in the presence of a static, isotropic and homogeneous gluon field with time component A_4. The latter can not be ruled out, as Lorentz symmetry is broken in the medium[7]. The renormalization scale independent quark self-energy $\Sigma(p)$, which is finite in Landau gauge, is given by

$$Z_2\Sigma(p) \;=\; Z_{1F}g^2\int\frac{d^4q}{(2\pi)^4}\,\Gamma^{(0)a}_{NG,\mu}\mathcal{S}(q)\Gamma^b_{NG,\nu}(q,p)D^{ab}_{\mu\nu}(k). \tag{2.43}$$

[6] In momentum space representation those are simply field configurations with opposite momenta, as $\psi_C(\vec{k}) = C\bar{\psi}(-\vec{k})^T$.

[7] More formally speaking, the heat bath/medium defines a reference frame.

Here $D^{ab}_{\mu\nu}(k)$ is the gluon propagator in the medium, furthermore the bare and full $q\bar{q}g$-vertex

$$\begin{aligned}\Gamma^{(0)a}_{NG\mu} &= \frac{1}{2}\begin{pmatrix}\gamma_\mu\lambda^a & 0\\ 0 & -\gamma_\mu\lambda^{aT}\end{pmatrix},\\ \Gamma^a_{NG\mu}(q,p) &= \frac{1}{2}\begin{pmatrix}\Gamma^{+,a}_\mu(q,p) & \Delta^{-,a}_\mu(q,p)\\ \Delta^{+,a}_\mu(q,p) & \Gamma^{-,a}_\mu(q,p)\end{pmatrix}\end{aligned} \tag{2.44}$$

have the shown components in Nambu-Gor'kov space. Flavor indices have been suppressed for the sake of clarity.

We will parameterize the propagator and self-energy in Nambu-Gor'kov space by

$$\begin{aligned}\mathcal{S}_0(p) &= \begin{pmatrix}S^+_0(p) & 0\\ 0 & S^-_0(p)\end{pmatrix},\\ \mathcal{S}(p) &= \begin{pmatrix}S^+(p) & T^-(p)\\ T^+(p) & S^-(p)\end{pmatrix},\\ \Sigma(p) &= \begin{pmatrix}\Sigma^+(p) & \Phi^-(p)\\ \Phi^+(p) & \Sigma^-(p)\end{pmatrix}\end{aligned} \tag{2.45}$$

and obtain by inverting Eq.(2.41) [84]

$$\begin{aligned}T^\pm &= -\left(S_0^{\mp\,-1}+\Sigma^\mp\right)^{-1}\Phi^\pm S^\pm,\\ S^{\pm\,-1} &= Z_2\left(S_0^{\pm\,-1}+\Sigma^\pm-\Phi^\mp\left(S_0^{\mp\,-1}+\Sigma^\mp\right)^{-1}\Phi^\pm\right)\end{aligned} \tag{2.46}$$

for the normal propagators $S^\pm$ and the anomalous propagators $T^\pm$.

The expectation value of A_4 in a covariant gauge is determined by its DSE, *i.e.* by its equation of motion (see Eq.(2.12)). In a covariant gauge this corresponds to a vanishing expectation value of

$$\begin{aligned}\left\langle\frac{\delta S_{QCD}[\psi,\bar\psi,A]}{\delta A^a_4(x)}\right\rangle &= \Big\langle -\left(Z_1\partial_\nu\delta^{ab}+Z_4 g f^{abc}A^c_\nu(x)\right)F^b_{\nu4}(x) - i\tilde{Z}_1 g f^{abc}\left(\partial_4\bar{c}_b(x)\right)c_c(x)\\ &\quad -\frac{Z_3}{Z_\xi\xi}\partial_4\partial_\nu A^a_\nu(x) - iZ_{1F}\frac{g}{2}\bar\Psi(x)\Gamma^{(0)a}_{NG4}\Psi(x)\Big\rangle\\ &= 0\,.\end{aligned} \tag{2.47}$$

Expectation values involving one field always come along with a derivative and therefore vanish in an isotropic and homogenous phase. Also using the anti-symmetry of $F^a_{\mu\nu}(x)$, we

only need to consider

$$\left\langle \frac{\delta S_{QCD}[\psi,\bar{\psi},A]}{\delta A_4^a(x)} \right\rangle = \Big\langle - Z_4 g f^{abc} A_i^c(x) F_{i4}^b(x) - i\tilde{Z}_1 g f^{abc} \left(\partial_4 \bar{c}_b(x)\right) c_c(x) - i Z_{1F} \frac{g}{2} \bar{\Psi}(x) \Gamma_{NG4}^{(0)a} \Psi(x) \Big\rangle , \quad (2.48)$$

where i sums over space indices. As A_i^a changes sign under time-reversal, whereas $F_{i4}^a(x)$ - being the chromo-electrical field - does not, we are left with

$$\left\langle \frac{\delta S_{QCD}[\psi,\bar{\psi},A]}{\delta A_4^a(x)} \right\rangle = \Big\langle - i\tilde{Z}_1 g f^{abc} \left(\partial_4 \bar{c}_b(x)\right) c_c(x) - i Z_{1F} \frac{g}{2} \bar{\Psi}(x) \Gamma_{NG4}^{(0)a} \Psi(x) \Big\rangle \quad (2.49)$$

in a T-symmetric phase. For the remaining terms we need to take care of normal-ordering to get a meaningful result. As the ghost propagator is real (as the ghost fields) and symmetric, the DSE of A_4 in an homogenous, isotropic and T-symmetric phase is given by

$$\rho^a(x) \stackrel{\text{def}}{=} \frac{Z_2}{2} \Big\langle : \bar{\Psi}(x) \Gamma_{NG4}^{(0)a} \Psi(x) : \Big\rangle = 0 , \quad (2.50)$$

with the colons, which are usually suppressed, explicitly indicating the normal-ordering. Therefore the static gluon fields A_4 ensure color neutrality ($\rho^a(x) = 0$) and can be implicitly determined by this condition [85, 86, 87].

To determine the normal-ordered expectation value, we consider the (real) time-ordered propagator

$$S_F(x,y) = \langle T \Psi(x) \bar{\Psi}(y) \rangle \quad (2.51)$$

in the limit

$$\begin{aligned} \lim_{y_0 \to x_0 + \epsilon} \frac{1}{2} \mathrm{Tr}_{D,c,f,NG} \left(S_F(x,y) \Gamma_{NG4}^{(0)a} \right) &= \frac{1}{2} \int \frac{d^3p}{(2\pi)^3} \int_C \frac{dp_0}{2\pi} \mathrm{Tr}_{D,c,f,NG} \left(S_F(p) \Gamma_{NG4}^{(0)a} \right) e^{ip\cdot(x-y)} \\ &= \Big\langle \bar{\Psi}(x_0,\vec{x}) \Gamma_{NG4}^{(0)a} \Psi(x_0,\vec{y}) \Big\rangle , \end{aligned} \quad (2.52)$$

where $\epsilon > 0$, which is implemented in the contour C of the energy integral. The latter goes along the real axis and closes as a asymptotically large semicircle in the lower complex plane. By this procedure, particle operators become normal-ordered and anti-particle operators anti-normal ordered. Bringing the anti-particle operators into a normal ordered form introduces an additional constant from the (anti-)commutation relation. This is however exactly canceled by the contribution from the semicircle in the lower complex plane (this is a similar argument as will be used to obtain sum rules for spectral functions in section 4.2). We can therefore safely take the limit $\vec{y} \to \vec{x}$ and obtain

$$\rho^a(x) = \frac{Z_2}{2} \int \frac{d^3p}{(2\pi)^3} \int \frac{dp_4}{2\pi} \mathrm{Tr}_{D,c,f,NG} \left(\mathcal{S}(p) \Gamma_{NG4}^{(0)a} \right) , \quad (2.53)$$

where we furthermore performed a Wick rotation to Euclidean energies. It is important to perform the energy integration first to get a finite result, although later it is not always clearly indicated.

2.3.3 Symmetry constraints on the Nambu-Gor'kov propagator

The quark propagator in the Nambu-Gor'kov formalism and also the $q\bar{q}g$-vertex carry $8N_cN_f$-components for each bispinor. It is therefore highly desirable to reduce the complexity with help of internal symmetries in order to make the solution of the qDSE trackable. By the use of the internal symmetries in Nambu-Gor'kov space it will turn out, that we can solely constrain ourself on S^+, T^+, Σ^+, Φ^+, Γ^+ and Δ^+ for positive Matsubara frequencies. The remnants of Poincaré invariance and global symmetries in a given phase will later in addition be used to constrain the parameterization of the most general set of solution.

Relations between Nambu-Gor'kov components: From the internal symmetry in Nambu-Gor'kov space given in Eq.(2.37), we obtain in coordinate space

$$\mathcal{S}(x,y) \;=\; -\mathcal{C}\mathcal{S}(y,x)^T\mathcal{C}\,, \tag{2.54}$$

which gives for an homogeneous phase in momentum space

$$\mathcal{S}(p) \;=\; -\mathcal{C}\mathcal{S}(-p)^T\mathcal{C}\,, \tag{2.55}$$

leading to

$$\begin{aligned} S^{\pm}(p) &= -CS^{\mp}(-p)^TC\,, \\ T^{\pm}(p) &= -CT^{\pm}(-p)^TC\,. \end{aligned} \tag{2.56}$$

As it is also true for the inverse propagator, we also obtain

$$\begin{aligned} \Sigma^{\pm}(p) &= -C\Sigma^{\mp}(-p)^TC\,, \\ \Phi^{\pm}(p) &= -C\Phi^{\pm}(-p)^TC\,. \end{aligned} \tag{2.57}$$

Similarly, the components of the full $q\bar{q}g$-vertex (see Appendix B for the conventions of the Fourier transformation) in Nambu-Gor'kov space are connected, as $\Gamma^{\pm,a}_{\mu}(q,p) = -C\Gamma^{\mp,a}_{\mu}(-p,-q)^TC$ and $\Delta^{\pm,a}_{\mu}(q,p) = -C\Delta^{\pm,a}_{\mu}(-p,-q)^TC$.

Imaginary time-ordering: As the path integral gives by construction imaginary time-ordered expectation values of an operator, the conjugate of an expectation value corresponds to the anti-time-ordered expectation value of the conjugate operator. From Eq.(2.38) we then get

$$\mathcal{S}_A(x,y) = \begin{pmatrix} \gamma_4 & 0 \\ 0 & \gamma_4 \end{pmatrix} \mathcal{S}(y,x)^\dagger \begin{pmatrix} \gamma_4 & 0 \\ 0 & \gamma_4 \end{pmatrix}, \tag{2.58}$$

where the subscript A denotes the unconventional time-ordering. Therefore we have

$$\mathcal{S}(p_4,\vec{p}) = \begin{pmatrix} \gamma_4 & 0 \\ 0 & \gamma_4 \end{pmatrix} \mathcal{S}(-p_4,\vec{p})^\dagger \begin{pmatrix} \gamma_4 & 0 \\ 0 & \gamma_4 \end{pmatrix}, \tag{2.59}$$

or in components

$$\begin{aligned} S^\pm(p_4,\vec{p}) &= \gamma_4 S^\pm(-p_4,\vec{p})^\dagger \gamma_4 \,, \\ T^\pm(p_4,\vec{p}) &= \gamma_4 T^\mp(-p_4,\vec{p})^\dagger \gamma_4 \,. \end{aligned} \tag{2.60}$$

These results follow also from the spectral representation of the propagator, as the spectral function is hermitian. Since ψ and $\bar{\psi}_C$ are anti-commuting, we furthermore get $T_A^\pm(x,y) = T^\pm(x,y)$ and therefore

$$T^\pm(p) = \gamma_4 T^\mp(p)^\dagger \gamma_4 \,. \tag{2.61}$$

With help of the qDSE we then get the substantial equalities

$$\begin{aligned} \Sigma^\pm(p_4,\vec{p}) &= \gamma_4 \Sigma^\pm(-p_4,\vec{p})^\dagger \gamma_4 \,, \\ \Phi^\pm(p_4,\vec{p}) &= \gamma_4 \Phi^\mp(-p_4,\vec{p})^\dagger \gamma_4 \\ &= \gamma_4 \Phi^\mp(+p_4,\vec{p})^\dagger \gamma_4 \,. \end{aligned} \tag{2.62}$$

Discrete Poincaré symmetries: In equilibrium we will furthermore impose time reversal invariance, which requires[8]

$$\mathcal{S}_T(p) = \begin{pmatrix} T & 0 \\ 0 & T \end{pmatrix} \mathcal{S}(-p)^* \begin{pmatrix} T & 0 \\ 0 & T \end{pmatrix}^\dagger, \tag{2.63}$$

Subsequently we have

$$\begin{aligned} S_T^\pm(p) &= T S^\pm(-p)^* T \,, \\ T_T^\pm(p) &= T T^\pm(-p)^* T \end{aligned} \tag{2.64}$$

[8]The derivation is an extention of the findings in [88].

and therefore

$$\begin{aligned} \Sigma_T^{\pm}(p) &= T\Sigma^{\pm}(-p)^* T\,, \\ \Phi_T^{\pm}(p) &= T\Phi^{\pm}(-p)^* T\,. \end{aligned} \tag{2.65}$$

We will also demand invariance under parity transformation, where a spinor in coordinate space transforms like $\psi_P(t,\vec{x}) = \eta_P\gamma_4\psi(t,-\vec{x})$ with $\eta_P = +1$ being intrinsic parity. From this, we get $\bar{\psi}_{CP}(t,\vec{x}) = -\bar{\psi}_C(t,-\vec{x})\gamma_4\eta_P$ and conclude

$$\mathcal{S}_P(p_4,\vec{p}) = \begin{pmatrix} \gamma_4 & 0 \\ 0 & -\gamma_4 \end{pmatrix} \mathcal{S}(p_4,-\vec{p}) \begin{pmatrix} \gamma_4 & 0 \\ 0 & -\gamma_4 \end{pmatrix}. \tag{2.66}$$

We therefore have

$$\begin{aligned} S_P^{\pm}(p_4,\vec{p}) &= \gamma_4 S^{\pm}(p_4,-\vec{p})\gamma_4\,, \\ T_P^{\pm}(p_4,\vec{p}) &= -\gamma_4 T^{\pm}(p_4,-\vec{p})\gamma_4 \end{aligned} \tag{2.67}$$

and

$$\begin{aligned} \Sigma_P^{\pm}(p_4,\vec{p}) &= \gamma_4 \Sigma^{\pm}(p_4,-\vec{p})\gamma_4\,, \\ \Phi_P^{\pm}(p_4,\vec{p}) &= -\gamma_4 \Phi^{\pm}(p_4,-\vec{p})\gamma_4\,. \end{aligned} \tag{2.68}$$

Internal symmetries: Apart from the symmetries in Nambu-Gor'kov space and the remnants of Poincaré invariance, global symmetries can give strong constraints on allowed solutions. Considering (direct products of) global $SU(N)$ symmetries, *i.e.* quarks forming a representation of $SU(N)$ such that $\psi' = U\psi$ for $U \in SU(N)$, we have

$$\Psi' = \mathcal{U}\Psi, \quad \bar{\Psi}' = \bar{\Psi}\,\gamma_4\mathcal{U}^{\dagger}\gamma_4\,, \tag{2.69}$$

with

$$\mathcal{U} = \begin{pmatrix} U & 0 \\ 0 & \gamma_4 C^{-1} U^* C \gamma_4 \end{pmatrix}. \tag{2.70}$$

With the group action on $\mathcal{S}\gamma_4$ then given by conjugation, an invariant propagator fulfills

$$[\mathcal{S}\gamma_4, \mathcal{T}] = 0\,, \tag{2.71}$$

with $\mathcal{T}$ being in the corresponding representation of the Lie algebra. For vector symmetries, where

$$\mathcal{T} = \begin{pmatrix} T & 0 \\ 0 & -T^T \end{pmatrix} \tag{2.72}$$

and $T \in \mathfrak{su}(N)$ only acting in color-flavor space, we then find

$$\left[S^+, T\right] = 0, \qquad T^T T^+ + T^+ T = 0 \tag{2.73}$$

and similar expressions for S^- and T^-. For axial symmetries, where

$$\mathcal{T} \;=\; \begin{pmatrix} \gamma_5 T & 0 \\ 0 & \gamma_5 T^T \end{pmatrix}, \tag{2.74}$$

we find

$$\gamma_5 T S^+ + S^+ T \gamma_5 = 0, \qquad \gamma_5 T^T T^+ + T^+ T \gamma_5 = 0 \tag{2.75}$$

and similar expressions for S^- and T^-.

2.3.4 A setup for truncations of the qDSE in the medium

It is, of course, expected that the gluon propagator and the $q\bar{q}g$-vertex undergo modifications when a non-vanishing chemical potential is introduced and/or the ground state changes. We are therefore concentrating on a truncation scheme that extends the qDSE to finite densities, such that weak-coupling investigations in the Hard-Dense-Loop (HDL) resummation scheme [89, 90] at leading order are reproduced at asymptotically large chemical potentials.

A suited truncation scheme is shown in Fig. 2.3: The medium polarization of the gluon self-energy is properly considered, which then enables to include Debye screening, Landau damping, the Meissner effect and other attributes in corresponding phases. However, we will neglect the medium modification in the Yang-Mills sector. On the one hand side this is for practical reasons, as we are aiming at a closed and also trackable set of equations. On the other hand it will become obvious in the following, that only the product of the dressing function of the gluon $Z(k^2)$ and our $q\bar{q}g$-vertex construction Γ^a_μ will be of relevance. As the product used in the vacuum investigations is essentially an effective running coupling, it agrees with the leading order HDL resummation scheme. Our truncation seems therefore trustworthy even when the infrared behavior of the Yang-Mills sector is significantly varying the gluon propagator and $q\bar{q}g$-vertex, but not their product.

The renormalized medium polarization tensor is generically given by

$$\Pi^{\mathrm{med}\,ab}_{\mu\nu}(k) \;=\; -Z_{1F}\, 2\pi\, \alpha_s(\nu) \int \frac{d^4p}{(2\pi)^4} \mathrm{Tr}_{D,c,f,NG} \Bigg(\Big[\Gamma^{(0)a}_{NG\mu} \mathcal{S}(p) \Gamma^b_{NG\nu}(p,q) \mathcal{S}(q) \Big] - \Big[\dots \Big]_{\mu=0} \Bigg), \tag{2.76}$$

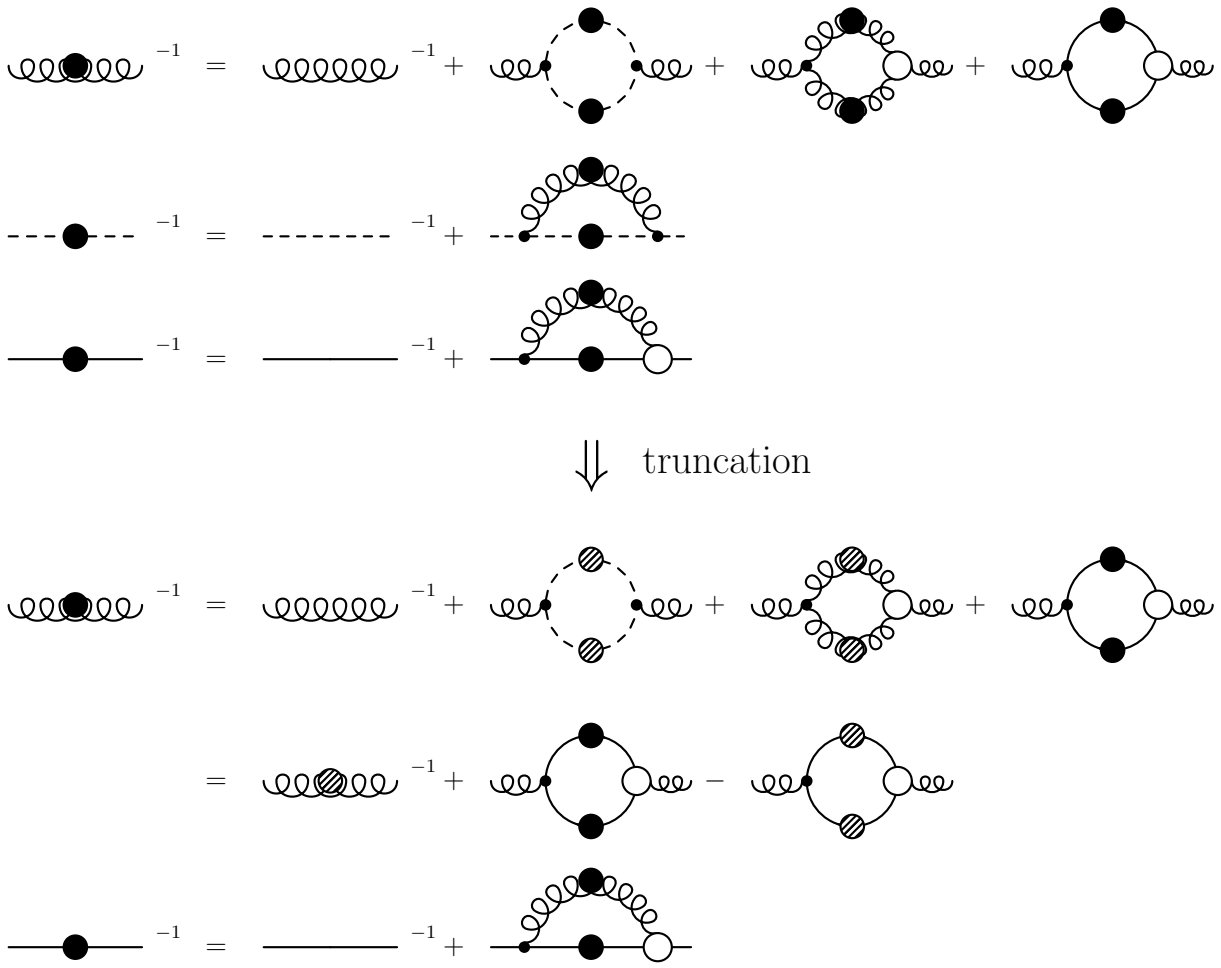

Figure 2.3: The coupled truncated Dyson-Schwinger equations of gluon (curly line), ghost (dashed line) and quark propagator (solid line) in Landau gauge (top) and a suitable truncation (bottom) in the medium. Full circles display connected n-point functions in the medium, shaded circles n-point functions in the vacuum, empty circles 1PI functions. All signs and prefactors have been absorbed in the diagrams.

where $q = p - k$. Due to gauge invariance, the medium polarization is constraint by

$$k_\mu \Pi^{\text{med}\,ab}_{\mu\nu}(k) k_\nu \;=\; 0 \tag{2.77}$$

in linear gauges [91]. In Landau gauge it even needs to fulfill

$$\Pi^{\text{med}\,ab}_{\mu\nu}(k) k_\nu \;=\; 0 \tag{2.78}$$

as can be seen by the BRST transformation of $\langle T_\tau \bar{c}(x) A(y) \rangle$ (see *e.g.* [91]). It is also interesting to note, that the dependence of the order parameter in color-superconducting

phases on the gauge parameter ξ has been investigated in the weakly coupled regime [92] and is has been argued in [93] that Landau gauge is most reliable. As in the vacuum, Landau gauge offers the most advantages and we will use it in the following.

The medium polarization tensor in Landau gauge can therefore by expressed with help of the so-called transverse and longitudinal projectors

$$P_{44}^T(k) = P_{i4}^T(k) = P_{4i}^T(k) = 0\,, \quad P_{ij}^T(k) = \delta_{ij} - \frac{k_i k_j}{\vec{k}^2} \tag{2.79}$$

and

$$P_{\mu\nu}^L(k) \;=\; \left(\delta_{\mu\nu} - \frac{k_\mu k_\nu}{k^2}\right) - P_{\mu\nu}^T(k)\,, \tag{2.80}$$

respectively, in the form

$$Z(k^2)\Pi^{\mathrm{med}\,ab}_{\mu\nu}(k) \;=\; \Pi_T^{ab}(k)P_{\mu\nu}^T(k) + \Pi_L^{ab}(k)P_{\mu\nu}^L(k)\,. \tag{2.81}$$

Adding the medium polarization to the inverse gluon propagator in the vacuum leads to the approximation

$$\begin{aligned} D_{\mu\nu}^{ab}(k) &\approx \left(D_{\mu\nu}^{vac\,-1}(k) + \Pi^{\mathrm{med}\,ab}_{\mu\nu}(k)\right)^{-1} \\ &= Z(k^2)\left(\left(\delta^{ab}k^2 + \Pi_T^{ab}(k)\right)^{-1} P_{\mu\nu}^T(k) + \left(\delta^{ab}k^2 + \Pi_L^{ab}(k)\right)^{-1} P_{\mu\nu}^L(k)\right)\,. \end{aligned} \tag{2.82}$$

This expression will be used in the qDSE when investigating color-superconducting phases.

2.4 Relevant properties and quantities

2.4.1 Ultraviolet finiteness of the gap functions

Similar to the ultraviolet analysis of the quark mass function in the chirally broken phase [77] we determine here the ultraviolet behavior of the gap functions. For large external momenta p, such that $\phi^2(p) \ll p^2$, $\mu^2 \ll p^2$ and $m^2 \ll p^2$, the breaking of Lorentz covariance is negligibly small, and thus the self-energies $\Sigma^{\pm}(p)$ and $\Phi^{\pm}(p)$ are to a very good approximation functions of the four-momentum squared, p^2, only. Furthermore, in the denominators of the integral kernels the renormalization scale independent self-energies can safely be neglected. Similar to Eq.(2.28) we substitute

$$Z_{1F}\frac{g^2}{4\pi}\,\Gamma^b_{NG\nu}(q, q+k)\,D^{ab}_{\mu\nu}(k) \;\simeq\; Z_2^2\,\frac{\alpha(k)}{k^2}\left(\delta_{\mu\nu} - \frac{k_\mu k_\nu}{k^2}\right)\begin{pmatrix} \frac{1}{2}\gamma_\mu\lambda^a & 0 \\ 0 & -\frac{1}{2}\gamma_\mu\lambda^{aT} \end{pmatrix} \tag{2.83}$$

in Eq.(2.43) and get in this approximation with Eq.(2.46)

$$\begin{aligned}\Phi^+(p) &\simeq \pi\int\frac{d^4q}{(2\pi)^4}\,\gamma_\mu\lambda^{aT}\left(S_0^-(q)\Phi^+(q)S_0^+(q)\right)\gamma_\nu\lambda^a\,\frac{\alpha(k)}{k^2}\left(\delta_{\mu\nu}-\frac{k_\mu k_\nu}{k^2}\right)\\ &\simeq -\pi\int\frac{d^4q}{(2\pi)^4}\,\gamma_\mu\not{q}\left(\lambda^{aT}\Phi^+(q)\lambda^a\right)\not{q}\gamma_\nu\,\frac{\alpha(k)}{q^4k^2}\left(\delta_{\mu\nu}-\frac{k_\mu k_\nu}{k^2}\right). \qquad (2.84)\end{aligned}$$

The gap function $\Phi^+(p)$ should then be decomposed in invariant channels

$$\Phi^+(p) = \sum_i \Phi_i^+(p)M_i\,, \qquad (2.85)$$

such that $\lambda^{aT}M_i\lambda = c_iM_i$. As one-gluon exchange comprises an $\bar{\mathbf{3}}$- and $\mathbf{6}$-channel, we find $c_{\bar{\mathbf{3}}} = -\frac{8}{3}$ and $c_{\mathbf{6}} = \frac{4}{3}$. Furthermore concentrating on the chirally symmetric components in an even-parity and T-symmetric phase (these will become of main interest), we have

$$\Phi_i^+(p) = \left(\gamma_4\not{p}\,\phi_{A,i}^+(p) + \phi_{C,i}^+(p)\right)\gamma_5 \qquad (2.86)$$

and the gap equations reduce to

$$\begin{aligned}\phi_{C,i}^+(p) &\simeq -3\pi c_i\int\frac{d^4q}{(2\pi)^4}\,\frac{\phi_{C,i}^+(q)}{q^2}\,\frac{\alpha(k^2)}{k^2}\\ \phi_{A,i}^+(p) &\simeq -\pi c_i\int\frac{d^4q}{(2\pi)^4}\,\frac{\phi_{A,i}^+(q)}{q^2}\,\frac{\alpha(k^2)}{k^2}\left(\hat{p}\cdot\hat{q}\left(1-2\frac{k_4^2+(\hat{q}\cdot\vec{k})^2}{k^2}\right)\right). \qquad (2.87)\end{aligned}$$

As the running coupling is a slowly varying function for large momenta it is safe to apply the angular approximation $\alpha(k^2)\approx\alpha(p^2\,\theta(p^2-q^2)+q^2\,\theta(q^2-p^2))$. The remaining angular integrations can then be done analytically. The gap function $\phi_{A,i}^+(p)$ decreases for large p^2 at least like $1/p^4$ times logarithmic corrections, and thus to order $1/p^2$ one has $\phi_{A,i}^+(p)\approx 0$. The equation for the gap function $\phi_{C,i}^+(p)$ then reads

$$\phi_{C,i}^+(p) \simeq -\frac{3}{16\pi}\,c_i\left(\frac{\alpha(p^2)}{p^2}\int^{p^2}dq^2\,\phi_{C,i}^+(q) + \int_{p^2}dq^2\,\frac{\alpha(q^2)\phi_{C,i}^+(q)}{q^2}\right). \qquad (2.88)$$

The anomalous dimensions of the gap functions $\gamma_{\phi,i}$ to 1-loop order can then be read off from the coefficient in Eq.(2.88). Comparing to the corresponding anomalous dimension of the mass function $\gamma_m = 12/(33-2N_f)$ they are given by

$$\gamma_{\phi,\bar{\mathbf{3}}} = \quad\gamma_m/2 = \quad 6/(33-2N_f) \qquad (2.89)$$

and

$$\gamma_{\phi,\mathbf{6}} = -\gamma_m/4 = -3/(33-2N_f) \qquad (2.90)$$

in $\bar{\mathbf{3}}$- and $\mathbf{6}$-channels, respectively. The asymptotic behavior of $\phi^+_{C,i}(p)$ is given by the so-called 'regular form', being the asymptotic solution of Eq.(2.88):

$$\phi^+_{C,i}(p) \;\propto\; \frac{1}{p^2}\left(\ln\left(\frac{p^2}{\Lambda^2}\right)\right)^{\gamma_{\phi,i}-1} . \tag{2.91}$$

The 'irregular form' as an asymptotic solution to Eq.(2.88) is of no importance, as there are no source terms in the theory and the condensate needs to vanish at large momenta.

Similar to the chiral quark condensate, see *e.g.* [12], we could now also define a renormalization-group independent diquark condensate from the asymptotic behavior of the gap function (see Eq.(2.21)).

2.4.2 Occupation numbers and diquark coherence lengths

Once the quark propagator is known, one can extract number densities, occupation numbers and the diquark coherence lengths. Within the Euclidean formalism, the number density ρ_a of a chosen charge (see Eq.(2.39)) is calculated as the derivative of the generating functional of the connected Green's functions W with respect to the corresponding chemical potential μ_a. For the homogeneous phases considered here it is given

$$\begin{aligned}
\rho_a &= \frac{Z_2}{2}\Big\langle :\Psi^\dagger(x)\begin{pmatrix} T^a & 0 \\ 0 & -T^{aT}\end{pmatrix}\Psi(x): \Big\rangle \\
&= \int\frac{d^3\vec{p}}{(2\pi)^3}\int\frac{dp_4}{2\pi}\,\frac{Z_2}{2}\,\mathrm{Tr}_{D,c,f,NG}\left(\begin{pmatrix} \gamma_4 T^a & 0 \\ 0 & -\gamma_4 T^{aT}\end{pmatrix}\mathcal{S}(p)\right) , \\
&= \int\frac{d^3\vec{p}}{(2\pi)^3}\int\frac{dp_4}{2\pi}\,\mathrm{Tr}_{D,c,f}\left(\gamma_4 T^a\, Z_2 S^+(p)\right) ,
\end{aligned} \tag{2.92}$$

where we again explicitly indicated the normal-ordering and used the same arguments as for the evaluation of Eq.(2.50). Since $T^a = \mathbb{1}$ for the quark number density, the form of Eq.(2.92) also suggests the definition of occupation numbers for a quasiparticle in color-flavor space

$$n_i(p) \;=\; \frac{g}{4\pi}\int_{-\infty}^{\infty} dp_4\;\mathrm{Tr}_D\left(\gamma_4\, Z_2 S_i^+(p_4,p)\right) , \tag{2.93}$$

with a degeneracy factor $g = 2$. The relation between the quark number density and the Fermi momentum will be further discussed in section 2.5.

The diquark coherence lengths provide a measure of the size of the pairing diquark correlations in a chosen channel. They can be determined from the anomalous propagator [93]

by first defining

$$\begin{aligned} T^{+}_{i,e}(x-y) &= \left\langle T_\tau\, \bar{\psi}_c(x) M_i \Lambda^e \psi(y) \right\rangle \\ &= \int \frac{d^4p}{(2\pi)^4}\, e^{ip(x-y)}\, \mathrm{Tr}_{D,c,f}\left(T^{+}_i(p) M_i \Lambda^e_{\vec{p}}\right) , \end{aligned} \tag{2.94}$$

where the matrix M_i singles out a chosen pairing pattern in color-flavor space and $\Lambda^e_{\vec{p}} = \frac{1}{2}\left(1 \pm i\gamma_4 \vec{\not{p}}\right)$ are the energy-projectors in Dirac space, for convenience taken in the chiral limit. The coherence length for this pairing pattern is then defined as

$$\begin{aligned} \xi^2_{i,e} &= \frac{\int d^3x\ |\vec{x}|^2 |T^{+}_{i,e}(0,\vec{x})|^2}{\int d^3x\ |T^{+}_{i,e}(0,\vec{x})|^2} \\ &= \frac{\int d^4p\ |\nabla_{\vec{p}} T^{+}_{i,e}(p)|^2}{\int d^4p\ |T^{+}_{i,e}(p)|^2} . \end{aligned} \tag{2.95}$$

This will be compared to the mean-particle distance.

2.4.3 The effective action

As we are investigating different phases, we also want to single out the energetically preferred one. To study this, we estimate the corresponding pressure difference by employing the Cornwall-Jackiw-Tomboulis (CJT) formalism [94], which provides the effective action Γ as a functional of the expectation values of fields and propagators in presence of local and bilocal source terms. In particular for QCD in the Nambu-Gor'kov formalism, the functional dependence on the quark propagator is given by [35, 95]

$$\Gamma[\mathcal{S}] = -\frac{1}{2}\mathrm{Tr}_{p,D,c,f,NG}\mathrm{Ln}\mathcal{S}^{-1} + \frac{1}{2}\mathrm{Tr}_{p,D,c,f,NG}\left(1 - Z_2\mathcal{S}_0^{-1}\mathcal{S}\right) + \Gamma_2[\mathcal{S}] . \tag{2.96}$$

Here $\Gamma_2[\mathcal{S}]$ is the sum of all 2-particle irreducible (2PI) diagrams without external legs and internal propagators replaced by the full ones, in particular the bare quark propagators replaced by $\mathcal{S}$.

The quark self-energy at the stationary point is then given by $Z_2\Sigma[\mathcal{S}] = -2\delta\Gamma_2[\mathcal{S}]/\delta\mathcal{S}$. Neglecting the functional dependence of the $q\bar{q}g$-vertex on the quark propagator, one can 'integrate' the DSE and obtains

$$\Gamma_2[\mathcal{S}] \simeq -\frac{1}{4}\mathrm{Tr}_{p,D,c,f,NG}(1 - Z_2\mathcal{S}_0^{-1}\mathcal{S}) + const. \tag{2.97}$$

at the stationary point. The approximate effective action at the stationary point is then

given by

$$\begin{aligned}\Gamma[\mathcal{S}] &= -\frac{1}{2}\mathrm{Tr}_{p,D,c,f,NG}\mathrm{Ln}\mathcal{S}^{-1} + \frac{1}{4}\mathrm{Tr}_{p,D,c,f,NG}\left(1 - Z_2\mathcal{S}_0^{-1}\mathcal{S}\right) + const. \\ &= -\frac{1}{2}\mathrm{Tr}_{p,D,c,f}\mathrm{Ln}\left(S^{+\,-1}\left(Z_2 S_0^{-\,-1} + Z_{1F}\Sigma^-\right)\right) + \\ &\quad +\frac{1}{4}\mathrm{Tr}_{p,D,c,f}\left(2 - Z_2 S^+ S_0^{+\,-1} - Z_2 S^- S_0^{-\,-1}\right) + const.\,. \end{aligned} \tag{2.98}$$

It is thermodynamically consistent, if the vertex construction is not depending on the quark propagator. In the weak coupling limit it gives the 2-loop result at the stationary point. Thermodynamically, Eq.(2.96) at the stationary point gives the negative pressure of the corresponding phase $p = -\Gamma[\mathcal{S}]$.

2.5 On Luttinger's theorem

Luttinger's theorem [96] can be summarized as follows: Provided the fermion propagator is positive at the Fermi energy, $p_4 = 0$, the volume of the Fermi surface at fixed density is independent of the interaction. The proof of this theorem is based on the fact that the functional $\Gamma_2[\mathcal{S}]$ is invariant under shifts in the momentum, *i.e.*,

$$\delta\Gamma_2[\mathcal{S}] \quad = \quad -\frac{1}{2}\,\mathrm{Tr}_{p,D,c,f,NG}\left[Z_2\Sigma[\mathcal{S}]\frac{\partial}{\partial p_4}\mathcal{S}\right] \quad = \quad 0\,. \tag{2.99}$$

Using $Z_2\,\gamma_4 \otimes \mathbb{1}_{NG} = i\frac{\partial}{\partial p_4}\left(\mathcal{S}^{-1} - Z_2\Sigma\right)$ obtained from the qDSE in Eq.(2.92), we are left with

$$\begin{aligned}\rho &= \int\frac{d^3\vec{p}}{(2\pi)^3}\int\frac{dp_4}{2\pi}\,\frac{1}{2}\,\mathrm{Tr}_{D,c,f,NG}\left(\left(i\frac{\partial}{\partial p_4}\left(\mathcal{S}^{-1}(p) - Z_2\Sigma(p)\right)\right)\mathcal{S}(p)\right) \\ &= \int\frac{d^3\vec{p}}{(2\pi)^3}\int\frac{dp_4}{2\pi}\,\frac{i}{2}\,\mathrm{Tr}_{D,c,f,NG}\left(\left(\frac{\partial}{\partial p_4}\mathcal{S}^{-1}(p)\right)\mathcal{S}(p)\right)\,. \end{aligned} \tag{2.100}$$

We can integrate analytically, however we need to take into account that there is the usual cut of the complex logarithm put onto the negative real half-axis. Then we find

$$\begin{aligned}\rho &= \int\frac{d^3\vec{p}}{(2\pi)^3}\left(\frac{i}{4\pi}\mathrm{Tr}_{D,c,f,NG}\mathrm{Log}\left(\mathcal{S}^{-1}\right)\Big|_{p_4=0^-} - \frac{i}{4\pi}\mathrm{Tr}_{D,c,f,NG}\mathrm{Log}\left(\mathcal{S}^{-1}\right)\Big|_{p_4=0^+}\right) \\ &= \int\frac{d^3\vec{p}}{(2\pi)^3}\left(\frac{i}{4\pi}\ln\left(\det\mathcal{S}^{-1}\right)\Big|_{p_4=0^-} - \frac{i}{4\pi}\ln\left(\det\mathcal{S}^{-1}\right)\Big|_{p_4=0^+}\right)\,. \end{aligned} \tag{2.101}$$

As an example, for a single fermion species, where

$$S^{-1}(p) \quad = \quad -i\vec{\not{p}}\,A(p) - i\omega_p\gamma_4 C(p) + B(p)\,, \tag{2.102}$$

this amounts to

$$\begin{aligned}\frac{i}{4\pi}\mathrm{Tr}_D\mathrm{Log}\left(S^{-1}\right)\Big|_{p_4=0^-} - \frac{i}{4\pi}\mathrm{Tr}_D\mathrm{Log}\left(S^{-1}\right)\Big|_{p_4=0^+} &= \frac{i}{2\pi}\ln\left(i\omega_p C + \sqrt{A^2p^2+B^2}\right)\Big|_{p_4=0^-} \\ &\quad -\frac{i}{2\pi}\ln\left(i\omega_p C + \sqrt{A^2p^2+B^2}\right)\Big|_{p_4=0^+} \\ &= \begin{cases} 1 & \text{if} \quad D(\vec{p},p_4=0)<0 \\ 0 & \text{if} \quad D(\vec{p},p_4=0)>0 \end{cases}, \end{aligned} \tag{2.103}$$

where $D = |\vec{p}|^2A^2 + \omega_p^2C^2 + B^2$. Since the Fermi surface in a Fermi liquid is defined by $D(\vec{p}=p_F, p_4=0)=0$, it is natural to extend this definition to a sign change in $D(\vec{p},p_4=0)$. For a gapped mode this will correspond to a singularity. Finally, we note that

$$\mathrm{Tr}_{NG}\mathrm{Log}\left(\mathcal{S}^{-1}\right) = \mathrm{Log}\left(S^{+\,-1}\left(Z_2S_0^{-\,-1}+Z_2\Sigma^-\right)\right), \tag{2.104}$$

as well as $D(\vec{p},p_4=0)$ of S^+ and $\left(Z_2S_0^{-\,-1}+Z_2\Sigma^-\right)^{-1}$ change sign at the same momenta, since S^+ is only invertible iff $Z_2(S_0^-)^{-1}+Z_2\Sigma^-$ is. In an isotropic phase we therefore conclude that

$$\rho = \frac{1}{3\pi^2}\sum_i p_{F,i}^3, \tag{2.105}$$

where the Fermi momenta $p_{F,i}$ are calculated by the zeros and poles in $\det_{D,c,f}\left(S^+\right)|_{p_4=0}$. We can therefore easily determine the density when only knowing the Fermi surfaces of the involved quasiparticles.

Chapter 3

A Hard-Dense-Loop-like truncation scheme

In section 2.3 we have sketched a setup for a truncated, but closed set of DSEs in the medium with focus on the quark propagator. We will know specify a truncation that recovers the HDL resummation scheme at large chemical potentials.

3.1 The truncation scheme

As the $q\bar{q}g$-vertex is already barely constrained in the vacuum and as we often restrict ourself to the tensor structure at tree level, we will follow the same lines in the medium and approximate

$$\Gamma^a_\mu(q,p) \;=\; \frac{Z_2\tilde{Z}_3}{\alpha_s(\nu)}\,\frac{\alpha_s(k)}{Z(k)}\,\Gamma^{(0)a}_{NG\mu}\,. \tag{3.1}$$

This way we ensure that we recover resummed perturbation theory for the dressing function of the quark propagator. At this stage, the sensitivity on the choice of our results on the running coupling constant α_s will serve as an indicator for the sensitivity of the $q\bar{q}g$-vertex. A more complicated vertex construction, also incorporating Goldstone boson effects and the anomalous vertices $\Delta^{\pm,a}_\mu$ in Eq.(2.45), will be subject of chapter 5. Furthermore the truncation seems more reasonable in the chirally unbroken medium than in the chirally broken vacuum, since some scalar-type tensor structures, which are expected to be important for understanding the relation between confinement and/or chiral symmetry breaking [41, 75, 97] are forbidden by chiral symmetry after chiral symmetry restoration.

Since we are primarily interested in chirally unbroken phases[1] at non-vanishing chem-

[1]Strictly speaking, we mean phases with (almost) vanishing chiral condensates in this context.

ical potential, it is important to incorporate medium effects like damping and screening by particle-hole excitations, as it is also done in the HDL approximation. In a first approach we will use 'bare' propagators for the determination of the medium polarization in Eq.(2.76). This is not self-consistent and its improvement will be subject of section 5.3. Nevertheless, the resulting qDSE turns out to be a generalization of the HDL approximation. Furthermore, even in the superconducting phases, the assumption of bare quark propagators will *a posteriori* turn out to be much better than neglecting the medium polarization (as in [98]) and we will be able to compare to weak coupling results for the gap functions.

Under these conditions, the expression in Eq.(2.76) can be reduced straightforwardly to

$$\Pi^{\mathrm{med}\,ab}_{\mu\nu}(k) \;=\; -\delta^{ab}\frac{2\pi N_f \alpha_s(k)}{Z(k)}\int\frac{d^4q}{(2\pi)^4}\mathrm{Tr}_D\left([\gamma_\mu S_0(p)\gamma_\nu S_0(q)] - [\ldots]_{\mu=0}\right). \quad (3.2)$$

The evaluation of this function is well known in the HDL approximation [91], and in the present case only the coupling is replaced by the running coupling. For small external momenta, the result for

$$\begin{aligned}\Pi^{ab}_T(k) &\stackrel{\mathrm{def}}{=} G(|\vec{k}|,k_4)\,\delta^{ab}\\ \Pi^{ab}_L(k) &\stackrel{\mathrm{def}}{=} F(|\vec{k}|,k_4)\,\delta^{ab}\end{aligned} \quad (3.3)$$

in Eq.(2.81) is given through

$$\begin{aligned}G(|\vec{k}|,k_4) &= m_g^2(k)\,\frac{ik_4}{|\vec{k}|}\left[\left(1-\left(\frac{ik_4}{|\vec{k}|}\right)^2\right)Q\left(\frac{ik_4}{|\vec{k}|}\right)+\frac{ik_4}{|\vec{k}|}\right]\\ F(|\vec{k}|,k_4) &= 2m_g^2(k)\,\frac{k_4^2+\vec{k}^2}{\vec{k}^2}\left[1-\frac{ik_4}{|\vec{k}|}Q\left(\frac{ik_4}{|\vec{k}|}\right)\right],\end{aligned} \quad (3.4)$$

where $Q(x)=\frac{1}{2}\ln\frac{x+1}{x-1}$ and

$$m_g^2(k) \;=\; \frac{N_f\alpha_s(k)\mu^2}{\pi}. \quad (3.5)$$

This approximation will be used for the medium polarization within this chapter. Summarizing the above considerations we arrive from Eq.(2.43) at a truncated, self-consistent DSE for the quark propagator:

$$\begin{aligned}\Sigma^+(p) &= Z_2\pi\int\frac{d^4q}{(2\pi)^4}\gamma_\mu\lambda^a S^+(q)\gamma_\nu\lambda^a\left(\frac{\alpha_s(k)}{k^2+G(k)}P^T_{\mu\nu}+\frac{\alpha_s(k)}{k^2+F(k)}P^L_{\mu\nu}\right)\\ \Phi^+(p) &= -Z_2\pi\int\frac{d^4q}{(2\pi)^4}\gamma_\mu\lambda^{aT}T^+(q)\gamma_\nu\lambda^a\left(\frac{\alpha_s(k)}{k^2+G(k)}P^T_{\mu\nu}+\frac{\alpha_s(k)}{k^2+F(k)}P^L_{\mu\nu}\right),\end{aligned} \quad (3.6)$$

where from Eq.(2.46)

$$\begin{aligned} T^+ &= -\left(S_0^{-\,-1} + \Sigma^-\right)^{-1} \Phi^+ S^+ \\ S^+ &= \frac{1}{Z_2}\left(S_0^{+\,-1} + \Sigma^+ - \Phi^- \left(S_0^{-\,-1} + \Sigma^-\right)^{-1} \Phi^+\right)^{-1} \end{aligned} \tag{3.7}$$

and $\Sigma^-(p) = -C\Sigma^+(-p)^T C$, $\Phi^-(p) = \gamma_4 \Phi^+(p)^\dagger \gamma_4$.

The running coupling $\alpha_s(k)$ is the only input into Eq.(3.6). Note that it also enters via the functions $G(|\vec{k}|, k_4)$ and $F(|\vec{k}|, k_4)$. In order to analyze the sensitivity on the running coupling, we employ the running coupling $\alpha_I(k)$ and $\alpha_{II}(k)$. The running coupling $\alpha_I(k)$ is known to underestimate chiral symmetry breaking in the vacuum (see section 2.2.3) for the bare vertex construction. Only for a more complicated Abelian $q\bar{q}g$-vertex construction in Eq.(2.29) it is in good agreement with lattice QCD results [41]. However this construction then contains a sizeable 'scalar' contribution, which is due to dynamical chiral symmetry breaking. Those are forbidden in a chirally symmetric phase. We therefore consider $\alpha_I(k)$ as some kind of lower bound. On the other hand, the running coupling $\alpha_{II}(k)$ extracted from quenched lattice data together with a bare vertex construction [81] serves as an upper bound, since a suitable coupling in the medium is likely to freeze out, *i.e.* become practically constant, below the Fermi energy. Furthermore effects from chiral symmetry breaking are modeled by this coupling.

3.2 Results for the unbroken phase

Before turning to the superconducting phases, we study the unbroken phase in the chiral limit first. This is to compare with analytical investigations [99, 100] and to emphasize that we will also consider the normal self-energy when studying superconducting phases, as they are very important at least in the weakly coupled regime [42] and have been neglected in previous numerical studies [93, 101]. The unbroken phase can be seen as the special case of setting the functions $\Phi^\pm$, and accordingly $T^\pm$, in Eq.(3.6) to zero. This yields a self-consistent integral equation for the self energy Σ^+. Due to the residual symmetries, we can parameterize the inverse quark propagator and its self-energy by

$$\begin{aligned} S^+(p)^{-1} &= -i\vec{\not{p}}\, A^+(p) - i\not{\omega}_p C^+(p) &&= \gamma_4 \sum_{e=\pm 1} S_e^+(p)^{-1} \Lambda_{\vec{p}}^e, \\ \Sigma^+(p) &= -i\vec{\not{p}}\, \Sigma_A^+(p) - i\not{\omega}_p \Sigma_C^+(p) &&= \gamma_4 \sum_{e=\pm 1} \Sigma_e^+(p) \Lambda_{\vec{p}}^e, \end{aligned} \tag{3.8}$$

where we introduced the notation $\vec{\not{p}} = \vec{p}\cdot\vec{\gamma}$, $\hat{p} = \vec{p}/|\vec{p}|$, $\not{\omega}_p = \omega_p\gamma_4$, $\omega_p = ip_4 + \mu$ and the energy projectors for massless particles $\Lambda_{\vec{p}}^\pm = \frac{1}{2}\left(1 \pm i\gamma_4 \vec{\not{p}}\right)$. The truncated qDSE

then becomes a system of integral equations for the dressing functions, which is solved numerically.

To understand the behavior of this numerical solution, we first derive an approximate form for the quasiparticle, *i.e.* positive energy, propagator

$$\begin{aligned} S_+^+(p) &= \frac{1}{Z_2}\left(-ip_4+\mu-|\vec{p}|+\Sigma_+^+(p)\right)^{-1} \\ &= \frac{1}{Z_2}\left(-ip_4\left(1-\frac{\mathrm{Im}\Sigma_+^+(p)}{p_4}\right)+\mu-|\vec{p}|+\mathrm{Re}\Sigma_+^+(p)\right)^{-1} \end{aligned} \tag{3.9}$$

near the Fermi surface, *i.e.* near $p_4 \approx 0$ and $|\vec{p}| \approx p_F$. This has been subject of several weak coupling analyses [99, 100]. Especially the imaginary part of the self energy, encoding the wave-function renormalization on the Fermi surface

$$Z_F = \left(1-\frac{\mathrm{Im}\Sigma_+^+(p)}{p_4}\right)^{-1}\Bigg|_{p_4=0,|\vec{p}|=p_F} \tag{3.10}$$

has been studied in detail. Within the present truncation we are able to generalize the investigation described in [100] such that the momentum dependence of the wave-function renormalization is taken into account. For bare quarks, corresponding to a 1-loop approximation, the contribution of the transversal gluons in Eq.(3.6) to the self-energy is given by

$$\Sigma_+^+(p) \simeq -\frac{4i}{3\pi^2}\int dk_4 \int dk \arctan\left(\frac{k}{p_4+k_4+il}\right)\frac{\alpha_s(k)k}{k^2+\frac{\pi}{2}m_g^2(k)\frac{|k_4|}{k}}\,, \tag{3.11}$$

where $l=|\vec{p}|-p_F$. The integrand is discontinuous for $|l|<k$, and the leading non-analytic contribution can be extracted from

$$\begin{aligned} i\frac{\mathrm{Im}\Sigma_+^+(p)}{p_4} &\simeq \frac{d}{dp_4}\Sigma_+^+(p) \\ &\simeq -\frac{4i}{3\pi}\int\limits_{k>|l|} dk \frac{\alpha_s(k)k}{k^2+\frac{\pi}{2}m_g^2(k)\frac{|p_4|}{k}}\,. \end{aligned} \tag{3.12}$$

The main contribution to this integral comes from scales of the implicitly given order $k_s \sim \left(\pi\, m_g^2(k_s)|p_4|\right)^{1/3}$. Note that $k_s \to 0$ for $p_4 \to 0$. Employing this scale we can approximate

$$\frac{\mathrm{Im}\Sigma_+^+(p)}{p_4} \simeq \frac{4}{9}\frac{\alpha_s(k_s)}{\pi}\ln\left(\frac{\left||\vec{p}|-p_F\right|^3+\frac{\pi}{2}m^2(k_s)|p_4|}{\Lambda_{UV}^3}\right)\,, \tag{3.13}$$

where Λ_{UV} is an ultraviolet cutoff. This demonstrates the well-known fact that the long-range (static) gluon interaction renders quark matter in the unbroken phase into a non-Fermi liquid, as the wave-function renormalization Z_F given by Eq.(3.10) vanishes. This will again show up in the results for the occupation numbers. In the present context it is obvious that this non-trivial feature depends on the infrared behavior of the product of gluon propagator and quark-gluon vertex.

Here also a qualitative difference between the couplings displayed in Fig. 2.2 becomes important. Since the coupling $\alpha_I(k)$ becomes almost constant for $q < 0.5\,\mathrm{GeV}$, we can estimate that k_s becomes negligibly small, *i.e.* $k_s \sim 0$, if

$$|p_4| \quad < \quad \frac{(0.5\,\mathrm{GeV})^3}{\pi m_g^2(0)} \quad \approx \quad \frac{10\,\mathrm{MeV}}{\mu^2[\mathrm{GeV}^2]}\,. \tag{3.14}$$

For the coupling $\alpha_{II}(k)$ this is not possible because the coupling vanishes in the infrared. One would need $|p_4| \ll (10\,\mathrm{MeV})/(\mu^2[\mathrm{GeV}^2])$ to study this effect, which is far beyond the scope of the present work.

In Fig. 3.1 we compare the non-analytic p_4 dependence at the Fermi surface to the corresponding numerical result at $\mu = 1\,\mathrm{GeV}$, employing the coupling $\alpha_I(k)$. One clearly sees that if k_s and Λ_{UV} are chosen accordingly, the approximation (3.13) works well. It is worth mentioning that for small coupling constants $\Lambda_{UV} = \frac{2^{5/2} m_g(\mu)}{\pi}$ [102]. This would give $\Lambda_{UV} = 2.1\,\mathrm{GeV}$ for $\mu = 1\,\mathrm{GeV}$ and is in reasonable agreement with $\Lambda_{UV} = 1.3\,\mathrm{GeV}$ used in Fig. 3.1. In addition, we display the dependence on $|\vec{p}|$ (which is neglected in weak coupling analyses) demonstrating that the singularity only occurs at $|\vec{p}| = p_F$.

For completeness, numerical results for the self-energy functions Σ_A^+ and Σ_C^+ in the unbroken phase are presented in Fig. 3.2. Displayed are their values at the Fermi surface as a function of the chemical potential μ and the momentum dependence for $p_4 = 0$ at $\mu = 0.5\,\mathrm{GeV}$ and $10\,\mathrm{GeV}$. We find $\Sigma_A^+, \Sigma_C^+ \ll 1$ in the unbroken phase, justifying the approximation of using bare quarks in the medium polarization *a posteriori*.

3.3 Color-superconductivity in the chiral limit

As the next step, we will investigate color-superconducting phases in the chiral limit. This will enable us to get an intuition for the choice, size and interpretation of the gap functions and for the relation of our numerical results to extrapolated weak-coupling studies. Since the relevant phases are (CFL) or at least are almost (2SC for 3 flavors) neutral, we neglect the neutrality condition in Eq.(2.50) and only consider the quark chemical potential μ.

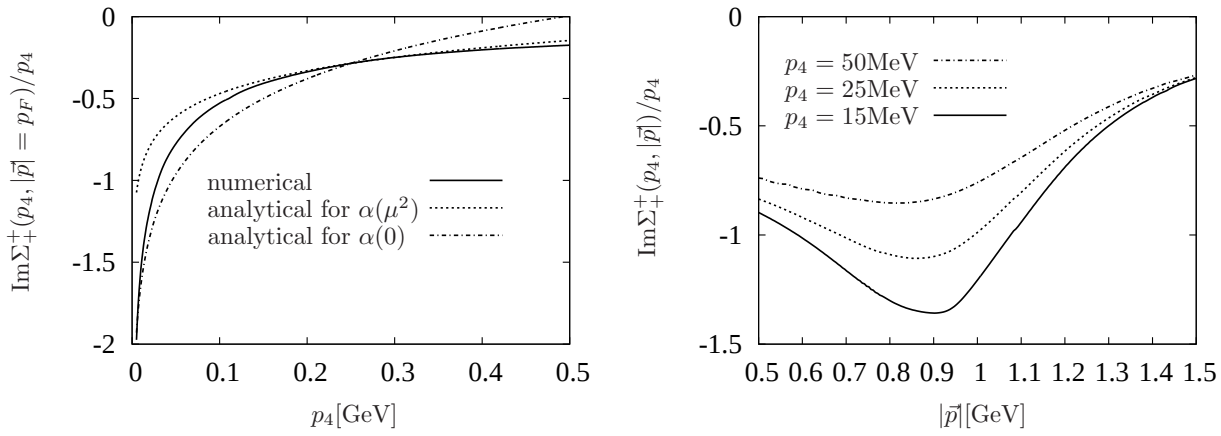

Figure 3.1: The logarithmic singularity on the Fermi surface as a function of p_4 at $\mu = 1\,\mathrm{GeV}$, compared to the approximation given in Eq.(3.13) at scales $k_s = 0$ and $k_s = \mu$, (left) and its momentum dependence for fixed $p_4 \neq 0$ (right). Here the coupling $\alpha_I(k)$ is employed. $\Lambda_{UV} = 1.3\,\mathrm{GeV}$ is chosen such that the analytical approximation fits the numerical result.

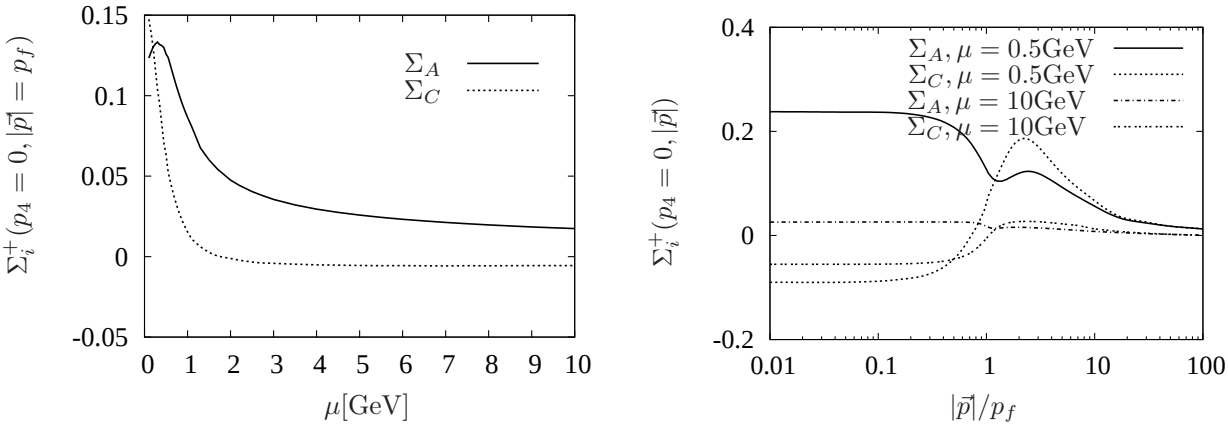

Figure 3.2: The self energies Σ_A^+ and Σ_C^+ in the unbroken phase at the Fermi surface as a function of the chemical potential μ (left) and as a function of the momentum $|\vec{p}|$ for $\mu = 0.5\,\mathrm{GeV}$ and $10\,\mathrm{GeV}$ for $p_4 = 0$ (right). Note that for $p_4 = 0$ all dressing functions are real.

3.3.1 Color-superconducting phases

In order to obtain a self-consistent solution of the system of equations (3.6) with (3.4), (3.5) and the running coupling as input, we will first consider the color-flavor structure of the normal and anomalous self-energies. We will restrict ourselves to scalar pairing, *i.e.* pairing to total spin 0, where one-gluon exchange and therefore also our truncation already has attractive channels. Pairing to higher total spin is known to lead to significantly smaller gap functions and therefore also gains less free energy [95]. It has been investigated for our approach in [48].

As Galilean invariance is still intact the normal and anomalous self-energies can be written as

$$\begin{aligned} \Sigma^+(p) &= \sum_i \Sigma_i^+(p) P_i \,, \\ \Phi^+(p) &= \sum_i \phi_i^+(p) M_i \,, \end{aligned} \tag{3.15}$$

where P_i and M_i parameterize all different allowed channels in color-flavor space and are constraint by the residual global symmetries in color-flavor space. They therefore form a closed basis under the transformations $P_i \to \lambda^a P_i \lambda^a$ and $M_i \to \lambda^{aT} M_i \lambda^a$, respectively, which appear when evaluating the self-energy integrals in Eq.(3.6). $\Sigma_i^+(p)$ and $\phi_i^+(p)$ are renormalization scale independent and take the form

$$\begin{aligned} \Sigma_i^+(p) &= -i\vec{\not{p}}\, \Sigma_{A,i}^+(p) - i\not{\omega}_p \Sigma_{C,i}^+(p) &&= \gamma_4 \sum_{e=\pm 1} \Sigma_i^e(p) \Lambda_{\vec{p}}^e \,, \\ \phi_i^+(p) &= \left(\gamma_4 \vec{\not{p}}\, \phi_{A,i}^+(p) + \phi_{C,i}^+(p)\right) \gamma_5 &&= \gamma_5 \sum_{e=\pm 1} \phi_i^e(p) \Lambda_{\vec{p}}^e \end{aligned} \tag{3.16}$$

in an even-parity[2], chirally and T-symmetric phase [103], where we again made use of the positive and negative energy projectors $\Lambda_{\vec{p}}^{\pm} = \frac{1}{2}\left(1 \pm i\gamma_4 \vec{\not{p}}\,\right)$. As the Nambu-Gor'kov propagator $\mathcal{S}$ possesses the same symmetries as the self-energy, we can also express

$$\begin{aligned} S^+(p) &= \sum_i S_i^+(p) P_i \,, \\ T^+(p) &= \sum_i T_i^+(p) M_i \,. \end{aligned} \tag{3.17}$$

The next task is to choose a self-consistent basis for P_i and M_i and thereby choosing a pairing pattern [31, 35]. Concentrating on the diquark correlation $T^+(p)$, the constraint

[2] In the chiral limit, our truncation is invariant under parity transformations. Instanton effects suggest however even-parity [30].

by the Pauli principle in Eq.(2.56) and by Eq.(2.61) gives

$$T^+(p) \;=\; -CT^+(p)^TC\,, \tag{3.18}$$

which leads to the constraint

$$M_i \;=\; M_i^T \tag{3.19}$$

in an even-parity, T-symmetric phase and for a linear independent basis. For the definition of a color-superconducting phase, we can therefore choose an ansatz M, which corresponds to the dominating pairing channel, and complete the basis. Motivated by one-gluon exchange we consider

$$M \;=\; \sum_{A=2,5,7;A'=2,5,7} s_{AA'}\;\lambda^A\otimes\tau^{A'}\,, \tag{3.20}$$

where λ^A and τ^A are the Gell-Mann matrices in color and flavor space, respectively. Those are antisymmetric for $A = 2,5,7$ and therefore parameterizing the attractive $\bar{\mathbf{3}}$-channel. For the pairing of up- and down-quark only, which will be labeled 2-flavor color-superconducting (2SC) phase [29, 30], we need to consider s_{A2} only and we can use the global color symmetry to rotate to

$$M_{2SC} \;=\; \lambda^2\otimes\tau^2\,. \tag{3.21}$$

The pairing of three degenerate quark flavors allows for more pairing patterns. Via a Ginzburg-Landau analysis [104, 105] it has been suggested that the color-flavor locked (CFL) phase [106] is energetically preferred. It is given by

$$M_{CFL} \;=\; \sum_{A=2,5,7}\lambda^A\otimes\tau^A \tag{3.22}$$

and also possesses the largest residual symmetry. The symmetries of these ansätze are determined by Eq.(2.73) and Eq.(2.75), which translate to

$$[P_i,T]=0\,,\qquad T^TM_i+M_iT=0 \tag{3.23}$$

for vector symmetries with generators T. The axial symmetries can be neglected, as they do not further constrain a basis $\{P_i\}$ and $\{M_i\}$, are broken dynamically or will be broken explicitly when introducing masses. The residual vector symmetry $\mathcal{G}$ of our ansätze is summarized in Tab. 3.1. In the 2SC phase the global color symmetry $SU_c(3)$ is broken to $SU_c(2)$. The generator λ^8 in addition forms a residual symmetry $U_{\tilde{B}}(1)$ in a linear combination with the generator of $U_B(1)$ having the generator $\mathbb{1}-\sqrt{3}\lambda^8$ only acting on

phase	ansatz M	residual vector symmetry $\mathcal{G}$
2SC	$\lambda^2 \otimes \tau^2$	$SU_c(2) \otimes SU_V(2) \otimes U_{\tilde{B}}(1) \otimes U_s(1)$
CFL	$\sum_{A=2,5,7} \lambda^A \otimes \tau^A$	$SU(3)_{c+V}$

Table 3.1: Residual vector symmetries of the 2SC and CFL phase.

blue quarks. Similar we have $U_s(1)$ with generator $\mathbb{1} - \sqrt{3}\tau^8$ only acting on strange-quarks. In the CFL phase we have the interesting color-flavor locked symmetry $SU(3)_{c+V}$, which is generated by $\tau_a - \lambda_a^T$, $a = 1 \ldots 8$. The determination of the largest basis $\{P_i\}$ and $\{M_i\}$ fulfilling Eq.(3.23) for the residual symmetry group $\mathcal{G}$ is then in general tedious, but straightforward and will be done for the more complicated pairing patterns in section 3.4 and 3.5. However, as we always start from a defining matrix M, it is enough to determine $\{P_i\}$ and set

$$M_i \;=\; MP_i\,. \tag{3.24}$$

By use of Eq.(3.23) we see that this forms a consistent basis $\{M_i\}$.

For the simple case of three degenerate quarks, we will follow [35] and can choose the basis $\{P_i\}$ to consist of orthogonal projectors fulfilling $P_iP_j = \delta_{ij}P_i$. The basis $\{M_i\}$ is then given by $M_i = MP_i = P_iM$ for the ansatz M. We furthermore introduce the parameters $\delta_i > 0$ via the decomposition

$$M^\dagger M \;=\; \sum_i \delta_i P_i\,. \tag{3.25}$$

For the 2SC phase we then find

$$\begin{aligned} \Sigma^+(p) &= \Sigma_1^+(p)P_{ur,ug,dr,dg} + \Sigma_2^+(p)P_{ub,db} + \Sigma_3^+(p)P_s\,, \\ \Phi^+(p) &= \phi_{2SC}^+(p)\,\lambda_2 \otimes \tau_2\,, \end{aligned} \tag{3.26}$$

where (r,g,b) and (u,d,s) label color and flavor (see also Appendix E.1). The red and green strange-quarks are degenerate with the blue ones due to our truncation.

The CFL phase is invariant under the $SU_{c+V}(3)$ symmetry for which the quarks form a $\mathbf{3} \otimes \bar{\mathbf{3}} = \mathbf{1} \oplus \mathbf{8}$ representation. The matrices $\{P_i\}$ turn out to project onto the irreducible representations. We therefore obtain (see also Appendix E.1)

$$\begin{aligned} \Sigma^+(p) &= \Sigma_{\mathbf{1}}^+ P_{\mathbf{1}}(p) + \Sigma_{\mathbf{8}}^+ P_{\mathbf{8}}(p)\,, \\ \Phi^+(p) &= \phi_{\mathbf{1}}^+(p) M_{\mathbf{1}} + \phi_{\mathbf{8}}^+(p) M_{\mathbf{8}} \\ &= \phi_{\bar{\mathbf{3}}}^+(p) \sum_{A=\{2,5,7\}} \lambda_A \otimes \tau_A + \phi_{\mathbf{6}}^+(p) \sum_{S=\{0,1,3,4,6,7,8\}} \lambda_S \otimes \tau_S\,, \end{aligned} \tag{3.27}$$

where we have also introduced the commonly used 'antitriplet' and 'sextet' pairing function $\phi^+_{\bar{\mathbf{3}}} = \frac{1}{3}\phi^+_{\mathbf{1}} + \frac{2}{3}\phi^+_{\mathbf{8}}$ and $\phi^+_{\mathbf{6}} = -\frac{1}{3}\phi^+_{\mathbf{1}} + \frac{1}{3}\phi^+_{\mathbf{8}}$. It is worth noting that the CFL phase is already color-neutral due to its large symmetry, as can be explicitly checked by evaluating $\mathrm{Tr}_{cf}\,(P_i\lambda^a) = 0$.

Due to the possibility of using energy projectors in chirally unbroken phases and the orthogonality of $\{P_i\}$, we can directly evaluate Eq.(3.7) to give the illustrative result

$$\begin{aligned} Z_2 S^+(p) &= -\sum_{i,e=\pm} \frac{(-ip_4-\mu)\left(1+\Sigma^+_{C,i}(p)^*\right) + e|\vec{p}|\left(1+\Sigma^+_{A,i}(p)^*\right) P_i \Lambda^e \gamma_4}{|(ip_4-\mu)(1+\Sigma^+_{C,i}(p)) + e|\vec{p}|(1+\Sigma^+_{A,i}(p))|^2 + \delta_i|\phi^e_i(p)|^2}\,, \\ T^+(p) &= -\sum_{i,e=\pm} \frac{\phi^e_i(p) M_i \Lambda^{-e}\gamma_5}{|(ip_4-\mu)(1+\Sigma^+_{C,i}(p)) + e|\vec{p}|(1+\Sigma^+_{A,i}(p))|^2 + \delta_i|\phi^e_i(p)|^2}\,, \end{aligned} \tag{3.28}$$

where we have made use of the relations $\Sigma_{F,i}(p) = \Sigma_{F,i}(-p)^*$ following from Eq.(2.62). The zero of the numerator at $p_4 = 0$ in the first equation defines the quasiparticle Fermi momenta p_F, and the zero in the denominator, which is the same for normal and anomalous propagator, provides the corresponding dispersion relation. To first approximation, *i.e.* evaluating the dressing functions on the Fermi surface, the energy gap Δ^e_i in the excitation spectrum is therefore given by

$$\Delta^e_i \simeq \left| \frac{\sqrt{\delta_i}\,\phi^+_i(p)}{1+\Sigma^+_{C,i}(p)} \right|_{|\vec{p}|=p_F, p_4=0}\,. \tag{3.29}$$

In the same approximation we can evaluate the negative pressure given in Eq.(2.96). For $\Delta^+_i \ll \mu$ and neglecting the anti-quasiparticle contribution similar to [35, 95, 101], we can estimate the pressure difference Δp between the color-superconducting and the chirally unbroken phase. Following the detailed calculation in [95] we obtain

$$\Delta p = \sum_i \mathrm{rank}(P_i)\,\frac{p^2_{F,i}\,{\Delta^+_i}^2}{8\pi^2} \tag{3.30}$$

for the gain through diquark condensation.

Both phases have been studied in a weak coupling analyses in the HDL approximation. Including the normal quark self-energies in this approximation, the quasiparticle gap at the Fermi surface is given by [42]

$$\phi^+_{weak,i} = 512\,\pi^4 \left(\frac{2}{N_f g^2}\right)^{\frac{5}{2}} e^{-\frac{\pi^2+4}{8}}\,\mu\, e^{-\frac{3\pi^2}{\sqrt{2}g}} \times \begin{cases} 1 & i = 2\mathrm{SC} \\ 2^{-1/3} & i = \bar{\mathbf{3}} \end{cases}\,. \tag{3.31}$$

The momentum dependence takes a more complicated form but for $g^2 \ln\left(\mu/\phi^+_{weak,i}\right) \ll 1$ one can neglect the quark self energies and obtains [42]

$$\phi^+_{weak,i}\,(|\vec{p}|) = \phi^+_{weak,i} \cos\left(\frac{g}{3\sqrt{2}\pi} \ln\left(\frac{\phi^+_{weak,i}}{|p-\mu|+\epsilon^+_i(p)}\right)\right), \tag{3.32}$$

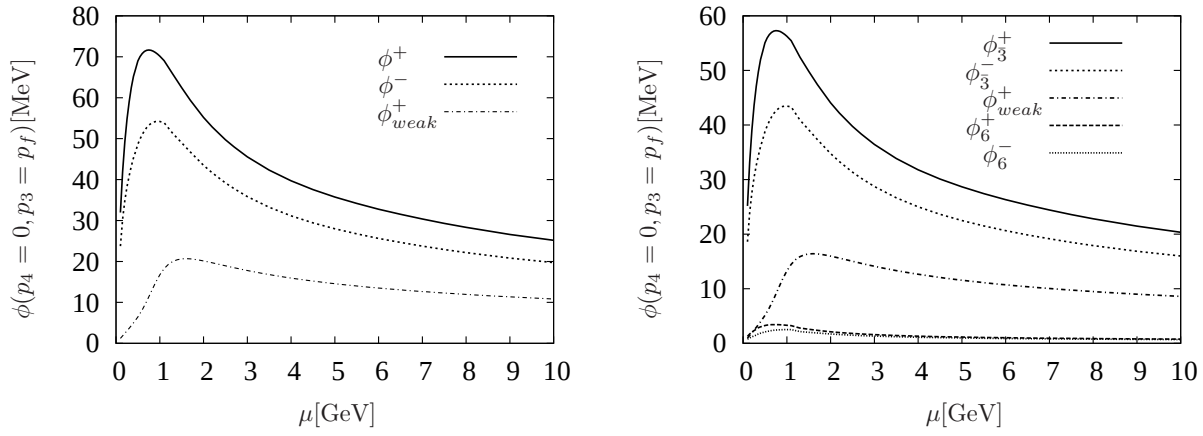

Figure 3.3: The quasiparticle gaps ϕ^+ and anti-quasiparticle gaps ϕ^- at the Fermi surface for the 2SC (left) and CFL (right) phases for the coupling $\alpha_I(k)$. These are compared to the extrapolated weak coupling result ϕ^+_{weak}.

with $\epsilon_i^+(p)^2 = (p-\mu)^2 + {\phi^+_{weak,i}}^2$. As our truncation recovers the HDL approximation in the weakly coupled regime, we should also recover these results.

3.3.2 Numerical results

We are now going to present the numerical results for our proposed truncation scheme. Our first focus is of course the value of the gap function at the Fermi surface, *i.e.* $p_4 = 0$ and $|\vec{p}| = p_{F,i}$ for a given channel i. The results for the gap functions at the Fermi surface the for 2SC and CFL phases are shown in Fig. 3.3 for the coupling $\alpha_I(k)$. In Fig. 3.4 the corresponding results are shown for the coupling $\alpha_{II}(k)$. In both cases the weak-coupling approximation of the gap functions is displayed, where we evaluated the identical running coupling $\alpha_s(k)$ as in the numerical solution[3] for $\sqrt{k^2} = \mu$.

In both figures it is evident that the extrapolated weak-coupling results for the value of the quasiparticle gap differs by a factor of more than five for $\mu \approx 500\,\mathrm{MeV}$, resulting in quasiparticle-pairing gaps larger than 50 MeV. It is worth noting that the results are less sensitive on the coupling than the mass function in the chirally broken phase. This can be attributed to the fact that a stronger coupling also results in stronger screening and damping. In addition, also the anti-quasiparticle gap functions are determined

[3]The relevant scale in weak-coupling investigations has so far not been determined, as it requires the next-to-leading order behavior. It is however generally believed to be of order μ [39]. In our truncation the relevant scale is implicitly given, as the 'soft' gluons dominate the dynamics and $\alpha_s(k)$ is evaluated at $k_s \sim g(k_s)\mu$. However to lowest order we have $g(k_s) \sim g(\mu)$ for small couplings.

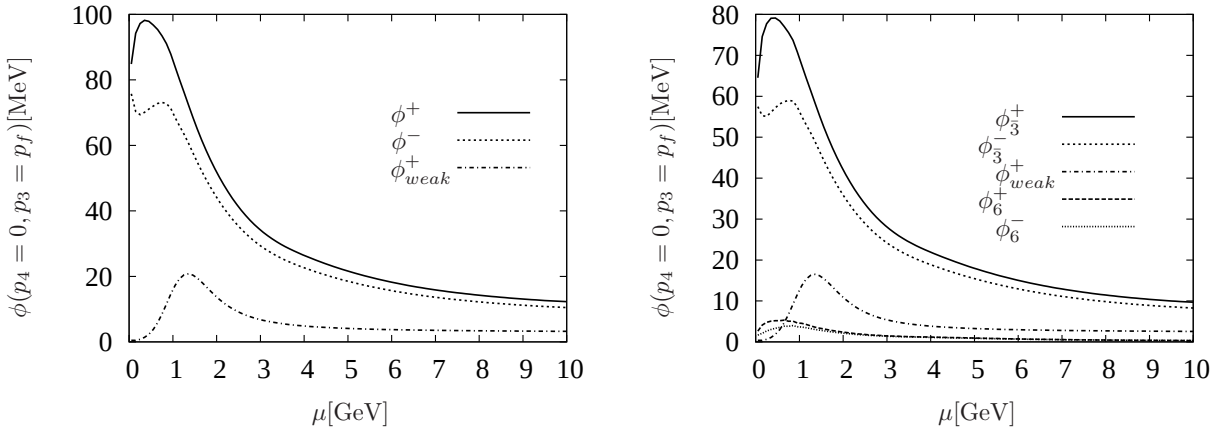

Figure 3.4: The quasiparticle gaps ϕ^+ and anti-quasiparticle gaps ϕ^- at the Fermi surface for the 2SC (left) and CFL (right) phases for coupling $\alpha_{II}(k)$. These are compared to the extrapolated weak coupling result ϕ^+_{weak}.

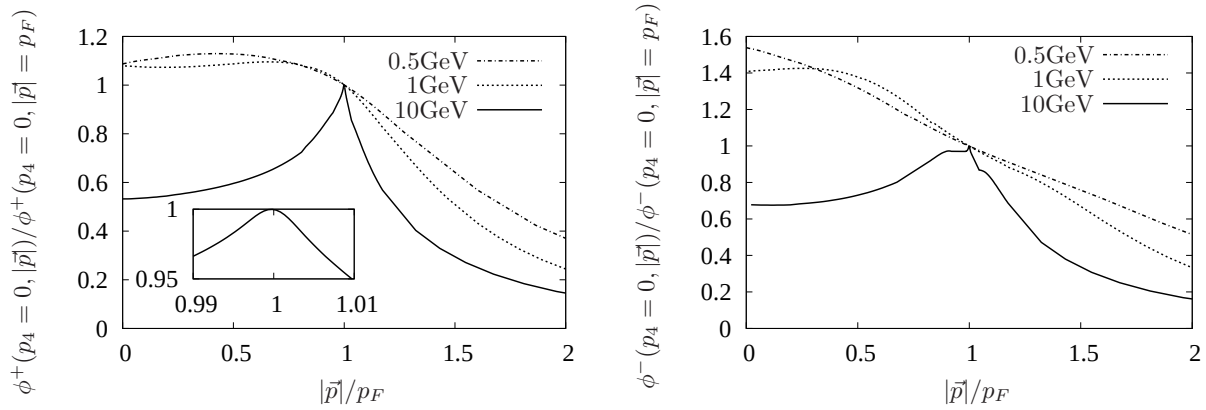

Figure 3.5: The momentum dependence of the quasiparticle gaps ϕ^+ (left) and anti-quasiparticle gaps ϕ^- (right) for $p_4 = 0$ normalized to their value at the Fermi surface.

self-consistently, which are important for low-energy constants of Goldstone modes (see section 5.2.1). Nevertheless, it is remarkable that the ratio of the 2SC and anti-triplet CFL gaps is almost equal to $2^{1/3}$ as in the weak coupling analysis. The reason for this behavior is that the normal self-energies Σ_i^+ are only weakly modified compared to the self energies in the unbroken phase. This amounts to an effective 'decoupling' of normal self-energies and gap functions, and thus the factor $2^{1/3}$ is directly inherited from the pairing pattern in color-flavor space.

As can be inferred from Fig. 3.2 and the estimate given in Eq.(3.29), the energy gap in the excitation spectrum Δ_i^+ is at most 15% smaller than the gap function at the corresponding kinematical point. (Note that the corresponding coefficients δ_i given in Appendix E.1 are: $\sqrt{\delta_{2SC}} = \sqrt{\delta_{\mathbf{8}}} = 1$ and $\sqrt{\delta_{\mathbf{1}}} = 2$.) We also emphasize that $\phi^+(p) \to \phi^-(p)$ for $\mu \to 0$, which can be non-zero, indicating a Bose-Einstein condensation of diquarks. This is found for the coupling $\alpha_{II}(k)$. However, this is not expected to be the energetically favored state in the vacuum, since spontaneous chiral symmetry breaking has not been taken into account here[4].

In Fig. 3.5 we present the momentum dependence of the quasiparticle gaps ϕ^+ and anti-quasiparticle gaps ϕ^- for $p_4 = 0$ for several chemical potentials, obtained with the coupling $\alpha_I(k)$. For large values of μ the gap function is concentrated around the Fermi surface and the quasiparticle gaps show a cosine-like behavior near the maximum, similar to the findings in Eq.(3.32). However, at chemical potentials of the order Λ_{QCD}, the Fermi surface is no longer the main contributing region to the gap integral, and even the maximum of the gap function is no longer on or close to the Fermi surface.

As described in section 2.4.2, the occupation numbers of the quasiparticles are calculated from the normal propagators. These are displayed in the left panel of Fig. 3.6 for the 2SC phase, employing the coupling $\alpha_I(k)$. The occupation number of the gapped red and green up- and down-quarks is, as expected and due to the pairing, a smooth function around the Fermi momentum. On the other hand, the occupation number of the blue up- and down-quarks changes rapidly. Within the present approximation, *i.e.* neglecting quark self energies in the medium polarization, these quarks are in a state at the borderline between a Fermi and a non-Fermi liquid.

The decoupled strange-quarks are in the unbroken phase and one clearly sees, especially when comparing to the blue up- and down-quarks, that the occupation number changes smoothly. As already mentioned, this is another feature of non-Fermi liquids which, strictly speaking, indicates the breakdown of the quasiparticle picture. We also find a significant

[4]Our approximation of the medium polarization requires the Fermi momentum of the quarks to be of order μ

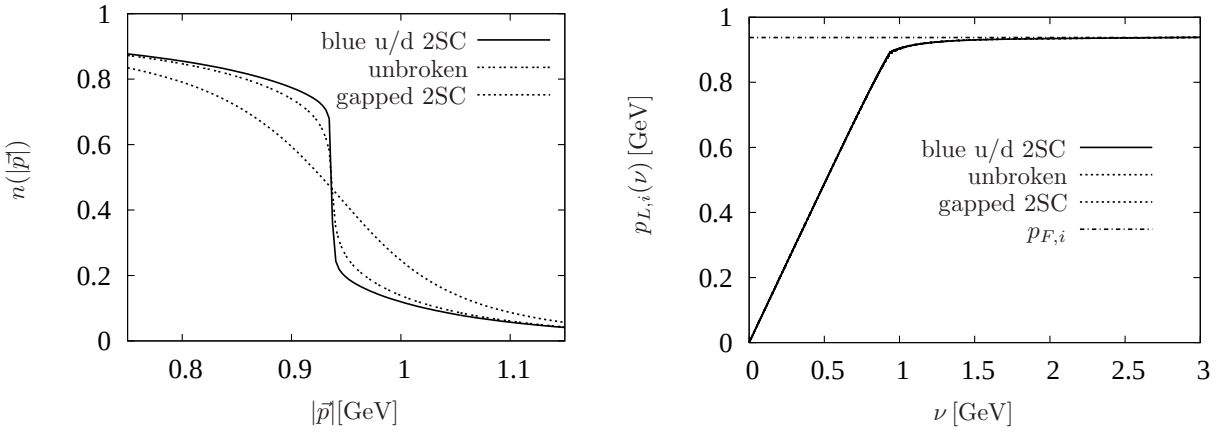

Figure 3.6: The occupation numbers (left) and the function defined in Eq.(3.33), $p_{L,i}(\nu)$, (right) for the different quark channels in the 2SC phase at $\mu = 1\,\mathrm{GeV}$ with the coupling $\alpha_I(k)$. As can be seen in the panels all Fermi momenta are (almost) equal and given by $p_{F,i} \approx .937\,\mathrm{GeV}$, *c.f.* the dashed-dotted line in the right panel. The lines of the different channels are nearly indistinguishable.

depletion at $|\vec{p}| = 0$ due to the interaction.

The density can either be obtained by integration of the occupation numbers or via Luttinger's theorem (see section 2.5). The conditions for the latter are fulfilled since all self-energies are real for $p_4 = 0$. To analyze this remarkable feature we define the function

$$p_{L,i}(\nu) \quad = \quad \left(3 \int_0^\nu dq q^2 n_i(q) \right)^{\frac{1}{3}} , \tag{3.33}$$

which has to obey the limiting behavior $\lim_{\nu\to\infty} p_{L,i}(\nu) = p_{F,i}$. From Fig. 3.6 one sees that this limit is assumed for $\nu \gg p_{F,i}$, and that the expectation derived from Luttinger's theorem is nicely fulfilled within the numerical accuracy. Note also that all Fermi momenta are very close to each other, a fact which justifies *a posteriori* the approximation of neglecting the neutrality conditions.

It is instructive to compare the coherence length of the diquarks $\xi_{i,+}$ given in Eq.(2.95) to the mean-particle distance λ_i as determined from the density ($\rho_i = 1/\lambda_i^3$ for the ith channel). The results are shown in Fig. 3.7 as a function of the chemical potential. Although the two different couplings lead to a distinctive pattern for these ratios it is safe to conclude that the size of a Cooper pair at moderate chemical potentials, $\mu \approx 500\,\mathrm{MeV}$, is only several times the mean-free path, the precise value depending on the diquark channel and the employed coupling (similar results were already presented in [93, 101].). Although there is an analogy to the crossover between a BCS-type superconductor in weak coupling

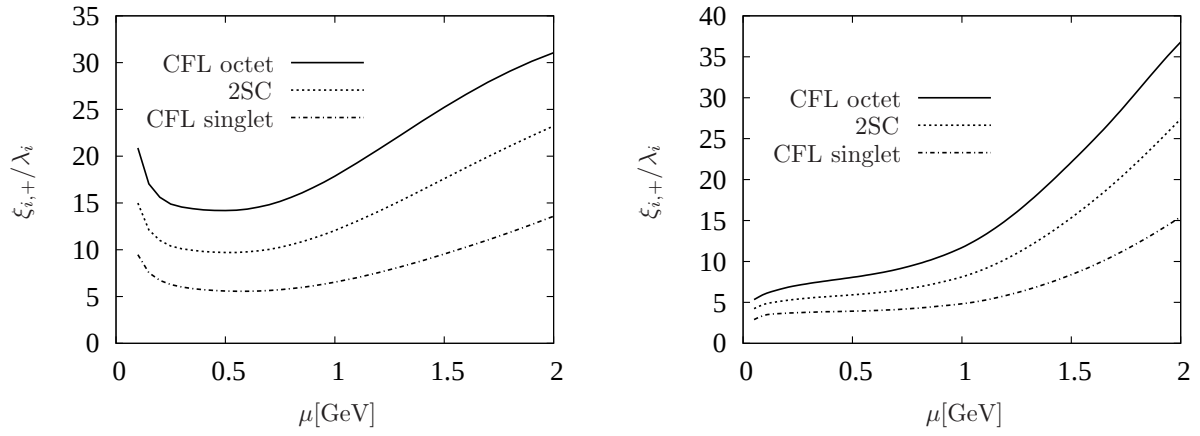

Figure 3.7: The ratio between the coherence length and mean-particle distance in 2SC and CFL phase for the coupling $\alpha_I(k)$ (left) and $\alpha_{II}(k)$ (right).

to the strongly coupled regime (Bose-Einstein condensate) the size of the diquarks suggest that the 2SC and CFL phases resemble a strongly coupled BCS system. However the result indicates that mean-field approximations are very questionable. In the limit $\mu \to 0$, we again find a different behavior for the two employed couplings indicating Bose-Einstein condensation of diquarks for $\alpha_{II}(k)$ for very small chemical potentials.

Finally, the pressure difference between the color-superconducting phases (2SC and CFL) and the unbroken phase are displayed in Fig. 3.8. This quantity is given by the negative effective action difference, and is here calculated within the approximate CJT formula given in Eq.(2.96). This is in good qualitative agreement with the parameterized form in Eq.(3.30). In the chiral limit, the CFL phase is the most favored phase, as expected.

3.3.3 Conclusions

Within our truncation, we include the in-medium modification of the gluon propagator and should recover weak-coupling expressions at asymptotically high densities. The most remarkable feature of these self-consistent solutions are the values of the gap functions: The quasiparticle-pairing gaps are several times larger than the extrapolated weak-coupling results even for sizeable chemical potentials $\mu \approx 1\,\mathrm{GeV}$. This is true irrespective of the considered phase (2SC or CFL) and the employed running coupling.

The investigation provides the starting point for the following more realistic studies involving finite current-quark masses. Using different quark masses the question of implementing neutrality conditions (which could be ignored here) becomes important.

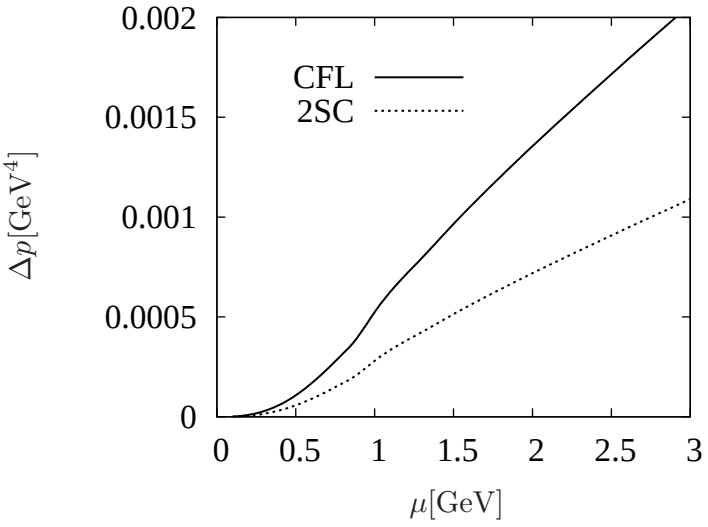

Figure 3.8: The pressure difference between the superconducting phases (2SC and CFL) and the unbroken phase employing $\alpha_I(k)$.

3.4 Unlocking of color and flavor

Having studied the chiral limit, the CFL phase turned out to be the energetically preferred ground state for three degenerate quark flavors, whereas the 2SC phase needs to be the ground state for only two quark flavors. Since the up- and down-quarks are to very good approximation massless, these results can be viewed as the case of vanishing strange-quark mass and infinite strange-quark mass. The obvious question is then, what the ground state for a realistic strange-quark mass is or metaphorically speaking at which value color and flavor become unlocked [107, 108].

The physical picture for this can be sketched as follows: In homogeneous phases, only quarks with opposite momenta pair. To pair a up- or down-quark with Fermi momentum $p_{F,ud}$ and a strange-quark, which has a lower Fermi momentum $p_{F,s}$, we need to lift the strange-quark to the Fermi surface of the other quarks. This costs kinetic energy and the amount needs to be smaller than the gain in condensation energy. In a simple model, with constant gap and mass functions and only considering the 'antitriplet' pairing, the rough estimate [109]

$$|p_{F,ud} - p_{F,s}| \quad \sim \quad \sqrt{3}\phi^+_{\bar{\mathbf{3}}} \tag{3.34}$$

for the unlocking transition has been obtained. This can also be obtained by using Eq.(2.98) under the model assumptions. The Fermi momenta of up- and down-quarks

is approximately given by $p_{F,ud} = \mu$. For a constituent strange-quark mass M_s we have $p_{F,s} = \sqrt{\mu^2 - M_s^2} \approx \mu - \frac{M_s^2}{2\mu}$. We therefore expect a critical strange-quark mass for color-flavor unlocking of $M_{s,critical} \sim O(\sqrt{\mu\phi_{\bar{\mathbf{3}}}^+})$.

In the following, this transition will be studies by solving the qDSE self-consistently for varying strange-quark mass and determine the pressure difference between 2SC and CFL phase. In contrast to a self-consistent treatment within models of the Nambu & Jona-Lasinio (NJL) type [110], the critical values for the renormalized strange-quark mass is much larger, which has a physical reason in the implemented consideration of the medium modification of the interaction.

The region of the 2SC phase possesses a rich (sub-)structure if furthermore neutrality conditions and β-equilibrium are taken into account [111]. The CFL phase and the boundary for unlocking are, however, only mildly affected. We therefore postpone the proper implementation of neutrality and β-equilibrium to section 3.5.

3.4.1 The parameterization of the CFL phase

We again focus on Eq.(3.6) within the approximation Eq.(3.4-3.5) and the two different couplings $\alpha_I(k)$ and $\alpha_{II}(k)$. In contrast to the chiral limit, we now consider the bare quark masses appearing in

$$S_{0,f}^+(p)^{-1} \;=\; -i(p_4 + i\mu)\gamma_4 - i\vec{p}\cdot\vec{\gamma} + m_{0,f} \tag{3.35}$$

for a quark flavor f.

The renormalization constants are determined in the (chirally broken) vacuum. For each flavor, we determine the quark wave-function renormalization constant, Z_2, and the renormalization constant Z_m, relating the unrenormalized quark mass $m_{0,q}(\Lambda^2)$ at an ultraviolet cutoff Λ to the renormalized mass $m_q(\nu)$ via

$$m_{0,q}(\Lambda^2) \;=\; Z_m(\nu^2, \Lambda^2) m_q(\nu)\,, \tag{3.36}$$

by requiring

$$S_f^+(p)^{-1}\Big|_{p^2=\nu^2} \;=\; -i\not{p} + m_f(\nu) \tag{3.37}$$

at a renormalization scale ν. The applied MOM scheme results in somewhat smaller numerical values for the quark current masses at a given renormalization scale (usually taken to be 2 GeV). We simply ignore here the difference between $\overline{\text{MS}}$ and MOM masses

because the effect is of the order of ten percent (when calculated within perturbation theory) and thus much smaller than the uncertainty in the value the current masses[5].

It turns out that, as expected, the mass dependence of the quark wave function renormalization constant, Z_2, is negligible as long as the renormalization scale is much larger than the mass. Therefore, we simply drop this dependence and Z_2 is determined once and for all in the chiral limit. To keep the number of parameters as small as possible, we work in the chiral isospin limit[6], *i.e.* we set the up and down current quark masses to zero, and vary only the strange quark current mass.

The self-energies again decompose into color-flavor and Dirac structure

$$\Sigma^+(p) = \sum_i \Sigma_i^+(p) P_i \,, \tag{3.38}$$

$$\Phi^+(p) = \sum_i \phi_i^+(p) M_i \,, \tag{3.39}$$

with suitable sets of matrices $\{P_i\}$ and $\{M_i\}$ in color-flavor space and renormalization-point independent component functions $\Sigma_i^+(p)$ and $\phi_i^+(p)$, which are matrix-valued in Dirac space. Full self-consistency is guaranteed in case a basis of all allowed matrices is considered. The dimensionality of this basis in a given phase depends on the residual symmetry in color-flavor space. For the CFL phase this will be detailed below.

The Dirac structure of the self-energies in an even-parity phase can be parameterized by [103]

$$\begin{aligned} \Sigma_i^+(p) &= -i\not{p}\ \Sigma_{A,i}^+(p) - i\not{\psi}_p\, \Sigma_{C,i}^+(p) + \Sigma_{B,i}^+(p) - i\gamma_4\not{p}\ \Sigma_{D,i}^+(p) \,, \\ \phi_i^+(p) &= \left(\gamma_4\not{p}\ \phi_{A,i}^+(p) + \gamma_4\, \phi_{B,i}^+(p) + \phi_{C,i}^+(p) + \not{p}\ \phi_{D,i}^+(p)\right) \gamma_5 \,, \end{aligned} \tag{3.40}$$

and we already note that $\Sigma_{D,i}^+(p)$ turns out to be negligibly small. This is to be expected since it has to vanish due to time reversal symmetry at vanishing temperatures in color-flavor symmetric channels. The gap functions ϕ_B and ϕ_D, which vanish in the chiral limit, will be discussed in section 3.4.2 where we provide an interpretation in a simplified setting.

Due to Eq.(2.62) the system of equations for the self-energies is symmetric under the transformations

$$\Sigma_{A/B/C,i}^+(p_4, |\vec{p}|) \rightarrow \Sigma_{A/B/C,i}^+(-p_4, |\vec{p}|)^* \,, \tag{3.41}$$

$$\Sigma_{D,i}^+(p_4, |\vec{p}|) \rightarrow -\Sigma_{D,i}^+(-p_4, |\vec{p}|)^* \,, \tag{3.42}$$

[5] In addition, it is worth mentioning that solutions of the Bethe-Salpeter equation within the DSE approach in MOM scheme favor small values for the physical strange-quark mass [112], a fact which is also related to the difference in renormalization schemes.

[6] As the shift of the Fermi momentum due to quark masses is of the order $\frac{m_f^2}{2\mu}$, this is a very good approximation.

which we find to be unbroken in the self-consistent scheme presented here. Therefore, the determinant of the quark propagator is positive for $p_4 = 0$, and the Luttinger theorem is applicable for determining the density.

For the anomalous propagator an inhomogeneous part is missing in Eqs.(3.6-3.7). Therefore we can choose a global phase for the gap functions. This is done such that the equations are invariant under

$$\phi^+_{A/D,i}(p_4, |\vec{p}|) \rightarrow \phi^+_{A/D,i}(-p_4, |\vec{p}|)^* , \tag{3.43}$$
$$\phi^+_{B/C,i}(p_4, |\vec{p}|) \rightarrow -\phi^+_{B/C,i}(-p_4, |\vec{p}|)^* , \tag{3.44}$$

and therefore ϕ_A and ϕ_D are real, and ϕ_B and ϕ_C purely imaginary, for $p_4 = 0$.

Neglecting $\Sigma^+_{D,i}$, the Dirac structure of the inverse normal propagator can be written as

$$S_i^{+\,-1}(p) = Z_2 S_{0,i}^{+\,-1} + Z_2\Sigma_i^+ = -i\not{p}\, A_i(p) - i\not{u}_p C_i(p) + B_i(p) , \tag{3.45}$$

which allows to define the mass function for the pairing quasiparticles for a given color-flavor channel q as

$$M_q(p) = \frac{m_{0,q} + \Sigma^+_{B,q}(p)}{1 + \Sigma^+_{C,q}(p)} . \tag{3.46}$$

In the following we will mostly present results for mass functions at $p_4 = 0$. To ease notations we will use $M_q(|\vec{p}|) = M_q(p_4 = 0, |\vec{p}|)$ except when stated explicitly otherwise.

As explained in section 3.3, the CFL phase is defined via its symmetry pattern in color-flavor space. For three degenerate quark flavors, one considers the $SU(3)_{c+V}$ symmetry generated by $\tau_a - \lambda_a^T$, with $a = 1, \ldots, 8$ and τ_a, λ_a being the Gell-Mann matrices in flavor and color space, respectively [106]. The quarks therefore are in a $\mathbf{3} \otimes \bar{\mathbf{3}} = \mathbf{1} \oplus \mathbf{8}$ representation of this symmetry. In the case of only two degenerate quarks and a strange-quark, the symmetry is broken down to $SU(2)_{c+V} \otimes U(1)_{c+V}$, which is generated by $\tau_a - \lambda_a^T$ with $a = 1, 2, 3$ and 8, *i.e.* the quarks form a $\mathbf{1} \oplus \mathbf{1} \oplus \mathbf{2} \oplus \mathbf{2} \oplus \mathbf{3}$ representation.

For the Nambu-Gor'kov propagator to be invariant under this transformation, we need to require (see Eq.(2.73))

$$U^\dagger S^+(p) U = S^+(p) , \quad U^T T^+(p) U = T^+(p) , \tag{3.47}$$

for $U \in SU(2)_{c+V} \otimes U(1)_{c+V}$. The matrices $\{P_i\}$ and $\{M_i\}$, needed for a self-consistent description are then those given explicitly in the Appendix E.2.

In section 3.4.3 we will also present results for the self-energies evaluated at different energies and momenta, in particular at the Fermi surface. In contrast to the chiral

limit, where the matrices $\{P_i\}$ can be chosen as constant projectors onto irreducible representations of the residual symmetry, the situation is more complex here. In principle, every dressing function of the normal propagator and self-energy can be decomposed into irreducible projectors in color-flavor space:

$$F = F_{\mathbf{1}}P_{\mathbf{1}} + F_{\mathbf{1}'}P_{\mathbf{1}'} + F_{\mathbf{2}}P_{\mathbf{2}} + F_{\bar{\mathbf{2}}}P_{\bar{\mathbf{2}}} + F_{\mathbf{3}}P_{\mathbf{3}}\,, \tag{3.48}$$

where, in particular, $P_{\mathbf{2}} = P_7$, $P_{\bar{\mathbf{2}}} = P_8$ and $P_{\mathbf{3}} = P_1 - \frac{1}{2}P_2$. However, for every dressing function, the singlets are not protected against mixing and therefore their projectors $P_{\mathbf{1}}$ and $P_{\mathbf{1}'}$ are in general energy and momentum dependent. We therefore find six different Fermi momenta, which are defined as sign changes of the determinant of the propagator, $\det(\mathcal{S})$, at $p_4 = 0$ and connected to the density by the Luttinger theorem. Three of them correspond to the upper 3×3 block-matrix in the ansatz employed (see Appendix E.2) and describe the mixing of the two singlet channels as well as the triplet channel. After ordering, these are denoted by $p_{F,\mathbf{1}_1}$, $p_{F,\mathbf{1}_2}$ and $p_{F,\mathbf{1}_3}$. In the lower 6×6 diagonal block-matrix, we find $p_{F,\mathbf{2}}$, $p_{F,\bar{\mathbf{2}}}$ and $p_{F,\mathbf{3}}$ corresponding to P_7, P_8 and P_6, respectively.

For the dressing functions of the anomalous propagators and the gap functions the situation is similar. With $M = \lambda_2 \otimes \tau_2 + \lambda_5 \otimes \tau_5 + \lambda_7 \otimes \tau_7$ being invertible and fulfilling $U^T M U = M$, we define $M_i = MP_i$. Every dressing function can then be written as

$$G = G_{\mathbf{1}}M_{\mathbf{1}} + G_{\mathbf{1}'}M_{\mathbf{1}'} + G_{\mathbf{2}}M_{\mathbf{2}} + G_{\bar{\mathbf{2}}}M_{\bar{\mathbf{2}}} + G_{\mathbf{3}}M_{\mathbf{3}}\,, \tag{3.49}$$

where $M_{\mathbf{2}} = M_7$, $M_{\bar{\mathbf{2}}} = M_8$ and $M_{\mathbf{3}} = M_1 - \frac{1}{2}M_2$. Furthermore $M_{\mathbf{1}}$ and $M_{\mathbf{1}'}$ are again in general energy and momentum dependent due to the possible mixing between the singlets.

3.4.2 The gap functions ϕ_B and ϕ_D

Having introduced the most general Dirac structure for the gap functions in an even-parity phase (see Eq.(3.40)) their interpretation and in particular their relation to the energy gap in the excitation spectrum is of interest. To this end one has to determine the dispersion relations as given by the poles of the propagators. This is a solvable task but leads already for degenerate quarks and constant dressing functions to very involved and intricate expressions. A physically motivated approximation with a simple interpretation of the gap function will be introduced in this section and will serve as an illustration. For simplicity, we consider the pairing of only two different quasiparticles a and b with inverse propagators in Dirac space, given by ${S^+_{a/b}}^{-1} = Z_2 {S^+_{0,a/b}}^{-1} + Z_2\Sigma^+_{a/b}$ for vanishing gap functions. This is in particular the case for the three lower 2×2 block-matrices in the ansatz presented in the Appendix E.2.

The gapped propagator S_c^+ in one channel, see Eq.(3.7), is then typically given by

$$S_c^{+\,-1} \;=\; S_a^{+\,-1} - \phi^- S_b^- \phi^+ \,, \tag{3.50}$$

with ϕ^+ of the form in Eq.(3.40). The propagators, being of the form in Eq.(3.45), can be expressed via the energy-projectors for massive fermions:

$$S_i^{+\,-1} \;=\; \sum_{e=\pm} \left(-i\omega C_i - eE_i\right) \gamma_4 \Lambda_i^e \,, \tag{3.51}$$

where

$$\Lambda_i^\pm \;=\; \frac{1}{2}\left(1 \pm \left(i\beta_i \gamma_4 \hat{\not{p}} + \alpha_i \gamma_4\right)\right), \tag{3.52}$$

and $E_i = \sqrt{\vec{p}^2 A_i^2 + B_i^2}$, $\alpha_i = B_i/E_i$, $\beta_i = |\vec{p}|A_i/E_i$ and $i = a, b, c$. Neglecting the p_4-dependence in the dressing-functions and absorbing C_a and C_b by rescaling E_a, E_b and ϕ_i correspondingly[7], we assume that no pairing between quasiparticles and anti-quasiparticles takes place. This reduces Eq.(3.50) to

$$\left(-i\omega C_c - E_c\right) \gamma_4 \Lambda_c^+ \;\approx\; \left(-i\omega - E_a\right) \gamma_4 \Lambda_a^+ - \phi^- \frac{1}{-i\omega^* + E_b} \Lambda_b^- \gamma_4 \phi^+ \,, \tag{3.53}$$

which is exact in the chiral limit and produces the results in Eq.(3.28). Note that it can also be justified, at least in leading order, in a ϕ^2/μ^2 expansion. Evaluating the roots of the right-hand side, we find the dispersion relation

$$\begin{aligned} -ip_4 \;=\; & \frac{E_a - E_b}{2} \pm \Bigg(\left(\frac{E_a + E_b}{2} - \mu\right)^2 + \phi_A^2 - \phi_B^2 - \phi_C^2 + \phi_D^2 \\ & + 2i\phi_C \left(\beta_2 \phi_A - \alpha_2 i \phi_B\right) - 2\phi_D \left(\alpha_2 \phi_A + \beta_2 i \phi_B\right) \Bigg)^{\frac{1}{2}} , \end{aligned} \tag{3.54}$$

where we have made use of the fact that ϕ_A and ϕ_D are real and ϕ_B and ϕ_C are imaginary at $p_4 = 0$ (see the discussion in the last section). Noting that $\alpha_i^2 + \beta_i^2 = 1$, the above expression suggests to introduce gap functions, which are transformed accordingly:

$$\tilde{\phi}_A = \beta_2 \phi_A - \alpha_2 i \phi_B \,, \qquad i\tilde{\phi}_B = \alpha_2 \phi_A + \beta_2 i \phi_B \,. \tag{3.55}$$

This transformation depends on the mass parameter of the quasiparticle, which makes evident that the existence of the functions ϕ_B and ϕ_D allows different energy gaps for

[7] In principle, we also need to rescale μ, formally leading to two chemical potentials. This introduces no further complication in principle but is neglected for the sake of simplicity.

quasiparticles with different masses. In terms of the 'rotated' gap functions $\tilde{\phi}_A$ and $\tilde{\phi}_B$ we obtain

$$-ip_4 = \frac{E_a - E_b}{2} \pm \left((\frac{E_a + E_b}{2} - \mu)^2 + (\tilde{\phi}_A + i\phi_C)^2 + (\phi_D - i\tilde{\phi}_B)^2\right)^{\frac{1}{2}} . \quad (3.56)$$

In analogy to the situation in the chiral limit, we arrive now at a simple interpretation: One has a chirally symmetric pairing via $\tilde{\phi}_A + i\phi_C$ and a chirality breaking pairing through $\phi_D - i\tilde{\phi}_B$. For anti-quasiparticle pairing $\tilde{\phi}_A$ and $\tilde{\phi}_B$ simply change sign. In the chiral limit we then recover $|\phi^{\pm}| = |\phi_A \pm i\phi_C|$ and $\phi_B = \phi_D = 0$.

3.4.3 Numerical results

As described above, the quark propagator is highly non-trivial. The Dirac structure of the self-energies and gap functions is given by four self-consistently determined functions, respectively, which are in addition functions of $|\vec{p}|$ and p_4. In accordance with the aim of our investigation, namely to investigate the phenomenological importance of the strange quark current mass, we mainly restrict ourself to the presentation of results at $p_4 = 0$ and some values of $|\vec{p}|$. This will also turn out to be sufficient to demonstrate the important differences of our results as compared to corresponding ones obtained in NJL-type models. As already mentioned we include self-energy effects, which have been analyzed so far only in the weak coupling regime [42]. For the dependence on $|\vec{p}|$ we refer to the results for the chiral limit in section 3.3. The role of a non-trivial p_4-dependence will reappear in chapter 4.

The following results will be presented for the couplings discussed above, $\alpha_I(k)$ and $\alpha_{II}(k)$. As explained we consider them as the limiting cases, which are allowed by the uncertainty within investigations of infrared QCD. We will see that gap functions and Fermi momenta are quite insensitive to the coupling used.

Fermi momenta

In Fig. 3.9 the results for the Fermi momenta at a chemical potential of $\mu = 400\,\mathrm{MeV}$ as a function of the renormalized strange quark current mass $m_s(\nu)$ at a renormalization scale $\nu = 2\,\mathrm{GeV}$ are presented. For the CFL phase these are of course only plotted below the critical value of the strange quark current mass. (For the definitions of the different components see section 3.4.1.) Above this critical value the 2SC phase is energetically preferred, and the three different Fermi momenta of the 2SC phase are shown: For the gapped red and green, up- and down-quarks and the ungapped blue up- and down-quarks, which are both independent of the strange quark mass and for the decoupled strange quarks

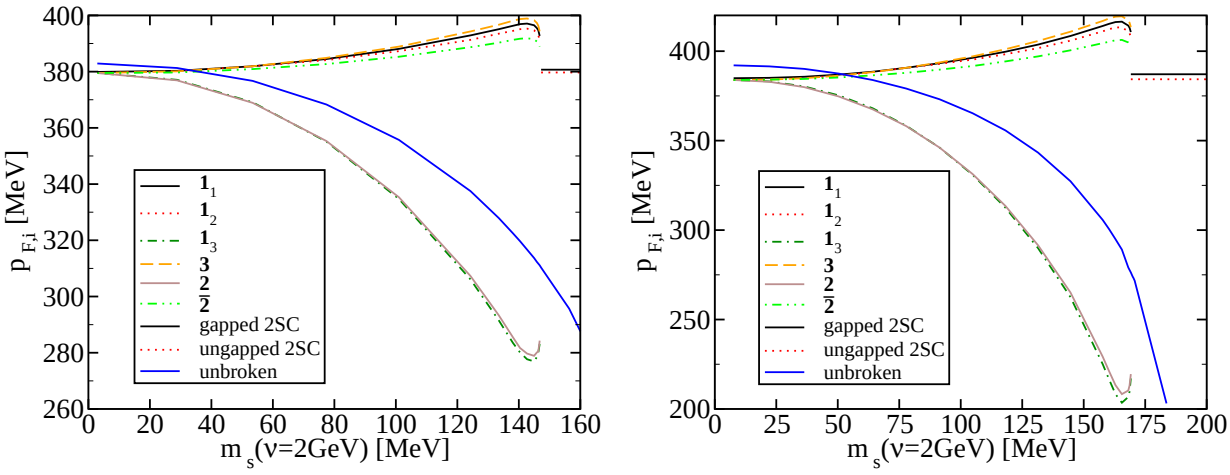

Figure 3.9: Fermi momenta in different channels (see text) at $\mu = 400\,\mathrm{MeV}$ for the coupling $\alpha_I(k)$ (left) and $\alpha_{II}(k)$ (right).

in the unbroken phase (which is also displayed below the critical of the strange-quark mass $m_{s,critical}$).

In the CFL phase the Fermi momenta are not monotonous functions of m_s. This is due to the behavior of the vector self-energies and not visible in the mass functions, *cf.* Fig. 3.10.

Mass functions

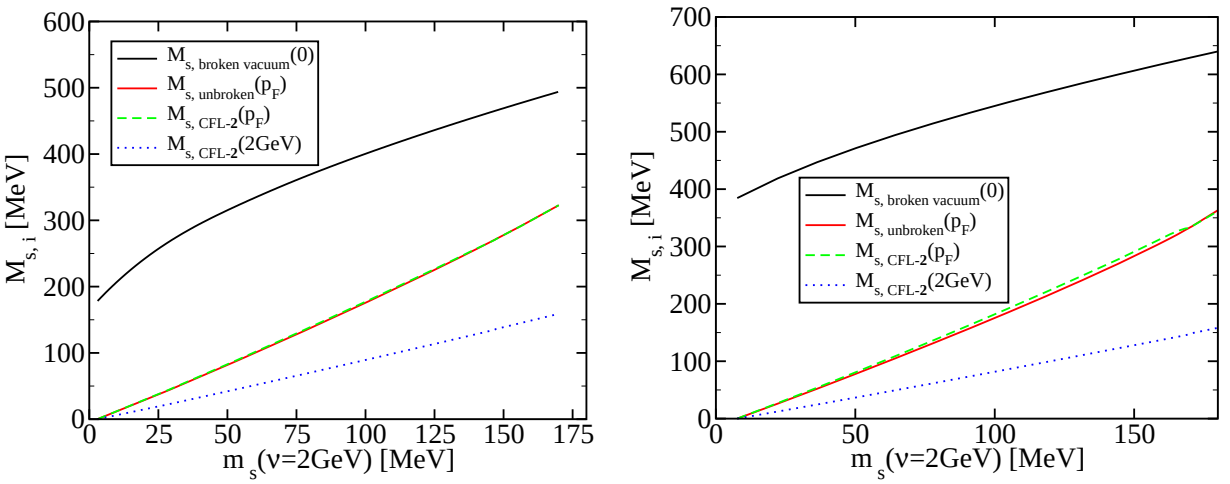

Figure 3.10: Mass functions at different values of three-momentum (see text) as function of the renormalized strange quark mass at a chemical potential of $\mu = 400\,\mathrm{MeV}$ for the coupling $\alpha_I(k)$ (left) and $\alpha_{II}(k)$ (right).

As a function of m_s, we display in Fig. 3.10 the results for the constituent quark mass function in the vacuum at vanishing momenta $M_{s,broken\,vacuum}(0)$, as well as the quark mass function in the unbroken phase $M_{s,unbroken}(p_F)$ and the doublet channel in the CFL phase $M_{s,CFL-\mathbf{2}}(p_F)$, both at their respective Fermi momenta and for a chemical potential of $\mu = 400\,\mathrm{MeV}$. Furthermore, the quark mass function in the unbroken phase $M_{s,unbroken}(2\,\mathrm{GeV})$ for the same chemical potential at the renormalization scale $\nu = 2\,\mathrm{GeV}$ is given.

Although the constituent quark mass in the vacuum $M_{s,broken\,vacuum}(0)$ is very sensitive to the choice of the coupling, especially for small renormalized strange quark masses, the mass functions at finite chemical potentials are not. As explained in the previous section, this is due to the medium modification of the coupling, which also leads to significantly smaller mass values at the Fermi surface. Note furthermore that the values of the mass functions at the Fermi surface in the chirally broken phase and the CFL phase are very close to each other. This leads to the conclusion that the dynamics near the Fermi surface, where gapped and ungapped propagators strongly differ, are not directly relevant for the dynamical mass generation. As expected, the mass functions at the renormalization scale are comparable to the values in the chirally broken vacuum, which confirms that ν is already sufficiently above the scale of dynamical mass generation and the Fermi energy.

Dependence of the gap functions on m_s

We now present results for the gap functions at the Fermi surface, *i.e.* at $p_4 = 0$, and selected values of the three-momentum. The renormalization-point independent gap functions (3.40) for the triplet, doublet and anti-doublet channel (*cf.* Eq.(3.49)) are evaluated at their corresponding Fermi momentum (see section 3.4.1). The functions $\phi_{i,\mathbf{1}(ud)}$, $\phi_{i,\mathbf{1}(uds)}$ and $\phi_{i,\mathbf{1}(bs)}$, corresponding to M_2, M_4 and M_3, given in the Appendix E.2, are evaluated at $(p_{F,\mathbf{1}_1} + p_{F,\mathbf{1}_2})/2$, $(p_{F,\mathbf{1}_1} + p_{F,\mathbf{1}_2} + 2p_{F,\mathbf{1}_3})/4$ and $p_{F,\mathbf{1}_3}$, respectively. Due to this, the functions are evaluated at momenta corresponding to the pairing quasiparticles. This also allows to recover the results at the Fermi surface for the CFL phase in the chiral limit. The corresponding numerical results are shown in Fig. 3.11 for the coupling $\alpha_I(k)$ and in Fig. 3.12 for the coupling $\alpha_{II}(k)$. Note again that due to the phase choice the gap functions $\phi_{A,i}$ and $\phi_{D,i}$ are real and $\phi_{B,i}$ and $\phi_{C,i}$ imaginary at $p_4 = 0$.

All functions, apart from $\phi_{i,\mathbf{1}(bs)}$, evolve towards the corresponding 2SC solution. However, $\phi_{i,\mathbf{1}(bs)}$ already shows that the transition must be first order. Furthermore, for the gap functions $\phi_{i,\mathbf{1}(ud)}$ and $\phi_{i,\mathbf{3}}$, describing non-strange pairing, ϕ_B and ϕ_D vanish, as expected. Finally, we see for the other gap functions, relevant to strange pairing, that ϕ_B is most varying and ϕ_D is non-vanishing, which is in line with the interpretation of the

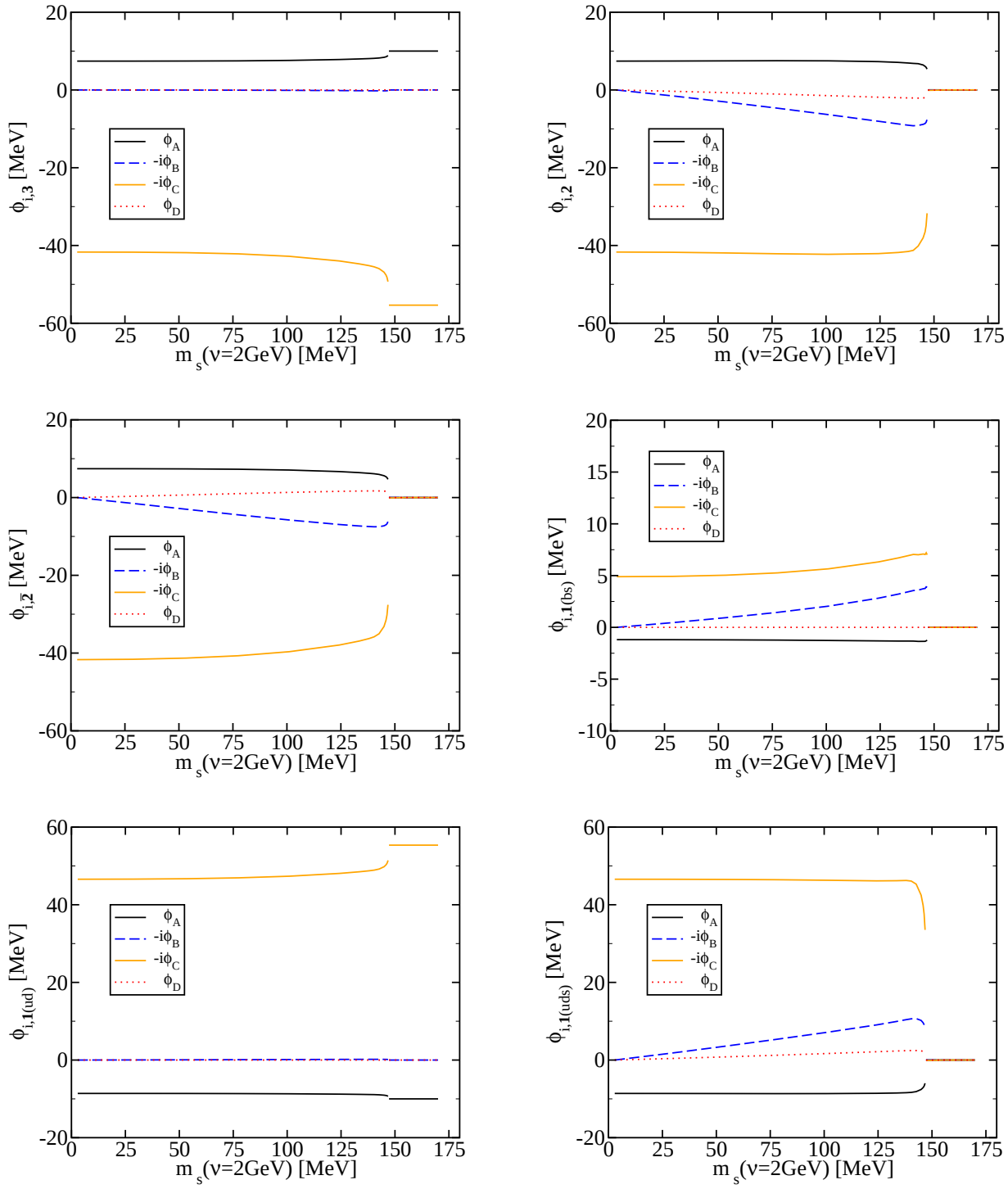

Figure 3.11: Gap functions at selected values of the three-momentum for different channels (see text) as a function of the renormalized strange-quark mass at a chemical potential of $\mu = 400\,\mathrm{MeV}$ and for the coupling $\alpha_I(k)$.

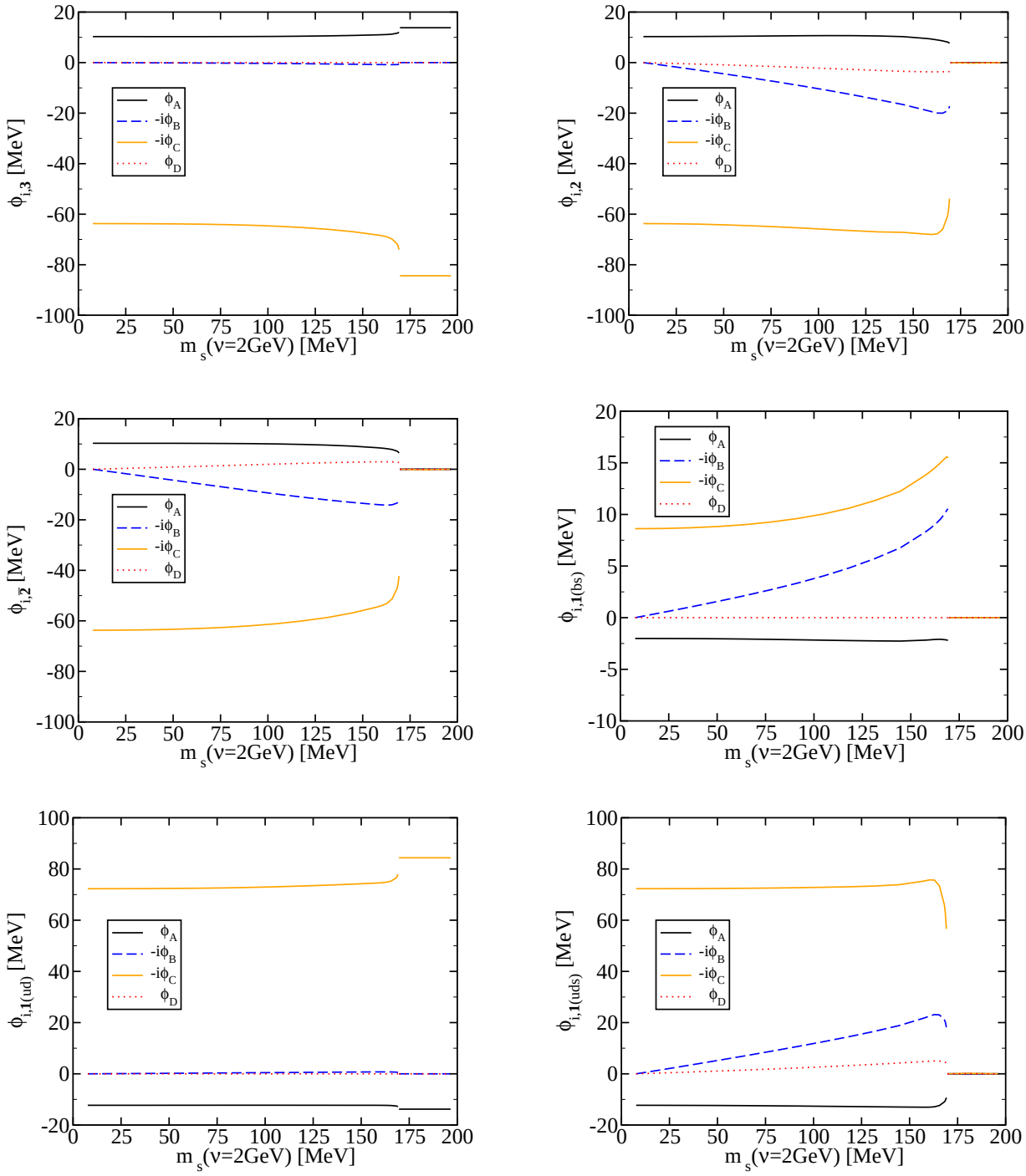

Figure 3.12: Gap functions at selected values of the three-momentum for different channels (see text) as function of the renormalized strange-quark mass at a chemical potential of $\mu = 400\,\mathrm{MeV}$ and for the coupling $\alpha_{II}(k)$.

gap functions given in section 3.4.2. It is again obvious that the sensitivity of the gap functions on the used coupling is much weaker than those of the mass functions.

Dependence of mass functions on the chemical potential μ

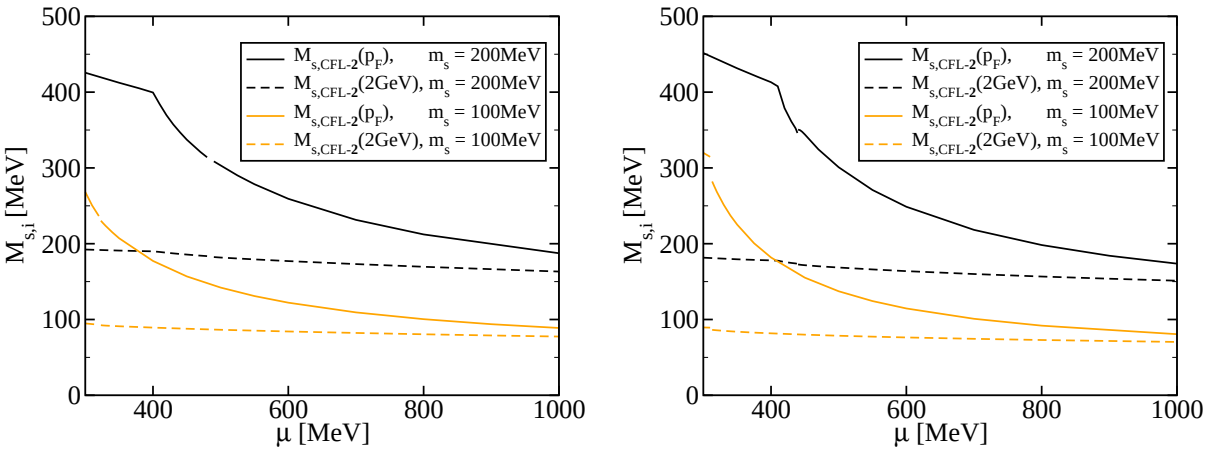

Figure 3.13: Mass functions at the Fermi surface and at a renormalization scale $\nu = 2\,\mathrm{GeV}$ for fixed renormalized strange quark mass in the vacuum as function of the chemical potential for the coupling $\alpha_I(k)$ (left) and $\alpha_{II}(k)$ (right).

We proceed by discussing the dependence on the chemical potential and treat the case of the mass functions first. Fig. 3.13 shows these mass functions in the doublet channel for two different renormalized strange-quark current masses, evaluated at the Fermi momentum and at the renormalization scale, respectively.

For small enough chemical potentials, the 2SC phase is preferred and the doublet channel corresponds to decoupled strange quarks in the truncation used. Depending on the value of the renormalized strange quark mass, the strange quarks may not condense for small enough chemical potential, *i.e.* not develop a Fermi surface. This can be seen from Fig. 3.13 for a renormalized strange-quark mass of $m_s = 200\,\mathrm{MeV}$. In this case, we evaluate the mass function at vanishing momentum and the onset of strange quark condensation is reflected as a kink in the curves. With rising chemical potential, the system undergoes a phase transition into the CFL phase. This effects the value of the mass function on the Fermi surface only slightly and is shown as a gap in the plots. For the coupling $\alpha_{II}(k)$ at $m_s = 100\,\mathrm{MeV}$ we find a direct transition of non-condensed strange quarks into the CFL phase.

The values of the mass functions at the renormalization scale show only a slight dependence on the chemical potential and are comparable to those in the chirally broken

vacuum, which again reflects the fact that the renormalization scale is well above the dynamical chiral symmetry breaking scale and the chemical potential. On the other hand, the values of the mass functions at the Fermi surface already at a chemical potential of $\mu = 1\,\mathrm{GeV}$ are close to their values at the renormalization scale. As a result, dynamical chiral breaking is suppressed and the mass function is only weakly dependent on the momentum below the renormalization scale.

Dependence of gap functions on the chemical potential

For completeness we also present results for the dependence of the gap functions on the chemical potential. In Fig. 3.14 we show the results for the gap functions in the CFL phase at a renormalized strange-quark mass of $m_s(\nu = 2\,\mathrm{GeV}) = 200\,\mathrm{MeV}$ and for the coupling $\alpha_I(k)$. As described above, the 2SC phase is preferred for smaller chemical potentials and we find again a visible jump in the $\phi_{i,\mathbf{1}(ud)}$ functions at a certain chemical potential. The gap functions in the CFL phase are remarkably insensitive in the chemical potential. Only the ϕ_B and ϕ_D functions evolve towards zero, which again reflects that the relevant values of the mass functions also become smaller.

Pressure difference and critical strange-quark mass

We now turn to the main result of this investigation: The determination of the critical value of the strange-quark current mass. Above this mass the Fermi surfaces are so far separated that pairing of up and down quarks with strange quarks is no longer energetically preferred. Based on the CJT-formalism we determine the pressure difference of CFL and 2SC using Eq.(2.98). The results as a function of the renormalized strange-quark current mass for different chemical potentials and for the couplings employed is shown in Fig. 3.15. One sees, as expected, that for small masses the CFL phase is preferred, and that there is a critical value of the strange-quark mass where the CFL phase becomes energetically disfavored.

We would like to emphasize, that we are no longer able to find a solution for the CFL phase in case the 2SC phase becomes favored. This is considered as a consequence of the numerical method to solve the truncated DSE being the functional derivative of the truncated CJT action. It turns out that we always only find the global minimum of the CJT action as long as the local minimum is not protected by a higher symmetry. The latter is the case for the 2SC phase, if the CFL one is preferred. Nevertheless we can judge from the behavior of the gap functions that the transition is first order.

In Fig. 3.16 the results for the critical value of the renormalized strange-quark mass as a function of the chemical potential are given and compared to the range of the physical

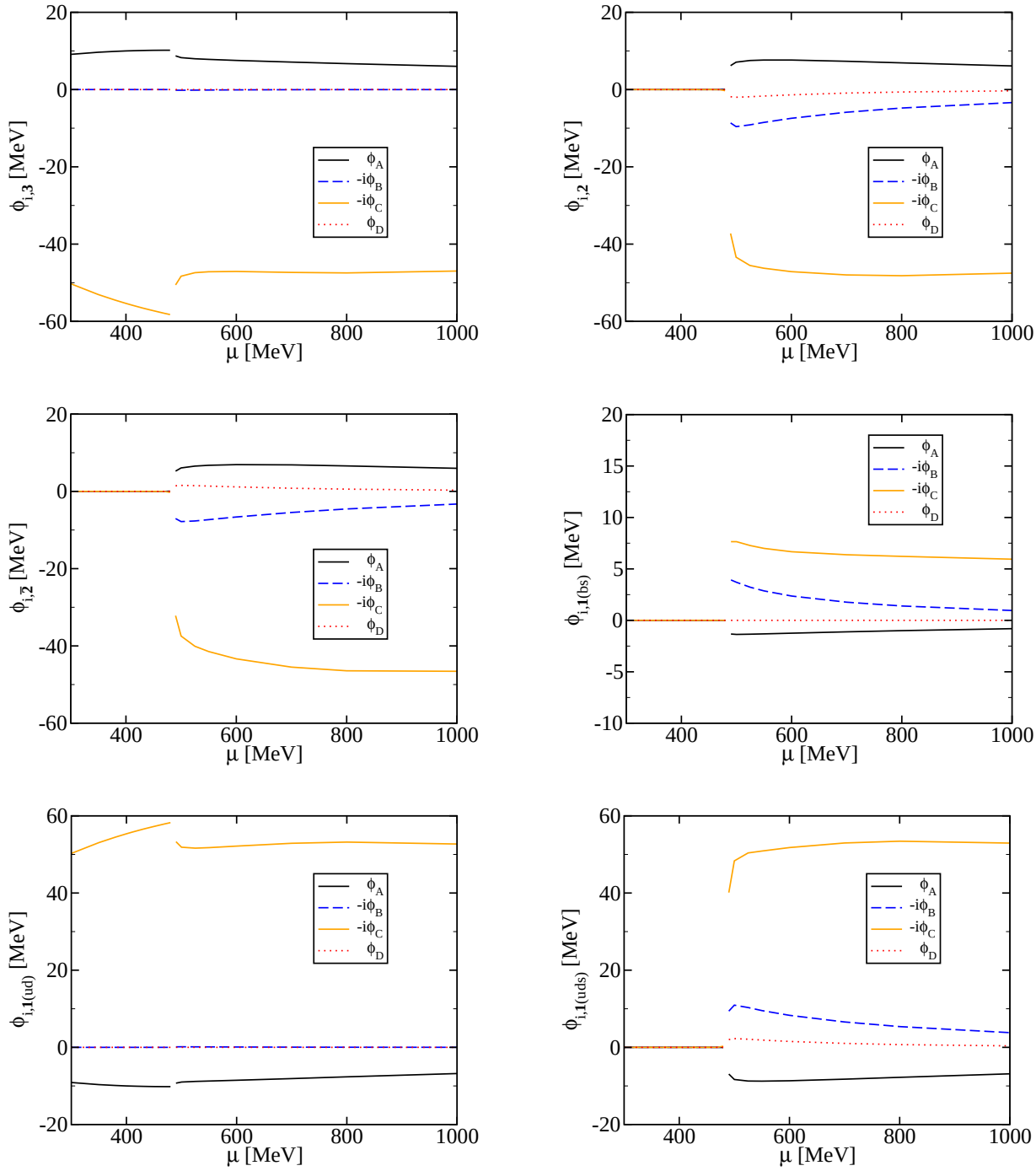

Figure 3.14: Gap functions on the Fermi surface at $m_s(\nu = 2\,\mathrm{GeV}) = 200\,\mathrm{MeV}$ for different channels (see text) as a function of chemical potential for the coupling $\alpha_I(k)$.

strange-quark current mass as determined by the particle data group [113]. (As stated above, the difference between this mass in the MOM and the $\overline{\mathrm{MS}}$ regularization scheme is negligible compared to the experimental uncertainty.) As can be seen, the approach

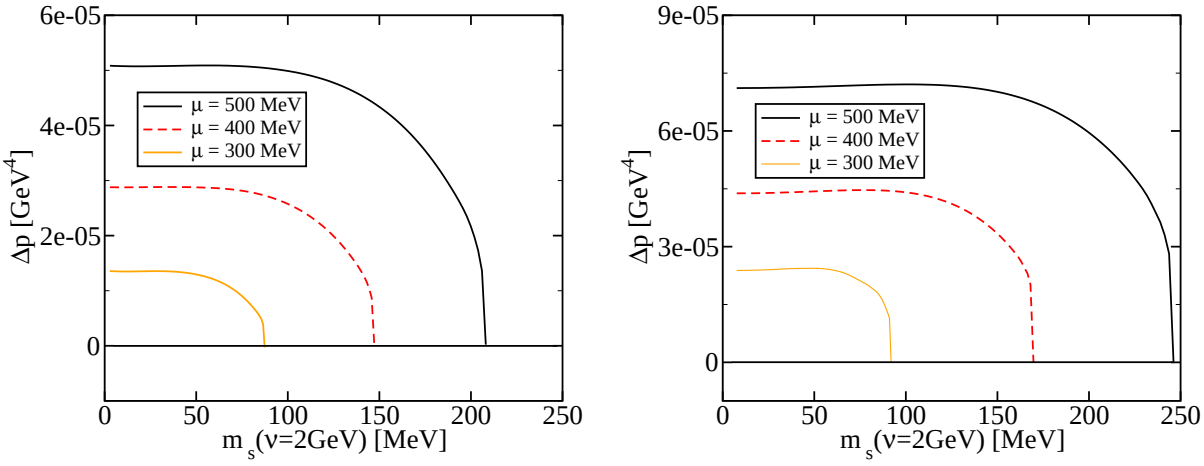

Figure 3.15: Pressure difference between 2SC and CFL phase as function of the renormalized strange quark mass at chemical potentials of $\mu = 300\,\mathrm{MeV}, 400\,\mathrm{MeV}, 500\,\mathrm{MeV}$ for the coupling $\alpha_I(k)$ (left) and $\alpha_{II}(k)$ (right).

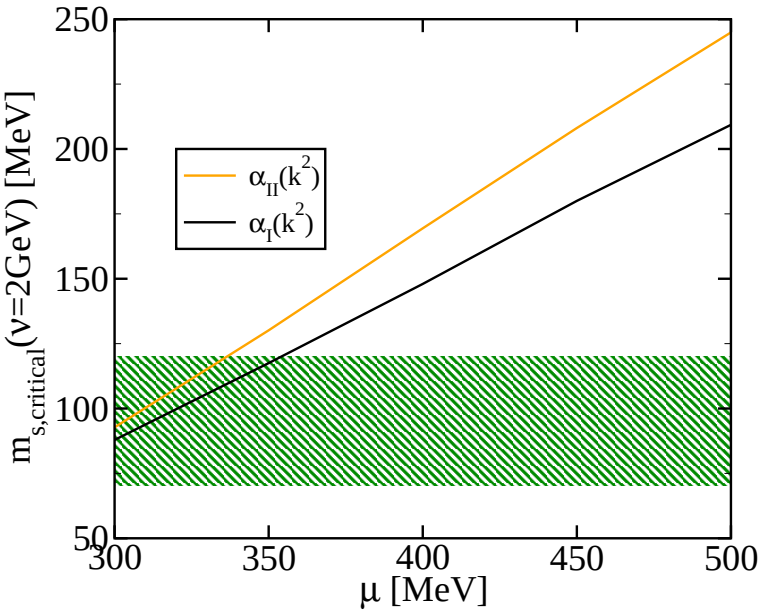

Figure 3.16: Critical renormalized strange-quark mass as a function of the chemical potential for the couplings $\alpha_I(k)$ and $\alpha_{II}(k)$ and the range stated by the particle data group [113] (shaded band).

taken here predicts that the physical strange-quark current mass is very likely too small for allowing a 2SC phase at zero temperature for any chemical potential. This result is remarkably stable against the variation of the running coupling $\alpha_s(k)$.

3.4.4 Conclusions

We have studied the quark propagator in the 2SC and CFL phase at zero temperature for different values of the strange-quark current mass employing only a truncation on the level of the qDSE, not on the parameterization of its solution. Due to the medium modification of the interaction we find the 2SC phase to be disfavored at any physically relevant chemical potential for the physical value of the strange-quark current mass. This result is robust against variation of the running of the strong coupling in the infrared within the given uncertainties. Since the CFL phase is only mildly influenced by neutrality conditions we expect the result to hold even when neutrality is required. The critical value of the strange-quark current mass should then be similar or even slightly larger. This will be explored in the next section.

Given this results a further investigation of the CFL phase by the inclusion of the Meissner effect and Goldstone-boson contributions is of interest, to study their effect on the value of the gap function. This will be subject of section 5.3.

3.5 Neutral quark matter

After our analysis of color-flavor unlocking, we also want to incorporate neutrality conditions. As the CFL phase in the chiral limit is neutral due to the residual symmetry, we do not expect it to be influenced strongly. In contrast, the 2SC phase for two flavors is far from being electrically neutral. Therefore, as known from investigations in NJL-type models [40, 111, 114, 115], the region of the 2SC phase is strongly affected by neutrality constraints.

The phenomenology when varying the strange-quark mass is shown in Fig. 3.17. In the chiral limit, all quarks have the same Fermi momentum and due to its connection by Luttinger's theorem also have the same density. With increasing strange-quark mass, the Fermi momentum of the strange quarks is lowered $p_{F,s} \approx \mu - \frac{M_s^2}{2\mu}$. To first approximation[8] the positive electrical charge of the up-quarks is then compensated by additional down quarks with Fermi momentum $p_{F,d} \approx \mu + \frac{M_s^2}{2\mu}$. This is also connected to a partial symmetry breaking of the full CFL symmetry. Eventually some channels get ungapped quasiparticle excitations, being referred to as the gapless CFL (gCFL) phase. At some stage pairing of down- and strange-quarks is no longer favorable and all remaining Cooper pairs involve an up-quark, which is characterizing the uSC phase. After this, the pairing of up- and strange-quarks might break and we may find an intermediate regime of the 2SC phase. Finally all

[8]The line of reasoning is strongly simplified and concentrated on the ungapped phase. If color-superconducting phases are energetically preferred, the Fermi surfaces rearrange in those phases.

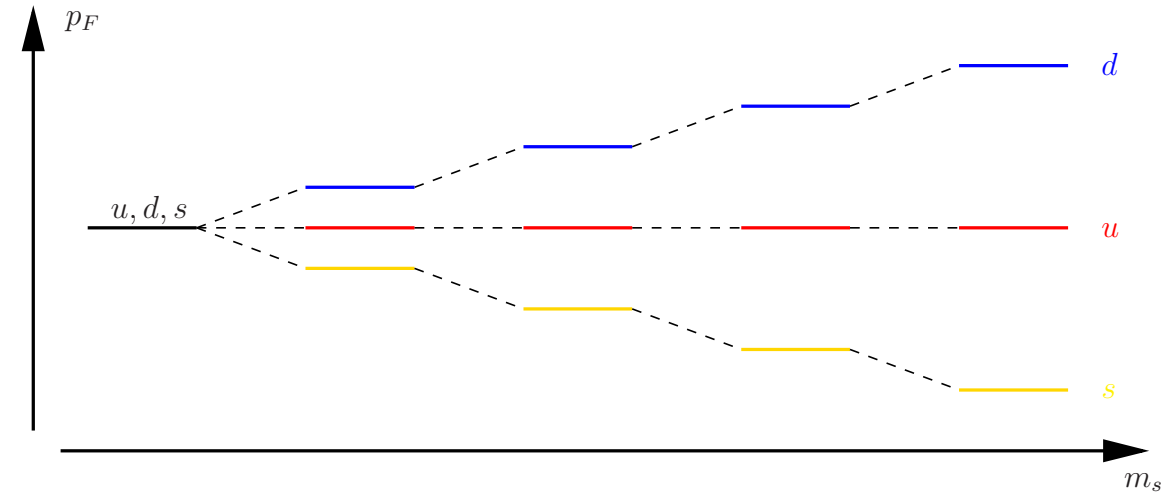

phase:	CFL	gCFL	uSC	2SC	unbroken
sym.:	$SU_{c+V}(3)$	$U_{c+V}(1) \otimes U_{c+V}(1)$		$\mathcal{G}_{2SC}$	$SU_c(3) \otimes SU_V(3)$

Figure 3.17: Schematic dependence of the phase structure on the strange-quark mass when considering neutrality constraints. Shown are the Fermi momenta in the ungapped phase, the energetically preferred phase and the residual symmetries in this phase.

Fermi surfaces are far separated and the ground state becomes unbroken. Ungapped uSC and 2SC phases have not been observed in our calculations.

3.5.1 Neutrality conditions and β-equilibrium for the CFL phase

Color neutrality

As has been discussed in section 2.3.2, we need to allow for constant values of A_4, whose DSE reduces to

$$\frac{Z_2}{2} \int \frac{d^3p}{(2\pi)^3} \int \frac{dp_4}{2\pi} \mathrm{Tr}_{D,c,f,NG} \left(\mathcal{S}(p) \Gamma^{(0)a}_{NG4} \right) \quad = \quad 0 \,. \tag{3.57}$$

As A_4 is anti-Hermitian within our conventions, we define by

$$\mu_C \quad \stackrel{\text{def}}{=} \quad \sum_a \mu_a \lambda^a \quad \stackrel{\text{def}}{=} \quad -i \frac{Z_{1F}}{Z_2} g A_4 \tag{3.58}$$

the effective color chemical potentials. The color chemical potentials are then adjusted to obtain color neutrality.

Electrical neutrality and β-equilibrium

Electrical neutrality within QCD only is meaningless. We need to include the electro-weak interaction and its particle content. The conserved electrical charge is then adjusted by its Lagrange multiplier μ_Q and the chemical potentials for the quarks are then, including the color chemical potentials, given by

$$\hat{\mu}_{ab,ij} \quad = \quad \mu\,\delta_{ab}\delta_{ij} + \sum_d \mu_d \lambda^d_{ab}\delta_{ij} + \mu_Q\,\delta_{ab}Q_{ij}\,, \tag{3.59}$$

where $a,b = 1,2,3$ are color and $i,j = 1,2,3$ flavor indices. The charges of the quark flavors are encoded by the matrix $Q = \mathrm{diag}_f\left(\frac{2}{3},-\frac{1}{3},-\frac{1}{3}\right) = \frac{1}{2}\tau^3 + \frac{1}{2\sqrt{3}}\tau^8$. Therefore the 'bare' inverse quark propagator takes the form

$$\mathcal{S}_0^{-1}(p) \quad = \quad \begin{pmatrix} -i\vec{p}_i\gamma_i - i(p_4 + i\hat{\mu})\gamma_4 + m & 0 \\ 0 & -i\vec{p}_i\gamma_i - i(p_4 - i\hat{\mu}^T)\gamma_4 + m \end{pmatrix}. \tag{3.60}$$

Compared to the strong interaction, we can consider leptons as non-interacting particles. Only the electrons will then be relevant, as the charge chemical potential will not or only slightly exceed the mass of other leptons. Therefore only electrons are present in the phase. With charge -1, their charge chemical potential is $\mu_e = -\mu_Q$. This also means

$$\mu_d \quad = \quad \mu_s \quad = \quad \mu_u + \mu_e \tag{3.61}$$

for each color, which is usually referred to as β-equilibrium. We consider the electrons as massless and their electrical charge density given by $\rho_{el} = \frac{1}{3\pi^2}\mu_Q^3$. Electrical neutrality then enforces

$$\rho_Q(x) \quad = \quad Z_2 \int \frac{d^3p}{(2\pi)^3} \int \frac{dp_4}{2\pi}\, \mathrm{Tr}_{D,c,f}\left(QS^+(p)\gamma_4\right) + \frac{1}{3\pi^2}\mu_Q^3 \quad = \quad 0\,. \tag{3.62}$$

Parameterization of the CFL phase

As in section 3.4, a finite strange-quark mass leads to a partial symmetry breaking of the CFL symmetry through the mass matrix $m = \frac{m_s}{3}\left(\mathbb{1} - \sqrt{3}\tau^8\right)$. If in addition $\mu_Q \neq 0$ due to the neutrality constraint, we can directly conclude from its generator $Q = \frac{1}{2}\tau^3 + \frac{1}{2\sqrt{3}}\tau^8$

$$SU_{c+V}(3) \overset{m_s\neq 0}{\longrightarrow} SU_{c+V}(2)\otimes U_{c+V}(1) \overset{\mu_Q\neq 0}{\longrightarrow} U_{c+V}(1)\otimes U_{c+V}(1)\,, \tag{3.63}$$

where the residual symmetry is generated by $\tau_3 - \lambda_3^T$ and $\tau_8 - \lambda_8^T$. Those form a Cartan subalgebra of the Lie algebra of $SU_{c+V}(3)$, *i.e.* a maximum set of commuting matrices. The most general choice of a basis $\{P_i\}$ and $\{M_i\}$ constructed as alluded in section 3.4 is given in Appendix E.3. It consists of 15 matrices for $\{P_i\}$ and $\{M_i\}$, respectively.

To preserve the remaining symmetry, we are only allowed to vary the color chemical potentials μ_3 and μ_8 and the question is, whether this is enough to fulfill the requirement $\rho^a(x) = 0$ for $a = 1, \ldots, 8$. To clarify this, we define the color-charge density matrix $\hat{\rho}$ by

$$\hat{\rho} \;=\; \int \frac{d^3p}{(2\pi)^3} \int \frac{dp_4}{2\pi} \, \mathrm{Tr}_{D,f} \left(S^+(p)\gamma_4 \right) . \tag{3.64}$$

This 3×3 matrix is symmetric and can be interpreted as the matrix of color-charges in the basis $\{u, d, s\}$. With its help the condition in Eq.(3.57) is reduced to

$$\mathrm{Tr}_c \left(\hat{\rho} \lambda^a \right) \;=\; 0 \, . \tag{3.65}$$

As the Gell-Mann matrices form an orthogonal basis, we conclude that we need to adjust $\{\mu_a\}$ to get

$$\hat{\rho} \;=\; \frac{\rho}{3} \mathbb{1} \, , \tag{3.66}$$

with ρ then being the quark number density.

Varying μ_3 and μ_8, we will surely achieve the requirement in Eq.(3.65), if the matrix is diagonal. This is the case for all NJL-type investigations [40, 111, 114, 115]. However, this is a further truncation on the self-consistency in those models and enforced by hand. In general the matrix $\hat{\rho}$ is only symmetric, as we also consider the color-flavor structures $P_4, \ldots, P_9$. Therefore we need to consider all μ_a for $a = 1, \ldots, 8$ and the residual symmetry gets completely broken. The same arguments also hold if $\mu_Q = 0$, but $\mu_3 \neq 0$ or $\mu_8 \neq 0$.

Therefore we conclude, that a finite strange quark mass induces backgrounds fields that breaks the CFL symmetry completely and the CFL phase can no longer be defined by a residual symmetry. It can only be defined by a continuous solution of the ground state as a function of m_s that is CFL symmetric for $m_s = 0$.

Instead of introducing further color chemical potentials aside μ_3 and μ_8, we will estimate those as described below and choose μ_3 and μ_8 such that $\rho^3 = 0$ and $\rho^8 = 0$. This approach is similar to the truncation being done in NJL-type investigation and we could otherwise not constrain $\{P_i\}$ and $\{M_i\}$. The ansatz becomes self-consistent in the 2SC and uSC phase.

Estimating μ_a not in the Cartan subalgebra

Varying μ_3 and μ_8 only, we adjust the 3×3-dimensional real and positive charge-density matrix $\hat{\rho}$ to have equal diagonal elements and we define $\mathrm{Tr}\,(\hat{\rho}) = \frac{3}{\pi^2}\hat{p}_F^3$. The off-diagonal elements of $\hat{\rho}$ are strongly suppressed. After diagonalization we obtain $\tilde{\rho} = \mathrm{diag}_c(\tilde{\rho}_1, \tilde{\rho}_2, \tilde{\rho}_3) = D^\dagger \hat{\rho} D$ and, approximating the system by a free gas, we estimate $\tilde{\rho}_i = \frac{1}{\pi^2}\tilde{p}_i^3$. For a free gas

we would therefore need to choose $\Delta\tilde{\mu}_3 = \frac{1}{2}(\tilde{p}_2 - \tilde{p}_1)$ and $\Delta\tilde{\mu}_8 = \frac{1}{2\sqrt{3}}(2\tilde{p}_3 - \tilde{p}_1 - \tilde{p}_2)$ for the color chemical potentials in the new basis, in order to obtain a neutral phase. This will be used as an estimate of μ_a for $a \neq 3, 8$ after the transformation into the old color basis.

The eigenvalues of $\hat{\rho}$ can be estimated in an expansion in $\hat{\rho}_{ij} \ll \rho_{11}$ for $i \neq j$ and are given by $\hat{\rho}_{11}$ and $\hat{\rho}_{11} \pm \delta\hat{\rho}$, with $\delta\hat{\rho} = \sqrt{\hat{\rho}_{12}\hat{\rho}_{21} + \hat{\rho}_{23}\hat{\rho}_{32} + \hat{\rho}_{13}\hat{\rho}_{31}}$. The corresponding Fermi momenta $\tilde{p}_i$ are approximately given by $\hat{p}_F$ and $\hat{p}_F(1 \pm \frac{\delta\hat{\rho}}{3\hat{\rho}_{11}})$. Therefore we have after ordering the Fermi momenta: $\Delta\tilde{\mu}_3 \approx \frac{\delta\hat{\rho}}{3\hat{\rho}_{ii}}$ and $\Delta\tilde{\mu}_8 \approx 0$. As for a free gas we also suspect the chemical potentials to transform like $\tilde{\mu} = D^\dagger \hat{\mu} D$ with $DD^\dagger = \mathbb{1}$. Therefore $\|\Delta\tilde{\mu}\| = \|\tilde{\mu} - \mu\mathbb{1}\| = \|\hat{\mu} - \mu\mathbb{1}\| = \|\Delta\hat{\mu}\|$ for any matrix norm and we obtain

$$\mu_a \quad \lesssim \quad \|\Delta\tilde{\mu}\| \quad \approx \quad \frac{\delta\hat{\rho}}{3\hat{\rho}_{ii}}, \quad a \neq 3, 8\,. \tag{3.67}$$

We will come back to this estimate when discussing our numerical results for the chemical potentials.

3.5.2 Are there electrons in the CFL phase?

It has been argued that the color-neutral CFL phase is automatically electrical neutral [116]. Therfore $\mu_Q = 0$ and no electrons are allowed in the phase, which would have important consequences. The same result is also found in self-consistent NJL-type investigations [40, 115]. Since we find deviations, we first describe the reasoning:

Apart from the $SU_c(3) \otimes SU_V(3)$, we can also consider the electrical $U_Q(1)$ generated by Q. In the dynamical symmetry breakdown $SU_c(3) \otimes SU_V(3) \to U_{c+V}(1) \otimes U_{c+V}(1)$ also $U_Q(1)$ gets broken, however the phase is still symmetric under the so-called $U_{\tilde{Q}}(1)$ symmetry that is generated by

$$\begin{aligned} \tilde{Q} &= Q - \frac{1}{2}\lambda^3 - \frac{1}{2\sqrt{3}}\lambda^8 \\ &= \frac{1}{2}\left(\tau^3 - \lambda^{3T}\right) + \frac{1}{2\sqrt{3}}\left(\tau^8 - \lambda^{8T}\right)\,. \end{aligned} \tag{3.68}$$

In the basis $((r,u),(g,d),(b,s),(r,d),(g,u),(r,s),(b,u),(g,s),(b,d))$ used in Appendix E.3 the matrix $\tilde{Q}$ is diagonal and the quasiparticles carry the charges $(0,0,0,-1,1,-1,1,0,0)$, respectively. From this it has been concluded that $\rho_{\tilde{Q}} = 0$ in the fully gapped CFL phase, which then is a $\tilde{Q}$-insulator [117]. The quark contribution to the thermodynamical potential $p_q[T,\mu,\mu_3,\mu_8,\mu_Q]$ would then be invariant under

$$p_q[T,\mu,\mu_3,\mu_8,\mu_Q] \;=\; p_q[T,\mu,\mu_3 - \frac{1}{2}\mu_{\tilde{Q}}, \mu_8 - \frac{1}{2\sqrt{3}}\mu_{\tilde{Q}}, \mu_Q + \mu_{\tilde{Q}}]\,. \tag{3.69}$$

Neglecting the leptons, we therefore have an array of degenerate ground states under varying $\mu_{\tilde{Q}}$. The ground state within this array is chosen by the minimum of the electronic (or leptonic) contribution to the thermodynamical potential, $p_{el}[T,\mu,\mu_3,\mu_8,\mu_Q] = \frac{1}{12\pi^2}\mu_Q^4$. We would therefore conclude $\mu_Q = 0$, which means that no electrons are allowed in the system.

The whole argument is therefore based on the assumption $\rho_{\tilde{Q}} = 0$. Considering the form of the charge $\tilde{Q}$, we can concentrate on the separate pairing of $\{(r,d),(g,u)\}$ and $\{(r,s),(b,u)\}$, respectively, as only those carry non-vanishing $\tilde{Q}$-charge (see Appendix E.3). The requirement $\rho_{\tilde{Q}} = 0$ is therefore equivalent to the statement, that two pairing fermion species with different chemical potentials have the same density in a fully gapped phase. We will now show that this is true for energy-independent gap functions, which are used in NJL-type models and emphasize that energy-dependent gap functions, as in our framework, do not require this.

For the case of two Fermion species a, b we neglect normal self-energies and consider

$$\begin{pmatrix} S_a^+ & & & T_a^- \\ & S_b^+ & T_b^- & \\ & T_a^+ & S_a^- & \\ T_b^+ & & & S_b^- \end{pmatrix}^{-1} = \begin{pmatrix} -i\not{p}+\mu_a\gamma_4 & & & -\gamma_5\Delta^* \\ & -i\not{p}+\mu_b\gamma_4 & -\gamma_5\Delta^* & \\ & \gamma_5\Delta & -i\not{p}-\mu_a\gamma_4 & \\ \gamma_5\Delta & & & -i\not{p}-\mu_b\gamma_4 \end{pmatrix}, \tag{3.70}$$

giving

$$S_{a/b}^{+\,-1} = -i\not{p}+\mu_{a/b}\gamma_4 - |\Delta|^2\frac{i\not{p}+\mu_{b/a}\gamma_4}{(p_4-i\mu_{b/a})^2+\vec{p}^2}\,. \tag{3.71}$$

With the definition of $D_{a/b} = (p_4+i\mu_{a/b})^2+\vec{p}^2$ and $\omega_{a/b} = p_4+i\mu_{a/b}$, the density $\rho_{a/b}(x)$ of the fermions species a and b turns out to be

$$\begin{aligned}\rho_{a/b}(x) &= \int\frac{d^3p}{(2\pi)^3}\int\frac{dp_4}{2\pi}\,\mathrm{Tr}_D\left(S_{a/b}^+(p)\gamma_4\right) \\ &= \int\frac{d^3p}{(2\pi)^3}\int\frac{dp_4}{2\pi}\,\frac{4iD_{b/a}^*\left(\omega_{a/b}D_{b/a}^*+|\Delta|^2\omega_{b/a}^*\right)}{\left(\omega_{a/b}D_{b/a}^*+\omega_{b/a}^*|\Delta|^2\right)^2+\vec{p}^2\left(D_{b/a}^*+|\Delta|^2\right)^2}\,.\end{aligned} \tag{3.72}$$

For an energy independent gap function Δ, we can perform the energy integral and obtain for $|\mu_a-\mu_b|<2|\Delta|$

$$\rho_{a/b}(x) = \int\frac{d^3p}{(2\pi)^3}\left(\frac{(\bar{\mu}-p)}{\sqrt{(p-\bar{\mu})^2+|\Delta|^2}}+\frac{(\bar{\mu}+p)}{\sqrt{(p+\bar{\mu})^2+|\Delta|^2}}\right), \tag{3.73}$$

where $\bar{\mu} = \frac{1}{2}(\mu_a + \mu_b)$. The momentum integral is finite for a sufficiently fast vanishing gap function and the result shows that for small differences in the chemical potential, the densities of both particle species are the same. This has also been found in [116]. For larger splittings, *i.e.* $|\mu_a - \mu_b| > 2|\Delta|$, gapless modes emerge, which will be discussed below.

If we have a non-trivial energy dependence, this argument does no longer hold, as can directly be tested by an ansatz. This effect is therefore connected to a finite width in the spectral function of the quasiparticles, which is included in our investigations and which will be discussed in section 4.4.

Gapless pairing

As a by-product of the previous discussion, we can also discuss gapless pairing. For illustration we will again use the simple parameterization in Eq.(3.70). If the difference in the chemical potentials $\delta\mu = \mu_a - \mu_b$ exceeds the value $2|\Delta|$, the gap in the excitation spectrum vanishes and we find gapless modes even for $\Delta \neq 0$. Their dispersion relation are given by $\det S^{+\,-1}_{a/b} = 0$, which are the zeros of the denominator of the integrand in Eq.(3.72). For the CFL phase, gapless pairing might occur in some channels [118] and has been found as the preferred homogeneous ground state in NJL-type investigations [119, 120, 121, 122] due to neutrality constraints. However they are expected to be unstable, as the Meissner masses become imaginary [123, 124, 125]. This finding led to a broad discussion of the appearance of inhomogeneous phases [126, 127, 128, 129]. We will postpone this subject to future investigations and consider homogeneous phases only. The problem of imaginary Meissner masses in the gap equation has not been addressed yet and does not appear in our truncation either. A suited truncation to study this back-reaction onto the pairing pattern is discussed in section 5.3.

For $|\delta\mu| > 2|\Delta|$, gapless modes create a breached pairing region [130]. For the occupation numbers implicitly given in Eq.(3.73) and choosing $\mu_a < \mu_b$, we get

$$n_{a/b}(p) \;=\; \begin{cases} \frac{\bar{\mu}+p\mp\sqrt{(p+\bar{\mu})^2+|\Delta|^2}}{2\sqrt{(p+\bar{\mu})^2+|\Delta|^2}}, & \bar{\mu}-\sqrt{\delta\mu^2-4|\Delta|^2} < p < \bar{\mu}+\sqrt{\delta\mu^2-4|\Delta|^2} \\ \frac{(\bar{\mu}-p)}{2\sqrt{(p-\bar{\mu})^2+|\Delta|^2}} + \frac{(\bar{\mu}+p)}{2\sqrt{(p+\bar{\mu})^2+|\Delta|^2}}, & \text{else} \end{cases} . \quad (3.74)$$

We see that in an interval of the Fermi momentum the occupation number is almost vanishing for one species and is almost unity for the other. The deviation of the occupation numbers from zero and unity in this interval for our simple parameterization is solely coming from the anti-quasiparticles and therefore of order $\frac{\Delta^2}{\mu^2} \ll 1$. The physical interpretation is that the quasiparticles in this 'breached pairing region' are not pairing.

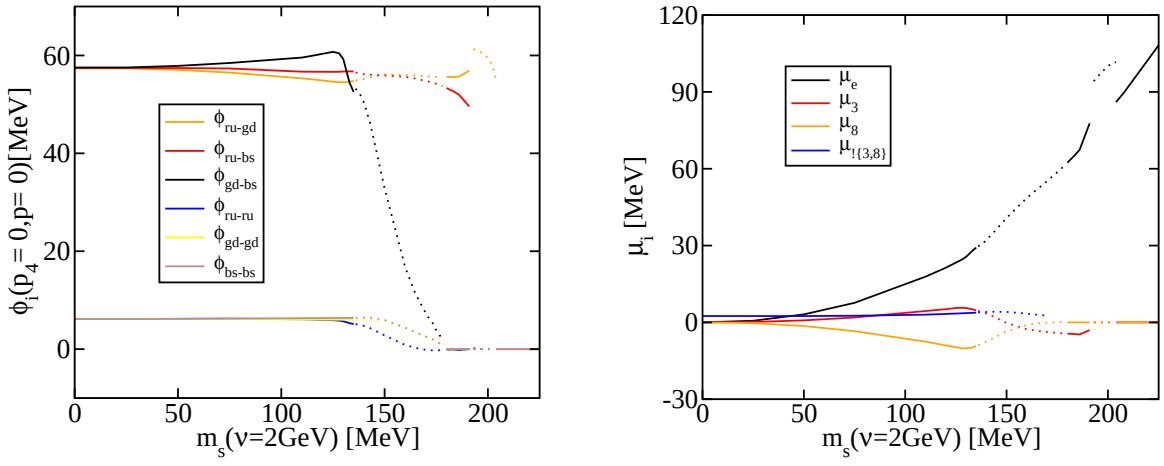

Figure 3.18: Dependence of some gap functions $\phi^+_{C,i}$ at the Fermi energy and for vanishing momentum (left) and of the (effective) chemical potentials (right) on the renormalized strange-quark mass. Both dependencies are determined at $\mu = 400\,\text{MeV}$ and with the coupling $\alpha_I(k)$.

3.5.3 Numerical results

We will now present numerical results for the neutral CFL phase. Again the amount of data is overwhelming, as we calculate 4×15 dressing functions depending on energy and momentum for normal self-energy, gap function, normal propagator and anomalous propagator, respectively. However, we refer to the previous results for details and will only highlight new features. The shown gap functions belong to the tensor structures P_1, P_2, P_3, P_4, P_6 and P_7 given in Appendix E.3 and are labeled according to the involved quarks.

In Fig. 3.18 we present the dependence on the renormalized strange-quark mass of gap functions at the Fermi surface, *i.e.* for $p_4 = 0$, and for vanishing momentum. As the color-flavor structure of the pairing is quite involved, we refrain from a determination of the Fermi momenta as we have done in section 3.4 and focus on the gap functions at vanishing momentum. This is reasonable as the gap functions $\phi^+_{C,i}$ for moderate chemical potentials are almost constant below the Fermi energy (see section 3.3). As can be seen, the gap functions are weakly dependent on the renormalized strange-quark mass up to values of $\sim 135\,\text{MeV}$. At this value, the pairing of green strange-quarks with blue down-quarks becomes ungapped as discussed in section 3.5.2. This can also be observed in the corresponding occupation numbers (see Fig. 3.19). From then on, the pairing gap of strange- and down-quarks 'melts' and from above $\sim 180\,\text{MeV}$ we are in the uSC phase. This phase exists up to a value of $\sim 190\,\text{MeV}$ and in the window of $\sim 190 - 200\,\text{MeV}$ we find the 2SC phase. Above this value no pairing takes place anymore.

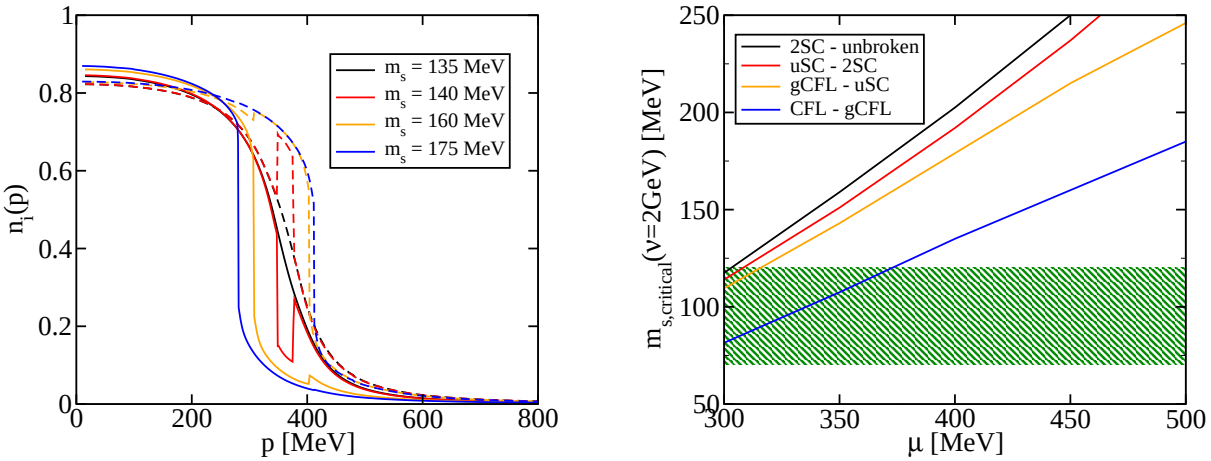

Figure 3.19: Occupation numbers of green strange-quarks (solid) and blue down-quarks (dashed) for various values of the renormalized strange-quark mass at $\mu = 400\,\mathrm{MeV}$ (left) and the critical renormalized strange-quark masses as a function of the chemical potential together with the range stated by the particle data group [113] (shaded area) (right). Both are determined with the coupling $\alpha_I(k)$.

We have to clarify that we can no longer compute the pressure difference between the phases for numerical reasons. However, the transition of CFL to gCFL to uSC seems to be at most of second order, as all parameters change continuously. In addition the intrinsic symmetry is not altered and the transitions might even be crossovers. For the transitions of uSC to 2SC and 2SC to the unbroken phase we refer to our observation in section 3.4, that it is much more difficult to find an energetically disfavored solution. As we solve the qDSE, being the variation of the CJT action, by iteration in a high-dimensional space of parameters (the discretized dressing functions), the domain of attraction for the global minimum is usually dominating. We also emphasize that those transitions are not in the physically relevant range of the strange-quark mass.

On the right hand side of Fig. 3.18 we present the electrical chemical potential μ_e, the color chemical potentials μ_3 and μ_8 as well as an upper bound for the chemical potentials not belonging to the Cartan subalgebra. It becomes obvious that electrical neutrality puts the strongest constraint on the phase structure and μ_e even exceeds the size of the largest gaps in the gCFL, uSC and 2SC phase. It is remarkable to note that μ_e is non-vanishing in the gapped CFL phase as discussed in section 3.5.2. This can also be seen in Fig. 3.19, which shows (in this case for green strange- and blue down-quarks) that the occupation numbers of pairing quarks in the gapped phase need not be identical as concluded for energy independent gap functions in Eq.(3.74). The bound for the chemical potentials not belonging to the Cartan subalgebra is of the order as the chemical μ_3 and μ_8. This shows

that all color chemical potentials are much smaller than the electrical chemical potential μ_e. However the treatment of μ_3 and μ_8 alone is equally justified as neglecting all color chemical potentials.

In Fig. 3.19 the occupation numbers for the ungapped pairing of green strange- and blue down-quarks at a chemical potential of $\mu = 400\,\mathrm{MeV}$ and for various renormalized strange-quark masses are presented. Qualitatively those show a breached pairing region as found in Eq.(3.74) for a simple model study Due to the interaction, the occupation numbers in the breached pairing region are not almost vanishing or close to unity, but bound by the occupation numbers in see unbroken phase (see also section 3.3).

Finally we present the critical value of the renormalized strange-quark mass, *i.e.* the values for the phase 'transitions', as a function of the chemical potential.

3.5.4 Conclusions

As expected from our study in section 3.4, the CFL phase seems to be the ground state for moderate chemical potentials and a realistic strange-quark mass. As our approach favors smaller values of the strange-quark mass in the parameter range stated by the particle data group [113] and nuclear saturation takes place at $\mu = 308\,\mathrm{MeV}$, gapless pairing is not present for our calculation. A surprising feature is the appearance of electrons in the CFL phase, which has not been expected. Furthermore it has been clarified that the CFL phase can not be defined by a symmetry pattern for a non-vanishing strange-quark mass.

As the CFL phase seems to be the physically most relevant phase, it will be the basis for improving out truncation scheme in section 5.

Chapter 4

Application of the Maximum Entropy Method

It will now be shown how to apply the Maximum Entropy Method (MEM) to numerical Dyson-Schwinger studies for the extraction of spectral functions of correlators from their corresponding Euclidean propagators. We will emphasize the differences to the application in lattice QCD and, as an example, extract the spectral functions of quarks in the 2SC phase.

4.1 Introduction

As already explained, investigations of QCD in the strongly coupled regime by non-perturbative numerical methods such as lattice QCD and truncated Dyson-Schwinger equations are often constrained or usually performed in Euclidean space (for recent reviews see [8, 9, 11]). Although Dyson-Schwinger studies rely on truncation schemes, they have the great advantage, that they can in principle be solved in the continuum limit and with much higher numerical accuracy.

An extraction of dynamical properties, in particular the spectral functions of propagators, is however highly desirable. In quantum Monte Carlo simulations, the Maximum Entropy Method (MEM) turns out to be an especially suited tool and has been successfully applied in condensed matter physics (see [43] for a review), lattice QCD in the vacuum (see [44] for a review), as well as at finite temperatures [131]. We will now show that it can also successfully be employed for the extraction of spectral functions in Dyson-Schwinger studies.

The starting point for the MEM is the linear relation between the spectral function and numerically determined Euclidean correlation functions via generalized Källen-Lehmann

representations. Since the inversion of the latter is in general ill-posed due to the spectral properties of the linear operator, further knowledge has to be implemented non-linearly. This can be done from a regularization point of view leading to the "historical maximum entropy" [132] or in a Bayesian approach leading to the "classic maximum entropy" [133, 134] and to "Bryan's method" [135].

The key idea in the latter case is the interpretation of the spectral function as a probability distribution due to its special properties and a proper consideration of the numerical error. As a result, the MEM determines the most plausible or expected spectral function for a given Euclidean correlator with known errors and some prior knowledge. It does not rely on a special form of the function and should, with decreasing errors, converge towards the exact solution.

For numerical Dyson-Schwinger studies, the method seems especially reliable, since the calculations can usually be performed with much higher numerical accuracy and for much more momentum points of the correlators than in lattice QCD.

The presentation is organized as follows: In section 4.2 we collect those properties of spectral functions for fermions and bosons, which make them suitable for the application of the MEM. In section 4.3 we discuss the MEM procedure itself, in particular its adaptation to Dyson-Schwinger studies and to fermions. After this we show in section 4.4 some results for massless quarks in the 2SC and in the unbroken phase. In Appendix F.2 we sketch the numerical implementation.

4.2 Spectral functions and their properties

Performing calculations for propagators in Euclidean space or rather within the imaginary time formalism means the determination of Matsubara propagators. These are related to spectral functions in Minkowski space via the generalized Källen-Lehmann representation (see *e.g.* [91]). Using the Euclidean conventions of [8] we have

$$S(\vec{p}, p_4) = \int_{-\infty}^{\infty} \frac{d\omega}{2\pi} \frac{\rho(\omega, \vec{p})}{-ip_4 + \mu - \omega}, \tag{4.1}$$

for a Dirac fermion propagator, where $p_4 = \omega_n$ denotes a given Matsubara frequency and μ is the chemical potential. The spectral function is given by

$$\begin{aligned} \rho(\omega, \vec{p})_{\alpha\beta} &= \frac{(2\pi)^4}{Z(\beta)} \sum_{l,n} e^{-\beta(E_l - \mu N_l)} (1 + e^{-\beta\omega}) \langle l|\psi_\alpha|n\rangle\langle n|\bar{\psi}_\beta|l\rangle \times \\ &\quad \times \delta\left(\omega + E_l - E_n\right) \delta^3\left(\vec{p} + \vec{p}_l - \vec{p}_n\right) . \end{aligned} \tag{4.2}$$

Therefore $\rho(\omega,\vec{p})\gamma_4$ is hermitian and has only positive eigenvalues in a given Hilbert space[1]. Furthermore it has to fulfill the sum rule

$$\gamma_4 \;=\; \frac{Z_2}{2\pi}\int_{-\infty}^{\infty} d\omega \;\; \rho(\omega,\vec{p})\,, \tag{4.3}$$

as a consequence of the (anti-)commutation relations. Thus $\rho(\omega,\vec{p})\gamma_4/4$ can be identified with a probability distribution, which is the key property for motivating the use of the MEM.

For a massive relativistic fermion in an isotropic, even parity and T-symmetric phase, we can parameterize

$$\rho(\omega,\vec{p}) \;=\; 2\pi\left(\omega\gamma_4\,\rho_e(\omega,\vec{p}) - i\vec{p}\cdot\vec{\gamma}\,\rho_v(\omega,\vec{p}) + \rho_s(\omega,\vec{p})\right) \tag{4.4}$$

and knowing that all eigenvalues have to be positive, we get

$$\omega\rho_e(\omega,\vec{p}) \geq \sqrt{\vec{p}^2\rho_v(\omega,\vec{p})^2 + \rho_s(\omega,\vec{p})^2} \geq 0 \tag{4.5}$$

and furthermore the sum rules

$$\begin{aligned} 1 \;&=\; Z_2\int_{-\infty}^{\infty} d\omega \;\; \omega\,\rho_e(\omega,\vec{p})\,, \\ 0 \;&=\; \int_{-\infty}^{\infty} d\omega \;\; \rho_v(\omega,\vec{p})\,, \\ 0 \;&=\; \int_{-\infty}^{\infty} d\omega \;\; \rho_s(\omega,\vec{p})\,. \end{aligned} \tag{4.6}$$

For the application discussed in section 4.4, we will for simplicity restrict ourself to the chiral limit, *i.e.* massless fermions (the case of massive fermions is discussed at the end of section 4.3). In this case, we can rewrite the propagators by using the energy projectors $\Lambda^{\pm} = \frac{1}{2}\left(1 \pm i\gamma_4\frac{\vec{p}\cdot\vec{\gamma}}{|\vec{p}|}\right)$ and obtain

$$\rho(\omega,\vec{p}) \;=\; 2\pi\left(\rho^+(\omega,\vec{p})\Lambda^+\gamma_4 + \rho^-(\omega,\vec{p})\Lambda^-\gamma_4\right)\,. \tag{4.7}$$

The spectral functions $\rho^{\pm}$ then fulfill

$$\begin{aligned} \rho^{\pm}(\omega,\vec{p}) \;&>\; 0\,, \\ Z_2\int_{-\infty}^{\infty} d\omega \;\; \rho^{\pm}(\omega,\vec{p}) \;&=\; 1\,, \end{aligned} \tag{4.8}$$

[1]This argument does therefore not hold *e.g.* for gauge fields.

with

$$S^{\pm}(\vec{p},p_4) \;=\; \int\limits_{-\infty}^{\infty} d\omega \;\frac{\rho^{\pm}(\omega,\vec{p})}{-ip_4+\mu-\omega}\,. \tag{4.9}$$

For completeness we also wish to show, how the solutions of the inhomogeneous Bethe-Salpeter equation (BSE) can be used to determine the spectral functions of mesons or diquarks. For a given current $J^a(x) = \bar{\psi}(x)T^a\psi(x)$, the solution for the corresponding Bethe-Salpeter amplitude $\Gamma^a(q;P)$ in momentum space (see *e.g.* [8]) determines the time-ordered product

$$\begin{aligned}\langle T\, J^a(x)\psi(y)\bar{\psi}(z)\rangle_\beta \;&=\; \int\frac{d^4P}{(2\pi)^4}\int\frac{d^4q}{(2\pi)^4}\; e^{-iP(x-\frac{y+z}{2})+iq(z-y)}\;\times \\ &\qquad\times\; S(q+\frac{P}{2})\Gamma^a(q;P)S(q-\frac{P}{2})\,,\end{aligned} \tag{4.10}$$

such that the current-current correlator is given by

$$\begin{aligned}\langle T\, J^a(x)J^b(y)\rangle_\beta \;&=\; \lim_{z\to y}\mathrm{Tr}\left(\langle T\, J^a(x)\psi(y)\bar{\psi}(z)\rangle_\beta T^b\right) \\ &=\; \int\frac{d^4P}{(2\pi)^4}\; e^{-iP(x-y)}\, D_{ab}(P)\,,\end{aligned} \tag{4.11}$$

with

$$D_{ab}(P) \;=\; \int\frac{d^4q}{(2\pi)^4}\mathrm{Tr}\left(S(q+\frac{P}{2})\Gamma^a(q;P)S(q-\frac{P}{2})T^b\right)\,. \tag{4.12}$$

Again $D_{ab}(P)$ possesses a generalized Källen-Lehmann representation and the spectral function has to fulfill positivity conditions.

4.3 Maximum Entropy Method (MEM)

The Maximum Entropy Method is a numerical tool for the inversion of potentially ill-posed linear equations by the implementation of additional information, *i.e.* constraints. It can be easily viewed from a standpoint of regularization as adding some non-linear auxiliary conditions, leading to the so-called "historical maximum entropy" [132]. This is known to underfit the data by overestimating the effective number of degrees of freedom, thus leading to solutions that are closer to the prior estimate. Usually, the somewhat converse Bayesian viewpoint is considered, since it essentially adjusts the number of effective degrees of freedom and also allows for an error estimation [43, 44]. We briefly review this here, emphasizing the adaption to our problem.

Given a (numerically evaluated) Euclidean correlator, which is treated as 'data' D, the objective is to determine the most plausible (related to "classic maximum entropy" [133, 134]) or the most expected (related to "Bryan's method" [135]) spectral function ρ_{MEM} by taking into account prior knowledge $H(m)$ of the solution, regulated by the prior estimate m to be defined below. The key entity is the plausibility functional $P[\rho|DH(m)]$ for the spectral function ρ under given D and $H(m)$. With help of the so called "Bayesian theorem" for conditional plausibilities

$$P[XY] = P[X|Y]P[Y] = P[Y|X]P[X]\,, \tag{4.13}$$

this can be brought into the form

$$\begin{aligned} P[\rho|DH(m)] &= \frac{P[D|\rho H(m)]P[\rho|H(m)]}{P[D|H(m)]} \\ &\propto P[D|\rho H(m)]P[\rho|H(m)]\,. \end{aligned} \tag{4.14}$$

Here, we have introduced the "likelihood function" $P[D|\rho H(m)]$ for the plausibility of the data D under given ρ and $H(m)$ and the "prior probability" $P[\rho|H(m)]$ for the plausibility of ρ under the prior knowledge $H(m)$. The constant plausibility $P[D|H(m)]$ of the data D under the prior knowledge $H(m)$ can be dropped, since we normalize the plausibility functional at the end.

Considering the function (or sequence at finite temperature) D in an interval $[a, b]$ as uncorrelated data points obeying a Gaussian distribution functional[2], we have

$$P[D|\rho H(m)] = \exp\left(-L\left[\rho\right]\right)\,, \tag{4.15}$$

with the likelihood

$$\begin{aligned} L\left[\rho\right] &= \frac{1}{b-a}\int_a^b dp_4 \frac{|D(p_4) - D[\rho](p_4)|^2}{2\sigma(p_4)^2} \\ &\simeq \frac{1}{b-a}\sum_i \Delta p_{4,i} \frac{|D_i - D[\rho]_i|^2}{2\sigma_i^2}\,, \end{aligned} \tag{4.16}$$

where $D[\rho]$ is given by the generalized Källen-Lehmann representation and a measure $\mathcal{D}D$ for the discretized integral

$$\mathcal{D}D = \prod_i \sqrt{\frac{\Delta p_{4,i}}{2\pi(b-a)\sigma_i^2}}\, dD_i\ . \tag{4.17}$$

[2]The justification of this needs to be discussed for a given application.

The prior probability $P[\rho|H(m)]$ is usually somewhat arbitrary and essentially implements the positivity conditions non-linearly, at least from the regularization point of view. It can be motivated by the law of large numbers or axiomatically constructed (see *e.g.* [43, 44]). The key idea in the latter case is to consider the spectral function as a probability distribution and derive the most general functional, fulfilling the requirements of subset independence, coordinate invariance, system independence and scaling. It is then of the form

$$P[\rho|H(m)] \;=\; \int_0^\infty d\alpha \;\; P[\rho|H(\alpha m)]P[\alpha|H(m)]\,, \tag{4.18}$$

with the scaling factor α for the prior estimate m and the plausibility for the scaled prior estimate

$$P[\rho|H(\alpha m)] \;=\; \exp\left(\alpha S\left[\rho\right]\right)\,. \tag{4.19}$$

Here $S\left[\rho\right]$ is the negative semi-definite entropy

$$\begin{aligned} S\left[\rho\right] \;&=\; \int_{-\infty}^{\infty} d\omega \;\; \left(\rho(\omega) - m(\omega) - \rho(\omega)\ln\left(\frac{\rho(\omega)}{m(\omega)}\right)\right) \\ &\simeq\; \sum_i \Delta\omega_i \left(\rho_i - m_i - \rho_i \ln\left(\frac{\rho_i}{m_i}\right)\right) \\ &=\; -\sum_i 2\Delta\omega_i \left(\sqrt{\rho_i} - \sqrt{m_i}\right)^2 + O\left(\left(\sqrt{\rho_i} - \sqrt{m_i}\right)^3\right) \end{aligned} \tag{4.20}$$

with the measure

$$\mathcal{D}\rho_\alpha \;\simeq\; \prod_i d\sqrt{\frac{2\alpha\Delta\omega_i\rho_i}{\pi}} \tag{4.21}$$

in the saddle point approximation around the prior estimate. The scaling factor α basically scales the maximum of the entropy and will be balanced by the likelihood. Furthermore we will assume that the plausibility $P[\alpha|H(m)]$ can be dropped, which is called Laplace's rule and can be justified *a posteriori*, as discussed in our example in section 4.4.

From Eq.(4.14) we therefore finally get

$$P[\rho|DH(m)] \;=\; \frac{1}{Z}\exp\left(Q\left[\rho\right]\right)\,, \tag{4.22}$$

with the negative semi-definite functional $Q\left[\rho\right] = \alpha S\left[\rho\right] - L\left[\rho\right]$, Z determined by normalization and the measure

$$\mathcal{D}\rho \;\simeq\; d\alpha \prod_i d\sqrt{\frac{2\alpha\Delta\omega_i\rho_i}{\pi}}\,. \tag{4.23}$$

It is worth noting that the "historic maximum entropy" [132] simply determines the maximum, which is unique if it exists [44], of the functional $Q[\rho]$ with α chosen, such that $L = 1$. We will however follow "Bryan's method" [135], aiming at the most expected spectral function, by computing

$$\begin{aligned} \rho_{\mathrm{MEM}} &= \int \mathcal{D}\rho \; \rho \; P[\rho|DH(m)] \\ &\simeq \int_0^\infty d\alpha \, \rho_\alpha \; \frac{1}{Z} \int \mathcal{D}\rho \; \exp\left(Q\left[\rho\right]\right) , \end{aligned} \tag{4.24}$$

where it is assumed that $P[\rho|DH(m)]$ is sharply peaked around its maximum ρ_α. We therefore define

$$\begin{aligned} P[\alpha|DH(m)] &= \frac{1}{Z} \int \mathcal{D}\rho \; \exp\left(Q\left[\rho\right]\right) \\ &\simeq \frac{1}{Z} \exp\left(Q\left[\rho_\alpha\right] + \frac{1}{2} \sum_k \ln\left(\frac{\alpha \Delta\omega_k}{\lambda_k} \right) \right) , \end{aligned} \tag{4.25}$$

with $\{\lambda_k\}$ being the eigenvalues of

$$M_{ij} = \alpha \Delta\omega_i \delta_{ij} + \sqrt{\rho_i} \, \frac{\partial^2 L}{\partial\rho_i \partial\rho_j} \, \sqrt{\rho_j} \tag{4.26}$$

and finally get the most expected spectral function via

$$\rho_{\mathrm{MEM}} = \int_0^\infty d\alpha \, \rho_\alpha \; P[\alpha|DH(m)] \, . \tag{4.27}$$

It should be noted that $P[\alpha|DH(m)]$ is formally not integrable due to the saddle point approximation. However, this becomes only relevant for very large values of α. In any numerically considered interval the function decreases exponentially for precise enough and many data points. For consistency, the choice for the upper cutoff for α should always be quoted. In the "classical maximum entropy", the most plausible spectral function $\rho_{\hat{\alpha}}$ is determined by maximizing $Q[\rho]$ and $P[\alpha|DH(m)]$ simultaneously. In our case, due to (in principle) arbitrarily many data points, this turns out and is known [43] to agree with the most expected spectral function ρ_{MEM}.

In comparison to previous applications, we have formulated the MEM for arbitrarily discretized functions D and ρ_α, since we want to deal with (in principle) continuous functions from truncated Dyson-Schwinger calculations. Therefore, the single-value decomposition as proposed in the Bryan algorithm [135] for the numerical determination of

ρ_α does not work. However, our new treatment of the spectral function opens the possibility of a better suited discretization, which can be adopted to the specific form of ρ_α. In this way, we are also able to significantly reduce the number of points which are needed for the numerically discretized spectral function.

As already mentioned, the Bayesian approach offers the possibility of an error estimation. If we consider an interval $I = [\omega_1, \omega_2]$ of the spectral function, the expectation value of ρ_a for fixed α in this interval for constant weighting is given by

$$\langle \rho_\alpha \rangle_I = \frac{1}{\omega_2 - \omega_1} \int\limits_I d\omega \ \rho_\alpha(\omega) \tag{4.28}$$

and, hence, for the most plausible function by

$$\langle \rho_{\mathrm{MEM}} \rangle_I = \int\limits_0^\infty d\alpha \, \langle \rho_\alpha \rangle_I P[\alpha | DH(m)] \, . \tag{4.29}$$

For the variance around this value, we first consider [133, 134]

$$\begin{aligned} \langle \delta\rho_\alpha(\omega_i) \delta\rho_\alpha(\omega_j) \rangle &\simeq 4\sqrt{\rho_\alpha(\omega_i)\rho_\alpha(\omega_j)} \left\langle \delta\sqrt{\rho_\alpha(\omega_i)} \delta\sqrt{\rho_\alpha(\omega_j)} \right\rangle \\ &\simeq -\sqrt{\rho_\alpha(\omega_i)\rho_\alpha(\omega_j)} \left(M^{-1}\right)_{ij} \\ &\simeq -\left. \frac{\partial^2 Q}{\partial\rho_i \partial\rho_j} \right|_{\rho=\rho_\alpha} , \end{aligned} \tag{4.30}$$

with fixed α and $\delta\rho_\alpha(\omega) = \rho(\omega) - \rho_\alpha(\omega)$. Therefore in the given interval I, we get

$$\left\langle (\delta\rho_\alpha)^2 \right\rangle_I \simeq -\frac{1}{(\omega_2 - \omega_1)^2} \int\limits_{I\times I} d\omega d\omega' \left(\frac{\delta^2 Q}{\delta\rho(\omega)\delta\rho(\omega')} \right)^{-1} \Bigg|_{\rho=\rho_\alpha} \tag{4.31}$$

and

$$\langle (\delta\rho_{\mathrm{MEM}})^2 \rangle_I = \int\limits_0^\infty d\alpha \, \left\langle (\delta\rho_\alpha)^2 \right\rangle_I P[\alpha | DH(m)] \, . \tag{4.32}$$

At the end of this section we want to indicate, how the MEM can be applied for massive fermions. For $\rho_e(\omega, \vec{p})$ the upper procedure can be performed analogously due to the properties given in Eq.(4.5) and Eq.(4.6). On the other hand, we would need to extend the procedure for the whole propagator by utilizing that $\rho(\omega, \vec{p})\gamma_4/4$ can be considered as

a probability distribution. With the propagator again denoted as data D, we generalize

$$\begin{aligned} L\left[\rho\right] &\rightarrow \frac{1}{b-a}\int_a^b dp_4 \frac{\mathrm{Tr}\left((D(p_4)-D[\rho](p_4))^\dagger (D(p_4)-D[\rho](p_4))\right)}{2\sigma(p_4)^2}\,, \\ S\left[\rho\right] &\rightarrow \int_{-\infty}^{\infty} d\omega\ \mathrm{Tr}\left(\left(\rho(\omega)-m(\omega)-\ln\left(\rho(\omega)m(\omega)^{-1}\right)\rho(\omega)\right)\gamma_4\right)\,, \end{aligned} \tag{4.33}$$

where the prior estimate m is now matrix-valued. Since $\rho(\omega,\vec{p})\gamma_4/4$ is hermitian and positive, it can be written as $g^\dagger\rho_D g$, with $g\in U(4)$ and ρ_D a diagonal matrix with positive eigenvalues. The unconstrained measure $\mathcal{D}\rho$ then becomes

$$\mathcal{D}\rho \rightarrow d\alpha \prod_{i,a} d\sqrt{\frac{2\alpha\Delta\omega_i\rho_{i,a}}{\pi}}\, d\lambda_i\,, \tag{4.34}$$

where $\rho_{i,a}$ is the a-th eigenvalue and $d\lambda_i$ the Haar measure for the group $U(4)$ at an energy ω_i. However, the path integral is usually constrained by symmetries, *i.e.* $\rho(\omega,\vec{p})\gamma_4 = h^\dagger\rho(\omega,\vec{p})\gamma_4 h$ for $h\in\mathcal{H}$. It can be easily seen that the group needs to be only integrated over the factor group of $U(4)$ and the conjugate closure of $\mathcal{H}$ and that only the independent eigenvalues need to be considered. For the case given by Eq.(4.4), we obtain with

$$\rho(\omega,\vec{p}) = \rho^+(\omega,\vec{p})\,\Lambda^+_{\omega,\vec{p}}\gamma_4 + \rho^-(\omega,\vec{p})\,\Lambda^-_{\omega,\vec{p}}\gamma_4\,, \tag{4.35}$$

where $\Lambda^\pm_{\omega,\vec{p}} = \frac{1}{2}(1\pm(i\cos\theta(\omega,\vec{p})\gamma_4\frac{\vec{p}\cdot\vec{\gamma}}{|\vec{p}|} - \sin\theta(\omega,\vec{p})\gamma_4))$, simply

$$\mathcal{D}\rho \rightarrow d\alpha \prod_i d\sqrt{\frac{2\alpha\Delta\omega_i\rho_i^+}{\pi}}\, d\sqrt{\frac{2\alpha\Delta\omega_i\rho_i^-}{\pi}}\,\frac{d\theta_i}{\pi}\,. \tag{4.36}$$

In the approximation of setting the integrand of the θ-integration to be constant and equal to the value θ_i given by the maximization of the functional $Q[\rho]$, the practical MEM procedure again becomes similar to the upper case.

4.4 Spectral functions of quarks in cold dense matter

4.4.1 Color-superconducting quark matter

As an example, we now present results for spectral functions of massless quarks in the 2SC phase at a quark chemical potential of $\mu = 1\,\mathrm{GeV}$, as they have been determined in section 3.3. The propagator is then of the form

$$S(p_4,\vec{p}) = S^+(p_4,\vec{p})\Lambda^+_{\vec{p}}\gamma_4 + S^-(p_4,\vec{p})\Lambda^-_{\vec{p}}\gamma_4 \tag{4.37}$$

and $S^+(p_4,\vec{p})$ is related to $\rho^+(\omega,\vec{p})$ by Eq.(4.9). For the bare normal quark propagator with a constant gap Δ in the gapped channel, the spectral function is then given by

$$\rho^+(\omega,\vec{p}) \;=\; \left(\frac{1}{2}+\frac{\mu-p}{2E_\Delta}\right)\delta\left(\omega+E_\Delta-\mu\right)+\left(\frac{1}{2}-\frac{\mu-p}{2E_\Delta}\right)\delta\left(\omega-E_\Delta-\mu\right)\,, \quad (4.38)$$

with $p=|\vec{p}|$ and $E_\Delta=\sqrt{(p-\mu)^2+\Delta^2}$. We will see below, how a non-trivial p_4-dependence generates a finite width.

4.4.2 Input data and error estimate

As described in section 4.3, the main input for the MEM is the data with a proper error estimate. In Dyson-Schwinger studies, these are obtained by self-consistent solutions of truncated integral equations. To lowest order, the error of S^+ therefore scales with the error of the numerical integrals, which determine the normal and anomalous self energies Σ^+ and Φ^+ (see Eq.(3.6)). In our case, we have chosen a simple Riemann quadrature for the multidimensional integrals, due to the principle-value-type behavior around the Fermi surface for ungapped channels. The error is therefore of order $O(h)$, where h is a scaling factor of the integration mesh. For the error estimation, we therefore calculate the propagator for two different h and extrapolate linearly to $h=0$. The data are then taken as the result for the smaller scaling factor h and the error as the difference between these data and the extrapolated result. In addition, the errors around nearest neighbors are averaged in order to avoid (artifically appearing) vanishing errors.

We also have to justify that correlations between the data points are negligible for the likelihood in the form given in Eq.(4.16). Since our numerical integrals for different values of p_4 are in principle independent, this is assumed to be true, at least when the discretized data is coarser than the numerical integral of the self energies.

The input data for $S^+(p_4,\vec{p})$ for the following example is chosen on an interval $[0,1\,\mathrm{GeV}]$ for the gapped channel in the 2SC phase at a quark chemical potential of $\mu=1\,\mathrm{GeV}$. As an illustration, the input for momentum $p=0.9\,\mathrm{GeV}$ is shown in Fig. 4.1. We consider the input as continuous due to our many data points and it has small errors of less than 1% in absolute value above 30 MeV.

4.4.3 Choice of the prior estimate

For the data input with given errors, we now need to choose an interval for the spectral function and a non-vanishing prior estimate. We take the comparatively large interval $[-1.5\,\mathrm{GeV},2\,\mathrm{GeV}]$. Furthermore we choose an interval for $P[\alpha|DH(m)]$ as discussed in

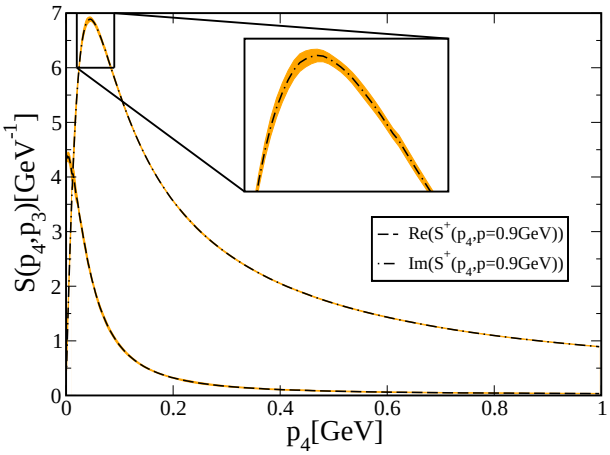

Figure 4.1: Real and imaginary part of the quasiparticle propagator S^+ in the gapped channel of the 2SC phase at a chemical potential of $\mu = 1\,\mathrm{GeV}$ and momentum $p = 0.9\,\mathrm{GeV}$ as a function of the Euclidean energy p_4. The errors are given as shaded regions around the lines and are of the order of their thickness.

the following section. For different prior estimates $m = 0.001, 0.01, 0.1$ and $1.0\,\mathrm{GeV}^{-1}$ at momentum $p = 0.9\,\mathrm{GeV}$, we then obtain the most expected spectral functions as shown in Fig. 4.2. It turns out that the extracted spectral function is remarkably insensitive on the variation of the prior estimate, even when varying it by more than three orders of magnitude. This is mainly related to the small errors of our data. We therefore fix $m = 0.1\,\mathrm{GeV}^{-1}$ in the following.

4.4.4 The α-dependence

It is also interesting to investigate the α-dependence of the maximum of the functional $Q[\rho]$ as well as of $P[\alpha|DH(m)]$. Since $P[\alpha|DH(m)]$ shows a pronounced maximum at α_{max}, we choose the interval $I = [\alpha_{low}, \alpha_{high}]$ for $P[\alpha|DH(m)]$ to be non-vanishing and normalized, such that $P[\alpha|DH(m)] > 10^{-1} \times P[\alpha_{max}|DH(m)]$ for $\alpha \in I$.

Again, for momentum $p = 0.9\,\mathrm{GeV}$, the results are shown in Fig. 4.3. On the left-hand side, we show $P[\alpha|DH(m)]$, normalized on I. On the right-hand side, we present the maximum of $Q[\rho]$ for $\alpha = \alpha_{min}, \alpha_{max}$ and α_{high}. They are only weakly varying, even when comparing the border of the interval I to the maximum. This also substantiates Laplace's rule for $P[\alpha|H(m)]$ *a posteriori*, assuming that its α-dependence is weaker.

Apart from this, in Fig. 4.3, the most expected spectral function is equal to the most probable spectral function given at α_{max} and therefore not shown. Thus the "classic maximum entropy" gives very similar results as "Bryan's method" in our case of "many"

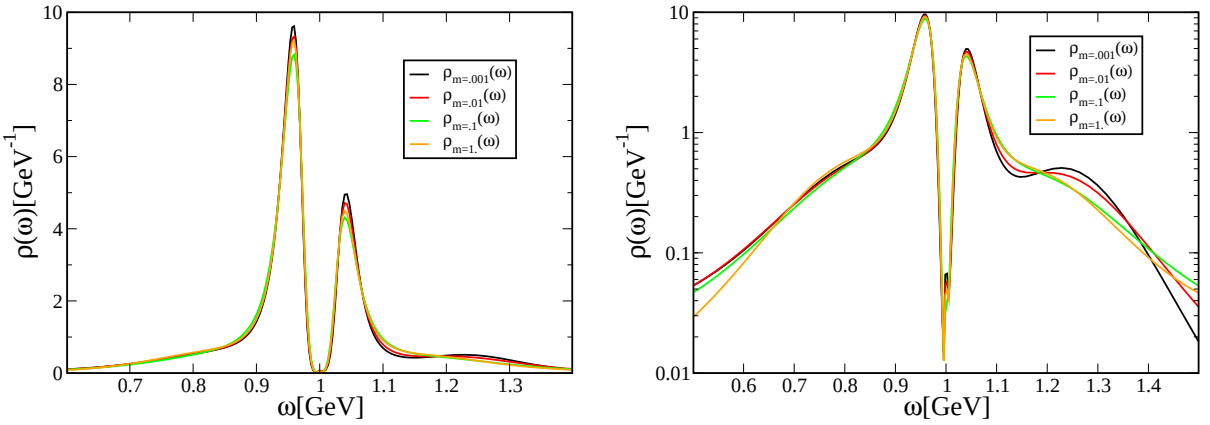

Figure 4.2: The most expected spectral function $\rho^+(\omega)$ in the gapped channel of the 2SC phase at momentum $p = 0.9\,\mathrm{GeV}$ for constant prior estimates $m = 0.001, 0.01, 0.1$ and $1.0\,\mathrm{GeV}^{-1}$ in linear (left) and logarithmic (right) presentation.

data points and small errors.

4.4.5 Error estimate

We are also able to perform an error estimate around the expectation value in a given interval. Since we have two pronounced peaks for quasiparticles and quasiparticle-holes in the spectral function, we choose the intervals associated to their full width at half maximum (FWHM). The exemplarily result for momentum $p = 0.9\,\mathrm{GeV}$ is shown on the right in Fig. 4.4. Again, the errors turn out to be very small.

4.4.6 Spectral densities in the 2SC and unbroken phase

Finally we come to the spectral densities in the gapped channel of the 2SC phase and also in the unbroken phase. In Fig. 4.5 we show a contour plot of the spectral density in the gapped channel as a function of the energy ω and momentum p. The yellow line shows the maxima of the quasiparticle and quasiparticle-hole branches, which show a similar behavior as we expect from BCS-type investigations (see Eq.(4.38)). However we also observe that the group velocity of the quasiparticles is significantly altered. We will come back to this point in section 5.2. For fixed momentum p, the difference between the blue lines below and above the yellow line gives the FWHM of the corresponding peak. This width results from the non-trivial energy dependence and is neglected in BCS- or NJL-type investigations. We see that even at the Fermi momentum, it is of the order of the gap in the excitation spectrum.

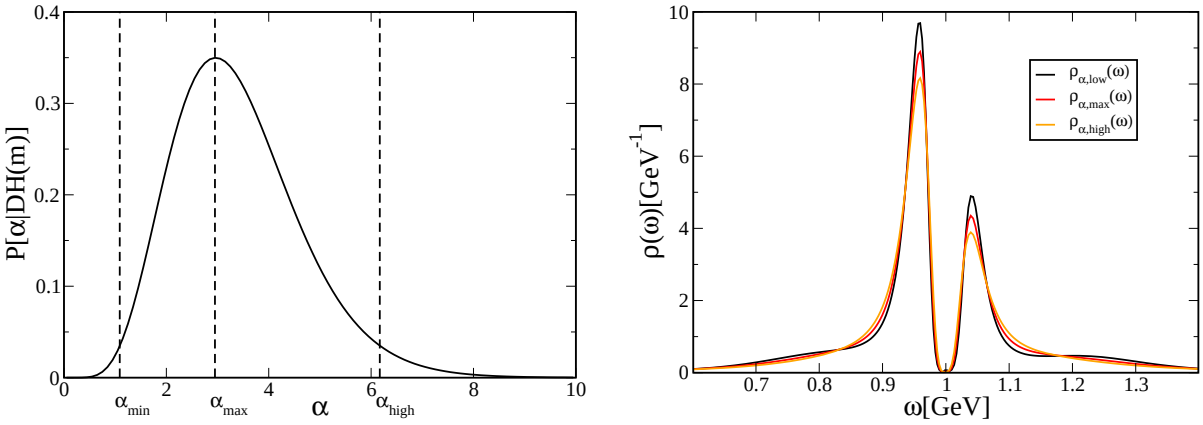

Figure 4.3: The function $P[\alpha|DH(m)]$ normalized between α_{min} and α_{high} (see text) with maximum α_{max} (left) and the maxima $\rho_{\alpha,low/max/high}$ of the functional $Q[\rho]$ for given α (right). Both for the gapped channel of the 2SC phase at momentum $p = 0.9\,\mathrm{GeV}$.

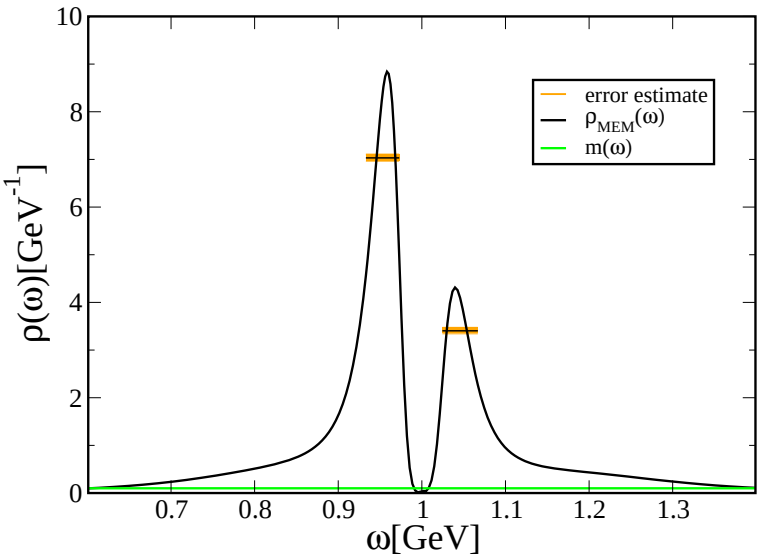

Figure 4.4: The spectral function for momentum $p = 0.9\,\mathrm{GeV}$ with the expectation value within the FWHM and its error estimate as shaded background.

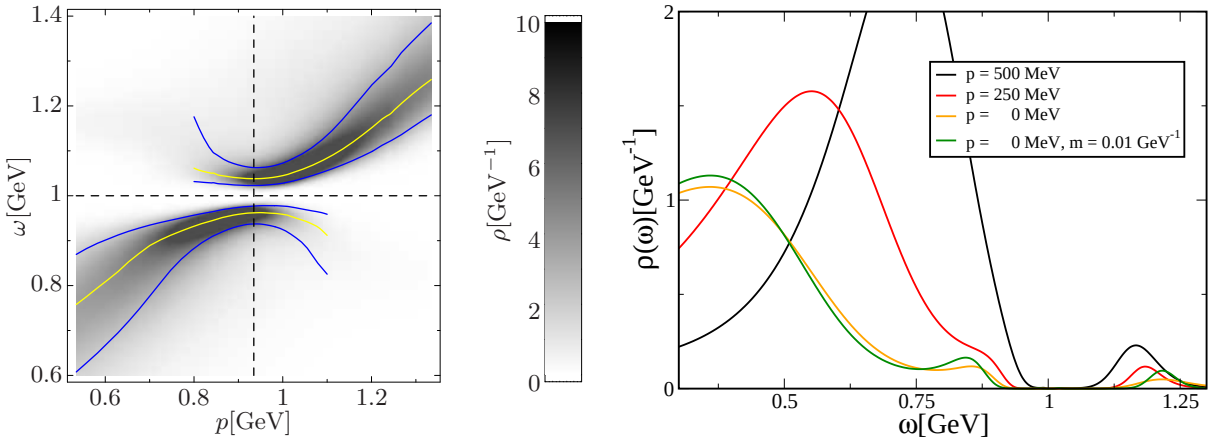

Figure 4.5: A contour plot of most expected spectral density in the gapped 2SC phase at $\mu = 1\,\mathrm{GeV}$ as described in the text (left) and the most expected spectral functions for momentum $|\vec{p}| = 0, 250, 500\,\mathrm{MeV}$ (right).

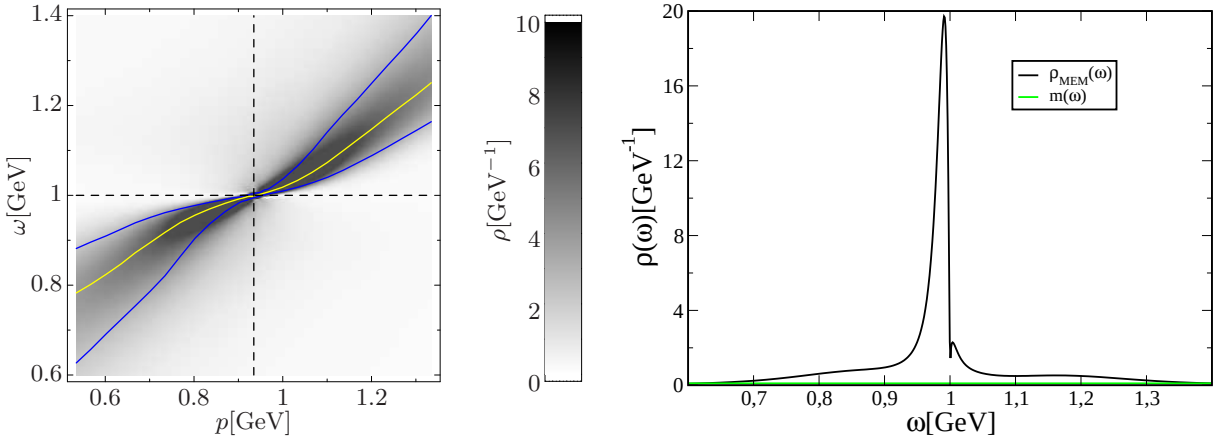

Figure 4.6: A contour plot of most expected spectral density in the unbroken phase at $\mu = 1\,\mathrm{GeV}$ as described in the text (left) and the most expected spectral functions for momentum $|\vec{p}| = 900\,\mathrm{MeV}$ (right).

As a by-product we can also see plasmino excitations in the color-superconducting phase as discussed in a model study for the weakly coupled regime [136]. On the right hand side of Fig. 4.5 we show the spectral functions in the gapped channel for small momenta. For vanishing momenta an additional collective excitation around $\sim 800\,\mathrm{MeV}$ appears, which is called plasmino. Its spectral strength is very small compared to the hole-excitation and its appearance in general depending on the kind of interaction. As our numerics are optimized for phenomena around the Fermi momentum, we also observe a stronger dependence on the prior estimate, which can be seen by the differing extracted spectral functions for $m = 0.1\,\mathrm{GeV}^{-1}$ and $0.01\,\mathrm{GeV}^{-1}$.

For the unbroken phase a contour plot of the spectral density is shown in Fig. 4.6. The yellow line again shows the maxima of the spectral function for a given momentum and it becomes apparent that this dispersion relation strongly differs from the free solution $p = \omega$. The Fermi velocity, *i.e.* the phase velocity at the Fermi surface, is (only almost due to the resolution) vanishing, as expected in a non-Fermi liquid. Also the spectral functions near the Fermi momentum shown on the right of Fig. 4.6 reveal significant deviations from a Fermi-liquid: The spectral maximum is not symmetric around its maximum, but strongly shifted towards the Fermi energy and the spectral function (almost) vanishes there.

4.5 Summary and conclusions

We have outlined, how the MEM can be adapted to numerical Dyson-Schwinger studies, in particular to fermions. It turns out that the extracted spectral functions are much more reliable and stable against variation, than in applications of the MEM in lattice QCD. Reasons for this are the comparatively small errors on the input functions and the almost arbitrary large number of data points. Compared to the systematic error, introduced by necessary truncations in Dyson-Schwinger studies, this error is negligible. Therefore this method can be useful for further applications in mesons or diquarks investigations, since currently all calculations have to be extended to complex momenta (see [97, 137, 138]). Avoiding this and reducing the numerical effort drastically, the MEM might help to improve or extent known truncation schemes, such as presented in section 5.1.

Concerning color-superconducting phases, the MEM turns out to be an interesting tool to determine spectral densities. It illuminates the role of the non-trivial energy dependence, which already plays an enormous role in the weakly coupled regime [42] and is usually neglected at moderate densities in other approaches. It gives a reasonable description for the allowance of electrons in the fully gapped CFL phase (see section 3.5.2) and we have access to non-trivial features of the quasiparticle excitation spectrum.

Chapter 5

Extending the truncation scheme

Given the results of the previous sections, we will now focus on an improvement of the HDL-like truncation scheme, restricting ourselves on the CFL phase in the chiral limit. We will incorporate Goldstone-boson effects in the qDSE, which are hidden in the $q\bar{q}g$-vertex. It turns out that the incorporation of pions, which are the Goldstone bosons connected to dynamical chiral symmetry breaking, in the qDSE can be done similarly and since vacuum investigations are usually more familiar, this will first serve as an illustration. In addition, we will determine the medium polarization self-consistently by inserting the full Nambu-Gor'kov propagator.

5.1 Pion effects in the quark propagator

Our first aim is the investigation of the qDSE beyond our $q\bar{q}g$-vertex construction. The purpose of this is manifold: Phenomenologically we want to include pion cloud effects, as a back-reaction of dynamical chiral symmetry breaking. For comparison to lattice QCD data, we need to incorporate dynamical sea-quarks when going from quenched to unquenched studies. It is also necessary for a proper description of hadrons, in particular the finite width of mesons due to hadronic intermediate states.

We limit ourself to the basic ideas and leave the details for future investigations [139].

5.1.1 Rainbow-ladder approximation

Let us briefly sketch the so-called renormalization-group-improved rainbow-ladder truncation. The starting point is the qDSE in the approximation

$$S^{-1}(p) \;=\; Z_2 S_0^{-1}(p) + Z_2 \Sigma^{(rainbow)}(p)\,, \tag{5.1}$$

where

$$\Sigma^{(rainbow)}(p) \;=\; 4\pi C_F \int \frac{d^4q}{(2\pi)^4}\,\frac{\alpha_s(k)}{k^2}\,\gamma_\mu\left(Z_2 S(q)\right)\gamma_\nu\left(\delta_{\mu\nu}-\frac{k_\mu k_\nu}{k^2}\right), \tag{5.2}$$

with the input $\alpha_s(k)$ being referred to as the strong running coupling [10, 11, 12]. The similarity to our truncation, especially using the tensor structure of the bare vertex, is evident (see section 2.2.3).

For a proper description of quark-antiquark bound states, the rainbow approximation needs to be combined with the ladder summation via the Bethe-Salpeter equation (BSE). The homogeneous BSE for a Bethe-Salpeter amplitude (BSA) $\Gamma(k;P)$ is given by

$$\Gamma(k;P)\big|_{tu} \;=\; \int \frac{d^4q}{(2\pi)^4}\,K^{rs}_{tu}(q,k;P)\,\left(S(q_+)\Gamma(q;P)S(q_-)\right)\big|_{sr}\,, \tag{5.3}$$

where we have introduced the kernel $K^{rs}_{tu}(q,p;P)$ and $k_\pm = k \pm \frac{P}{2}$. The choice for an appropriate approximation of the kernel is constrained by the axial-vector Ward-Takahashi identity (axWTI)

$$P_\mu\Gamma^a_{5\mu}(k;P) \;=\; S^{-1}(k_+)i\gamma_5\frac{\tau^a}{2}+i\gamma_5\frac{\tau^a}{2}S^{-1}(k_-)-i\sum_b \mathrm{Tr}_f\left(\left\{m,\frac{\tau^a}{2}\right\}\tau^b\right)\Gamma^b_5(k;P)\,, \tag{5.4}$$

where $\Gamma^a_{5\mu}(k;P)$ is the isovector axial-vector and $\Gamma^a_5(k;P)$ the isovector pseudo-scalar vertex (see Appendix B.3). Using the inhomogeneous BSE

$$\Gamma^a_{5\mu}(k;P)\big|_{tu} \;=\; Z_2\gamma_\mu\gamma_5\frac{\tau^a}{2}+\int\frac{d^4q}{(2\pi)^4}\,K^{rs}_{tu}(q,k;P)\,\left(S(q_+)\Gamma^a_{5\mu}(q;P)S(q_-)\right)\big|_{sr} \tag{5.5}$$

of the isovector axial-vector vertex and exploiting the axWTI, we get

$$Z_2\left(\Sigma(k_+)i\gamma_5\frac{\tau^a}{2}+i\gamma_5\frac{\tau^a}{2}\Sigma(k_-)\right)\Big|_{tu} \;= \int\frac{d^4q}{(2\pi)^4}\,K^{rs}_{tu}(q,k;P)\,\left(S(q_+)i\gamma_5\frac{\tau^a}{2}+i\gamma_5\frac{\tau^a}{2}S(q_-)\right)\Big|_{sr} \tag{5.6}$$

in the chiral limit. We conclude that

$$K^{(ladder)rs}_{\quad tu}(q,p;P) \;=\; -4\pi Z_2^2\frac{\alpha_s(k)}{k^2}\left(\delta_{\mu\nu}-\frac{k_\mu k_\nu}{k^2}\right)\left(\frac{\lambda^a}{2}\gamma_\mu\right)\Big|_{ts}\left(\frac{\lambda^a}{2}\gamma_\nu\right)\Big|_{ru} \tag{5.7}$$

is an appropriate, *i.e.* consistent and therefore symmetry conserving, choice of the kernel.

5.1.2 Low-energy properties from chiral symmetry

The particular importance of the axWTI is due to its role when proving the Goldstone theorem [140, 141]. With the quark propagator in Landau gauge for the chirally broken vacuum being parameterized via

$$S^{-1}(p) \;=\; -i\not{p}A(p) + B(p)\,, \tag{5.8}$$

chiral symmetry for vanishing quark masses is spontaneously broken for non-vanishing scalar dressing function $B(p)$. Therefore the right hand side of Eq.(5.4) is non-vanishing for $P_\mu \to 0$:

$$\lim_{P_\mu\to 0} P_\mu \Gamma^a_{5\mu}(k;P) \;=\; i\gamma_5\tau^a B(k)\,. \tag{5.9}$$

As a consequence, the isovector axial-vector vertex needs to be of the form

$$\Gamma^a_{5\mu}(k;P) \;=\; \frac{P_\mu}{P^2}\,\phi^a(k;P) + R^a_{5\mu}(k;P)\,, \tag{5.10}$$

with $\phi^a(k;P)$ and $R^a_{5\mu}(k;P)$ being regular at $P^2 = 0$. Furthermore the residue $\phi^a(k;P)$ of the inhomogeneous BSE for the isovector axial-vector vertex reduces to the homogenous BSE in the pseudo-scalar channel when approaching $P^2 \to 0$. Since $\phi^a(k;0) = i\gamma_5\tau^a B(k) \neq 0$ we then have a non-trivial solution for the BSA at $P^2 = 0$ and therefore massless Goldstone bosons of the spontaneously broken symmetry. This proves the Goldstone theorem in general.

Properly normalizing the BSA of the Goldstone-boson, $\Gamma^a_\pi(k;P)$, we find [141]

$$\Gamma^a_\pi(k;0) \;=\; \frac{\phi^a_\pi(k;0)}{r_A}\,, \tag{5.11}$$

with $r_A = f_\pi$ being the pion decay constant[1]. In the following, we will apply the approximation

$$\Gamma^a_\pi(k;P) \;\approx\; \Gamma^a_\pi(k;0) \;=\; i\gamma_5\tau^a\frac{B(k)}{f_\pi}\,, \tag{5.12}$$

which is the leading contribution and completely constrained by symmetry. This is the generalized Goldberger-Trieman relation, which now describes the coupling of pions to a quark instead of a nucleon. Within this approximation, we can determine the pion decay constant, giving the coupling strength of pions to the electro-weak axial-current [12]:

$$\delta^{ab} f_\pi P_\mu \;=\; -Z_2\int\frac{d^4q}{(2\pi)^4}\mathrm{Tr}_{c,f,D}\left(\gamma_5\gamma_\mu\frac{\tau^a}{2}S(q_+)i\gamma_5\tau^a\frac{B(k)}{f_\pi}S(q_-)\right) \tag{5.13}$$

[1] As shown in [141], a proper normalization of the pseudo-scalar BSA [142] from the residue of the axial-vector vertex always gives the Goldstone decay constant.

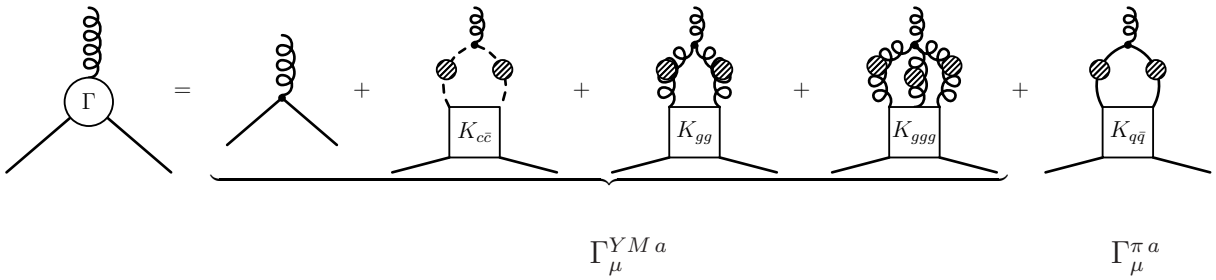

Figure 5.1: Dyson-Schwinger equation of the $q\bar{q}g$-vertex, separating the diagram containing the fully-amputated quark-antiquark scattering amplitude. All signs and prefactors have been absorbed in the diagrams.

for $P^2 \to -m_\pi^2 \equiv 0$. We therefore do not need to solve the BSE of the Goldstone bosons.

Also considering the inhomogeneous BSE of the isovector pseudo-scalar vertex, we can deduce the Gell–Mann-Oakes-Renner (GOR) relation, as has been done in [10]. In this context we define the chiral condensate

$$-\langle\bar{\psi}\psi\rangle_\nu \;=\; Z_m(\nu,\Lambda)\int^{\Lambda}\frac{d^4q}{(2\pi)^4}\;\mathrm{Tr}_{D,c,f}\left(S(p;\nu)Z_2(\nu,\Lambda)\right)\,, \tag{5.14}$$

which is also the order parameter of chiral symmetry breaking. As the integrand is renormalization scale independent (see section 2.2.3), the condensate scales with $Z_m(\nu,\Lambda)$ given by Eq.(2.24). Contemporary phenomenological approaches employ the 1-loop expression for Z_m and following this expedient we obtain, practically as a matter of definition,

$$\langle\bar{\psi}\psi\rangle_\nu \;=\; \left(\frac{\ln\left(\frac{\nu}{\Lambda_{QCD}}\right)}{\ln\left(\frac{\Lambda}{\Lambda_{QCD}}\right)}\right)^{\gamma_m}\langle\bar{\psi}\psi\rangle_\Lambda\,. \tag{5.15}$$

The result may be compared with a best-fit phenomenological value [143]: $-\langle\bar{\psi}\psi\rangle_{1\mathrm{GeV}} = (0.24\pm0.01\,\mathrm{GeV})^3$.

At the end we want to remark that the findings via the axWTI only require it to be fulfilled in the limit $P^2 \to 0$. In order to obtain a Goldstone boson, a consistent kernel $K^{rs}_{tu}(q,k;P)$ is therefore only constrained in this limit.

5.1.3 Pion contribution and the $q\bar{q}g$-vertex

Considering the Dyson-Schwinger equation of the $q\bar{q}g$-vertex as shown in Fig. 5.1, we separate the contribution containing the fully-amputated quark-antiquark scattering amplitude $M^{rs}_{tu}(q,p;P)$ (also denoted by $K_{q\bar{q}}$). We assume the other contributions to be only mildly affected by the presence of dynamical fermions as we will focus on the leading modification

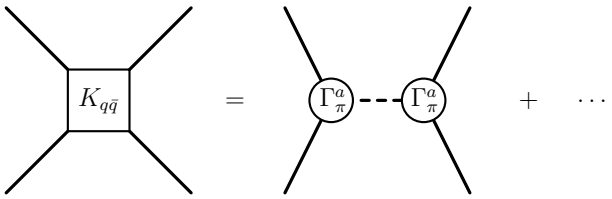

Figure 5.2: Resonant Goldstone contributions in the fully-amputated quark-antiquark scattering amplitude. The dashed line indicates a bare pseudo-scalar boson propagator. Empty circles attached to a dashed line denote the BSA of the Goldstone bosons.

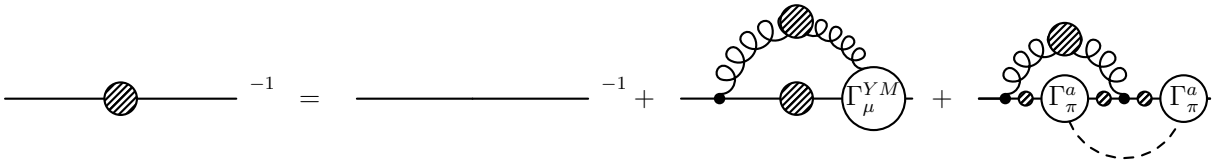

Figure 5.3: qDSE with our proposed vertex construction. The dashed line indicates a bare pseudo-scalar boson propagator. Empty circles attached to a dashed line denote the BSA of the Goldstone bosons.

by Goldstone bosons. Since those contributions are also present in the 'quenched' theory, we apply the same approximation as in Eq.(2.29) and Eq.(2.33) by setting

$$\Gamma^{YM\,a}_\mu(q,p) \;=\; \frac{Z_2\tilde{Z}_3}{\alpha_s(\nu)}\,\frac{\alpha_s(k)}{Z(k)}\,\gamma_\mu\frac{\lambda^a}{2}\,. \tag{5.16}$$

This seems especially appropriate for the coupling $\alpha_{II}(k)$, as this vertex has been constructed such that the solutions of the qDSE agree with quenched lattice QCD data.

The contribution containing the fully-amputated quark-antiquark scattering amplitude certainly contains resonant Goldstone contributions in the t-channel, which are diagrammatically shown in Fig. 5.2. Instead of solving its BSE given by

$$M^{rs}_{tu}(q,p;P) \;=\; K^{rs}_{tu}(q,p;P) + \int\frac{d^4k}{(2\pi)^4}\,K^{vw}_{tu}(q,k;P)S_{wa}(k_+)M^{rs}_{ab}(k,p;P)S_{bv}(k_-)\,, \tag{5.17}$$

where we would first need to find a symmetry preserving kernel $K^{rs}_{tu}(q,p;P)$, we approximate

$$M^{rs}_{tu}(q,k;P) \;=\; \big(\bar{\Gamma}^a_\pi(q;0)\big)\big|_{rs}\,\frac{1}{P^2}\,\big(\Gamma^a_\pi(k;0)\big)\big|_{tu} + R^{rs}_{tu}(q,k;P)\,, \tag{5.18}$$

where $R^{rs}_{tu}(q,k;P)$ is regular for $P^2\to 0$ and will be neglected in the following.

Using this approximation, we arrive at the qDSE shown in Fig. 5.3. In a last step we assume the BSA of the pion to be similar to the solution in rainbow-ladder approximation,

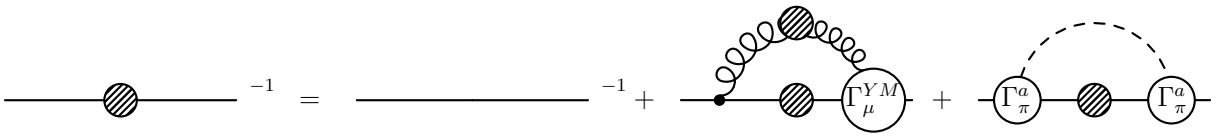

Figure 5.4: Final approximation for the qDSE including dynamical Goldstone contributions. The dashed line indicates a bare pseudo-scalar boson propagator. Empty circles attached to a dashed line denote the BSA of the Goldstone bosons.

which then allows us to reduce the qDSE shown in Fig. 5.3 to the one in Fig. 5.4. We have obtained

$$Z_2\Sigma(p) \;=\; Z_2\Sigma^{(rainbow)}(p) + Z_2\Sigma^{\pi}(p)\,, \tag{5.19}$$

with

$$Z_2\Sigma^{\pi}(p) \;=\; -3\int\frac{d^4q}{(2\pi)^4}\frac{B(\frac{p+q}{2})^2}{f_\pi^2}\,\gamma_5 S(q)\gamma_5\,\frac{1}{k^2}\,. \tag{5.20}$$

Here we used $N_f = 2$ in $\tau^a\tau^a = 4C_F(N_f) = 3$. Using Eq.(5.13) for f_π, this truncated equation becomes closed on the level of the quark propagator.

5.1.4 $1/N_c$-expansion

It is interesting to note that this approximation can be viewed as the (approximate) next-to-leading order in a $1/N_c$-expansion for models that can be motivated by an effective one-gluon exchange. Examples are the NJL-model [144, 145, 146], the global-color model [147] or the usual truncations of Dyson-Schwinger equations with focus on hadron phenomenology [8, 10, 11, 12]. As described in section 2.4.3, the qDSE can equally be derived from the variation of the effective action Γ in the CJT-formalism. For models with effective one-gluon exchange it is given by

$$\Gamma[S] \;=\; -\mathrm{TrLn}S^{-1} + \mathrm{Tr}\left(1 - Z_2 S_0^{-1} S\right) + \Gamma_2[S]\,. \tag{5.21}$$

For the diagrammatic expansion of the two-particle irreducible functional $\Gamma_2[S]$ we can then apply a $1/N_c$ ordering. The $1/N_c$-expansion of vacuum-vacuum contributions can nicely be arranged by the topology of the contributing diagrams [148]. Since we do not consider pure gluonic contributions at order $O(N_c^2)$, the leading contribution is given by planar gluonic diagrams with a quark line as a boundary, being $O(N_c)$. The corresponding contribution to $\Gamma_2[S]$ is shown in Fig. 5.5. To next-to-leading order, i.e. $O(1)$, we have the topology of a cylinder with two quark lines as boundaries. Those contributions to

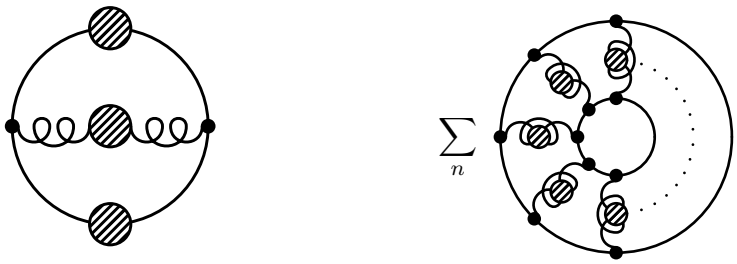

Figure 5.5: Leading (sunset diagram on the left) and next-to-leading (right, the sum is over the number of gluon lines) order contribution to $\Gamma_2[S]$ in a model with effective one-gluon exchange. All signs and prefactors have been absorbed in the diagrams.

$\Gamma_2[S]$ are also shown in Fig. 5.5. It is worth mentioning that we also need to consider the $O(1)$ contributions from the leading-order contribution to be consistent to next-to-leading order.

Therefore the truncated qDSE to next-to-leading order in a $1/N_c$-expansion, as derived from Eq.(5.21), turns out to be

$$S^{-1}(p) \;=\; Z_2 S_0^{-1}(p) + \Sigma^{(0)}(p) + \Sigma^{(1)}(p), \tag{5.22}$$

where $\Sigma^0(p) = Z_2\Sigma^{(rainbow)}(p)$ is the rainbow self-energy from Eq.(5.2) and

$$\Sigma^{(1)}_{ts}(p) \;=\; \int \frac{d^4q}{(2\pi)^4}\, S_{ur}(q)\, M^{rs}_{tu}(\frac{p+q}{2}, \frac{p+q}{2}; p-q) \tag{5.23}$$

with

$$M^{rs}_{tu}(q,p;P) \;=\; K^{rs}_{tu}(q,p;P) + \int \frac{d^4k}{(2\pi)^4}\, K^{vw}_{tu}(q,k;P) S_{wa}(k_+) M^{rs}_{ab}(k,p;P) S_{bv}(k_-) \tag{5.24}$$

is the next-to-leading order contribution. At this stage we emphasize that the ladder summation in Eq.(5.24) is also consistent with next-to-leading order for the self-energy, when leading order quark propagators, *i.e.* the results from the rainbow truncation, are used.

Within the approximation given in Eq.(5.18) for the fully-amputated quark-antiquark scattering amplitude, we obtain the same scheme as in the previous section. The scalar dressing function $B(k)$ in the BSA of the Goldstone boson can equally be taken from the rainbow truncation or be treated self-consistently.

5.1.5 Some numerical results

We now sketch some results for the truncation scheme proposed by Eq.(5.2), Eq.(5.13), Eq.(5.19) and Eq.(5.20). As it is determined from quenched lattice QCD data, we will use

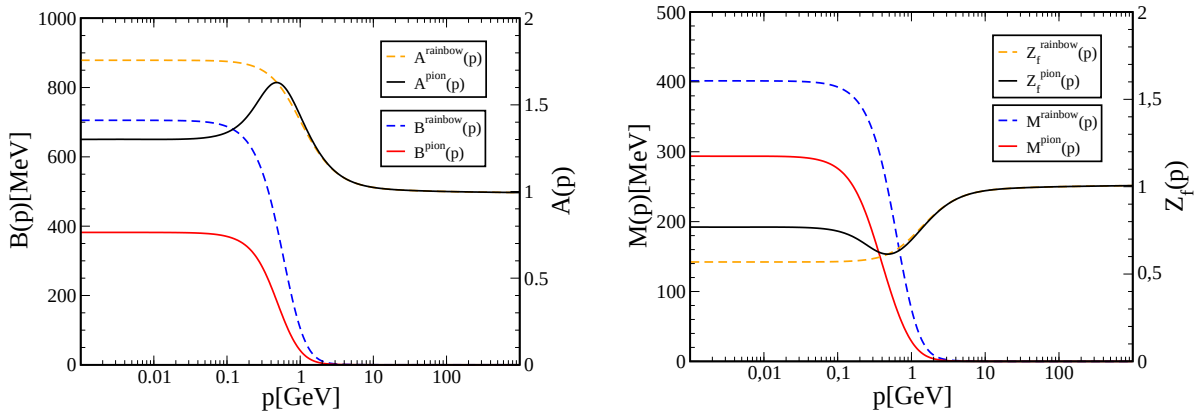

Figure 5.6: The dressing functions $A(p)$, $B(p)$ (left) and $Z_f(p)$, $M(p)$ (right) for $\alpha_{II}(k)$ in rainbow approximation (dashed lines) and including the pion contribution (solid lines).

the running coupling $\alpha_{II}(k)$ for this purpose.

We start with the effect of the pion contribution in the chiral limit. In Fig. 5.6 we show our results for the dressing functions $A(p)$, $B(p)$, $Z_f(p)$ and $M(p)$. As expected from Eq.(5.20), the pion contribution reduces the scalar dressing function $B(p)$ significantly. The vector dressing function $A(p)$ and therefore also the wave function $Z_f(p) = 1/A(p)$ is mainly altered in the low-momentum region. As a consequence, the mass function is lowered by about 100 MeV at small momentum. It also secedes at a smaller momentum, a fact probably connected to a larger charge radius of the pion [10]. The phenomenon of Goldstone fluctuation to lower the order parameter of the spontaneous symmetry breaking is generic, *e.g.* in 2-dimensions this even excludes spontaneous dynamical symmetry breaking [149] for continuous symmetries. This statement can easily be understood in our truncation: With a non-vanishing BSA of the Goldstone bosons, the integral of the Goldstone contribution is diverging in the infrared in 2-dimensions. This leads to an infinite repulsive back-reaction on the symmetry breaking function.

To estimate the role of the pion mass, we substitute

$$\frac{1}{k^2} \quad \rightarrow \quad \frac{1}{k^2 + m_\pi^2} \tag{5.25}$$

in Eq.(5.20), *i.e.* neglect the mass-dependence of the BSA and stick to the on-shell approximation for the pion. The pion can be linked to the current-quark mass by the GOR relation, which we postpone to future investigations. Our results for the dressing functions $Z_f(0)$, $M(0)$ at vanishing momentum, the pion decay constant f_π and the chiral condensate $\langle \bar{q}q \rangle_{1\text{GeV}}$ are shown in Fig. 5.7. As in [81] we used $\Lambda_{QCD} = 234\,\text{MeV}$ in Eq.(5.15). We observe a significant shift in the mass function up to pion masses $> 1\,\text{GeV}$. For pion masses

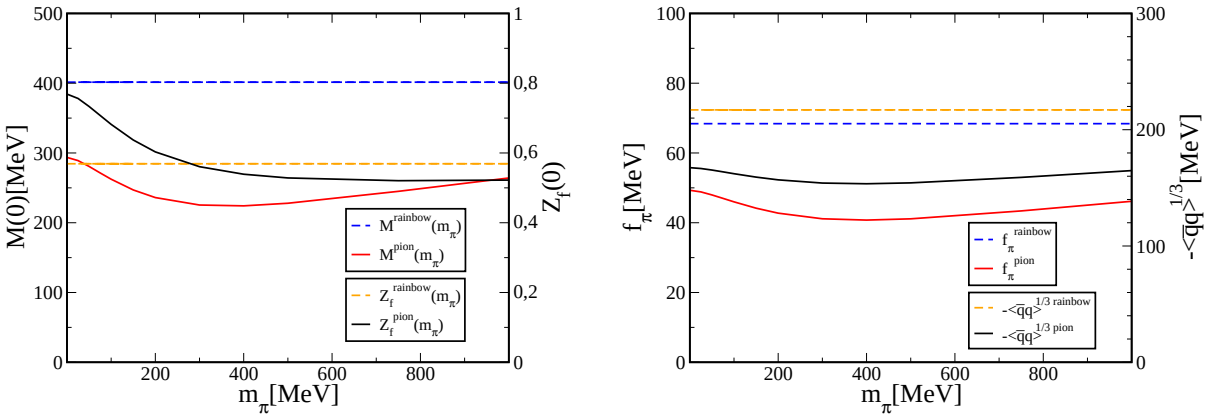

Figure 5.7: The dressing functions $Z_f(0)$, $M(0)$ at vanishing momentum (left) and f_π, $-\langle\bar{q}q\rangle^{\frac{1}{3}}_{1\mathrm{GeV}}$ (right) for $\alpha_{II}(k)$ in rainbow approximation (dashed lines) and including the pion contribution (solid lines) as a function of the pion mass m_π.

$< 300\,\mathrm{MeV}$ the dependence seems to become non-linear and the question of appearing chiral non-analyticities can be addressed [150].

A remark concerning the absolute values of f_π and $\langle\bar{q}q\rangle$ is in order: Those values turn out to be significantly smaller than the physical values being $f_\pi^{physical} = 92\,\mathrm{MeV}$ and $\langle\bar{\psi}\psi\rangle^{physical}_{1\mathrm{GeV}} = -(0.24 \pm 0.01\,\mathrm{GeV})^3$ although we use the coupling $\alpha_{II}(k)$ for vanishing mass function (see Appendix D for details). This has already been noted in [81] and needs to be clarified in future studies. In particular the underestimation of f_π, appearing in the denominator of Eq.(5.20), might overestimate the contribution of the Goldstone bosons.

5.2 Goldstone modes in the CFL phase

We now apply the truncation of the previous section to color-superconducting phases. For this purpose we need to specify the broken global symmetries and consider the corresponding Ward-Takahashi identities for the quark propagator.

The derivation of these at finite temperature and chemical potential in the Nambu-Gor'kov formalism is similar as in the vacuum (see Appendix B.4). With the internal symmetry transformations given in section 2.3.3 we obtain for vector symmetries

$$P_\mu \Gamma^M_\mu(k;P) \;=\; \mathcal{S}^{-1}(k_+) i\mathcal{T}^M - i\mathcal{T}^M \mathcal{S}^{-1}(k_-) \tag{5.26}$$

and for axial symmetries

$$P_\mu \Gamma^M_{5\mu}(k;P) \;=\; \mathcal{S}^{-1}(k_+) i\gamma_5 \mathcal{T}^M_5 + i\gamma_5 \mathcal{T}^M_5 \mathcal{S}^{-1}(k_-)\,, \tag{5.27}$$

where

$$\mathcal{T}^M = \begin{pmatrix} T^M & 0 \\ 0 & -T^{M\,T} \end{pmatrix}, \quad \mathcal{T}_5^M = \begin{pmatrix} T^M & 0 \\ 0 & T^{M\,T} \end{pmatrix}, \quad T^M \in \mathfrak{u}(1) \otimes \mathfrak{su}(N_f) \tag{5.28}$$

and in the chiral limit. If a symmetry is spontaneously broken, the right hand side of Eq.(5.26) or Eq.(5.27) is finite in the limit $P_\mu \to 0$ and the corresponding vector or axial-vector current needs to couple to a Goldstone boson with the same quantum numbers. With a remaining $O(3)$-symmetry in an isotropic phase those have a dispersion relation [151] $ip_4 = \pm v_{GB,M}|\vec{p}|$, where $v_{GB,M}$ is the group velocity of the Goldstone modes and we have

$$\Gamma_\mu^M(k;P) = \frac{\tilde{P}_\mu}{P_4^2 + v_{GB,M}^2 \vec{P}^2}\, \phi^M(k;P) + O(P_\mu)\,, \tag{5.29}$$

$$\Gamma_{5\mu}^M(k;P) = \frac{\tilde{P}_\mu}{P_4^2 + v_{GB,M}^2 \vec{P}^2}\, \phi_5^M(k;P) + O(P_\mu)\,, \tag{5.30}$$

with $\tilde{P}_\mu = \left(v_{GB,M}^2 \vec{P}, P_4\right)$. Considering the BSEs of the vector and axial-vector vertices at the poles, we again find the residues to obey the homogeneous BSE. Therefore $\phi^M(k;P)$ and $\phi_5^M(k;P)$ are proportional to the BSAs of Goldstone bosons. At the residue those are then given by

$$\Gamma^M(k;0) = \frac{1}{r^M}\left(\mathcal{S}^{-1}(k) i\mathcal{T}^M - i\mathcal{T}^M \mathcal{S}^{-1}(k)\right)\,, \tag{5.31}$$

$$\Gamma_5^M(k;0) = \frac{1}{r_5^M}\left(\mathcal{S}^{-1}(k) i\gamma_5\mathcal{T}_5^M + i\gamma_5\mathcal{T}_5^M \mathcal{S}^{-1}(k)\right)\,. \tag{5.32}$$

The normalization constants r^M and r_5^M can be determined in an analogous fashion as in the chirally broken phase in the vacuum [141]: The vector and axial-vector vertices can be written as

$$\Gamma_\mu^M(k;P)\big|_{tu} = \frac{Z_2}{2}\int\frac{d^4q}{(2\pi)^4}\left[\mathcal{S}(q_+)\gamma_\mu\mathcal{T}^M\mathcal{S}(q_-)\right]_{sr}\mathcal{M}_{tu}^{rs}(q,k;P)\,, \tag{5.33}$$

$$\Gamma_{5\mu}^M(k;P)\big|_{tu} = \frac{Z_2}{2}\int\frac{d^4q}{(2\pi)^4}\left[\mathcal{S}(q_+)\gamma_\mu\gamma_5\mathcal{T}_5^M\mathcal{S}(q_-)\right]_{sr}\mathcal{M}_{tu}^{rs}(q,k;P)\,, \tag{5.34}$$

where $\mathcal{M}_{tu}^{rs}(q,k;P)$ is the fully-amputated quark-antiquark scattering amplitude in the Nambu-Gor'kov basis and the prefactor $\frac{1}{2}$ prevents a double-counting in the Nambu-Gor'kov formalism. For $P^2 \to 0$ we consider as in Eq.(5.18)

$$\mathcal{M}_{tu}^{rs}(q,k;P) = \sum_{M,GB}\left(\bar{\Gamma}_{GB}^M(q;-P)\right)\big|_{rs}\frac{1}{P_4^2 + v_{GB,M}^2\vec{P}^2}\left(\Gamma_{GB}^M(k;P)\right)\big|_{tu} + \mathcal{R}_{tu}^{rs}\,, \tag{5.35}$$

	axial symmetry		vector symmetry	
T^M	$\frac{\mathbb{1}}{2}$	$\frac{\tau^a}{2}$	$\frac{\mathbb{1}}{2}$	$\frac{\tau^a}{2}$
r^M, r_5^M	f_η	f_π	f_σ	f_{a_0}
$v_{GB,M}$	v_η	v_π	v_σ	v_{a_0}

Table 5.1: Basis and low-energy constants of Goldstone bosons in the CFL phase.

with a regular function $\mathcal{R}^{rs}_{tu}(q,k;P)$, the sum over all Goldstone modes and $\bar{\Gamma}^M_{GB}(q;P) = \gamma_4 \left(\Gamma^M_{GB}(-q;-P)\right)^\dagger \gamma_4$ for vanishing diagonal elements in Nambu-Gor'kov space. Using Eqs.(5.29-5.32) on the left side of Eqs.(5.33-5.34) and Eq.(5.35) on the right, we obtain

$$\frac{r^M \tilde{P}_\mu}{P_4^2 + v_M^2 \vec{P}^2}\,\Gamma^M(k;P) = \frac{Z_2}{2}\sum_{M',GB}\int\frac{d^4q}{(2\pi)^4}\mathrm{Tr}\left[\mathcal{S}(q_+)\gamma_\mu\mathcal{T}^M\mathcal{S}(q_-)\bar{\Gamma}^{M'}_{GB}(q;-P)\right]\times \frac{1}{P_4^2 + v^2_{GB,M'}\vec{P}^2}\Gamma^{M'}_{GB}(k;P)\,, \tag{5.36}$$

$$\frac{r_5^M \tilde{P}_\mu}{P_4^2 + v_{5,M}^2 \vec{P}^2}\,\Gamma^M_5(k;P) = \frac{Z_2}{2}\sum_{M',GB}\int\frac{d^4q}{(2\pi)^4}\mathrm{Tr}\left[\mathcal{S}(q_+)\gamma_\mu\gamma_5\mathcal{T}_5^M\mathcal{S}(q_-)\bar{\Gamma}^{M'}_{GB}(q;-P)\right]\times \frac{1}{P_4^2 + v^2_{GB,M'}\vec{P}^2}\Gamma^{M'}_{GB}(k;P)\,. \tag{5.37}$$

Choosing a basis with $\mathrm{Tr}\left[\mathcal{S}\gamma_\mu\mathcal{T}^M\mathcal{S}\bar{\Gamma}^{M'}_{GB}\right] \propto \delta^{M,M'}$ and $\mathrm{Tr}\left[\mathcal{S}\gamma_\mu\gamma_5\mathcal{T}_5^M\mathcal{S}\bar{\Gamma}^{M'}_{GB}\right] \propto \delta^{M,M'}$ for the Goldstone bosons yields

$$r^M\tilde{P}_\mu = \frac{Z_2}{2}\int\frac{d^4q}{(2\pi)^4}\mathrm{Tr}\left[\mathcal{S}(q_+)\gamma_\mu\mathcal{T}^M\mathcal{S}(q_-)\bar{\Gamma}^M_{GB}(q;-P)\right]\,, \tag{5.38}$$

$$r_5^M\tilde{P}_\mu = \frac{Z_2}{2}\int\frac{d^4q}{(2\pi)^4}\mathrm{Tr}\left[\mathcal{S}(q_+)\gamma_\mu\gamma_5\mathcal{T}_5^M\mathcal{S}(q_-)\bar{\Gamma}^{M'}_{GB}(q;-P)\right] \tag{5.39}$$

for $P^2 \to 0$, when approximating the Goldstone BSAs by Eqs.(5.31-5.32).

We are now ready to choose a basis for the Goldstone bosons in the CFL phase. Using the convention in Eq.(5.28) we consider the Goldstone bosons stated in Tab. 5.1. As the normalization conditions in Eq.(5.38) and Eq.(5.39) are identical to the coupling of the Goldstone bosons to the corresponding currents, the constants r^M and r_5^M are referred to as decay constants in analogy to the chirally broken phase.

For the axial symmetries this is straightforward as there is no residual symmetry left. The quasiparticle spectrum is similar to the chirally broken phase [152, 153], with a definition of color-singlet baryons even for the fermions [154]. For the vector symmetries the situation is slightly more complicated as we have a residual $SU(3)_{c+V}$ symmetry

group in $SU(3)_c \otimes SU(3)_V$ left. The Goldstone bosons are fluctuations on the coset $SU(3)_c \otimes SU(3)_V / SU(3)_{c+V}$. This means that the matrices $\frac{\tau^a}{2}$ stated in Tab. 5.1 for the vector symmetry are actually only representatives for the equivalence class

$$\left[\frac{\tau^a}{2}\right] \stackrel{\text{def}}{=} \left\{\frac{\tau^a}{2} + g : g \in \mathfrak{su}(3)_{c+V}\right\} \tag{5.40}$$

as the propagator commutes with the generators of the residual symmetry. We could therefore equally choose $\frac{\lambda^{aT}}{2}$ as a representative, which is generating the color symmetry. For this reason, the flavor symmetry is often not considered as the Goldstone bosons are assumed to be 'eaten' by the gluons [153]. This is not the case in our framework, as we are working in a fixed gauge and are not able to choose an implicit, *i.e.* order parameter dependent gauge, such as a unitary gauge [155].

On the other hand, the BSA of the Goldstone boson of the gauge group is exactly known due to the connection of color and flavor symmetry by the pairing pattern. This is a non-trivial result and we like to emphasize that the approximation of the STI of the quark propagator stated in the context of Eq.(2.31) is consistent with this result. In the Nambu-Gor'kov formalism it is given by

$$\tilde{f}(P) P_\mu \Gamma^a_\mu(k_+, k_-) = \mathcal{S}^{-1}(k_+) i \begin{pmatrix} \frac{\lambda^a}{2} & 0 \\ 0 & -\frac{\lambda^{aT}}{2} \end{pmatrix} - i \begin{pmatrix} \frac{\lambda^a}{2} & 0 \\ 0 & -\frac{\lambda^{aT}}{2} \end{pmatrix} \mathcal{S}^{-1}(k_-)\,, \tag{5.41}$$

with some real function $\tilde{f}(k) = -g\left(f(k)G(k)\right)^{-1}$. We can then equally deduce the BSA in Eq.(5.31) for the gauge symmetry by means of the approximated STI and the function $\tilde{f}(P)$ chancels out when normalizing the BSA.

5.2.1 Low-energy properties from WTIs

We are now able to derive the low-energy constants for the Goldstone modes from first principles and without using an effective field theory as in [156]. Using the qDSE in the Nambu-Gor'kov formalism given by Eq.(2.41) in the expression for BSA of the Goldstone bosons given by Eq.(5.31) and Eq.(5.32), we obtain for the parameterization in Eq.(3.15)

$$\Gamma^M(k;P) \simeq \frac{iZ_2}{r^M} \sum_i \begin{pmatrix} 0 & -\phi_i^-(k)\left(M_i T^{M\,T} + T^M M_i\right) \\ \phi_i^+(k)\left(M_i T^M + T^{M\,T} M_i\right) & 0 \end{pmatrix}, \tag{5.42}$$

$$\Gamma^M_5(k;P) \simeq \frac{iZ_2}{r^M_5} \sum_i \begin{pmatrix} 0 & \gamma_5\phi_i^-(k)\left(M_i T^{M\,T} + T^M M_i\right) \\ \gamma_5\phi_i^+(k)\left(M_i T^M + T^{M\,T} M_i\right) & 0 \end{pmatrix}. \tag{5.43}$$

Here we already neglected the normal self-energies $\Sigma^\pm$ as they are only weakly modified compared to the ungapped phase and are therefore almost symmetric. Using this approx-

imation in Eqs.(5.38-5.39) and remembering that $\phi_i^{\pm} = \gamma_4 \left(\phi_i^{\mp}\right)^{\dagger} \gamma_4$, we find

$$\begin{aligned}
\left(r^M\right)^2 \tilde{P}_\mu &= \left(r_5^M\right)^2 \tilde{P}_\mu \\
&= \frac{iZ_2^2}{2} \sum_{ijk} \int \frac{d^4q}{(2\pi)^4} \mathrm{Tr}_{c,f} \left(M_j T^M P_k \left(T^M M_i + M_i T^{M\,T}\right)\right) \times \\
&\qquad \Big(+ \mathrm{Tr}_D \left(T_j^-(q_+)\gamma_\mu S_k^-(q_-)\phi_i^+(q)\right) \\
&\qquad\quad + \mathrm{Tr}_D \left(T_j^+(q_+)\gamma_\mu S_k^+(q_-)\phi_i^-(q)\right) \\
&\qquad\quad - \mathrm{Tr}_D \left(S_k^+(q_+)\gamma_\mu T_j^-(q_-)\phi_i^+(q)\right) \\
&\qquad\quad - \mathrm{Tr}_D \left(S_k^-(q_+)\gamma_\mu T_j^+(q_-)\phi_i^-(q)\right) \Big) \\
&= \frac{iZ_2^2}{2} \sum_{ijk} \int \frac{d^4q}{(2\pi)^4} \mathrm{Tr}_{c,f} \left(M_j T^M P_k \left(T^M M_i + M_i T^{M\,T}\right)\right) \times \\
&\qquad\qquad \left(f_{ijk}(P) - f_{ijk}(P)^* + f_{ijk}(-P)^* - f_{ijk}(-P)\right) , \quad (5.44)
\end{aligned}$$

with $f_{ijk}(P) = \mathrm{Tr}_D \left(T_j^-(q_+)\gamma_\mu S_k^-(q_-)\phi_i^+(q)\right)$. This expression needs to be evaluated in the limit $P_\mu \to 0$. For $P_\mu = (0, P_4)$ it determines r^M and for $P_\mu = (\vec{P}, 0)$ it determines $v_M r^M$. We therefore obtain the decay constant and the group velocity of the Goldstone mode. In addition we observe the Goldstone bosons of vector and axial symmetry to have the same low-energy behavior, *i.e.* $r^M = r_5^M$ and $v_M = v_{5,M}$.

Results for simple parameterization Before coming to numerical results it is worth evaluating Eq.(5.44) for a simple parameterization near the Fermi surface. We approximate $Z_2 = 1$, $\phi_i^e(p) \to \Delta^e$ and $S_0^{+\,-1} + \Sigma^+ \to -ip_4 + v_F(p_F - i\vec{p}\,)$, which gives with Eq.(3.28)

$$\begin{aligned}
S_i^+(p) &= -\sum_{e=\pm} \frac{-ip_4 + v_F\left(e|\vec{p}| - p_F\right)}{p_4^2 + v_F^2\left(e|\vec{p}| - p_F\right)^2 + \delta_i |\Delta^e|^2} \Lambda_{\vec{p}}^e \gamma_4 \,, \\
T_i^+(p) &= -\sum_{e=\pm} \frac{\Delta^e}{p_4^2 + v_F^2\left(e|\vec{p}| - p_F\right)^2 + \delta_i |\Delta^e|^2} \Lambda_{\vec{p}}^{-e} \gamma_5 \,, \\
\phi_i^+(p) &= \sum_{e=\pm} \Delta^e \Lambda_{\vec{p}}^e \gamma_5 \,. \qquad (5.45)
\end{aligned}$$

Using this in Eq.(5.44) yields

$$\left(r^M\right)^2 = \frac{p_F^2}{\pi^2} \sum_{jk} \mathrm{Tr}\left(M_j T^M P_k \left(T^M M + M T^{M\,T}\right)\right) \frac{\delta_j - \delta_k + \delta_k \ln\left(\frac{\delta_k}{\delta_j}\right)}{\left(\delta_j - \delta_k\right)^2} + O(\Delta^{\pm}) \,, \quad (5.46)$$

where we used some regularization for the momentum integral, which is actually irrelevant to leading order in Δ^e. This remarkable result of being finite for $\Delta^e \to 0$ although Γ_{GB}^M

vanishes, is due to the fact that taking the limit and performing the integration is not commutable and the integrand is essentially a representation of the Dirac distribution. Evaluating this expression gives

$$\begin{aligned} f_\pi^2 = f_{a_0}^2 &= \frac{21-8\ln 2}{36}\,\frac{p_F^2}{\pi^2}\,, \\ f_\eta^2 = f_\sigma^2 &= \frac{3}{8}\,\frac{p_F^2}{\pi^2}\,, \\ v_\pi = v_\eta = v_{a_0} = v_\sigma &= \frac{v_F}{\sqrt{3}}\,, \end{aligned} \tag{5.47}$$

which has already been found in [156] by using an effective field theory approach. We therefore expect the decay constant to be essentially proportional to the chemical potential, whereas the group velocity of the Goldstone modes depends on the Fermi velocity of the quasiparticles. As we have seen in section 4.4.6 for the 2SC phase, this can significantly differ from the speed of light.

Explicit symmetry breaking As chiral symmetry is explicitly broken by non-vanishing current-quark masses, the Goldstone bosons are no longer massless. However for small explicit symmetry breaking, their masses obey a generalized GOR relation. The latter has been determined from effective theories [157, 158], but it is interesting to see that it can directly be deduced from the axWTI. Our procedure will also enable us to elucidate results obtained within NJL model calculations [159], which show a different behavior than QCD in the weakly coupled regime [157].

The axWTI at finite current-quark masses is given by

$$\begin{aligned} P_\mu \Gamma_{5\mu}^M(k;P) &= \mathcal{S}^{-1}(k_+) i\gamma_5 \mathcal{T}_5^M + i\gamma_5 \mathcal{T}_5^M \mathcal{S}^{-1}(k_-) \\ &\quad -2i \sum_{M'} \mathrm{Tr}_f(\{\hat{m}, T^M\} T^{M'})\, \tilde{\Gamma}_5^{M'}(k;P)\,. \end{aligned} \tag{5.48}$$

In order to avoid a confusion with the BSA of the Goldstone bosons, the scalar vertex function is denoted by $\tilde{\Gamma}_5^M(k;P)$ in this context. As the Goldstone modes no longer need to be massless, we assume the vertices to be of the form

$$\begin{aligned} \Gamma_{5\mu}^M(k;P) &= \frac{\tilde{P}_\mu}{P_4^2 + v_{5,M}^2 \vec{P}^2 + m_{5,M}^2}\, r_5^M \Gamma_5^M(k;0)\,, \\ \tilde{\Gamma}_5^M(k;P) &= \frac{-i}{P_4^2 + v_{5,M}^2 \vec{P}^2 + m_{5,M}^2}\, r_P^M \Gamma_5^M(k;0)\,, \end{aligned} \tag{5.49}$$

near the putative poles $P_4^2 + v_{5,M}^2 \vec{P}^2 + m_{5,M}^2 = 0$ and with the normalization condition

$$r_P^M = \frac{Z_4}{2} \int \frac{d^4q}{(2\pi)^4} \mathrm{Tr}\left[\mathcal{S}(q)\gamma_5 \mathcal{T}_5^M \mathcal{S}(q) \bar{\tilde{\Gamma}}_{GB}^M(q;0)\right]\,. \tag{5.50}$$

Equating Eq.(5.48) on the putative poles then gives for $\hat{m} = m\mathbb{1}$

$$m_{5,M}^2 \, r_5^M \;=\; 2\, m \, r_P^M \,. \tag{5.51}$$

We are therefore left to evaluate Eq.(5.50) to obtain a generalized GOR relation. In contrast to the chirally broken phase in the vacuum, r_P^M vanishes in the chiral limit and we need to consider a finite constituent quark mass. For a simple parameterization as in Eq.(5.45), the latter can be considered as an insertion, since

$$\begin{aligned} \mathcal{S}(p) &= \left(\mathcal{S}_{m=0}^{-1}(p) + \begin{pmatrix} M & \\ & M \end{pmatrix} \right)^{-1} \\ &= \mathcal{S}_{m=0}(p) \sum_n (-1)^n \left(\begin{pmatrix} M & \\ & M \end{pmatrix} \mathcal{S}_{m=0}(p) \right)^n . \end{aligned} \tag{5.52}$$

We mind the difference between the current-quark mass m and the constituent quark mass M. Evaluating Eq.(5.50) to lowest order for the pion gives

$$r_P^\pi f_\pi \;=\; \frac{\left(c_R + \ln \frac{\mu}{\Delta^+}\right)}{\pi^2} M \Delta^+ \Delta^- \,, \tag{5.53}$$

with the constant c_R depending on the regularization of the integral.

Several remarks are in order: As the integrand in Eq.(5.50) does not represent a distribution, the result is of order $O(\Delta^\pm)$. We get however a regularization scheme independent leading non-analytic contribution. Secondly, the mass insertion flips the chirality of the quarks and therefore in our expansion a quasiparticle to an anti-quasiparticle. Consequently the result depends on the anti-quasiparticle spectrum as can directly be seen when using Eq.(5.45). This also explains the appearance and importance of Δ^-. In the weakly coupled regime, we therefore need to determine the anti-quasiparticle gaps at least implicitly, which has been done in [157]. In the NJL-model we have $\Delta^+ = \Delta^-$ from the ansatz and for the commonly used $O(3)$-cutoff we obtain furthermore

$$c_R \;=\; \frac{-6 + 4\ln(2) + 3\ln\left(\frac{\Lambda^2 - \mu^2}{\mu^2}\right)}{6} \,. \tag{5.54}$$

We then have

$$m_\pi^2 f_\pi^2 \;=\; 2mM \frac{\left(c_R + \ln \frac{\mu}{\Delta^+}\right)}{\pi^2} \Delta^+ \Delta^- \,, \tag{5.55}$$

where $m_\pi \stackrel{\text{def}}{=} m_{5,M}$ for the axial $SU(3)$ symmetry. This is in very nice agreement with the masses determined within NJL model investigations by solving the BSE [159, 160].

The Goldstone boson masses play an important role when including neutrality constraints at a finite value of the strange-quark mass, as some Goldstone bosons, the kaons, might condense [158, 161, 162].

Connection to effective field theory As the expressions in Eq.(5.39), Eq.(5.50) and Eq.(5.51) are in principle exact, it is not surprising that the explicit expressions can be directly mapped onto those obtained in an effective field theory. When using the approximation

$$\Gamma_5^M(k;P) \;=\; \frac{1}{r_5^M}\left(\mathcal{S}^{-1}(k_+)i\gamma_5\mathcal{T}_5^M + i\gamma_5\mathcal{T}_5^M\mathcal{S}^{-1}(k_-)\right)\,, \tag{5.56}$$

which can be justified on equal footing, and considering the masses as insertion the use of the parameterization in Eq.(5.45) leads to identical expressions as in [156]. We can then think of an ordering scheme in a parameter x and set $\frac{M}{p_F} \sim \frac{m}{p_F} \sim \frac{\Delta^+}{p_F} \sim x^1$ as well as $\frac{m_{GB,M}}{p_F} \sim x^2$, which should be valid in a fully gapped and neutral phase.

5.2.2 The extended truncation scheme for the qDSE

Having worked out an extension scheme that exploits low-energy properties of Goldstone modes in the chirally broken vacuum, the application to color-superconducting phases is straightforward. We will focus on the most prominent phase, the CFL phase, and limit ourself to the chiral limit and the HDL-like approximation for the gluon in the qDSE.

As in Eq.(5.19) and section 5.1.4 the truncated self-energy is then given by

$$Z_2\Sigma(p) \;=\; Z_2\Sigma^{(HDL-like)}(p) + Z_2\Sigma^{(GB)}(p)\,, \tag{5.57}$$

with $Z_2\Sigma^{(HDL-like)}(p)$ approximated as in section 3 and

$$Z_2\Sigma^{(GB)}(p) \;=\; \sum_{M,GB}\int\frac{d^4q}{(2\pi)^4}\,\Gamma_{GB}^M(\frac{p+q}{2};0)\,\mathcal{S}(q)\,\bar{\Gamma}_{GB}^M(\frac{p+q}{2};0)\frac{1}{k_4^2+v_{GB,M}^2\vec{k}^2}\;. \tag{5.58}$$

The BSAs $\Gamma_{GB}^M(q;0)$ and low-energy constants r_{GB}^M, $v_{GB,M}$ are obtained from Eqs.(5.42-5.44). For simplicity all of these are determined from the HDL-like solution first, which is in accordance with the $1/N_c$-counting scheme in section 5.1.4.

As the gauge-dependent Goldstone bosons associated with vector symmetries are often not considered, we also show results for the pseudo-scalar Goldstone bosons only. In this case we assume

$$Z_2\Sigma^{(GB)}(p) \;=\; \sum_{M}\int\frac{d^4q}{(2\pi)^4}\,\Gamma_5^M(\frac{p+q}{2};0)\,\mathcal{S}(q)\,\bar{\Gamma}_5^M(\frac{p+q}{2};0)\frac{1}{k_4^2+v_{5,M}^2\vec{k}^2}\;. \tag{5.59}$$

However we emphasize that this treatment is not appropriate: Not only have we fixed the gauge, but also the BSAs of the 'colored' Goldstone modes are exactly determined from the propagator through color-flavor locking.

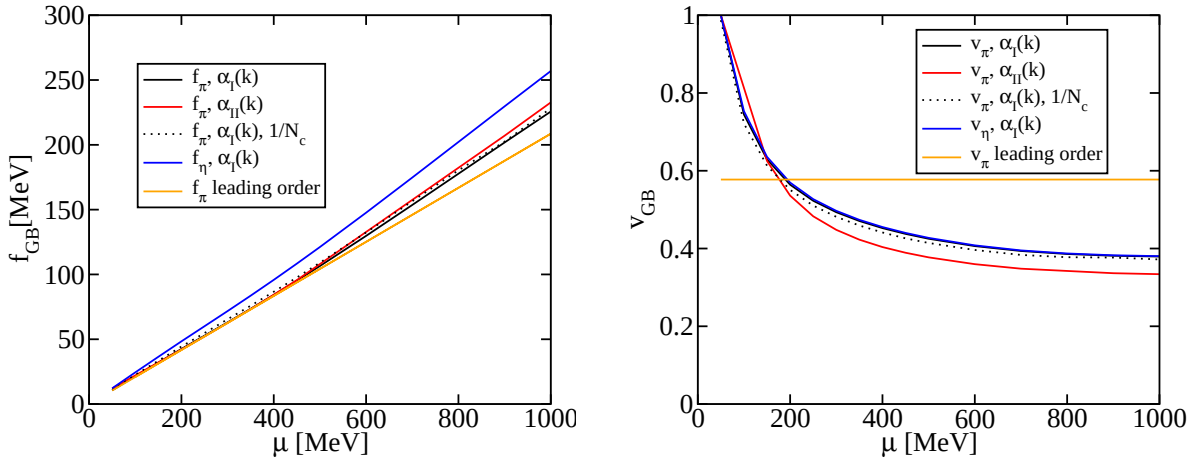

Figure 5.8: Decay constants (left) and group velocity (right) of Goldstone modes in the CFL phase. Shown are the results for f_π in the HDL-like approximation with $\alpha_I(k)$ (black) and $\alpha_{II}(k)$ (red). In addition f_π for the final solution including Goldstone modes with $\alpha_I(k)$ (black dotted) and for f_η (blue) are presented. The analytical result from Eq.(5.47) with $p_F \to \mu$ is also shown (yellow).

5.2.3 Numerical results

The numerical results for the low-energy constants obtained from the solutions of the HDL-like approximation shown in section 3 are presented in Fig. 5.8. We see the results for the decay constants to be in nice agreement with the lowest order results of the simple parameterization in Eq.(5.47). This is due to the fact that the result is to lowest order independent of the gap function and therefore of the coupling. As a consequence the decay constants obtained with different couplings for the HDL-like solution as well as for the solution including the Goldstone modifications in the self-energy are almost identical. For the group velocity of the Goldstone modes we obtain non-trivial results. This can be understood by a Fermi velocity differing from the speed of light, which has already been indicated in section 4.4.6 for the 2SC phase and which is in accordance with Eq.(5.47). For very small chemical potentials, which are not of phenomenological interest for color-superconductivity, the group velocity even exceeds the speed of light. This indicates a breakdown of our approximation and should be compensated by the condensation of Goldstone modes. Again the results with and without the Goldstone fluctuation almost agree, even between the different Goldstone modes, *i.e* v_η and v_π. However a dependence on $\alpha_s(k)$ becomes apparent.

In Fig. 5.9 and Fig. 5.10 we present the momentum dependence of the gap functions at the Fermi energy and for $\mu = 400\,\mathrm{MeV}$. As expected, we find the Goldstone modes to

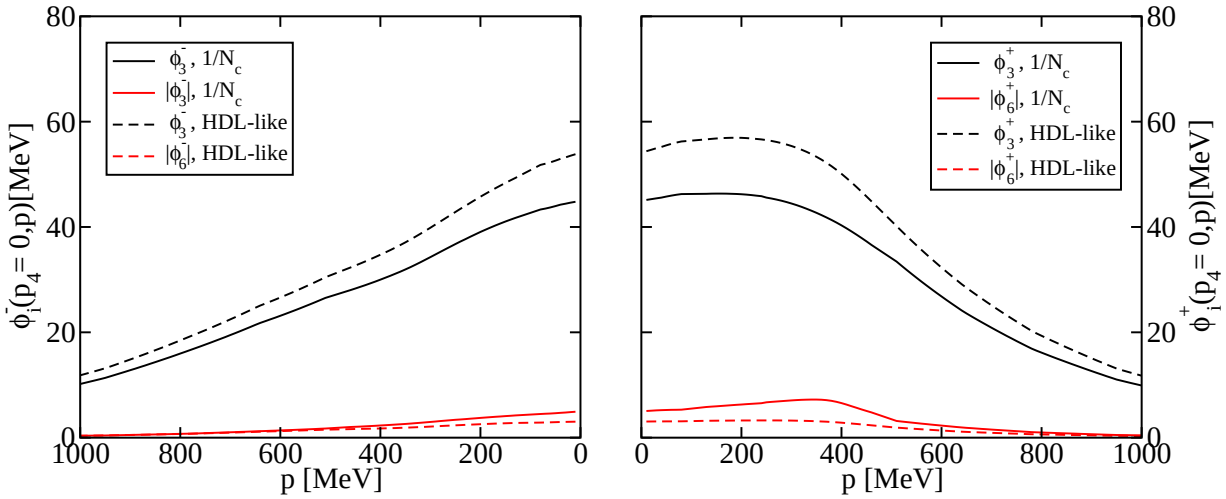

Figure 5.9: Quasiparticle gap functions ϕ^+ (right) and anti-quasiparticle gap functions ϕ^- (left) at the Fermi energy, *i.e.* $p_4 = 0$, for $\alpha_I(k)$ and $\mu = 400\,\text{MeV}$. Shown are the results for the $\bar{\mathbf{3}}$-gap functions (black) and the $\mathbf{6}$-gap functions (red) obtained the the HDL-like approximation (dashed) and including the Goldstone fluctuations (solid).

lower the magnitude of the $\bar{\mathbf{3}}$-gap function. The decrease can be as large as 30% for $\alpha_{II}(k)$ and is of course larger for larger BSAs, *i.e.* gap functions. As a result the differences of the results obtained with $\alpha_I(k)$ and $\alpha_{II}(k)$ decrease. In the repulsive $\mathbf{6}$-channel the gap function are increased and become sizable, even though they are still small compared to the $\bar{\mathbf{3}}$-channel. This is due to the fact that the interaction via Goldstone modes cannot be decomposed into a $\bar{\mathbf{3}}$- and a $\mathbf{6}$-channel, but is rather suited for $\mathbf{1}$- and $\mathbf{8}$-channels.

Finally we present the results for the value of the gap functions at the Fermi surface on the right hand side of Fig. 5.10. As in the chirally broken vacuum, we observe the Goldstone modes to lead to a sizable but not crucial effect in the order parameter. The magnitude of the gap functions are not altered and the sensitivity on the choice of $\alpha_s(k)$ is even reduced. For the running coupling $\alpha_{II}(k)$ we cannot investigate $\mu \to 0$ as gap functions for the HDL-like approximation do not vanish in the vacuum and therefore the BSAs of the Goldstone modes in our truncation diverge as $\frac{1}{\mu}$. From the solution excluding scalar Goldstone modes we see the variation in gap functions to be almost proportional to the number of Goldstone modes. This would allow us to treat the Goldstone modes as a perturbation.

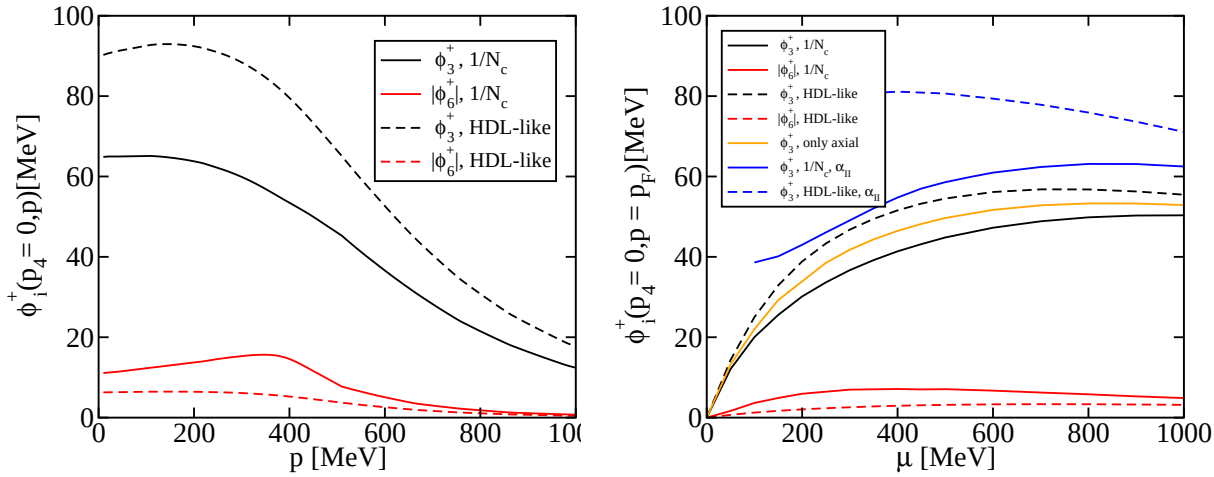

Figure 5.10: Left: Quasiparticle gap functions ϕ^+ at the Fermi energy, *i.e.* $p_4 = 0$, for $\alpha_{II}(k)$ and $\mu = 400\,\mathrm{MeV}$. Shown are the results for the $\bar{\mathbf{3}}$-gap functions (black) and the **6**-gap functions (red) obtained the the HDL-like approximation (dashed) and including the Goldstone fluctuations (solid). Right: Results for the gap functions at the Fermi surface, *i.e.* $p_4 = 0$ and $|\vec{p}| = p_F$, in the HDL-like approximation (dashed) and those including the Goldstone fluctuations (solid). Shown are the results for the $\bar{\mathbf{3}}$-gap functions with $\alpha_I(k)$ (black) and $\alpha_{II}(k)$ (blue). Also shown is the result excluding scalar Goldstone modes for $\alpha_I(k)$ as in Eq.(5.59) (yellow) and for the **6**-gap functions (red).

5.3 QRPA for the medium polarization

Having improved the vertex-construction in the qDSE, we can now turn to the medium polarization and aim for a self-consistent inclusion of the quark-propagator in the medium polarization (see section 2.3.4). Considering gauge invariance properly via STIs will also force us to improve the $q\bar{q}g$-vertex construction in the medium polarization. Connected to curious findings in the unbroken phase, the gap functions within this treatment are strongly enhanced compared to the HDL-like truncation scheme.

5.3.1 Is the unbroken phase meta-stable?

Considering the approximation in Eq.(3.2), we restricted ourselves to small, *i.e.* 'soft', external momenta to obtain the expressions in Eq.(3.4). This HDL-like approximation is

not really necessary and we are even able to obtain analytical results for

$$\begin{aligned} F(\vec{k}, k_4 = 0) &= \frac{4\alpha_s C_r}{\pi} \,\mathrm{Re} \int_0^\infty dq q^2 \frac{\theta(\mu - E_q)}{E_q} \left(1 + \frac{-4E_q^2 + |\vec{k}|^2}{4|\vec{k}|q} \ln\left(\frac{|\vec{k}| - 2q}{|\vec{k}| + 2q} \right) \right) , \\ G(\vec{k}, k_4 = 0) &= \frac{2\alpha_s C_r}{\pi} \,\mathrm{Re} \int_0^\infty dq q^2 \frac{\theta(\mu - E_q)}{E_q} \left(1 + \frac{4q^2 + |\vec{k}|^2}{4|\vec{k}|q} \ln\left(\frac{|\vec{k}| - 2q}{|\vec{k}| + 2q} \right) \right) , \end{aligned} \tag{5.60}$$

where $E_q = \sqrt{q^2 + m^2}$, $C_r = \frac{N_f}{2}$ and m is the bare quark mass[2]. For the transversal medium polarization function $G(\vec{k}, k_4)$ we then have

$$\begin{aligned} G(\vec{k}, k_4 = 0) &= \frac{2\alpha_s C_r}{3\pi} \,\mathrm{Re} \Bigg(p_F \mu + |\vec{k}|^2 \ln\left(\frac{m}{p_F + \mu} \right) + \\ &\quad \frac{\mu}{4|\vec{k}|} \left(3|\vec{k}|^2 + 4\left(\mu^2 - 3m^2 \right) \right) \ln\left(\frac{2p_F - |\vec{k}|}{2p_F + |\vec{k}|} \right) - \\ &\quad \frac{|\vec{k}|^4 + 2m^2|\vec{k}|^2 - 8m^4}{2|\vec{k}|\sqrt{|\vec{k}|^2 + 4m^2}} \ln\left(\frac{|\vec{k}|\mu - \sqrt{|\vec{k}|^2 + 4m^2} p_F}{|\vec{k}|\mu + \sqrt{|\vec{k}|^2 + 4m^2} p_F} \right) \Bigg) , \end{aligned} \tag{5.61}$$

where $\mu^2 = p_F^2 + m^2$. For finite m we find

$$G(\vec{k}, k_4 = 0) = \frac{2\alpha_s C_r}{3\pi} |\vec{k}|^2 \ln\left(\frac{m}{p_F + \mu} \right) + O(|\vec{k}|^4) \tag{5.62}$$

and in the chiral limit, *i.e.* $m = 0$,

$$\begin{aligned} G(\vec{k}, k_4 = 0) &= \frac{2\alpha_s C_r \mu^2}{3\pi} \left(1 - \frac{4\mu^2 + 3|\vec{k}|}{4\mu|\vec{k}|} \ln\left(\frac{2\mu + |\vec{k}|}{2\mu - |\vec{k}|} \right) - \frac{|\vec{k}|^2}{2\mu^2} \ln\left(-1 + \frac{4\mu^2}{|\vec{k}|^2} \right) \right) \\ &= -\frac{\alpha_s C_r}{3\pi} |\vec{k}|^2 \left(\ln\left(\frac{4\mu^2}{|\vec{k}|^2} \right) + \frac{5}{3} \right) + O(|\vec{k}|^4) . \end{aligned} \tag{5.63}$$

space-like pole and linear response Similar to what is shown in [163] for an external classical electrical field $\vec{E}_{cl}(\vec{k})$, we can determine the linear response to a static external (chromo-)magnetic field $\vec{B}_{cl}(\vec{k})$. We find for the total field $\vec{B}^{total}(\vec{k}) = \vec{B}_{cl}(\vec{k}) + \delta\vec{B}(\vec{k})$

$$\vec{B}^{total}(\vec{k}) = P^T(\vec{k}) \vec{B}_{cl}(\vec{k}) \frac{|\vec{k}|^2}{|\vec{k}|^2 + G(k_4 = 0, \vec{k})} . \tag{5.64}$$

[2]We allow for a finite quark mass as we will also address the non-relativistic limit.

Therefore a space-like pole in the transversal propagator - being the response function - results into a breakdown of linear response and signals an instability of the phase. Neglecting the vacuum polarization the 1-loop medium polarization produces such a pole as can be estimated from Eq.(5.63) by considering the slope. We find

$$k^2_{pole} \gtrsim 4\mu^2 \exp\left(\frac{2}{3} - \frac{3\pi}{\alpha_s C_r}\right) . \tag{5.65}$$

non-relativistic limit In the non-relativistic limit we have $\mu = m + \delta\mu$ with $\delta\mu \ll m$. We therefore get

$$G(\vec{k}, k_4 = 0) = -\frac{2\sqrt{2}\alpha_s C_r}{3\pi}|\vec{k}|^2\sqrt{\frac{\delta\mu}{m}} + O(|\vec{k}|^4, \frac{\delta\mu}{m}) . \tag{5.66}$$

In principle we have now one more dimension-full parameter m and can define the reliability of the non-relativistic approximation by its ratio with the chemical potential. For

$$\alpha_s C_r < \pi\sqrt{\frac{9\,m}{8\,\delta\mu}} \ll 1 \tag{5.67}$$

we do not expect a space-like pole in the transversal part of the medium polarization, which can be considered as the non-relativistic regime. It is also worth remarking that $G(\vec{k}, k_4 = 0)$ vanishes for $m \to \mu$ in general.

vacuum polarization In QCD the quark-loop contribution to the 1-loop vacuum polarization of the gluons in the $\overline{\rm MS}$ scheme is given by [3]

$$G^{q,vac}(k) = \frac{\alpha_s C_r}{3\pi}\, k^2 \left(\ln\left(\frac{\nu^2}{k^2}\right) + \frac{5}{3}\right) \tag{5.68}$$

and the Yang-Mills contribution by

$$G^{YM,vac}(k) = -\frac{\alpha_s C_F}{36\pi}\, k^2 \left(15\ln\left(\frac{\nu^2}{k^2}\right) + 34\right) , \tag{5.69}$$

with the renormalization scale ν. The total 1-loop polarization is then

$$\begin{aligned} G^{total}(\vec{k}, k_4 = 0) &= G^{vac}(\vec{k}, k_4 = 0) + G(\vec{k}, k_4 = 0) \\ &= -\frac{\alpha_s C_r}{3\pi}|\vec{k}|^2 \ln\left(\frac{4\mu^2}{\nu^2}\right) - \frac{\alpha_s C_F}{36\pi}|\vec{k}|^2 \left(15\ln\left(\frac{\nu^2}{|\vec{k}|^2}\right) + 34\right) \\ &\quad + O(|\vec{k}|^4) \end{aligned} \tag{5.70}$$

and our instability is connected to the Landau pole in the infrared. Note the singularity of the medium polarization to be exactly compensated by the quark-loop contribution.

In the Abelian case, where the Yang-Mills contribution disappears, we therefore at least expect a charge renormalization in the medium. Nevertheless it is unclear, whether the pole from the medium polarization is an artefact of the Landau pole, as the latter should already be cured (it is also absent in our truncation setting proposed in section 2.3.4) and the vacuum polarization is usually neglected in medium studies. In addition the pole in the propagator only appears in a certain kinematical region, *i.e.* for $k_4/|\vec{k}| \ll 1$ when $k^2 \to 0$.

Choosing $\nu = 2\mu$ we estimate the space-like pole in $\left(|\vec{k}|^2 + G^{total}(\vec{k}, k_4 = 0)\right)^{-1}$ by the vanishing derivative

$$\begin{aligned} |\vec{k}|_{pole} &\gtrsim 2\mu \exp\left(\frac{17}{15}\right) \exp\left(-\frac{6\pi}{5\alpha_s C_F}\right) \\ &\gtrsim \mu \exp\left(-\frac{6\pi}{5\alpha_s C_F}\right) . \end{aligned} \tag{5.71}$$

Interestingly enough this is independent of N_f. Assuming $k_4 \approx |\vec{k}|^3/m_g^2$ as we have found in section 3 for the unbroken phase, the parametric energy scale is

$$k_{4,pole} \sim \mu \exp\left(-\frac{18\pi}{5\alpha_s C_F}\right) . \tag{5.72}$$

This can be compared to the non-Fermi liquid scale [100]

$$k_{4,non-Fermi-liquid} \sim \mu \exp\left(-\frac{3\pi}{\alpha_s C_F}\right) . \tag{5.73}$$

We emphasize that the identification $k_4 \approx |\vec{k}|^3/m_g^2$ from the HDL-like solution may not need to apply.

open questions We find a space-like pole in the gluon propagator, which would signal an instability of the unbroken phase. In other words it would not even be meta-stable. It is however unclear, whether the pole relies on the 1-loop approximation, *e.g.* its scale is that related to the Landau pole. Nevertheless it will also influence our following investigations due to our truncation.

It is however remarkable that it is of the same order as the non-Fermi liquid scale. The investigation of those, as has been done in [100, 102, 164], is therefore highly questionable.

Also interesting would be the study of the temperature dependence of this behavior and whether the space-like pole disappears for a hot enough quark-gluon plasma.

5.3.2 $q\bar{q}g$-vertex construction from STI

In order to find a transversal medium polarization, *i.e.* $\Pi_{\mu\nu}k_\nu = 0$, we need to have a suited $q\bar{q}g$-vertex. As motivated in section 2.2.3 we can use an Abelian vertex construction under assumptions for the unconstrained ghost-gluon scattering kernel. This is in particular an appropriate choice for the BSAs of the Goldstone modes (see section 5.2) and gives perturbatively the 2-loop result in the kinematical regime of interest [165]. We therefore consider as in the context of Eq.(2.31)

$$k_\mu \mathcal{V}^a_\mu(p,q) = \mathcal{S}^{-1}(p) i \begin{pmatrix} \frac{\lambda^a}{2} & 0 \\ 0 & -\frac{\lambda^{aT}}{2} \end{pmatrix} - i \begin{pmatrix} \frac{\lambda^a}{2} & 0 \\ 0 & -\frac{\lambda^{aT}}{2} \end{pmatrix} \mathcal{S}^{-1}(q)\,, \tag{5.74}$$

with

$$\Gamma^a_\mu(q,p;\nu) = \frac{\tilde{Z}_3(\nu,\Lambda)}{\alpha_s(\nu)} \frac{\alpha_s(k)}{Z(k;\nu)} \mathcal{V}^a_\mu(q,p;\nu)\,. \tag{5.75}$$

Ball-Chiu vertex for unbroken phase in medium The idea of the Ball-Chiu vertex construction [79] is to use the WTI in Eq.(5.74) and consider

$$\begin{aligned} \mathcal{V}^a_\mu(p,q) &= \left(\delta_{\mu\nu} - \frac{k_\mu k_\nu}{k^2}\right) \mathcal{V}^a_\nu(p,q) \\ &\quad + i\frac{k_\mu}{k^2} \left(\mathcal{S}^{-1}(p) \begin{pmatrix} \frac{\lambda^a}{2} & 0 \\ 0 & -\frac{\lambda^{aT}}{2} \end{pmatrix} - \begin{pmatrix} \frac{\lambda^a}{2} & 0 \\ 0 & -\frac{\lambda^{aT}}{2} \end{pmatrix} \mathcal{S}^{-1}(q) \right)\,. \end{aligned} \tag{5.76}$$

The transversal part

$$\mathcal{V}^{T,a}_\mu(p,q) = \left(\delta_{\mu\nu} - \frac{k_\mu k_\nu}{k^2}\right) \mathcal{V}^a_\nu(p,q) \tag{5.77}$$

is partially constrained by the requirement not to generate an artificial kinematic singularity coming from $1/k^2$. For the unbroken phase we have $[S^\pm(p)^{-1}, \lambda^a] = 0$ leading to

$$V^{+a}_\mu(p,p) = i\frac{\partial S^+(p)^{-1}}{\partial p_\mu}\frac{\lambda^a}{2} \tag{5.78}$$

for

$$\mathcal{V}^a_\mu(p,q) = \begin{pmatrix} V^{+a}_\mu(p,q) & W^{-a}_\mu(p,q) \\ W^{+a}_\mu(p,q) & V^{-a}_\mu(p,q) \end{pmatrix}\,. \tag{5.79}$$

In addition we of course have $W^a_\mu(p,q) = 0$. In order to avoid an artifical kinematic singularity in the transversal part of the vertex, this property needs to be implemented into the truncation. For

$$S^+(p)^{-1} = -i\not{p}\, A(p) - i\not{\omega}_p\, C(p) \tag{5.80}$$

we get

$$\begin{aligned}\frac{\partial S^+(p)^{-1}}{\partial p_i} &= -i\gamma_i A(p) - 2i\vec{\not{p}}\, p_i \frac{\partial A(p)}{\partial \vec{p}^2} - 2i\not{\psi}_p p_i \frac{\partial C(p)}{\partial \vec{p}^2}\,, \\ \frac{\partial S^-(p)^{-1}}{\partial p_4} &= -i\gamma_4 C(p) - 2i\vec{\not{p}}\, p_4 \frac{\partial A(p)}{\partial p_4^2} - 2i\not{\psi}_p p_4 \frac{\partial C(p)}{\partial p_4^2}\,. \end{aligned} \tag{5.81}$$

To get this limit in a symmetric way in q and p, we generalize

$$\begin{aligned}V_\mu^{+a}(p,q) &= \Bigg(\frac{A(p)+A(q)}{2}\,(1-\delta_{4\mu})\gamma_\mu + \frac{C(p)+C(q)}{2}\,\delta_{4\mu}\gamma_\mu + \\ &\quad \frac{(p+q)_\mu(\vec{\not{p}}+\vec{\not{q}})}{2}\,\frac{A(p)-A(q)}{p^2-q^2} + \\ &\quad \frac{(p+q)_\mu(\not{\psi}_p+\not{\psi}_q)}{2}\,\frac{C(p)-C(q)}{p^2-q^2}\Bigg)\frac{\lambda^a}{2}. \end{aligned} \tag{5.82}$$

It fulfills Eq.(5.74) and Eq.(5.78). The construction is however not as unique as usually claimed [80].

Ball-Chiu vertex in color-superconducting phase With the color symmetry in a fixed gauge explicitly broken, we get Goldstone bosons with the quantum numbers of the gluons. In the vertex this is reflected by a kinematic singularity of the form

$$\mathcal{V}_\mu^a(p,q) = \frac{\tilde{k}_\mu}{k_4^2 + v_{a_0}^2 \vec{k}^2} f_{a_0}\Gamma^a_{GB}(\frac{p+q}{2};k) + \mathcal{V}_\mu^{reg,a}(p,q), \tag{5.83}$$

with $\tilde{k}_\mu = \left(v_{a_0}^2 \vec{k}, k_4\right)$, corresponding to an s-channel Goldstone boson (see Eq.(5.41)). The regular part $\mathcal{V}_\mu^{reg,a}(p,q)$ of the vertex function should not contain kinematic singularities. In the approximation

$$\begin{aligned} f_{a_0}\Gamma^a_{GB}(p;k) &\approx f_{a_0}\Gamma^a_{GB}(p;k=0) \\ &= \mathcal{S}^{-1}(p)\, i\frac{\Lambda^a}{2} - i\frac{\Lambda^a}{2}\,\mathcal{S}^{-1}(p)\,, \end{aligned} \tag{5.84}$$

where

$$\Lambda^a = \begin{pmatrix} \lambda^a & 0 \\ 0 & -\lambda^{a,T} \end{pmatrix}, \tag{5.85}$$

we get for the regular part of the vertex:

$$\begin{aligned}
\mathcal{V}_\mu^{reg,a}(p,q) &= \mathcal{V}_\mu^{T,a}(p,q) + i\frac{\tilde{k}_\mu}{k\cdot\tilde{k}}\left(\mathcal{S}^{-1}(p)\frac{\Lambda^a}{2} - \frac{\Lambda^a}{2}\mathcal{S}^{-1}(q) + if_{a_0}\Gamma^a_{GB}(\frac{p+q}{2};k)\right) \\
&= \mathcal{V}_\mu^{T,a}(p,q) + \\
&\quad i\frac{\tilde{k}_\mu}{k\cdot\tilde{k}}\left(\left(\mathcal{S}^{-1}(p) - \mathcal{S}^{-1}(\frac{p+q}{2})\right)\frac{\Lambda^a}{2} - \frac{\Lambda^a}{2}\left(\mathcal{S}^{-1}(q) - \mathcal{S}^{-1}(\frac{p+q}{2})\right)\right) \\
&= \left(\mathcal{V}_\mu^{left}(p,q) + i\frac{\tilde{k}_\mu}{k\cdot\tilde{k}}\left(\mathcal{S}^{-1}(p) - \mathcal{S}^{-1}(\frac{p+q}{2})\right)\right)\frac{\Lambda^a}{2} - \\
&\quad \frac{\Lambda^a}{2}\left(\mathcal{V}_\mu^{right}(p,q) + i\frac{\tilde{k}_\mu}{k\cdot\tilde{k}}\left(\mathcal{S}^{-1}(q) - \mathcal{S}^{-1}(\frac{p+q}{2})\right)\right) . \qquad (5.86)
\end{aligned}$$

Here we decomposed the transversal part of the vertex $\mathcal{V}_\mu^{reg,a}(p,q)$ into $\mathcal{V}_\mu^{left}(p,q)$ and $\mathcal{V}_\mu^{right}(p,q)$. We can then again construct the transversal part of the vertex in order to avoid further kinematic singularities by extending the Ball-Chiu vertex construction to

$$\mathcal{V}_\mu^{left}(p,q) + i\frac{\tilde{k}_\mu}{k\cdot\tilde{k}}\left(\mathcal{S}(p)^{-1} - \mathcal{S}(\frac{p+q}{2})^{-1}\right) \qquad (5.87)$$

and

$$\mathcal{V}_\mu^{right}(p,q) + i\frac{\tilde{k}_\mu}{k\cdot\tilde{k}}\left(\mathcal{S}(q)^{-1} - \mathcal{S}(\frac{p+q}{2})^{-1}\right) . \qquad (5.88)$$

Explicit expressions More explicitly we get with

$$\mathcal{S}^{-1}(p) = Z_2\mathcal{S}_0^{-1}(p) + Z_2\Sigma(p) \qquad (5.89)$$

and

$$\begin{aligned}
\mathcal{S}_0^{-1}(p) &= \begin{pmatrix} -i\vec{p}\cdot\vec{\gamma} - i(p_4 + i\mu + \frac{Z_{1F}}{Z_2}gA_4)\gamma_4 & 0 \\ 0 & -i\vec{p}\cdot\vec{\gamma} - i(p_4 - i\mu - \frac{Z_{1F}}{Z_2}gA_4^T)\gamma_4 \end{pmatrix} \\
&= \begin{pmatrix} S_0^+(p)^{-1} & 0 \\ 0 & S_0^-(p)^{-1} \end{pmatrix} \qquad (5.90)
\end{aligned}$$

for our common parameterization with help of basis matrices $\{P_i\}$ and $\{M_i\}$, *i.e.*

$$\mathcal{S}^{-1}(p) = Z_2\sum_i \begin{pmatrix} \left(S_{0,i}^+(p)^{-1} + \Sigma_i^+(p)\right)P_i & \phi_i^-(p)M_i \\ \phi_i^+(p)M_i & \left(S_{0,i}^-(p)^{-1} + \Sigma_i^-(p)\right)P_i \end{pmatrix} , \qquad (5.91)$$

the regular part of the vertex to be given by

$$\begin{aligned}\mathcal{V}_{\mu}^{reg,a}(p,q) &= \sum_i \begin{pmatrix} \frac{1}{2}V_{i,\mu}^{BC+}\left(p,\frac{p+q}{2}\right)P_i & \frac{1}{2}W_{i,\mu}^{BC-}\left(p,\frac{p+q}{2}\right)M_i \\ \frac{1}{2}W_{i,\mu}^{BC+}\left(p,\frac{p+q}{2}\right)M_i & \frac{1}{2}V_{i,\mu}^{BC-}\left(p,\frac{p+q}{2}\right)P_i \end{pmatrix}\frac{\Lambda^a}{2} + \\ &\quad \frac{\Lambda^a}{2}\sum_i \begin{pmatrix} \frac{1}{2}V_{i,\mu}^{BC+}\left(\frac{p+q}{2},q\right)P_i & \frac{1}{2}W_{i,\mu}^{BC-}\left(\frac{p+q}{2},q\right)M_i \\ \frac{1}{2}W_{i,\mu}^{BC+}\left(\frac{p+q}{2},q\right)M_i & \frac{1}{2}V_{i,\mu}^{BC-}\left(\frac{p+q}{2},q\right)P_i \end{pmatrix}, \end{aligned} \tag{5.92}$$

where $V_{i,\mu}^{BC\pm}(p,q)$ and $W_{i,\mu}^{BC\pm}(p,q)$ are Ball-Chiu constructions. The latter are given by

$$\begin{aligned} V_{i,\mu}^{BC+}(p,q) &= Z_2\Big(\frac{2+\Sigma_{A,i}^+(p)+\Sigma_{A,i}^+(q)}{2}(1-\delta_{4\mu})\gamma_\mu + \frac{2+\Sigma_{C,i}^+(p)+\Sigma_{C,i}^+(q)}{2}\delta_{4\mu}\gamma_\mu + \\ &\quad \frac{(p+q)_\mu(\not{p}+\not{q})}{2}\frac{\Sigma_{A,i}^+(p)-\Sigma_{A,i}^+(q)}{p^2-q^2} + \\ &\quad \frac{(p+q)_\mu(\not{\omega}_{p,i}+\not{\omega}_{q,i})}{2}\frac{\Sigma_{C,i}^+(p)-\Sigma_{C,i}^+(q)}{p^2-q^2}\Big), \\ W_{i,\mu}^{BC+}(p,q) &= Z_2\Big(\frac{\phi_{C,i}^+(p)-\phi_{C,i}^+(q)}{p^2-q^2}(p_\mu+q_\mu) + \frac{\not{p}\,\phi_{A,i}^+(p)-\not{q}\,\phi_{A,i}^+(q)}{p^2-q^2}\gamma_4(p_\mu+q_\mu)\Big), \end{aligned} \tag{5.93}$$

where $\omega_{p,i}=p_4+i\mu+\frac{Z_{1F}}{Z_2}gA_{4.i}$. The Goldstone mode contribution is given by

$$\begin{aligned} f_{a_0}\Gamma_{GB}^a(p;k) &= \mathcal{S}^{-1}(p)\,i\frac{\Lambda^a}{2} - i\frac{\Lambda^a}{2}\,\mathcal{S}^{-1}(p) \\ &= \frac{iZ_2}{2}\sum_i \begin{pmatrix} (S_{0,i}^+(p)^{-1}+\Sigma_i^+(p))\,[P_i,\lambda^a] & -\phi_i^-(p)\,(\lambda^a M_i + M_{i,T}\lambda^a) \\ +\phi_i^+(p)\left(\lambda^{a,T}M_i + M_i\lambda^a\right) & (S_{0,i}^-(p)^{-1}+\Sigma_i^-(p))\left[\lambda^{a,T},P_i\right] \end{pmatrix} \end{aligned} \tag{5.94}$$

A remark is in order: Applying this vertex construction to the unbroken phase is possible on an equal footing, however, the vertex construction is not identical to the one in Eq.(5.82). This is connected to our statement that the Ball-Chiu construction is not unique and stems from $\Gamma(p,q)\neq\frac{1}{2}\Gamma(p,\frac{p+q}{2})+\frac{1}{2}\Gamma(\frac{p+q}{2},q)$. The applicability of Eq.(5.93) for the unbroken phase is actually a constraint on the vertex construction, since one might be tempted to use $(\tilde{p}_\mu+\tilde{q}_\mu)/(p\cdot\tilde{p}-q\cdot\tilde{q})$ instead of $(p_\mu+q_\mu)/(p^2-q^2)$ in the explicit Ball-Chiu construction. As $v_{a_0}\neq 1$ for $\phi^\pm\to 0$ only the employed construction makes the vertex construction independent of the low-energy constants of Goldstone bosons when going to the unbroken phase continuously.

Transversality of the polarization tensor For the transverality we simply need

$$\begin{aligned}
\Pi^{ab}_{\mu\nu}(k)k_\nu &\propto \int\frac{d^4q}{(2\pi)^4}\mathrm{Tr}_{D,c,f,NG}\left[\gamma_\mu\Lambda^a\mathcal{S}^{-1}\Gamma^b_\nu k_\nu\mathcal{S}^{-1}\right]\\
&\propto \int\frac{d^4q}{(2\pi)^4}\mathrm{Tr}_{D,c,f,NG}\left[\gamma_\mu\Lambda^a\Lambda^b\mathcal{S}^{-1}-\gamma_\mu\Lambda^a\mathcal{S}^{-1}\Lambda^b\right]\\
&\propto \int\frac{d^4q}{(2\pi)^4}\mathrm{Tr}_{D,c,f,NG}\left[\gamma_\mu\left[\Lambda^a,\Lambda^b\right]\mathcal{S}^{-1}\right]\\
&\propto \sum_i\mathrm{Tr}_{c,f}\left[\left[\lambda^a,\lambda^b\right]P_i\right]\,. \qquad (5.95)
\end{aligned}$$

The integrals are formally divergent. Focusing on the medium polarization, we subtract the vacuum polarization which regularizes the integrals. For the vacuum polarization we assume a symmetry conserving renormalization scheme and therefore a transversal propagator in Landau gauge. In the CFL phase we can perform the flavor trace first, get the remains of P_i to be proportional to the Casimir and therefore finally zero for the color trace. In the 2SC phase, we could get contributions to the $\Pi_{4\nu}(k)k_\nu$ component for the antisymmetric part in a and b.

5.3.3 Medium polarization and the Meissner effect

Using our extended Ball-Chiu construction in Eq.(2.76) gives

$$\begin{aligned}
\Pi^{\mathrm{med}\,ab}_{\mu\nu}(k) &= -\frac{Z_2\,2\pi\alpha_s(k)}{Z(k)}\int\frac{d^4p}{(2\pi)^4}\mathrm{Tr}_{D,c,f,NG}\Bigg(\left[\Gamma^{(0)a}_{NG\mu}\mathcal{S}(p)\mathcal{V}^b_\nu(p,q)\mathcal{S}(q)\right]\\
&\qquad -\Big[\dots\Big]_{\mu=0}\Bigg)\,, \qquad (5.96)
\end{aligned}$$

which splits into two parts by Eq.(5.83):

$$\Pi^{\mathrm{med}\,ab}_{\mu\nu}(k) = \Pi^{\mathrm{med}\,ab}_{GB\,\mu\nu}(k)+\Pi^{\mathrm{med}\,ab}_{reg\,\mu\nu}(k)\,, \qquad (5.97)$$

where

$$\begin{aligned}
\Pi^{\mathrm{med}\,ab}_{GB\,\mu\nu}(k) &= -\frac{Z_2\,2\pi\alpha_s(k)}{Z(k)}\frac{k_\nu}{k^2}f_{a_0}\int\frac{d^4p}{(2\pi)^4}\mathrm{Tr}_{D,c,f,NG}\left(\left[\Gamma^{(0)a}_{NG\mu}\mathcal{S}(p)\Gamma^a_{GB}(\frac{p+q}{2};k)\mathcal{S}(q)\right]\right),\\
\Pi^{\mathrm{med}\,ab}_{reg\,\mu\nu}(k) &= -\frac{Z_2\,2\pi\alpha_s(k)}{Z(k)}\int\frac{d^4p}{(2\pi)^4}\mathrm{Tr}_{D,c,f,NG}\Bigg(\left[\Gamma^{(0)a}_{NG\mu}\mathcal{S}(p)\mathcal{V}^{reg,b}_\mu(p,q)\mathcal{S}(q)\right]\\
&\qquad -\Big[\dots\Big]_{\mu=0}\Bigg)\,. \qquad (5.98)
\end{aligned}$$

The chemical potential μ should not be confused with the Lorentz index μ here. In our approximation for the BSA of the Goldstone modes in Eq.(5.94) we then obtain as in Eq.(5.38)

$$\Pi^{\text{med}\,ab}_{GB\;\mu\nu}(k) \;=\; -\frac{4\pi\alpha_s(k)f_{a_0}^2}{Z(k)}\frac{\tilde{k}_\mu\tilde{k}_\nu}{k_4^2+v_{a_0}^2\vec{k}^2}\,\delta^{ab} \tag{5.99}$$

for $k^2\to 0$. Due to Galilean invariance we also have

$$\Pi^{\text{med}\,ab}_{reg\;\mu\nu}(k) \;=\; A^{ab}\delta_{4\mu}\delta_{4\nu}+B^{ab}\delta_{4\mu}\hat{k}_\nu+C^{ab}\hat{k}_\mu\delta_{4\nu}+D^{ab}\hat{k}_\mu\hat{k}_\nu\,, \tag{5.100}$$

with functions A^{ab}, B^{ab}, C^{ab}, D^{ab} to be determined and $\hat{k}_\nu=(\vec{k}/k,0)$, $k=|\vec{k}|$. Since the polarization tensor should be symmetric in μ and ν we should have $B^{ab}=C^{ab}$. This might be violated by our truncation, but we postpone this problem for the moment. Due to the transversality $\Pi^{\text{med}\,ab}_{\mu\nu}(k)k_\nu=0$ we find however

$$0 \;=\; k_4A^{ab}\delta_{4\mu}+kB^{ab}\delta_{4\mu}+k_4C^{ab}\hat{k}_\mu+kD^{ab}\hat{k}_\mu-\frac{4\pi\alpha_s(k)f_{a_0}^2}{Z(k)}\,\tilde{k}_\mu\,\delta^{ab}\,. \tag{5.101}$$

For $k_4=0$ and $\vec{k}\to 0$ we then find

$$D^{ab} \;=\; \frac{4\pi\alpha_s(k)v_{a_0}^2f_{a_0}^2}{Z(k)}\,\delta^{ab} \tag{5.102}$$

and with help of the parameterization in Eq.(2.81) we get the amazing result

$$\begin{aligned} m^2_{M,ab} &\stackrel{\text{def}}{=} \lim_{\vec{k}\to 0}\Pi_T^{ab}(\vec{k},k_4=0) \\ &= 4\pi\alpha_s(0)v_{a_0}^2f_{a_0}^2\,\delta^{ab} \end{aligned} \tag{5.103}$$

for the Meissner mass[3]. This has already been found in the weak coupling limit [156, 166] and the role of the gauge invariance has been clarified in [155]. However, the Debye mass

$$m^2_{D,ab} \;\stackrel{\text{def}}{=}\; \lim_{\vec{k}\to 0}\Pi_L^{ab}(\vec{k},k_4=0) \tag{5.104}$$

is not constrained by gauge symmetry as we only have

$$0 \;=\; k_4A^{ab}-\frac{4\pi\alpha_s(k)f_{a_0}^2}{Z(k)}\,k_4\,\delta^{ab} \tag{5.105}$$

for $\vec{k}=0$ and $k_4\to 0$, which is fulfilled trivially. We therefore do not need to and will not find

$$m^2_{D,ab} \;=\; 4\pi\alpha_s(0)f_{a_0}^2\,\delta^{ab} \tag{5.106}$$

[3]Due to the dressing function $Z(k)\neq 1$ this parameter takes the role of the Meissner mass in the gap equation, but is strictly speaking not the Meissner mass defined by the response function.

as in the weakly coupled regime [155, 156, 166].

The evaluation of Eq.(5.98) is tedious but straightforward. For $\Pi^{\text{med}\,ab}_{GB\;\mu\nu}(k)$ we refer to the similar evaluation in Eq.(5.44). For $\Pi^{\text{med}\,ab}_{reg\;\mu\nu}(k)$ the use of Eq.(5.92) gives

$$\begin{aligned}
\Pi^{\text{med}\,ab}_{\mu\nu}(k) \;=\; & -\frac{Z_2\,\pi\alpha_s(k)}{4Z(k)}\,\text{Re}\!\int\!\frac{d^4p}{(2\pi)^4}\,\times \\
& \times\Bigg[\Big(\text{Tr}_D\big[\gamma_\mu S_i^+(p)V^{BC+}_{i,\nu}\left(p,\frac{p+q}{2}\right)S_j^+(q)\big]\,\text{Tr}_{c,f}\big[\lambda^a P_i\lambda^b P_j\big] + \\
& \quad \text{Tr}_D\big[\gamma_\mu S_i^+(p)V^{BC+}_{j,\nu}\left(\frac{p+q}{2},q\right)S_j^+(q)\big]\,\text{Tr}_{c,f}\big[\lambda^a P_i\lambda^b P_j\big] - \\
& \quad \text{Tr}_D\big[\gamma_\mu T_i^+(p)V^{BC+}_{i,\nu}\left(p,\frac{p+q}{2}\right)T_j^-(q)\big]\,\text{Tr}_{c,f}\big[\lambda^{a,T} M_i\lambda^b M_j\big] - \\
& \quad \text{Tr}_D\big[\gamma_\mu T_i^+(p)V^{BC+}_{j,\nu}\left(\frac{p+q}{2},q\right)T_j^-(q)\big]\,\text{Tr}_{c,f}\big[\lambda^{a,T} M_i\lambda^b M_j\big] + \\
& \quad \text{Tr}_D\big[\gamma_\mu T_i^-(p)W^{BC+}_{i,\nu}\left(p,\frac{p+q}{2}\right)S_j^+(q)\big]\,\text{Tr}_{c,f}\big[\lambda^a(\delta_i P_i)\lambda^b P_j\big] - \\
& \quad \text{Tr}_D\big[\gamma_\mu T_i^-(p)W^{BC+}_{j,\nu}\left(\frac{p+q}{2},q\right)S_j^+(q)\big]\,\text{Tr}_{c,f}\big[\lambda^a M_i\lambda^{b,T} M_j\big] - \\
& \quad \text{Tr}_D\big[\gamma_\mu S_i^-(p)W^{BC+}_{i,\nu}\left(p,\frac{p+q}{2}\right)T_j^-(q)\big]\,\text{Tr}_{c,f}\big[\lambda^{a,T} M_i\lambda^b M_j\big] + \\
& \quad \text{Tr}_D\big[\gamma_\mu S_i^-(p)W^{BC+}_{j,\nu}\left(\frac{p+q}{2},q\right)T_j^-(q)\big]\,\text{Tr}_{c,f}\big[\lambda^{a,T} P_i\lambda^{b.T}(\delta_j P_j)\big]\Big) \\
& \quad -\Big(\dots\Big)_{\mu=0}\Bigg]\,. \qquad (5.107)
\end{aligned}$$

This way we have factorized the Dirac structure and the color-flavor structure. We just need to perform similar integrals for the Dirac structures and can then apply the expression to any given phase by considering simply properties of the bases $\{P_i\}$ and $\{M_i\}$.

For a simple parameterization as in Eq.(5.45) we would obtain the weak coupling results in Eq.(5.103) and Eq.(5.106) as obtained in [167] for the 2SC phase, in [166] for the CFL phase and in [124, 125] for neutral phases. For our self-consistent truncation scheme, those integrals will be performed numerically with the fully dressed Nambu-Gor'kov propagators.

We are therefore left with the elaboration of the color-flavor traces. For the CFL phase in the chiral limit this is especially coherent and the remaining $SU(3)_{c+V}$ symmetry forces the color-flavor structure of $\Pi^{\text{med}\,ab}_{reg\;\mu\nu}(k)$ to be proportional to the Casimir operator, *i.e.*

unity. A direct evaluation gives

$$\mathrm{Tr}_{c,f}\left[\lambda^a P_i \lambda^b P_j\right] = \left(\frac{14}{3}\,\delta_{i1}\delta_{j1} + \frac{2}{3}\,\delta_{i1}\delta_{j2} + \frac{2}{3}\,\delta_{i2}\delta_{j1}\right)\delta^{ab}, \tag{5.108}$$

$$\mathrm{Tr}_{c,f}\left[\lambda^a M_i \lambda^{T,b} M_j\right] = -\frac{4}{3}\left(\delta_{i1}\delta_{j1} + \delta_{i1}\delta_{j2} + \delta_{i2}\delta_{j1}\right)\delta^{ab}. \tag{5.109}$$

In the 2SC phase the situation is a bit more involved. The case of the neutral 2SC phase with two flavors is shown in Appendix E.4.

5.3.4 The extended truncation scheme for the medium polarization

We will now apply our self-consistent truncation scheme to the medium polarization by assuming $\Pi^{\mathrm{med}\,ab}_{\mu\nu}(k)$ in the CFL phase to be of the form (see Eq.(2.81))

$$Z(k^2)\Pi^{\mathrm{med}\,ab}_{\mu\nu}(k) = \left(G(|\vec{k}|,k_4)P^T_{\mu\nu}(k) + F(|\vec{k}|,k_4)P^L_{\mu\nu}(k)\right)\delta^{ab} \tag{5.110}$$

and determine $G(|\vec{k}|,k_4)$ and $F(|\vec{k}|,k_4)$ by

$$\begin{aligned} G(|\vec{k}|,k_4)\delta^{ab} &= \frac{1}{2}Z(k^2)\Pi^{\mathrm{med}\,ab}_{\mu\nu}(k)P^T_{\nu\mu}(k)\,, \\ F(|\vec{k}|,k_4)\delta^{ab} &= Z(k^2)\Pi^{\mathrm{med}\,ab}_{\mu\nu}(k)P^L_{\nu\mu}(k)\,. \end{aligned} \tag{5.111}$$

The only approximation here is to replace B^{ab} and C^{ab} in Eq.(5.100) by their arithmetic mean in order to avoid possible asymmetries in μ and ν. Those functions become irrelevant in the most important kinematical regime near $k_4 = 0$. In the qDSE we will use the same vertex construction as in section 3, *i.e.* the one in Eq.(3.1). This may look inadequate, as already in simple models for the Higgs mechanism a proper consideration of Goldstone bosons is required to maintain gauge independence of observables (see *e.g.* [3]) and we are already able to consider those effects as shown in section 5.2. We will comment on this after showing the numerical results.

5.3.5 Numerical results

To get a first impression we present the results for the momentum dependence of the gap functions at the Fermi energy, for the coupling $\alpha_I(k)$ and a chemical potential $\mu = 400\,\mathrm{MeV}$ in Fig 5.11. We see that the overall shape of the gap functions and their relative ratios using the QRPA approximation for the medium polarization is similar to the HDL-like approximation used in section 3. However that absolute value of the functions is a factor 2-3 times larger.

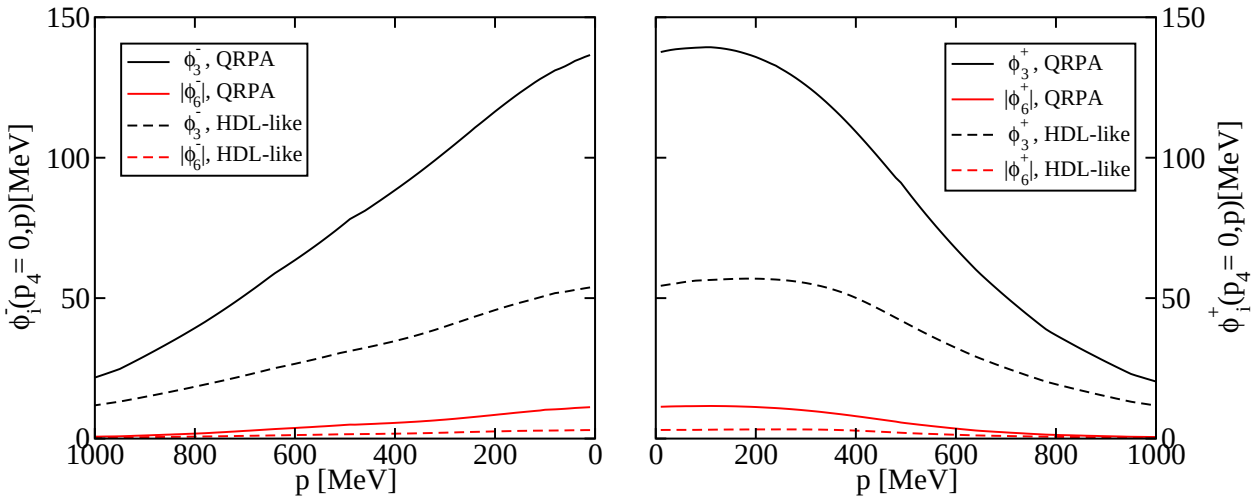

Figure 5.11: Quasiparticle gap functions ϕ^+ (right) and anti-quasiparticle gap functions ϕ^- (left) at the Fermi energy, *i.e.* $p_4 = 0$, for $\alpha_I(k)$ and $\mu = 400\,\mathrm{MeV}$. Shown are the results for the $\bar{\mathbf{3}}$-gap functions (black) and the $\mathbf{6}$-gap functions (red) obtained the the HDL-like approximation (dashed) and using the QRPA approximation for the medium polarization (solid).

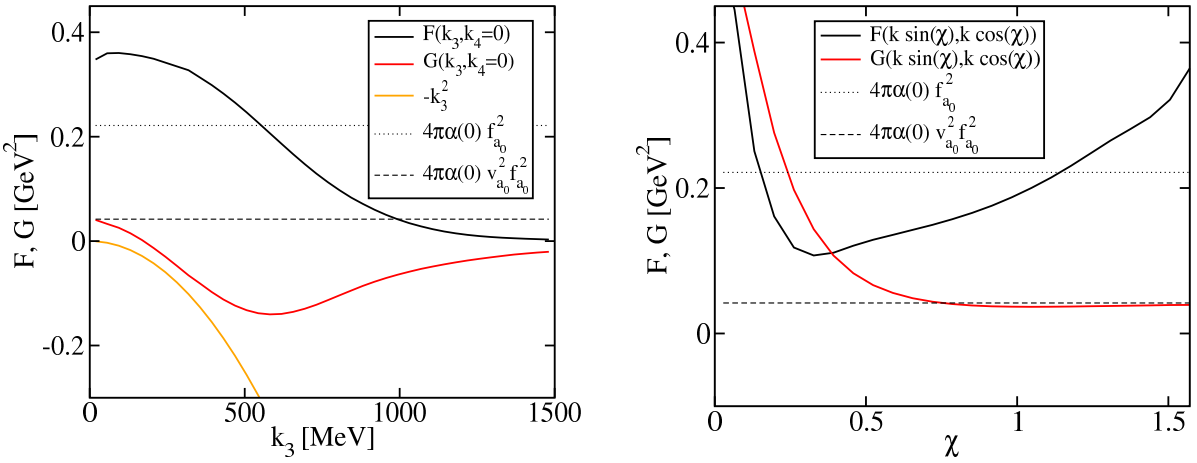

Figure 5.12: The dressing functions $F(|\vec{k}|, k_4)$ (black) and $G(|\vec{k}|, k_4)$ (red) for $\alpha_I(k)$ and $\mu = 400\,\mathrm{MeV}$. Left: The result for vanishing energies, *i.e.* $k_4 = 0$ together with $-|\vec{k}|^2$. Right: The dependence on the relative ratio of $|\vec{k}|$ and k_4 parameterized by the hyperspherical coordinate χ, for which $(|\vec{k}|, k_4) = (k \sin\chi, k\cos\chi)$ and $k = 50\,\mathrm{MeV}$. In both plots, the value of the Meissner mass and the value of the Debye mass in the weak coupling limit are also shown (dashed lines).

The reason for this enhancement is hidden in the behavior of the dressing functions $F(|\vec{k}|, k_4)$ and $G(|\vec{k}|, k_4)$ of the medium polarization. To point out this connection, we present the results of these functions in Fig. 5.12. On the left hand side we present our results for vanishing gluon energies. We see that the chromo-electric dressing function $F(|\vec{k}|, k_4 = 0)$ takes a rather large value in the infrared, which is even larger than the suggested value in Eq.(5.106) from the weak coupling analysis. The static chromo-electric gluons are therefore subleading compared to the chromo-magnetic ones, whose properties are encoded in the dressing function $G(|\vec{k}|, k_4)$. The latter function shows however an unexpected and novel feature as it was already discussed in section 5.3.1 for the unbroken phase. It is not strictly positive and compared to k^2, which also appears in the transversal part of the propagator (see Eq.(3.6)), we even conclude that the static chromo-magnetic gluon propagator is not most enhanced in the infrared. Instead it is strongly contributing within a whole interval in $|\vec{k}|$ near $k_4 = 0$, which is independent of the gap function. As a consequence we are not able to find a meta-stable solution of the unbroken phase even within our self-consistent treatment. In the infrared the Meissner mass agrees however with the result in Eq.(5.103) given by the transversality of the polarization tensor. On the right hand side of Fig. 5.12 we show the dependence on the relative ratio of $|\vec{k}|$ and k_4 for small absolute 4-momentum being parameterized by the hyperspherical coordinate χ, for which $(|\vec{k}|, k_4) = (k \sin\chi, k \cos\chi)$. We again observe the chromo-magnetic gluons to dominate the dynamics at $k_4 \lesssim |\vec{k}|$. We cannot really access the plasmon spectrum, which is encoded in the behavior at $k_4 \gtrsim |\vec{k}|$ as investigated in [168]. This is due to the fact that the behavior of F and G in this kinematical regime is not constrained by gauge symmetry and even sensitive to the actual choice of our Ball-Chiu construction of the vertex. Choosing *e.g.* $(\tilde{p}_\mu + \tilde{q}_\mu)/(p \cdot \tilde{p} - q \cdot \tilde{q})$ instead of $(p_\mu + q_\mu)/(p^2 - q^2)$ in Eq.(5.93), which can be equally justified, whould introduce an additional factor $v_{a_0}^2 \sim 0.1$ in $F(|\vec{k}| = 0, k_4) = G(|\vec{k}| = 0, k_4)$ and damp the strong enhancement for $\lim_{|\vec{k}|\to 0} F(|\vec{k}|, k_4)$ and $\lim_{|\vec{k}|\to 0} G(|\vec{k}|, k_4)$. However this kinematical regime does only mildly affect the gap functions, especially as the damping here is very strong anyway. We therefore prefer the Ball-Chiu construction with a sensible limit to the unbroken phase when taking $\phi \to 0$.

The final result for the value of the gap function on the Fermi surface is summarized in Fig. 5.13. As elaborated and explained in the following, the gap function takes very large values compared to the HDL-like solution. It is strictly increasing up to chemical potentials of $\mu \sim 800\,\mathrm{MeV}$ and even exceeding values of 200 MeV in the attractive channel.

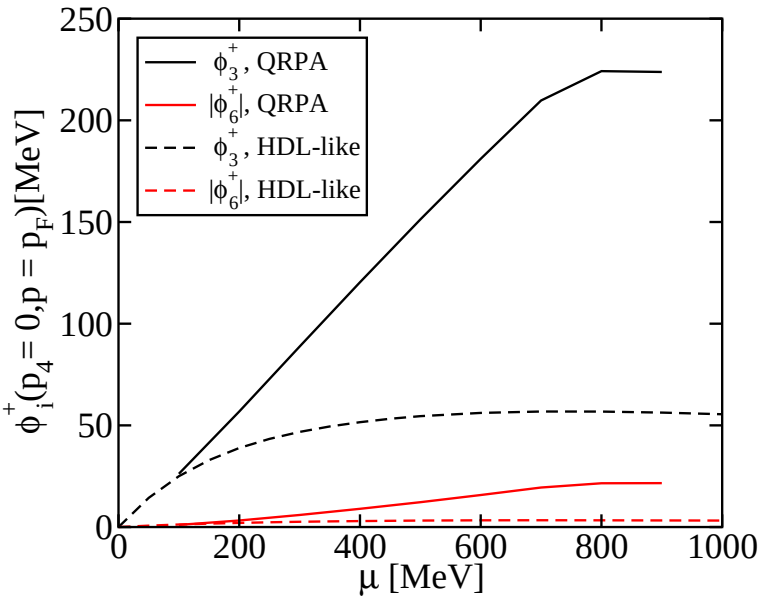

Figure 5.13: Results for the gap functions at the Fermi surface, *i.e.* $p_4 = 0$ and $|\vec{p}| = p_F$, in the HDL-like approximation (dashed) and using the QRPA approximation for the medium polarization (solid). Shown are the results for the $\bar{\mathbf{3}}$-gap functions with $\alpha_I(k)$ (black) and for the $\mathbf{6}$-gap functions (red).

5.3.6 Conclusions

We have worked out a novel feature of the medium polarization in the unbroken phase, which might point to an spontaneous instability of the unbroken phase and which questions investigations of its Fermi-liquid behavior. Extending the Ball-Chiu construction of the Abelian vertex to finite chemicals potentials and Nambu-Gor'kov space then allowed us to find a self-consistent truncation of the medium polarization which fulfills the transversality criterion from gauge symmetry. Within a self-consistent numerical treatment we find the unbroken phase not to be meta-stable either. In addition the findings for the unbroken phase have remnants in the CFL phase and are in particular enhancing the values of the gap functions significantly. Therefore a further elaboration of this effect is highly desirable. In this context it is worth mentioning that similar non-analycities have been found for the spin susceptibility in clean Fermi systems [169] and especially for smaller space-time dimensions possible instabilities are discussed.

As a practical next step in our investigation of color-superconducting phases a combination of section 5.2 and 5.3 is evident. As the Goldstone contribution in the quark self-energy will however be strong, the treatment of the BSA amplitude, *i.e.* self-consistent

or not, will be crucial. Due to the appearance of repulsive and attractive channels the existence of a self-consistent solution is however questionable as the expression of the self-energy need not to vanish for $\|\phi^+\| \to \infty$. Nevertheless Goldstone contributions are likely to lower the $\phi^+_{\bar{\mathbf{3}}}$-gap function and raise $\phi^+_{\mathbf{6}}$. As a result the $\phi^+_{\mathbf{6}}$-gap function might exceed a value of 20 MeV.

Chapter 6

Conclusions and Outlook

The aim of this thesis has been the application of Dyson-Schwinger equations to the phenomenology of color-superconducting phases. A variety of different questions could be addressed and further directions for future investigations can be pointed out.

In chapter 2 we presented the basis of our framework. Analytical properties such as the ultraviolet behavior of the gap-functions and the applicability of Luttinger's theorem to color-superconducting phases have been worked out.

A minimal truncation scheme was discussed in chapter 3. It is capable to recover known results in the vacuum as well as the leading order Hard-Dense-Loop approximation at asymptotically large densities. To illustrate the complexity of our calculations, especially the non-trivial energy-dependence of the propagators, we presented results for the non-Fermi liquid behavior in the unbroken phase first. Color-superconductivity in the chiral limit then served as an indicator for the applicability of analytical results obtained in weak coupling when extrapolating to smaller densities. We found large deviations between the extrapolated weak coupling results and our numerical calculations for chemical potentials smaller than 10 GeV. At moderate values of the quark density, the pairing functions at the Fermi surface acquire sizeable values, comparable to those obtained within NJL-type models. In contrast to those investigations, these results were found to be rather insensitive to the effective running coupling, at least within the considered range of uncertainty. The underlying reason for this is the inclusion of a medium modification in the gluon propagator. In addition, the size of the the diquark correlations were determined and the consistency of our numerical results and Luttinger's theorem was demonstrated. As the structure of the QCD phase diagram in the color-superconducting regime is strongly depending on the relative Fermi surfaces of the pairing quasiparticles, finite strange-quark masses were considered in a next step. Their self-energies and therefore also the constituent-quark masses were treated self-consistently. As the main result we found the color-flavor locked

(CFL) phase, which is expected to be the ground state in the weakly coupled regime, to be favored at any relevant quark chemical potential. This is in contrast to NJL-type investigations and stems from the different values of the constituent-quark masses which regulate the Fermi momenta. Including a medium modification in the interaction leads to smaller dynamically generated masses here and therefore to a weaker sensitivity on the strange-quark mass. The inclusion of neutrality conditions into our framework completed this investigation. Interestingly enough, we then found the CFL phase no longer to be definable by a residual symmetry due to the presence of gluonic background fields. Moreover, we showed that electrons are not forbidden in the CFL phase as has been claimed from NJL-type investigations and we presented the occupation number of quasiparticles for gapless pairing.

The canonical next step for future investigations would be a finite temperature study, which only amounts to a modification of the numerically performed energy integration in the quark self-energy. Another interesting point would be the determination of the density as a function of the chemical potential by Luttinger's theorem. As the primitive of this function is the pressure, this could then be used as input in the Tolman-Oppenheimer-Volkoff equation and be compared to compact star phenomenology.

The applicability of the Maximum Entropy Method to Dyson-Schwinger studies performed in Euclidean space has been shown in chapter 4. Due to the non-trivial energy-dependence of our propagators, we could determine the quasiparticle spectral functions in the unbroken and color-superconducting phases. In the unbroken phase the non-Fermi liquid behavior again became apparent. For the color-superconducting phase we got direct access to the excitation spectrum. This included the Fermi velocity of the quasiparticles, a finite width even at the Fermi surface and an insight to the presence of plasminos in our approach. The results nicely complemented and explained the findings in chapter 3 and 5.

For future investigations an application to bound-state solutions via the inhomogeneous Bethe-Salpeter equation would be interesting and has already been suggested.

In chapter 5 we presented extensions of our truncation scheme. First concentrating on the Dyson-Schwinger equation of the quark propagator, we extended the truncation of the involved vertex-function by considering its corresponding Dyson-Schwinger equation. We found a trackable truncation scheme which essentially describes a back-reaction of Goldstone bosons onto the quark propagator in spontaneously broken phases. It is worth remarking that the truncation scheme can be viewed as a next-to-leading order approximation in an expansion in the number of colors. As this scheme has not yet been applied for the chirally broken phase in the vacuum either, an application to this case served as an introduction and motivation. We successfully determined low-energy prop-

erties of Goldstone bosons that are needed for a description of the long-range dynamics by an effective theory. The corresponding low-energy constants for the Goldstone bosons in the CFL phase were compared with a simple parameterization as used in NJL-type investigations. As a by-product, we have found a generalized Gell–Mann-Oakes-Renner relation for the Goldstone boson masses in the NJL-model, which perfectly agrees with numerical calculations.

In the second part of this chapter, we constructed a self-consistent truncation scheme for the medium polarization of the gluon propagator. We found a novel feature in the unbroken phase that might indicate an instability on the non-Fermi liquid scale. In the color-superconducting phase this treatment properly includes the Meissner effect self-consistently. Due to remnants of the findings in the unbroken phase the gap-functions turned out to be rather large.

Several directions for future investigations are obvious: For the study of pion effects on the quark propagator an extension to bound-states via the Bethe-Salpeter equation is feasible. As can be seen from the effective action in the CJT-formalism, those are already included in the thermodynamic potential and therefore an extension to finite temperatures towards the chiral phase transition would be interesting. Furthermore an investigation of the analytic structure of the quark propagator and a comparison to lattice QCD results for the quark propagator in Landau gauge with dynamical sea-quarks can be put onto the agenda.

For the color-superconducting phases a combination of both extensions of our truncation scheme, *i.e.* the Goldstone contribution to the quark self-energy and the improved medium modification, is desirable. The chromo-magnetic instability in the CFL as well as in the 2SC phase can be studied. Finally, an extension to finite temperatures would again be of interest as the self-consistent consideration of the medium polarization might alter the order of the phase transition.

Acknowlegdements

Many people have contributed to make this work possible and it is a pleasure to thank all of them.

First of all I would like to express my gratitude to Jochen Wambach for giving me the opportunity to work on this subject, for his continuous interest and stimulating discussions. I also appreciate the opportunities to visit workshops and schools to get in contact with experienced scientists from whom I have learned a lot.

I am very grateful to Reinhard Alkofer for the fruitful engagement in our collaboration and for the warm hospitality in Tübingen and especially in Graz.

I would like to thank Jürgen Berges for being the second examiner of this work and his interest in its content.

Special thanks go to the local experts in Darmstadt, especially to Michael Buballa for numerous discussions about color-superconductivity and for a critical reading of the manuscript as well as to Christian Fischer and Axel Maas for sharing their knowledge about Dyson-Schwinger equations. I am indebted to Robert Roth, Heiko Hergert, Markus Hild and Mathias Wagner for the computer administration and support. With pleasure I recall the stimulating atmosphere on the 4^{th} floor at the Institut für Kernphysik and I also thank Florian Marhauser for discussions and a critical reading of the manuscript. In addition I appreciate the interest and impact of Norbert Grewe as a condensed matter physicist.

I also enjoyed the regular meetings of the Frankfurt-Darmstadt Color Superconductivity Group of the Virtual Institute for Dense Hadronic Matter and QCD Phase Transitions funded by the Helmholtz Association and in particular the discussions with Dirk Rischke and Igor Shovkovy.

During my time in Graz I found an inspiring environment and I liked the discussions with Bernd-Jochen Schaefer and Andreas Krassnigg as well as the atmosphere with all people in the Mozartgasse 5, especially Verena Hermann.

For enlightening discussions I would also like to thank Krishna Rajagopal, Craig Roberts and Thomas Schäfer.

Finally I would like to thank my family and friends, in particular my parents for their long-lasting support and my beloved future wife Dan Wang for all the love and patience she gave me in the past years.

This work has been furthermore supported in part by the Helmholtz association (Virtual Theory Institute VH-VI-041) by the BMBF under grant number 06DA916 and by a DAAD fellowship for PhD students.

Appendix A

Conventions

A.1 Parameterizations in the Euclidean framework

In Euclidean space-time we have the metric $g_{\mu\nu} = \delta_{\mu\nu}$ in a Cartesian basis, therefore covariant and contravariant coordinates are equal and we can work with lower indices only. Scalar products and the modulus of vectors will usually denoted like

$$p^2 = p_\mu p_\mu = \sum_{\mu=1}^{4} p_\mu p_\mu,\ xp = x_\mu p_\mu = \sum_{\mu=1}^{4} x_\mu p_\mu,\quad \vec{p}^2 = p_i p_i = \sum_{i=1}^{3} p_i p_i,\ \vec{x}\vec{p} = x_i p_i = \sum_{i=1}^{3} x_i p_i. \tag{A.1}$$

We work with Hermitian Dirac matrices γ_μ related to those in Minkowski space [2] by

$$\begin{aligned} \gamma_j &= -i\gamma_M^j\,, \qquad j = 1,2,3\,, \\ \gamma_4 &= \gamma_M^0\,. \end{aligned} \tag{A.2}$$

Here and in the following Roman letters indicate space components, *e.g.* $j = 1,..,3$, whereas Greek letters denote space-time components, *e.g.* $\mu = 1,..,4$. The Clifford algebra is then given through

$$\{\gamma_\mu, \gamma_\nu\} = 2\delta_{\mu\nu}\,, \tag{A.3}$$

for which we choose the Dirac-like representation

$$\sigma_j = \begin{pmatrix} 0 & -i\sigma_j \\ i\sigma_j & 0 \end{pmatrix},\ \gamma_4 = \begin{pmatrix} \sigma_0 & 0 \\ 0 & -\sigma_0 \end{pmatrix}, \tag{A.4}$$

where the 2×2 Pauli matrices and the unit matrix are

$$\sigma_0 = \begin{pmatrix} 1 & 0 \\ 0 & 1 \end{pmatrix},\ \sigma_1 = \begin{pmatrix} 0 & 1 \\ 1 & 0 \end{pmatrix},\ \sigma_2 = \begin{pmatrix} 0 & -i \\ i & 0 \end{pmatrix},\ \sigma_3 = \begin{pmatrix} 1 & 0 \\ 0 & -1 \end{pmatrix}. \tag{A.5}$$

We then define

$$\gamma_5 = -\gamma_1\gamma_2\gamma_3\gamma_4\,, \tag{A.6}$$
$$C = \gamma_2\gamma_4\,, \tag{A.7}$$
$$T = -i\gamma_1\gamma_3\,, \tag{A.8}$$

satisfying

$$\{\gamma_\mu,\gamma_5\} = 0\,, \qquad \gamma_5^2 = \mathbb{1}\,, \tag{A.9}$$
$$C^\dagger = C^{-1} = C^T = -C\,, \qquad C\gamma_\mu C^{-1} = -\gamma_\mu^T\,, \qquad C\gamma_5 C^{-1} = \gamma_5^T\,, \tag{A.10}$$
$$T^\dagger = T^{-1} = T\,, \qquad T\gamma_\mu T^{-1} = \gamma_\mu^* = \gamma_\mu^T\,. \tag{A.11}$$

A.2 $SU(N)$ symmetry groups

Throughout this work we use standard conventions for the special unitary group of degree N, denoted $SU(N)$. In contrast to mathematics, only one of the $N-1$ non-equivalent representations by $N\times N$-dimensional matrices is called *fundamental representation*, its conjugate *anti-fundamental representation*.

Important are the fundamental and adjoint representation of the corresponding Lie algebra $\mathfrak{su}(N)$. Being semi-simple, the Killing Form is positive definite and we can choose an orthogonal basis $\{T^a\}$ according to

$$\mathrm{Tr}\left(T^aT^b\right) = \frac{1}{2}\delta_{ab} \tag{A.12}$$

for the fundamental representation. The second Casimir operator is then given by

$$C_F(N) = T^aT^a = \frac{N^2-1}{2N}\,. \tag{A.13}$$

The adjoint representation in this basis is given by the antisymmetric structure constants f^{abc} defined in

$$\left[T^a,T^b\right] = if^{abc}T^c \tag{A.14}$$

and has the second Casimir

$$C_A(N)\delta^{ab} = f^{acd}f^{bcd} = N. \tag{A.15}$$

Instead of T^a, the generalized Pauli matrices $\lambda^a = \tau^a \stackrel{\text{def}}{=} 2T^a$ are often used. For $N=2$ those are the Pauli matrices in Eq.(A.5), for $N=3$ the Gell-Mann matrices. We eventually complete the basis by defining $2T^0 = \lambda^0 \stackrel{\text{def}}{=} \sqrt{\frac{2}{N}}\mathbb{1}$.

Appendix B

Definitions and parameterizations of correlation functions

B.1 Ghost, gluon and quark propagators

The full (imaginary time-ordered, *i.e.* Matsubara) connected ghost, gluon and quark propagators in coordinate space are given as

$$D_G^{ab}(x,y) \stackrel{\text{def}}{=} \langle T_\tau\, c^a(x)\bar{c}^b(y)\rangle_c = \left.\frac{\delta^2 W[\chi,\bar{\chi},\sigma,\bar{\sigma},j]}{\delta\sigma^b(y)\delta\bar{\sigma}^a(x)}\right|_{\chi=\bar{\chi}=\sigma=\bar{\sigma}=j=0}, \quad \text{(B.1)}$$

$$D_{\mu\nu}^{ab}(x,y) \stackrel{\text{def}}{=} \langle T_\tau\, A_\mu^a(x)A_\nu^b(y)\rangle_c = \left.\frac{\delta^2 W[\chi,\bar{\chi},\sigma,\bar{\sigma},j]}{\delta j_\nu^b(y)\delta j_\mu^a(x)}\right|_{\chi=\bar{\chi}=\sigma=\bar{\sigma}=j=0}, \quad \text{(B.2)}$$

$$S(x,y) \stackrel{\text{def}}{=} \langle T_\tau\, \psi(x)\bar{\psi}(y)\rangle_c = \left.\frac{\delta^2 W[\chi,\bar{\chi},\sigma,\bar{\sigma},j]}{\delta\chi(y)\delta\bar{\chi}(x)}\right|_{\chi=\bar{\chi}=\sigma=\bar{\sigma}=j=0}, \quad \text{(B.3)}$$

where we introduced the generating functional $W[\chi,\bar{\chi},\sigma,\bar{\sigma},j] = \ln Z[\chi,\bar{\chi},\sigma,\bar{\sigma},j]$ of connected Green's functions (see Eq.(2.7) and Eq.(2.34)). The subscript c denotes connected Green's functions.

By use of the effective action

$$\Gamma\big[c,\bar{c},\psi,\bar{\psi},A\big] = -W[\chi,\bar{\chi},\sigma,\bar{\sigma},j] + \int d^4x\left(\bar{\chi}\psi + \bar{\psi}\chi + \bar{\sigma}c + \bar{c}\sigma + j_\mu^a A_\mu^a\right), \quad \text{(B.4)}$$

where

$$\psi = \frac{\delta W[\chi,\bar{\chi},\sigma,\bar{\sigma},j]}{\delta\bar{\chi}}, \qquad \bar{\psi} = -\frac{\delta W[\chi,\bar{\chi},\sigma,\bar{\sigma},j]}{\delta\chi},$$
$$c = \frac{\delta W[\chi,\bar{\chi},\sigma,\bar{\sigma},j]}{\delta\bar{\sigma}}, \qquad \bar{c} = -\frac{\delta W[\chi,\bar{\chi},\sigma,\bar{\sigma},j]}{\delta\sigma}, \qquad A_\mu^a = \frac{\delta W[\chi,\bar{\chi},\sigma,\bar{\sigma},j]}{\delta j_\mu^a}, \quad \text{(B.5)}$$

i.e. the (negative) Legendre transform of W, we can equally express

$$D_G^{ab}(x,y)^{-1} = \frac{\delta^2\Gamma\left[c,\bar{c},\psi,\bar{\psi},A\right]}{\delta c^b(y)\delta\bar{c}^a(x)}, \tag{B.6}$$

$$D_{\mu\nu}^{ab}(x,y)^{-1} = \frac{\delta^2\Gamma\left[c,\bar{c},\psi,\bar{\psi},A\right]}{\delta A_\nu^b(y)\delta A_\mu^a(x)}, \tag{B.7}$$

$$S(x,y)^{-1} = \frac{\delta^2\Gamma\left[c,\bar{c},\psi,\bar{\psi},A\right]}{\delta\psi(y)\delta\bar{\psi}(x)}, \tag{B.8}$$

which are to be evaluated at the stationary point.

At tree level, the effective action is equal to the classical action and we get the inverse bare (unrenormalized) propagators in the vacuum

$$D_G^{(0)ab}(x,y)^{-1} = \frac{\delta^2 S_{QCD}\left[c,\bar{c},\psi,\bar{\psi},A\right]}{\delta c^b(y)\delta\bar{c}^a(x)} = i\delta^{ab}\partial^2\delta(x-y), \tag{B.9}$$

$$D_{\mu\nu}^{(0)ab}(x,y)^{-1} = \frac{\delta^2 S_{QCD}\left[c,\bar{c},\psi,\bar{\psi},A\right]}{\delta A_\nu^b(y)\delta A_\mu^a(x)} = \delta^{ab}\left(-\partial^2\delta_{\mu\nu}+\left(1-\frac{1}{\xi}\right)\partial_\mu\partial_\nu\right)\delta(x-y), \tag{B.10}$$

$$S^{(0)}(x,y)^{-1} = \frac{\delta^2 S_{QCD}\left[c,\bar{c},\psi,\bar{\psi},A\right]}{\delta\psi(y)\delta\bar{\psi}(x)} = (-\not{\partial}_x+m_0)\,\delta(x-y). \tag{B.11}$$

As we are always considering homogeneous phases in equilibrium, the propagators only depend on $u=x-y$ and we define

$$D(p) = \int d^4u\, D(x,y)e^{-ipu} \tag{B.12}$$

for all propagators.

B.2 $q\bar{q}g$-vertex

The connected $q\bar{q}g$-vertex is given by

$$\begin{aligned}\langle T_\tau\, A_\mu^a(x)\psi(y)\bar{\psi}(z)\rangle_c &= \left.\frac{\delta^3 W[\chi,\bar{\chi},\sigma,\bar{\sigma},j]}{\delta\chi(z)\delta\bar{\chi}(y)\delta j_\mu^a(x)}\right|_{\chi=\bar{\chi}=\sigma=\bar{\sigma}=j=0}\\ &= \left.\frac{\delta}{\delta j_\mu^a(x)}\left(\frac{\delta^2\Gamma\left[c,\bar{c},\psi,\bar{\psi},A\right]}{\delta\psi(z)\delta\bar{\psi}(y)}\right)^{-1}\right|_{\chi=\bar{\chi}=\sigma=\bar{\sigma}=j=0}.\end{aligned} \tag{B.13}$$

With help of

$$\begin{aligned}\frac{d}{dx}A^{-1} &= -A^{-1}\frac{dA}{dx}A^{-1}\\ \frac{\delta}{\delta j_\mu^a(x)} &= \int d^4u\, D_{\mu\nu}^{ab}(x,u)\frac{\delta}{\delta A_\nu^b(u)},\end{aligned} \tag{B.14}$$

we obtain

$$\langle T_\tau\, A^a_\mu(x)\psi(y)\bar\psi(z)\rangle_c \;=\; -\int d^4u\, d^4v\, d^4w\, D^{ab}_{\mu\nu}(x,u)S(y,v)g\Gamma^b_\nu(u;v,w)S(w,z)\,, \quad \text{(B.15)}$$

where the proper, *i.e.* 1PI, $q\bar qg$-vertex

$$g\Gamma^a_\mu(x;y,z) \;\stackrel{\text{def}}{=}\; \frac{\delta^3\Gamma\big[c,\bar c,\psi,\bar\psi,A\big]}{\delta\psi(z)\delta\bar\psi(y)\delta A^a_\mu(x)} \quad \text{(B.16)}$$

has been introduced. For its Fourier transform, the momentum of the gluon is defined as incoming whereas the two quark momenta are chosen differently, one incoming and one outgoing (see figure)

$$g\Gamma^a_\mu(k,q,p) \;=\; \int d^4x\, d^4y\, d^4z\, e^{-ikx}e^{-iqy}e^{ipz}g\Gamma^a_\mu(x;y,z)\,. \quad \text{(B.17)}$$

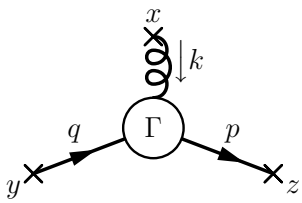

Momentum conservation allows to define a reduced vertex function

$$g\Gamma^a_\mu(k,q,p) \;=\; -ig\,(2\pi)^4\delta^4(k+q-p)\Gamma^a_\mu(q,p)\,. \quad \text{(B.18)}$$

At tree level we have again $\Gamma = S_{QCD}$ and find

$$\Gamma^{(0)a}_\mu \;\stackrel{\text{def}}{=}\; \Gamma^{(0)a}_\mu(q,p) \;=\; \gamma_\mu\frac{\lambda^a}{2} \;=\; \gamma_\mu T^a\,. \quad \text{(B.19)}$$

B.3 Bethe-Salpeter amplitudes (BSAs)

Instead of solving the BSE for the quark-antiquark scattering amplitude, usually certain channels are selected by focusing on vertices

$$\langle T_\tau\, J^M(x)\psi(y)\bar\psi(z)\rangle_c \;=\; \int d^4v\, d^4w\, S(y,v)\Gamma^M(x;v,w)S(w,z)\,, \quad \text{(B.20)}$$

where $J^M(x) = \bar\psi(x)T^M\psi(x)$. Those vertices obey an inhomogeneous BSE. In momentum space, we then use the convention

$$\Gamma^M(P,q,p) \;=\; \int d^4x\, d^4y\, d^4z\, e^{iPx}e^{-iqy}e^{ipz}\Gamma^M(x;y,z) \quad \text{(B.21)}$$

and momentum conservation again allows us to define a reduced vertex function

$$\begin{aligned}\Gamma^M(P,q,p) &= (2\pi)^4\delta^4(q-p-P)\Gamma^M(q,p)\\ &= (2\pi)^4\delta^4(q-p-P)\Gamma^M(\frac{q+p}{2};P)\,,\end{aligned} \quad \text{(B.22)}$$

where the latter definition is often more convenient. At tree level we then have $\Gamma^{M(0)}(q,p) = T^M$. Within this work we consider the axial currents J_5^M generated by $T^M = \gamma_\mu\gamma_5$, γ_5, $\gamma_\mu\gamma_5\frac{\tau^a}{2}$, $\gamma_5\frac{\tau^a}{2}$, the flavor currents J^M generated by $T^M = \gamma_\mu$, $\mathbb{1}$, $\gamma_\mu\frac{\tau^a}{2}$, $\frac{\tau^a}{2}$ and the color currents J_c^M generated by $T^M = \gamma_\mu\frac{\lambda^a}{2}$, $\frac{\lambda^a}{2}$. Note the different definition of the vector currents compared to [10].

If the vertex function possesses poles, *i.e.* couples to bound-states, the inhomogeneous BSE reduces to the homogeneous for the residue. The latter determines the wave function of the bound state. When restricting ourself to the homogeneous equation, we need to normalize the wave function in order to keep unitarity [10, 142].

B.4 Generalized Ward-Takahashi identities

Generalized WTIs can be derived from infinitesimal symmetry transformations $\psi(x) \to (1 + i\alpha(x))\psi(x)$ with $\alpha(x)^\dagger = \alpha(x)$ and either $[\alpha(x), \gamma_\mu] = 0$ or $\{\alpha(x), \gamma_\mu\} = 0$. For $\mathcal{L}_q = \bar\psi(-\not{D} + m + \gamma_4)\psi$ we find[1]

$$\delta\mathcal{L}_q \;=\; i\left(\bar\psi\,\gamma_4\left[\gamma_4 m, \alpha\right]\psi + \bar\psi\,\gamma_4\left[\mu, \alpha\right]\psi - \bar\psi\not{\partial}\,\alpha\psi\right) . \tag{B.23}$$

The generalized WTIs then follow, in a somewhat sloppy notation, from

$$\begin{aligned} 0 \;&=\; \int \mathcal{D}\left[\psi\bar\psi A\right]\;\delta\left(Oe^{-S}\right) \\ &=\; \left\langle -\left(\delta S\right)O + \delta O\right\rangle . \end{aligned} \tag{B.24}$$

For $O = \psi(y)\bar\psi(z)$ we get with $\alpha(x) = \epsilon(x)T^M$

$$\begin{aligned} i\partial_\mu^x \left\langle\bar\psi(x)\gamma_\mu T^M\psi(x)\,\psi(y)\bar\psi(z)\right\rangle_c \;=\;& \delta(x-y)iT^M\left\langle\psi(y)\bar\psi(z)\right\rangle_c - \\ & \left\langle\psi(y)\bar\psi(z)\right\rangle_c\delta(x-z)i\gamma_4T^M\gamma_4 \\ & i\left\langle\bar\psi(x)\gamma_4\left[\gamma_4 m, T^M\right]\psi(x)\psi(y)\bar\psi(z)\right\rangle_c - \\ & i\left\langle\bar\psi(x)\gamma_4\left[\mu, T^M\right]\psi(x)\psi(y)\bar\psi(z)\right\rangle_c . \end{aligned} \tag{B.25}$$

This is a relation of propagators and vertex functions and its Fourier transform to momentum space is often used within this thesis.

[1] The extension to the Nambu-Gor'kov formalism is straightforward.

Appendix C

Derivation of the qDSE in the medium

As explained by section 2.2.1, we can expand

$$\left\langle \frac{\delta S_{QCD}\left[c,\bar{c},\psi,\bar{\psi},A\right]}{\delta\bar{\psi}(x)} - \chi(x) \right\rangle \;=\; 0 \tag{C.1}$$

in the external sources to get a set of DSEs. The Taylor coefficient to $\chi(y)$ is the qDSE and of the form

$$\left\langle T_\tau \, \frac{\delta S_{QCD}\left[c,\bar{c},\psi,\bar{\psi},A\right]}{\delta\bar{\psi}(x)} \, \bar{\psi}(y) - \delta(x-y) \right\rangle \Bigg|_{\chi=\bar{\chi}=\sigma=\bar{\sigma}=j=0} \;=\; 0\,. \tag{C.2}$$

In the medium we then find

$$\begin{aligned} \delta(x-y) \;&=\; Z_2\left(-\not{\partial}_x + m + \mu\gamma_4\right)\left\langle T_\tau\, \psi(x)\bar{\psi}(y)\right\rangle \\ &\quad -iZ_{1F} g\gamma_\mu T^a \left\langle T_\tau\, A^a_\mu(x)\psi(x)\bar{\psi}(y)\right\rangle . \end{aligned} \tag{C.3}$$

Decomposing the correlators into connected parts, we allow for a non-vanishing expectation value of A^a_μ in particular and get

$$\delta(x-y) \;=\; \int d^4z\, Z_2 S^{(0)}(x,z)^{-1} S(z,y) - iZ_{1F} g\gamma_\mu T^a \left\langle T_\tau\, A^a_\mu(x)\psi(x)\bar{\psi}(y)\right\rangle_c , \tag{C.4}$$

where we have used the inverse 'bare' quark propagator in the medium:

$$S^{(0)}(x,z)^{-1} \;\stackrel{\text{def}}{=}\; \left(-\not{\partial}_x + m + \mu\gamma_4 - i\frac{Z_{1F}}{Z_2} g\gamma_\mu T^a \langle A^a_\mu\rangle_c\right)\delta(x-z)\,. \tag{C.5}$$

With Eq.(B.15) we rewrite Eq.(C.4) to get the qDSE in coordinate space

$$S(x,y)^{-1} \;=\; Z_2 S^{(0)}(x,y)^{-1} + iZ_{1F} g^2 \int d^4u\, d^4v\, \Gamma^{(0)a}_\mu S(x,v)\Gamma^b_\nu(u;v,y) D^{ab}_{\mu\nu}(x,u)\,. \tag{C.6}$$

Fourier transforming this expression according to Eq.(B.12) gives the qDSE in momentum space (see Eq.(2.15) and following).

The derivation in the Nambu-Gor'kov formalism is very similar. We introduce external sources

$$X = \frac{1}{\sqrt{2}} \begin{pmatrix} \chi \\ \chi_C = C\bar{\chi}^T \end{pmatrix} , \quad \bar{X} = \frac{1}{\sqrt{2}} \left(\bar{\chi}, \bar{\chi}_C = \chi^T C\right) . \tag{C.7}$$

and only need to consider the Jacobian matrix of $(\psi, \bar{\psi})$ and $(\Psi, \bar{\Psi})$ in Eq.(2.12).

Appendix D

The strong running coupling constants

The running coupling constants $\alpha_s(k)$ are the essential input in our truncation scheme. For $\alpha_I(k)$ we take a fit to the numerical solution obtained in [170]:

$$\alpha_I(k) = \frac{\alpha_I(0)}{\ln\left(e + a_1\,(k^2/\Lambda_I^2)^{a_2} + b_1\,(k^2/\Lambda_I^2)^{b_2}\right)}\,, \tag{D.1}$$

with $\alpha_I(0) = 2.972$, $a_1 = 1.106$, $a_2 = 2.324$, $b_1 = 0.004$, $b_2 = 3.169$ and $\Lambda_I = 0.714\,\mathrm{GeV}$. For $\alpha_{II}(k^2)$ we take the coupling constructed in [81], which reproduces quenched lattice QCD results for the quark propagator [171] in the bare vertex approximation:

$$\alpha_{II}(k) = \frac{Z_{cor}}{4\pi}\,k^2 D(k^2)\,\Gamma_1(k^2)\,, \tag{D.2}$$

where

$$\begin{aligned} D(k^2) &= Z_g\left[\frac{A\Lambda_g^{2\alpha}}{(k^2+\Lambda_g^2)^{1+\alpha}} + \frac{L(k^2,\Lambda_g)}{k^2+\Lambda_g^2}\right]\,, \\ L(k^2,\Lambda_g) &= \left(\frac{1}{2}\ln\left[(k^2+\Lambda_g^2)(\frac{1}{k^2}+\frac{1}{\Lambda_g^2})\right]\right)^{-d_D}\,, \end{aligned} \tag{D.3}$$

with

$$\begin{aligned} A &= 9.8^{+0.1}_{-0.9}\,, & \Lambda_g &= 1.020 \pm 0.1 \pm 0.025\,\mathrm{GeV}\,, \\ \alpha &= 2.2^{+0.1+0.2}_{-0.2-0.3}\,, & Z_g &= 2.01^{+0.04}_{-0.05}\,. \end{aligned} \tag{D.4}$$

Furthermore

$$\begin{aligned}
\Gamma_1(k^2) &= 4\pi^2\gamma_m \frac{1}{Z_g} \frac{\left(\frac{1}{2}\ln(e^2-1+k^2/\Lambda_g^2)\right)^{d_D}}{\ln(e^2-1+k^2/\Lambda_{QCD}^2)}\, v(k^2)\,, \\
v(k^2) &= \frac{a_v(m)+k^2/\Lambda_g^2}{b+k^2/\Lambda_g^2}\,, \\
a_v(m) &= \frac{a_1}{1+a_2\,(m(\nu)/\Lambda_g)+a_3\,(m(\nu)/\Lambda_g)^2}\,,
\end{aligned} \tag{D.5}$$

where

$$a_1 = 1.5\,, \quad a_2 = 7.35\,, \quad a_3 = 63.\,, \quad b = 0.005\,, \quad \Lambda_{QCD} = 0.234\,\mathrm{GeV}\,. \tag{D.6}$$

For the anomalous dimensions $d_D = (39-4N_f)\,/\,(2(33-2N_f))$ and γ_m with $N_c = 3$, $N_f = 0$ is taken for the fit to quenched lattice data and $N_f = 3$ in our calculations. Furthermore we set $m(\nu) = 0$ in our calculations for the medium as the dynamical mass function, even when explicit symmetry breaking is taken into account, is relatively small. Finally we introduced a correction factor $Z_{cor} = 1/Z_2(\nu = 19\,\mathrm{GeV})^2 = 1.043$ allowing an arbitrary renormalization scale by keeping multiplicative renormalizibility.

Appendix E

Parameterization of phases in color-flavor space

E.1 Parameterization of 2SC and CFL phase in the chiral limit

For the 2SC phase, defined by the pairing pattern $M_{2SC} = \lambda_2 \otimes \tau_2$, we find

$$P_1 = \lambda_2^2 \otimes \tau_2^2 \,, \quad P_2 = (\mathbb{1} - \lambda_2^2) \otimes \tau_2^2 \,, \quad P_3 = \mathbb{1} - P_1 - P_2 \tag{E.1}$$

and trivially the parameters δ_i from

$$M_{2SC}^\dagger M_{2SC} = \sum_i \nu_i P_i = P_1 \,. \tag{E.2}$$

With

$$\begin{aligned} &\lambda_a P_1 \lambda_a = \frac{10}{3} P_1 + 4 P_2 \,, \quad \lambda_a P_2 \lambda_a = 2 P_1 + \frac{4}{3} P_2 \,, \quad \lambda_a P_3 \lambda_a = \frac{16}{3} P_3 \,, \\ &\lambda_a^T P_i M_{2SC} \lambda_a = \delta_{i1} \lambda_a^T M_{2SC} \lambda_a = -\frac{8}{3} \delta_{i1} M_{2SC} \end{aligned} \tag{E.3}$$

the dynamics of the channels in color-flavor space is completely determined for the truncation used in section 3.

For the CFL phase, given through $M_{CFL} = \sum_{A=2,5,7} \lambda^A \otimes \tau^A$, we find

$$P_{\mathbf{8}} = \begin{pmatrix} 2 & & & & & & -1 & & & & & & -1 \\ & 3 & & & & & & & & & & & \\ & & 3 & & & & & & & & & & \\ & & & 3 & & & & & & & & & \\ -1 & & & & 2 & & & & & & & & -1 \\ & & & & & 3 & & & & & & & \\ & & & & & & 3 & & & & & & \\ & & & & & & & 3 & & & & & \\ -1 & & & & -1 & & & & & & 2 & & \end{pmatrix}, \quad P_{\mathbf{1}} = \begin{pmatrix} 1 & & & & & & 1 & & & & & & 1 \\ & & & & & & & & & & & & \\ & & & & & & & & & & & & \\ & & & & & & & & & & & & \\ 1 & & & & & & 1 & & & & & & 1 \\ & & & & & & & & & & & & \\ & & & & & & & & & & & & \\ & & & & & & & & & & & & \\ 1 & & & & & & 1 & & & & & & 1 \end{pmatrix}, \tag{E.4}$$

with

$$M_{CFL}^{\dagger} M_{CFL} = \sum_i \nu_i P_i = P_{\mathbf{8}} + 4P_{\mathbf{1}}. \tag{E.5}$$

The dynamics of the channels in color-flavor space is encoded by

$$\begin{aligned} &\lambda_a P_{\mathbf{8}} \lambda_a = \frac{14}{3} P_{\mathbf{8}} + \frac{16}{3} P_{\mathbf{1}}\,, \quad \lambda_a P_{\mathbf{1}} \lambda_a = \frac{2}{3} P_{\mathbf{8}}\,, \\ &\lambda_a^T P_{\mathbf{8}} M_{CFL} \lambda_a = -\frac{4}{3}(P_{\mathbf{8}} + 2P_{\mathbf{1}}) M_{CFL}\,, \quad \lambda_a^T P_{\mathbf{1}} M_{CFL} \lambda_a = -\frac{4}{3} P_{\mathbf{8}} M_{CFL} \end{aligned} \tag{E.6}$$

for the truncation used in section 3.

E.2 The color-flavor structure of the CFL phase for finite m_s

We generalize the ansatz for the CFL phase with two degenerate quarks as given in [107] by choosing the matrices

$$P_i = \begin{pmatrix} \delta_{i1}+\delta_{i2} & \delta_{i2} & \delta_{i4} & & & & & & & \\ \delta_{i2} & \delta_{i1}+\delta_{i2} & \delta_{i4} & & & & & & & \\ \delta_{i5} & \delta_{i5} & \delta_{i3} & & & & & & & \\ & & & \delta_{i1} & & & & & & \\ & & & & \delta_{i1} & & & & & \\ & & & & & \delta_{i7} & & & & \\ & & & & & & \delta_{i8} & & & \\ & & & & & & & \delta_{i7} & & \\ & & & & & & & & \delta_{i8} & \end{pmatrix}, \tag{E.7}$$

$$M_i = \begin{pmatrix} \delta_{i1}+\delta_{i2} & \delta_{i2} & \delta_{i4} & & & & & & \\ \delta_{i2} & \delta_{i1}+\delta_{i2} & \delta_{i4} & & & & & & \\ \delta_{i5} & \delta_{i5} & \delta_{i3} & & & & & & \\ & & & \delta_{i1} & & & & & \\ & & & & \delta_{i1} & & & & \\ & & & & & \delta_{i8} & & & \\ & & & & & & \delta_{i7} & & \\ & & & & & & & \delta_{i8} & \\ & & & & & & & & \delta_{i7} \end{pmatrix}, \tag{E.8}$$

which fulfill the requirements of Eq. (3.47). The basis is redefined compared to the chiral limit by

$$\{(r,u),(g,d),(b,s),(r,d),(g,u),(r,s),(b,u),(g,s),(b,d)\},$$

with r, g, b denoting the color and u, d, s the flavor of the quarks.

E.3 The color-flavor structure of the neutral CFL phase

For the neutral CFL phase and finite strange-quark mass m_s, we generalize the ansatz of Appendix E.2. In the same basis, we choose the matrices:

$$P_i = \begin{pmatrix} \delta_{i1} & \delta_{i4} & \delta_{i6} & & & & & & \\ \delta_{i5} & \delta_{i2} & \delta_{i7} & & & & & & \\ \delta_{i8} & \delta_{i9} & \delta_{i3} & & & & & & \\ & & & \delta_{i10} & & & & & \\ & & & & \delta_{i11} & & & & \\ & & & & & \delta_{i12} & & & \\ & & & & & & \delta_{i13} & & \\ & & & & & & & \delta_{i14} & \\ & & & & & & & & \delta_{i15} \end{pmatrix}, \tag{E.9}$$

$$M_i = \begin{pmatrix} \delta_{i1} & \delta_{i4} & \delta_{i6} & & & & & & & & & & \\ \delta_{i5} & \delta_{i2} & \delta_{i7} & & & & & & & & & & \\ \delta_{i8} & \delta_{i9} & \delta_{i3} & & & & & & & & & & \\ & & & \delta_{i10} & & & & & & & & & \\ & & & & \delta_{i11} & & & & & & & & \\ & & & & & & & \delta_{i12} & & & & & \\ & & & & & & \delta_{i13} & & & & & & \\ & & & & & & & & & & & \delta_{i14} & \\ & & & & & & & & & & \delta_{i15} & & \end{pmatrix}. \tag{E.10}$$

E.4 The color-flavor structure of the neutral 2SC phase

In the basis

$$\{(r,u),(g,u),(b,u),(r,d),(g,d),(b,d)\}$$

we define the projectors

$$P_i = \begin{pmatrix} \delta_{i1} & & & & & \\ & \delta_{i1} & & & & \\ & & \delta_{i3} & & & \\ & & & \delta_{i2} & & \\ & & & & \delta_{i2} & \\ & & & & & \delta_{i4} \end{pmatrix}, \quad M_i = \begin{pmatrix} 0 & & & & & -\delta_{i2} \\ & 0 & & \delta_{i2} & & \\ & & 0 & & & \\ & \delta_{i1} & & 0 & & \\ -\delta_{i1} & & & & 0 & \\ & & & & & 0 \end{pmatrix} \tag{E.11}$$

for the 2SC ansatz $M_{2SC} = \lambda_2 \otimes \tau_2$ with two flavors. Furthermore

$$Q_i = \begin{pmatrix} \delta_{i1} & & & & & & & \\ & \delta_{i1} & & & & & & \\ & & \delta_{i1} & & & & & \\ & & & \delta_{i3} & i\delta_{i4} & & & \\ & & & -i\delta_{i4} & \delta_{i3} & & & \\ & & & & & \delta_{i3} & -i\delta_{i4} & \\ & & & & & i\delta_{i4} & \delta_{i3} & \\ & & & & & & & \delta_{i2} \end{pmatrix} \tag{E.12}$$

is the largest basis for the color structure of the medium polarization $\Pi^{\mathrm{med}\,ab}_{\mu\nu}(k)$ allowed by the residual symmetries.

Appendix F

Numerical implementation

F.1 Implementation of the qDSE

Due the complexity of our calculations in the number of basis elements as well as keeping the full energy- and momentum-dependence, an object-oriented programming is strongly advised. In particular to handle possible sources of errors.

The basic object is the quark propagator in Nambu-Gor'kov space. It requires the following data members: The discretized (discretization will be discussed below) dressing functions as given in Eq.(3.38-3.40), the chemical potentials and the vacuum solution with all physical parameters, especially the renormalization constants and masses (see *e.g.* [41] for the implementation in the vacuum). For this data members the following methods are needed: A method for reading necessary parameters and data, a method to export the data and methods that implement the algebraic field structure of the quark propagator. For the latter we include methods for addition, subtraction, multiplication and inversion of the quark propagator at every fixed energy and momentum. Those algebraic manipulations can be performed with a computer algebra system, such as *Mathematica*® and it is convenient to store those properties in separate parameter files, such that the object is applicable to any chosen phase. In addition we have implemented an interpolation routine of the discretized dressing functions to any chosen energy and momentum. It is crucial to perform the interpolation in the inverse propagator, as self-energies and gap-functions are in contrast to the propagators rather smooth, and then invert the propagator. For the effective action an implementation of the determinant is also suited.

In order to reduce the computer-time and memory consumption, it is necessary to exploit internal symmetries. With help of the symmetries detailed in section 2.3.3, we can restrict ourself to the dressing functions of $\Sigma^+(p_4, \vec{p})$ and $\Phi^+(p_4, \vec{p})$ for $p_4 > 0$. For convenience we also store the dressing functions of $S^+(p_4, \vec{p})$ and $T^+(p_4, \vec{p})$ for $p_4 > 0$.

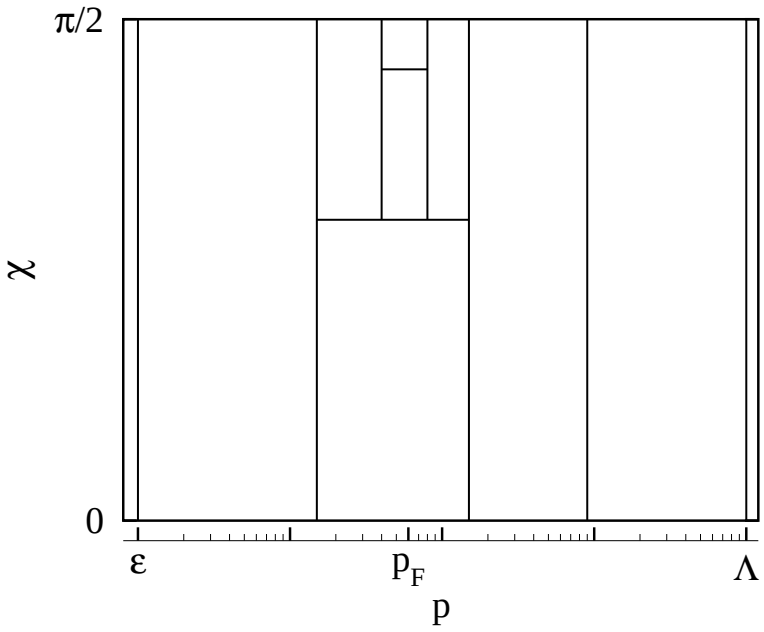

Figure F.1: Schematic presentation of subsets used for the discretization of the propagators.

The discretization of those dressing functions is then adjusted to the involved scales in the numerical integrations, namely a scale Λ_{QCD} encoded in the effective running coupling $\alpha_s(k)$ and the chemical potential μ determining the Fermi surface. We use hyperspherical coordinates, such that $(|\vec{p}|, p_4) = (p\sin\chi, p\cos\chi) = p_0 e^x(\sin\chi, \cos\chi)$. A schematic discretization is shown in Fig. F.1: We choose an infrared cutoff $\epsilon \lesssim 0.1$MeV small enough to be irrelevant and take the ultraviolet cutoff Λ from the regularization of the vacuum solution. The set $[\epsilon, \Lambda] \times [0, \pi/2]$ is then split into smaller subsets, such that in each subset the dressing functions can be discretized on the abscissae needed for a numerical integration in x and χ. We use simple Riemann quadrature as we need to handle a principle value integral at Fermi surface for the unbroken phase. Using other quadratures for color-superconducting phases has not been found more advantageous.

Given a Nambu-Gor'kov propagator and an effective running coupling $\alpha_s(k)$, we can then directly perform the numerical integral for our approximation in chapter 3. The self-energy is projected on the tensor structure of each dressing function and the loop integral in the quark self-energy is written in hyperspherical coordinates

$$\int \frac{d^4q}{(2\pi)^4} \;=\; \frac{1}{(2\pi)^3} \int_\epsilon^\Lambda dq q^3 \int_0^\pi d\chi \sin^2\chi \int_0^\pi d\theta \sin\theta \,, \tag{F.1}$$

where we analytically performed the ϕ-integration. In addition the θ-integration is in-

dependent of the propagator and can first be performed numerically for each abscissa of outer and inner momentum. Storing the result of this integration enhances the numerical algorithm significantly, but also puts a restriction on the extend of the discretization.

The qDSE for the truncation in chapter 3 is then solved by iterating the quark propagator in the self-energy integral. In some cases a damping factor accelerates the convergence.

For the chemical potentials in section 3.5 we need to determine the occupation numbers and densities first. The $|\vec{p}|$-integral over the occupation numbers is numerically very demanding and a bilinear interpolation in the self-energy necessary. For a free propagator, the integrand of the $|\vec{p}|$-integration has support on $[0, \mu]$. In the numerics we chose $[0, \max(2.5\mu, 1\text{GeV})]$. Varying the cutoff up to $\max(7.5\mu, 1\text{GeV})$ left the results almost invariant, a much larger cutoff $\sim \Lambda$ is however numerically impossible. For the minimization of the charge-densities, the conjugate gradient method can then be applied.

The qDSE proposed in section 5.2 can also be solved by iteration. Here the θ-integration is depending on the propagator and cannot be performed once before the iteration. In addition an interpolation of the dressing functions appearing the the BSAs is required. This considerably slows down the iteration and it is advisable not to perform the integral of the Goldstone contribution in each step, but to store this contribution separately.

Similarly the qDSE in section 5.3 requires the θ-integration to be performed with the self-consistently determined medium polarization. This constitutes an additional iteration.

F.2 Implementation of the Maximum Entropy Method

For the numerical determination of the most plausible spectral function, we first need the data D with errors σ on an interval $[a, b]$. Furthermore we have to choose a suitable interval $[\omega_1, \omega_2]$ for the considered part of the spectral function and a prior estimate m. The interval $[\omega_1, \omega_2]$ is usually suggested by the involved scales and can be chosen to be rather large. The prior estimate m is in our case taken as a constant and can be estimated from the sum rules (see Eq. (4.6)), if the spectral function varies only in a certain interval ΔI. It can also be adopted to the knowledge from other methods. Since the main purpose is the implementation of positivity, the results turn out to be comparatively insensitive to its choice. The advantage of our method is that, after an eventual test calculation, we can choose the discretization, i.e. the abscissas and weights, of the spectral function, such that it is interpolated by a small number of points.

We summarize the procedure as follows:

- Take the data D with errors σ on an interval $[a, b]$ and choose a prior estimate m on

an interval $[\omega_1, \omega_2]$.

- Determine the maximum of the functional $Q[\rho] = L[\rho] - \alpha S[\rho]$ for a fixed value of α and an adjusted discretization of ρ. Due to its simple form, the Marquardt-Levenberg method [132] is very well suited.

- Choose a discretized interval for α, such that $P[\alpha|DH(m)]$ is strongly peaked. Z in Eq.(4.22) is determined by normalization. For consistency, the choice for the upper cutoff for α should always be quoted.

- Calculate ρ_{MEM} and eventually $\langle\rho_{\mathrm{MEM}}\rangle_I$ and $\langle(\delta\rho_{\mathrm{MEM}})^2\rangle_I$ for a chosen interval I.

F.3 Implementation of the medium polarization

For the medium polarization it is again necessary to perform the energy integration first. With the propagator being given by interpolation at any energy and momentum, we can concentrate on the numerical integration for any given outer momentum. For the outer momentum $(|\vec{k}|, k_4)$ we take

$$\int\frac{d^4p}{(2\pi)^4} \;=\; \frac{1}{(2\pi)^3}\int_0^\Lambda d|\vec{p}||\vec{p}|^2\int_0^\pi d\theta\sin\theta\int_{-\Lambda}^{\Lambda} dp_4\,, \tag{F.2}$$

i.e. the $\vec{p}$-integration is performed in spherical coordinates. As θ- and p_4-integration are interchangeable, we perform the θ-integration first and adjust the remaining integration according to the pole-structure of the quark propagators. This can be done in a similar fashion as shown in Fig. F.1 for the integrand in the qDSE.

The final $|\vec{p}|$-integral has support on $[0, \mu]$ for a free propagator. In the numerics we again chose $[0, \max(2.5\mu, 1\mathrm{GeV})]$. Varying the cutoff up to $\max(7.5\mu, 1\mathrm{GeV})$ also left the results almost invariant in this case, a much larger cutoff $\sim \Lambda$ is however numerically impossible. It is also necessary to calculate the quark propagator for the chirally broken phase, being needed for the subtraction, on the same grid as the propagator in the medium. This removes numerical artefacts that spoil the subtraction at large momentum.

For the medium polarization required by the approximation of the qDSE in section 5.3, we determine the dressing functions of the medium polarization on a grid $[0, \Lambda_{FG}]\times[0, \pi/2]$ for hyperspherical coordinates k, χ and interpolate bilinearly. The cutoff Λ_{FG} can be chosen quite small: $\Lambda_{FG} \sim \max(2.5\mu, 1\mathrm{GeV})$.

Bibliography

[1] T. P. Cheng and L. F. Li, "Gauge theory of elementary particle physics,". Oxford, UK: Clarendon (1984) 536 p.

[2] C. Itzykson and J. B. Zuber, "Quantum field theory,". New York, USA: Mcgraw-hill (1980) 705 p.

[3] M. E. Peskin and D. V. Schroeder, "An Introduction to Quantum Field Theory,". Reading, USA: Addison-Wesley (1995) 842 p.

[4] S. Weinberg, "The quantum theory of fields. vol. 1-3,". Cambridge, UK: Univ. Pr. (1996).

[5] D. J. Gross and F. Wilczek, "Ultraviolet behavior of non-abelian gauge theories," *Phys. Rev. Lett.* **30** (1973) 1343–1346.

[6] H. D. Politzer, "Reliable perturbative results for strong interactions?," *Phys. Rev. Lett.* **30** (1973) 1346–1349.

[7] H. J. Rothe, "Lattice gauge theories: An introduction," *World Sci. Lect. Notes Phys.* **74** (2005) 1–605.

[8] R. Alkofer and L. von Smekal, "The infrared behavior of QCD Green's functions: Confinement, dynamical symmetry breaking, and hadrons as relativistic bound states," *Phys. Rept.* **353** (2001) 281, `hep-ph/0007355`.

[9] C. S. Fischer, "Infrared properties of QCD from Dyson-Schwinger equations," *J. Phys.* **G32** (2006) R253–R291, `hep-ph/0605173`.

[10] P. Maris and C. D. Roberts, "Dyson-Schwinger equations: A tool for hadron physics," *Int. J. Mod. Phys.* **E12** (2003) 297–365, `nucl-th/0301049`.

[11] C. D. Roberts and S. M. Schmidt, "Dyson-Schwinger equations: Density, temperature and continuum strong QCD," *Prog. Part. Nucl. Phys.* **45** (2000) S1–S103, `nucl-th/0005064`.

[12] C. D. Roberts and A. G. Williams, "Dyson-Schwinger equations and their application to hadronic physics," *Prog. Part. Nucl. Phys.* **33** (1994) 477–575, `hep-ph/9403224`.

[13] J. C. Collins and M. J. Perry, "Superdense matter: Neutrons or asymptotically free quarks?," *Phys. Rev. Lett.* **34** (1975) 1353.

[14] N. Cabibbo and G. Parisi, "Exponential hadronic spectrum and quark liberation," *Phys. Lett.* **B59** (1975) 67.

[15] F. Karsch and E. Laermann, "Thermodynamics and in-medium hadron properties from lattice QCD," `hep-lat/0305025`.

[16] Y. Aoki, Z. Fodor, S. D. Katz, and K. K. Szabo, "The QCD transition temperature: Results with physical masses in the continuum limit," *Phys. Lett.* **B643** (2006) 46–54, `hep-lat/0609068`.

[17] M. Cheng *et al.*, "The transition temperature in QCD," *Phys. Rev.* **D74** (2006) 054507, `hep-lat/0608013`.

[18] S. Datta, F. Karsch, P. Petreczky, and I. Wetzorke, "Behavior of charmonium systems after deconfinement," *Phys. Rev.* **D69** (2004) 094507, `hep-lat/0312037`.

[19] E. V. Shuryak, "Strongly coupled quark-gluon plasma: The status report," `hep-ph/0608177`.

[20] A. Maas, "Gluons at finite temperature in Landau gauge Yang-Mills theory," *Mod. Phys. Lett.* **A20** (2005) 1797–1811, `hep-ph/0506066`.

[21] A. Maas, J. Wambach, and R. Alkofer, "The high-temperature phase of Landau-gauge Yang-Mills theory," *Eur. Phys. J.* **C42** (2005) 93–107, `hep-ph/0504019`.

[22] A. Maas, J. Wambach, B. Gruter, and R. Alkofer, "High-temperature limit of Landau-gauge Yang-Mills theory," *Eur. Phys. J.* **C37** (2004) 335–357, `hep-ph/0408074`.

[23] C. R. Allton *et al.*, "Thermodynamics of two flavor QCD to sixth order in quark chemical potential," *Phys. Rev.* **D71** (2005) 054508, hep-lat/0501030.

[24] P. de Forcrand and O. Philipsen, "The QCD phase diagram for small densities from imaginary chemical potential," *Nucl. Phys.* **B642** (2002) 290–306, hep-lat/0205016.

[25] P. de Forcrand and O. Philipsen, "The chiral critical line of N(f) = 2+1 QCD at zero and non- zero baryon density," *JHEP* **01** (2007) 077, hep-lat/0607017.

[26] Z. Fodor and S. D. Katz, "Critical point of QCD at finite T and mu, lattice results for physical quark masses," *JHEP* **04** (2004) 050, hep-lat/0402006.

[27] B. C. Barrois, "Superconducting quark matter," *Nucl. Phys.* **B129** (1977) 390.

[28] D. Bailin and A. Love, "Superfluidity and superconductivity in relativistic fermion systems," *Phys. Rept.* **107** (1984) 325.

[29] M. G. Alford, K. Rajagopal, and F. Wilczek, "QCD at finite baryon density: Nucleon droplets and color superconductivity," *Phys. Lett.* **B422** (1998) 247–256, hep-ph/9711395.

[30] R. Rapp, T. Schafer, E. V. Shuryak, and M. Velkovsky, "Diquark Bose condensates in high density matter and instantons," *Phys. Rev. Lett.* **81** (1998) 53–56, hep-ph/9711396.

[31] M. Buballa, "NJL-model analysis of quark dense matter," *Phys. Rept.* **407** (2005) 205–376, hep-ph/0402234.

[32] G. Nardulli, "Effective description of QCD at very high densities," *Riv. Nuovo Cim.* **25N3** (2002) 1–80, hep-ph/0202037.

[33] K. Rajagopal and F. Wilczek, "The condensed matter physics of QCD," hep-ph/0011333.

[34] S. Reddy, "Novel phases at high density and their roles in the structure and evolution of neutron stars," *Acta Phys. Polon.* **B33** (2002) 4101–4140, nucl-th/0211045.

[35] D. H. Rischke, "The quark-gluon plasma in equilibrium," *Prog. Part. Nucl. Phys.* **52** (2004) 197–296, nucl-th/0305030.

[36] T. Schafer, "Quark matter," hep-ph/0304281.

[37] I. A. Shovkovy, "Two lectures on color superconductivity," *Found. Phys.* **35** (2005) 1309–1358, nucl-th/0410091.

[38] D. K. Hong, V. A. Miransky, I. A. Shovkovy, and L. C. R. Wijewardhana, "Schwinger-Dyson approach to color superconductivity in dense QCD," *Phys. Rev.* **D61** (2000) 056001, hep-ph/9906478.

[39] T. Schafer and F. Wilczek, "Superconductivity from perturbative one-gluon exchange in high density quark matter," *Phys. Rev.* **D60** (1999) 114033, hep-ph/9906512.

[40] S. B. Ruster, V. Werth, M. Buballa, I. A. Shovkovy, and D. H. Rischke, "The phase diagram of neutral quark matter: Self-consistent treatment of quark masses," *Phys. Rev.* **D72** (2005) 034004, hep-ph/0503184.

[41] C. S. Fischer and R. Alkofer, "Non-perturbative propagators, running coupling and dynamical quark mass of Landau gauge QCD," *Phys. Rev.* **D67** (2003) 094020, hep-ph/0301094.

[42] Q. Wang and D. H. Rischke, "How the quark self-energy affects the color-superconducting gap," *Phys. Rev.* **D65** (2002) 054005, nucl-th/0110016.

[43] M. Jarrell and J. E. Gubernatis, "Bayesian inference and the analytic continuation of imaginary-time quantum monte carlo data," *Phys. Rept.* **269** (1996) 133–195.

[44] M. Asakawa, T. Hatsuda, and Y. Nakahara, "Maximum entropy analysis of the spectral functions in lattice QCD," *Prog. Part. Nucl. Phys.* **46** (2001) 459–508, hep-lat/0011040.

[45] D. Nickel, J. Wambach, and R. Alkofer, "Color-superconductivity in the strong-coupling regime of landau gauge qcd," *Phys. Rev.* **D73** (2006) 114028, hep-ph/0603163.

[46] D. Nickel, R. Alkofer, and J. Wambach, "On the unlocking of color and flavor in color- superconducting quark matter," *Phys. Rev.* **D74** (2006) 114015, hep-ph/0609198.

[47] D. Nickel, "Extraction of spectral functions from dyson-schwinger studies via the maximum entropy method," *Annals of Physics* **In Press** (2006) hep-ph/0607224.

[48] F. Marhauser, D. Nickel, M. Buballa, and J. Wambach, "Color-spin locking in a selfconsistent Dyson-Schwinger approach," *Phys. Rev.* **D75** (2007) 054022, `hep-ph/0612027`.

[49] C. Vafa and E. Witten, "Restrictions on symmetry breaking in vector-like gauge theories," *Nucl. Phys.* **B234** (1984) 173.

[50] K. Fujikawa, "Path integral measure for gauge invariant fermion theories," *Phys. Rev. Lett.* **42** (1979) 1195.

[51] I. M. Singer, "Some remarks on the Gribov ambiguity," *Commun. Math. Phys.* **60** (1978) 7–12.

[52] V. N. Gribov, "Quantization of non-Abelian gauge theories," *Nucl. Phys.* **B139** (1978) 1.

[53] C. Becchi, A. Rouet, and R. Stora, "Renormalization of gauge theories," *Annals Phys.* **98** (1976) 287–321.

[54] M. Z. Iofa and I. V. Tyutin, "Gauge invariance of spontaneously broken nonabelian theories in the Bogolyubov-Parasiuk-Hepp-Zimmermann method. (in russian)," *Teor. Mat. Fiz.* **27** (1976) 38–47.

[55] T. Kugo and I. Ojima, "Local covariant operator formalism of nonabelian gauge theories and quark confinement problem," *Prog. Theor. Phys. Suppl.* **66** (1979) 1.

[56] D. Zwanziger, "Vanishing of zero momentum lattice gluon propagator and color confinement," *Nucl. Phys.* **B364** (1991) 127–161.

[57] D. Zwanziger, "Critical limit of lattice gauge theory," *Nucl. Phys.* **B378** (1992) 525–590.

[58] S. Elitzur, "Impossibility of spontaneously breaking local symmetries," *Phys. Rev.* **D12** (1975) 3978–3982.

[59] L. Baulieu and J. Thierry-Mieg, "The principle of BRS symmetry: An alternative approach to Yang-Mills theories," *Nucl. Phys.* **B197** (1982) 477.

[60] J. C. Taylor, "Ward identities and charge renormalization of the Yang- Mills field," *Nucl. Phys.* **B33** (1971) 436–444.

[61] W. J. Marciano and H. Pagels, "Quantum Chromodynamics: A review," *Phys. Rept.* **36** (1978) 137.

[62] R. J. Rivers, "Path integral methods in quantum field theory,". Cambridge, UK: Univ. Pr. (1987) 339 p.

[63] A. Cucchieri, T. Mendes, and A. Mihara, "Numerical study of the ghost-gluon vertex in Landau gauge," *JHEP* **12** (2004) 012, hep-lat/0408034.

[64] W. Schleifenbaum, A. Maas, J. Wambach, and R. Alkofer, "Infrared behaviour of the ghost gluon vertex in Landau gauge Yang-Mills theory," *Phys. Rev.* **D72** (2005) 014017, hep-ph/0411052.

[65] L. von Smekal, R. Alkofer, and A. Hauck, "The infrared behavior of gluon and ghost propagators in Landau gauge QCD," *Phys. Rev. Lett.* **79** (1997) 3591–3594, hep-ph/9705242.

[66] C. Lerche and L. von Smekal, "On the infrared exponent for gluon and ghost propagation in Landau gauge QCD," *Phys. Rev.* **D65** (2002) 125006, hep-ph/0202194.

[67] D. Zwanziger, "Time-independent stochastic quantization, DS equations, and infrared critical exponents in QCD," *Phys. Rev.* **D67** (2003) 105001, hep-th/0206053.

[68] R. Alkofer, C. S. Fischer, and F. J. Llanes-Estrada, "Vertex functions and infrared fixed point in Landau gauge SU(N) Yang-Mills theory," *Phys. Lett.* **B611** (2005) 279–288, hep-th/0412330.

[69] C. S. Fischer and J. M. Pawlowski, "Uniqueness of infrared asymptotics in Landau gauge Yang- Mills theory," *Phys. Rev.* **D75** (2007) 025012, hep-th/0609009.

[70] T. Kugo, "The universal renormalization factors Z(1) / Z(3) and color confinement condition in non-Abelian gauge theory," hep-th/9511033.

[71] A. Cucchieri and T. Mendes, "Propagators, running coupling and condensates in lattice QCD," hep-ph/0605224.

[72] E. M. Ilgenfritz, M. Muller-Preussker, A. Sternbeck, A. Schiller, and I. L. Bogolubsky, "Landau gauge gluon and ghost propagators from lattice QCD," hep-lat/0609043.

[73] P. O. Bowman, U. M. Heller, and A. G. Williams, "Lattice quark propagator with staggered quarks in Landau and Laplacian gauges," *Phys. Rev.* **D66** (2002) 014505, hep-lat/0203001.

[74] P. O. Bowman *et al.*, "Unquenched quark propagator in Landau gauge," *Phys. Rev.* **D71** (2005) 054507, hep-lat/0501019.

[75] R. Alkofer, C. S. Fischer, and F. J. Llanes-Estrada, "Dynamically induced scalar quark confinement," hep-ph/0607293.

[76] H. D. Politzer, "Effective quark masses in the chiral limit," *Nucl. Phys.* **B117** (1976) 397.

[77] V. A. Miransky, "On dynamical chiral symmetry breaking," *Phys. Lett.* **B165** (1985) 401–404.

[78] J. I. Skullerud, P. O. Bowman, A. Kizilersu, D. B. Leinweber, and A. G. Williams, "Nonperturbative structure of the quark gluon vertex," *JHEP* **04** (2003) 047, hep-ph/0303176.

[79] J. S. Ball and T.-W. Chiu, "Analytic properties of the vertex function in gauge theories. 1," *Phys. Rev.* **D22** (1980) 2542.

[80] D. C. Curtis and M. R. Pennington, "Truncating the Schwinger-Dyson equations: How multiplicative renormalizability and the Ward identity restrict the three point vertex in QED," *Phys. Rev.* **D42** (1990) 4165–4169.

[81] M. S. Bhagwat, M. A. Pichowsky, C. D. Roberts, and P. C. Tandy, "Analysis of a quenched lattice-QCD dressed-quark propagator," *Phys. Rev.* **C68** (2003) 015203, nucl-th/0304003.

[82] L. P. Gor'kov, "Quasi-particles and gauge invariance in the theory of superconductivity," *Sov. Phys. JETP* **9** (1959) 1364.

[83] Y. Nambu, "Quasi-particles and gauge invariance in the theory of superconductivity," *Phys. Rev.* **117** (1960) 648–663.

[84] C. Manuel, "Lifetime effects in color superconductivity at weak coupling," *Phys. Rev.* **D62** (2000) 114008, hep-ph/0006106.

[85] A. Gerhold and A. Rebhan, "Gauge dependence identities for color superconducting QCD," *Phys. Rev.* **D68** (2003) 011502, hep-ph/0305108.

[86] D. D. Dietrich and D. H. Rischke, "Gluons, tadpoles, and color neutrality in a two-flavor color superconductor," *Prog. Part. Nucl. Phys.* **53** (2004) 305–316, nucl-th/0312044.

[87] M. Buballa and I. A. Shovkovy, "A note on color neutrality in NJL-type models," *Phys. Rev.* **D72** (2005) 097501, hep-ph/0508197.

[88] J. J. Rusnak and R. J. Furnstahl, "Two point fermion correlation functions at finite density," *Z. Phys.* **A352** (1995) 345–350.

[89] E. Braaten and R. D. Pisarski, "Soft amplitudes in hot gauge theories: A general analysis," *Nucl. Phys.* **B337** (1990) 569.

[90] E. Braaten and R. D. Pisarski, "Simple effective Lagrangian for hard thermal loops," *Phys. Rev.* **D45** (1992) 1827–1830.

[91] M. Le Bellac, "Thermal field theory,". Cambridge, UK: Cambridge University Press (1996).

[92] K. Rajagopal and E. Shuster, "On the applicability of weak-coupling results in high density QCD," *Phys. Rev.* **D62** (2000) 085007, hep-ph/0004074.

[93] H. Abuki, T. Hatsuda, and K. Itakura, "Structural change of Cooper pairs and momentum-dependent gap in color superconductivity," *Phys. Rev.* **D65** (2002) 074014, hep-ph/0109013.

[94] J. M. Cornwall, R. Jackiw, and E. Tomboulis, "Effective action for composite operators," *Phys. Rev.* **D10** (1974) 2428–2445.

[95] A. Schmitt, "The ground state in a spin-one color superconductor," *Phys. Rev.* **D71** (2005) 054016, nucl-th/0412033.

[96] J. M. Luttinger, "Fermi surface and some simple equilibrium properties of a system of interacting fermions," *Phys. Rev.* **119** (1960) 1153.

[97] R. Alkofer, W. Detmold, C. S. Fischer, and P. Maris, "Analytic properties of the Landau gauge gluon and quark propagators," *Phys. Rev.* **D70** (2004) 014014, hep-ph/0309077.

[98] J. C. R. Bloch, C. D. Roberts, and S. M. Schmidt, "Diquarks: Condensation without bound states," *Phys. Rev.* **C60** (1999) 065208, nucl-th/9907086.

[99] C. Manuel, "Dispersion relations in ultradegenerate relativistic plasmas," *Phys. Rev.* **D62** (2000) 076009, hep-ph/0005040.

[100] T. Schafer and K. Schwenzer, "Non-Fermi liquid effects in QCD at high density," *Phys. Rev.* **D70** (2004) 054007, hep-ph/0405053.

[101] H. Abuki, "Color superconductivity in Schwinger-Dyson approach: Strange quark mass and color-flavor unlocking line," *Prog. Theor. Phys.* **110** (2003) 937–961, hep-ph/0306074.

[102] T. Schafer and K. Schwenzer, "Low energy dynamics in ultradegenerate QCD matter," *Phys. Rev. Lett.* **97** (2006) 092301, hep-ph/0512309.

[103] R. D. Pisarski and D. H. Rischke, "Superfluidity in a model of massless fermions coupled to scalar bosons," *Phys. Rev.* **D60** (1999) 094013, nucl-th/9903023.

[104] R. D. Pisarski and D. H. Rischke, "A first order transition to, and then parity violation in, a color superconductor," *Phys. Rev. Lett.* **83** (1999) 37–40, nucl-th/9811104.

[105] T. Schafer, "Patterns of symmetry breaking in QCD at high baryon density," *Nucl. Phys.* **B575** (2000) 269–284, hep-ph/9909574.

[106] M. G. Alford, K. Rajagopal, and F. Wilczek, "Color-flavor locking and chiral symmetry breaking in high density QCD," *Nucl. Phys.* **B537** (1999) 443–458, hep-ph/9804403.

[107] M. G. Alford, J. Berges, and K. Rajagopal, "Unlocking color and flavor in superconducting strange quark matter," *Nucl. Phys.* **B558** (1999) 219–242, hep-ph/9903502.

[108] T. Schafer and F. Wilczek, "Quark description of hadronic phases," *Phys. Rev.* **D60** (1999) 074014, hep-ph/9903503.

[109] M. G. Alford, K. Rajagopal, S. Reddy, and F. Wilczek, "The minimal CFL-nuclear interface," *Phys. Rev.* **D64** (2001) 074017, hep-ph/0105009.

[110] M. Buballa and M. Oertel, "Color-flavor unlocking and phase diagram with self-consistently determined strange quark masses," *Nucl. Phys.* **A703** (2002) 770–784, hep-ph/0109095.

[111] A. W. Steiner, S. Reddy, and M. Prakash, "Color-neutral superconducting quark matter," *Phys. Rev.* **D66** (2002) 094007, hep-ph/0205201.

[112] C. S. Fischer, P. Watson, and W. Cassing, "Probing unquenching effects in the gluon polarisation in light mesons," *Phys. Rev.* **D72** (2005) 094025, hep-ph/0509213.

[113] W.-M. Yao *et al.*, "Review of Particle Physics," *Journal of Physics G* **33** (2006) 1+.

[114] S. B. Ruster, I. A. Shovkovy, and D. H. Rischke, "Phase diagram of dense neutral three-flavor quark matter," *Nucl. Phys.* **A743** (2004) 127–146, hep-ph/0405170.

[115] H. Abuki and T. Kunihiro, "Extensive study of phase diagram for charge neutral homogeneous quark matter affected by dynamical chiral condensation: Unified picture for thermal unpairing transitions from weak to strong coupling," *Nucl. Phys.* **A768** (2006) 118–159, hep-ph/0509172.

[116] K. Rajagopal and F. Wilczek, "Enforced electrical neutrality of the color-flavor locked phase," *Phys. Rev. Lett.* **86** (2001) 3492–3495, hep-ph/0012039.

[117] M. Alford and K. Rajagopal, "Absence of two-flavor color superconductivity in compact stars," *JHEP* **06** (2002) 031, hep-ph/0204001.

[118] M. G. Alford, J. Berges, and K. Rajagopal, "Gapless color superconductivity," *Phys. Rev. Lett.* **84** (2000) 598–601, hep-ph/9908235.

[119] I. Shovkovy and M. Huang, "Gapless two-flavor color superconductor," *Phys. Lett.* **B564** (2003) 205, hep-ph/0302142.

[120] M. Huang and I. Shovkovy, "Gapless color superconductivity at zero and at finite temperature," *Nucl. Phys.* **A729** (2003) 835–863, hep-ph/0307273.

[121] M. Alford, C. Kouvaris, and K. Rajagopal, "Gapless color-flavor-locked quark matter," *Phys. Rev. Lett.* **92** (2004) 222001, hep-ph/0311286.

[122] M. Alford, C. Kouvaris, and K. Rajagopal, "Evaluating the gapless color-flavor locked phase," *Phys. Rev.* **D71** (2005) 054009, hep-ph/0406137.

[123] M. Huang and I. A. Shovkovy, "Chromomagnetic instability in dense quark matter," *Phys. Rev.* **D70** (2004) 051501, hep-ph/0407049.

[124] M. Huang and I. A. Shovkovy, "Screening masses in neutral two-flavor color superconductor," *Phys. Rev.* **D70** (2004) 094030, hep-ph/0408268.

[125] R. Casalbuoni, R. Gatto, M. Mannarelli, G. Nardulli, and M. Ruggieri, "Meissner masses in the gCFL phase of QCD," *Phys. Lett.* **B605** (2005) 362–368, hep-ph/0410401.

[126] T. Schafer, "P-wave meson condensation in high density QCD," *Phys. Rev. Lett.* **96** (2006) 012305, hep-ph/0508190.

[127] K. Rajagopal and R. Sharma, "The crystallography of three-flavor quark matter," *Phys. Rev.* **D74** (2006) 094019, hep-ph/0605316.

[128] E. V. Gorbar, M. Hashimoto, and V. A. Miransky, "Gluonic phase in neutral two-flavor dense QCD," *Phys. Lett.* **B632** (2006) 305–312, hep-ph/0507303.

[129] D. K. Hong, "RG analysis and magnetic instability in gapless superconductors," hep-ph/0506097.

[130] E. Gubankova, W. V. Liu, and F. Wilczek, "Breached pairing superfluidity: Possible realization in QCD," *Phys. Rev. Lett.* **91** (2003) 032001, hep-ph/0304016.

[131] F. Karsch, E. Laermann, P. Petreczky, S. Stickan, and I. Wetzorke, "A lattice calculation of thermal dilepton rates," *Phys. Lett.* **B530** (2002) 147–152, hep-lat/0110208.

[132] W. H. Press *et al.*, "Numerical Recipes in C,". Cambridge, UK: Cambridge University Press (1992).

[133] J. Skilling, "Maximum entropy and Bayesian methods,". Dordrecht, NL: Kluwer Academic Publishers (1989).

[134] S. F. Gull, "Maximum entropy and Bayesian methods,". Dordrecht, NL: Kluwer Academic Publishers (1989).

[135] R. K. Bryan, "Maximum entropy analysis of oversampled data problems," *Eur. Biophys. J.* **18** (1990) 165.

[136] B. Betz and D. H. Rischke, "Are there plasminos in superconductors?," nucl-th/0609019.

[137] P. Maris and C. D. Roberts, "pi and k meson Bethe-Salpeter amplitudes," *Phys. Rev.* **C56** (1997) 3369–3383, nucl-th/9708029.

[138] R. Alkofer, P. Watson, and H. Weigel, "Mesons in a Poincare covariant Bethe-Salpeter approach," *Phys. Rev.* **D65** (2002) 094026, hep-ph/0202053.

[139] C. S. Fischer, D. Nickel, and J. Wambach, "Studying pion effects in the quark propagator,". in preparation.

[140] A. Bender, C. D. Roberts, and L. Von Smekal, "Goldstone theorem and diquark confinement beyond rainbow- ladder approximation," *Phys. Lett.* **B380** (1996) 7–12, nucl-th/9602012.

[141] P. Maris, C. D. Roberts, and P. C. Tandy, "Pion mass and decay constant," *Phys. Lett.* **B420** (1998) 267–273, nucl-th/9707003.

[142] C. H. Llewellyn-Smith, "A relativistic formulation for the quark model for mesons," *Ann. Phys.* **53** (1969) 521–558.

[143] D. B. Leinweber, "QCD sum rules for skeptics," *Annals Phys.* **254** (1997) 328–396, nucl-th/9510051.

[144] V. Dmitrasinovic, H. J. Schulze, R. Tegen, and R. H. Lemmer, "Chirally symmetric o (1/n(c corrections to the nambu-jona- lasinio model," *Annals Phys.* **238** (1995) 332–369.

[145] E. N. Nikolov, W. Broniowski, C. V. Christov, G. Ripka, and K. Goeke, "Meson loops in the nambu-jona-lasinio model," *Nucl. Phys.* **A608** (1996) 411–436, hep-ph/9602274.

[146] M. Oertel, M. Buballa, and J. Wambach, "Meson loop effects in the njl model at zero and non-zero temperature," *Phys. Atom. Nucl.* **64** (2001) 698–726, hep-ph/0008131.

[147] P. C. Tandy, "Hadron physics from the global color model of QCD," *Prog. Part. Nucl. Phys.* **39** (1997) 117–199, nucl-th/9705018.

[148] G. 't Hooft, "A planar diagram theory for strong interactions," *Nucl. Phys.* **B72** (1974) 461.

[149] S. R. Coleman, "There are no Goldstone bosons in two-dimensions," *Commun. Math. Phys.* **31** (1973) 259–264.

[150] J. Gasser and H. Leutwyler, "Quark masses," *Phys. Rept.* **87** (1982) 77–169.

[151] T. Brauner, "Goldstone bosons in presence of charge density," hep-ph/0701110.

[152] T. Schafer and F. Wilczek, "Continuity of quark and hadron matter," *Phys. Rev. Lett.* **82** (1999) 3956–3959, hep-ph/9811473.

[153] R. Casalbuoni and R. Gatto, "Effective theory for color-flavor locking in high density QCD," *Phys. Lett.* **B464** (1999) 111–116, hep-ph/9908227.

[154] A. Kryjevski and T. Schafer, "An effective theory for baryons in the CFL phase," *Phys. Lett.* **B606** (2005) 52–58, hep-ph/0407329.

[155] D. H. Rischke and I. A. Shovkovy, "Longitudinal gluons and Nambu-Goldstone bosons in a two- flavor color superconductor," *Phys. Rev.* **D66** (2002) 054019, nucl-th/0205080.

[156] D. T. Son and M. A. Stephanov, "Inverse meson mass ordering in color-flavor-locking phase of high density QCD," *Phys. Rev.* **D61** (2000) 074012, hep-ph/9910491.

[157] D. T. Son and M. A. Stephanov, "Inverse meson mass ordering in color-flavor-locking phase of high density QCD: Erratum," *Phys. Rev.* **D62** (2000) 059902, hep-ph/0004095.

[158] P. F. Bedaque and T. Schafer, "High density quark matter under stress," *Nucl. Phys.* **A697** (2002) 802–822, hep-ph/0105150.

[159] V. Werth, M. Buballa, and M. Oertel, "Goldstone bosons in the color-flavor locked phase," hep-ph/0611392.

[160] V. Kleinhaus, M. Buballa, D. Nickel, and M. Oertel, "Goldstone bosons in the color-flavor locked phase,". in preparation.

[161] M. Buballa, "NJL-model description of Goldstone boson condensation in the color-flavor locked phase," *Phys. Lett.* **B609** (2005) 57–67, hep-ph/0410397.

[162] H. J. Warringa, "The phase diagram of neutral quark matter with pseudoscalar condensates in the color-flavor locked phase," hep-ph/0606063.

[163] J. I. Kapusta, "Finite Temperature Field Theory,". Cambridge, UK: Univ. Pr. (1989).

[164] A. Gerhold, A. Ipp, and A. Rebhan, "Non-Fermi-liquid specific heat of normal degenerate quark matter," *Phys. Rev.* **D70** (2004) 105015, hep-ph/0406087.

[165] W. E. Brown, J. T. Liu, and H.-c. Ren, "Non-Fermi liquid behavior, the BRST identity in the dense quark-gluon plasma and color superconductivity," *Phys. Rev.* **D62** (2000) 054013, hep-ph/0003199.

[166] D. H. Rischke, "Debye screening and Meissner effect in a three-flavor color superconductor," *Phys. Rev.* **D62** (2000) 054017, nucl-th/0003063.

[167] D. H. Rischke, "Debye screening and Meissner effect in a two-flavor color superconductor," *Phys. Rev.* **D62** (2000) 034007, nucl-th/0001040.

[168] H. Malekzadeh and D. H. Rischke, "Gluon self-energy in the color-flavor-locked phase," *Phys. Rev.* **D73** (2006) 114006, hep-ph/0602082.

[169] D. Belitz, T. R. Kirkpatrick, and T. Vojta, "Nonanalytic behavior of the spin susceptibility in clean fermi systems," *Phys. Rev. B* **55** (Apr, 1997) 9452–9462.

[170] C. S. Fischer and R. Alkofer, "Infrared exponents and running coupling of SU(N) Yang-Mills theories," *Phys. Lett.* **B536** (2002) 177–184, hep-ph/0202202.

[171] P. O. Bowman, U. M. Heller, D. B. Leinweber, and A. G. Williams, "Modelling the quark propagator," *Nucl. Phys. Proc. Suppl.* **119** (2003) 323–325, hep-lat/0209129.

Lebenslauf

Name	Marcel Dominik Johannes Nickel
Geburtsdatum	3. Januar 1979
Geburtsort	Hanau
Staatsangehörigkeit	deutsch
Familienstand	ledig

1985-1989	Besuch der Grundschule in Birstein
1989-1995	Besuch der Gesamtschule in Wächtersbach
1995-1998	Besuch des Grimmelshausen Gymnasium in Gelnhausen
Juni 1998	Abitur
Juli 1998 - April 1999	Wehrdienst im 2.PzBtl 143 in Stadtallendorf
Mai 1999	Beginn des Physikstudiums an der TU Darmstadt
September 2000	Vordiplom
Oktober 2001 - März 2002	Studium am Trinity College Dublin (2 Trimester)
November 2001 - November 2003	Stipendiat der Studienstiftung des deutschen Volkes
Januar 2002 - Januar 2007	Stipendiat bei e-fellows.net
November 2003	Diplom, Gesamtnote: mit Auszeichung bestanden
seit Dezember 2003	Wissenschaftlicher Mitarbeiter am Institut für Kernphysik der TU Darmstadt
Dezember 2005	DAAD Kurzstipendium für Doktoranden
Dezember 2005 - März 2006	Forschungsaufenthalt Karl-Franzens-Universität Graz

Eidesstattliche Erklärung

Hiermit erkläre ich eidesstattlich, dass ich die vorliegende Dissertation selbständig verfasst, keine anderen als die angegebenen Hilfsmittel verwendet und noch keinen Promotionsversuch unternommen habe.

Darmstadt, den 30. April 2007,

gez. Dominik Nickel

Unterschrift